UNIVERSITAT DE BARCELONA

Microarray Strategies for Multiplexed Immunochemical Analysis

Julian Guercetti

UNIVERSITAT DE BARCELONA

FACULTAT DE FARMÀCIA I CIÈNCIES DE L'ALIMENTACIÓ

MICROARRAY STRATEGIES FOR MULTIPLEXED IMMUNOCHEMICAL ANALYSIS

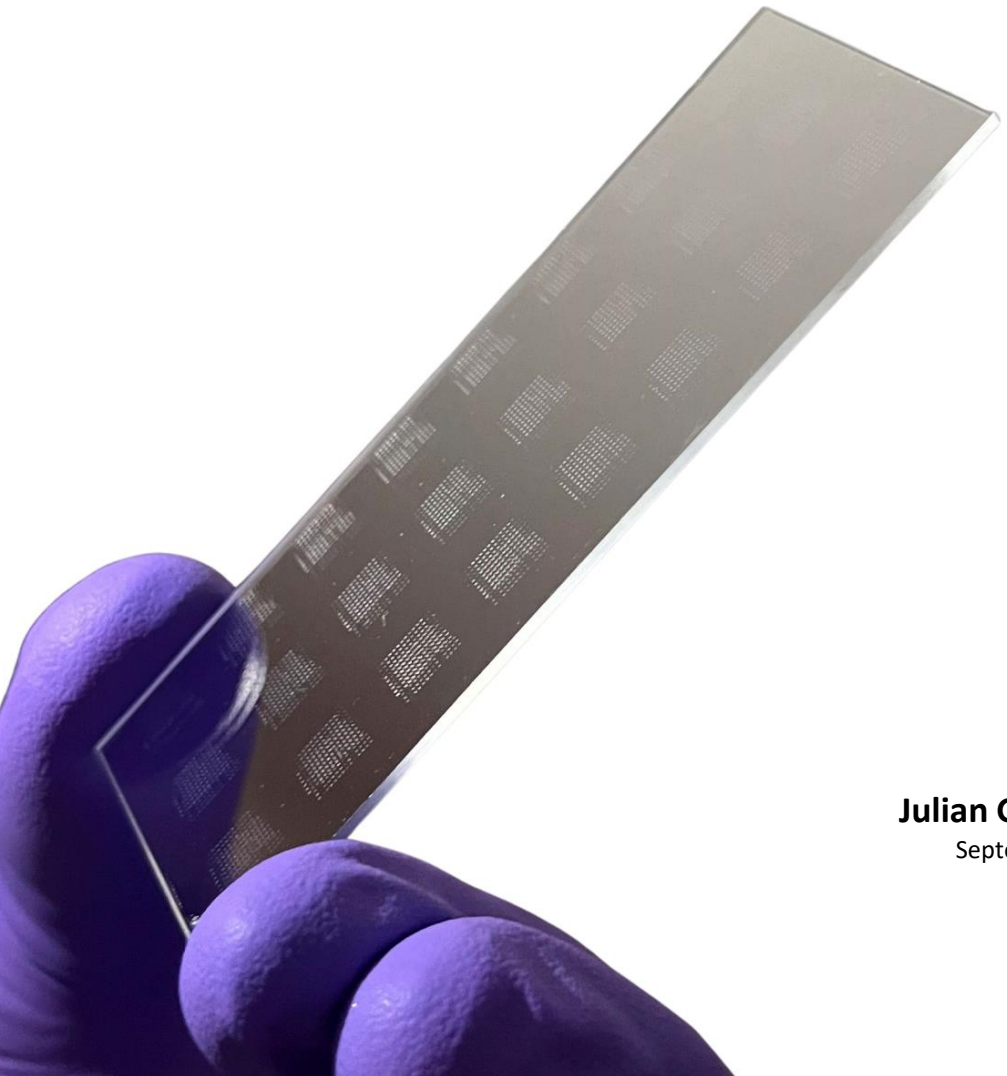

Julian Guercetti

September, 2023

UNIVERSITAT DE BARCELONA

Facultat de Farmàcia
i Ciències de l'Alimentació

Doctoral program in Biotechnology

"MICROARRAY STRATEGIES FOR MULTIPLEXED IMMUNOCHEMICAL ANALYSIS"

"Dissertation presented by Julian Guercetti in fulfillment of the requirements for the degree of doctor by Universitat de Barcelona"

Supervisors:

Prof. Mª Pilar Marco Colás
Research Professor
Head of Nanotechnology for Diagnostic group,
IQAC-CSIC

Dr. J-Pablo Salvador
Research Associate
Nanomedicine Program
Nb4D group, IQAC-

Tutor:
Dr. Laura Baldomà Llavinés
University of Barcelona

AGRADECIMIENTOS

Se acerca el final de este viaje… un viaje repleto de experiencias, desafíos, algo de turbulencias y muchos aprendizajes. Pero sin dudas esto no hubiera sido posible sin todas esas personas que formaron parte del recorrido y a las cuales me gustaría dejarles un pequeño agradecimiento.

Con origen en Argentina, mi familia y amigos fueron fundamentales para emprender este camino. Gracias a mi madre, porque a pesar de creer que me iba a otro planeta no dudo en darme su apoyo y acompañarme siempre. A mi padre por motivarme a comenzar esta etapa y disfrutar de cada pequeño logro conseguido a pesar de los kilómetros de distancia. A mi hermano, quien también decidió compartir este viaje mucho mas cerca para seguir creciendo juntos. Mis abuelos, Elena, Merchi y Ricardo incondicionales en todo momento, y también al que más insistió para que llegara este día, Emilio.

Durante el viaje, tuve la suerte de contar con dos pilotos excepcionales, quienes depositaron su confianza y me enseñaron el valor de la vocación científica. Muchas gracias Pilar, por haberme dado la oportunidad de formarme en tu grupo tanto profesional como personalmente y de impulsar ese camino. Y que decir de Pablo, quien luego de muchos intentos fallidos se resignó a dejarme poner la foto de una vaca con sombrero en las presentaciones, gracias por tu paciencia y dedicación continua.

Otra parte esencial en esta travesía fue sin dudas la tripulación del Nb4d, de quienes pude aprender y conocer grandes personas. A Roger, por las charlas científicas y de la vida. A Nuria, por tantas risas y la ayuda en todo momento (especialmente con el AKTA). A Lluïsa, por ser una gran consejera científica y amiga, compartiendo horas y horas de charlas. Monste, por los debates experimentales y los alfajores que me regalabas en secreto. David, por explicarme cada reacción sabiendo que entendía un 10% de lo que decías y por tantas risas, en síntesis.

Como en todo viaje, hay pasajeros que suben y se bajan en distintos momentos, pero con ellos siempre quedan los mejores recuerdos. A aquellos que estaban cuando comencé e hicieron que la llegada al laboratorio sea como estar en casa. Gracias Ana por el legado del microarray, Ginevra, profesora de italiano, fisio

personal y gran amiga. Enric compañero de anécdotas, experimentos y festivales. Klaudia, porque la seguridad alimentaria nos regaló una amistad y muchos momentos tan divertidos. Luciano, por las magníficas libretas y charlas de cualquier tema. Ellen, por ese gran corazón. Astrid, por tu generosidad. A todos los que formaron parte del proyecto FoodSmarpthone en especial a Javi, Ariadni, Gina.

Con el tiempo, se sumaron nuevos pasajeros que poco a poco se volvieron grandes amigos. Carlins, gracias por tantas charlas, suspiros y esos momentos inspección de tuppers tan emblemáticos. Juan, por esas discusiones existenciales intentando entender fenómenos inexplicables y todas las anécdotas que hay para contar. Francesc, por los grandes consejos, reflexiones, algunos traumas frutales y momentos de tensión con la bolsa del CSIC. Nere, por ese entusiasmo contagioso, y por enseñarme que el tofu se puede comer con cualquier cosa. A Idoia, por los cuestionarios del FBI y por animarte a incursionar en festivales sin bandas catalanas y aun así darlo todo. Andreita, por tomarte tu tiempo para guardar las cosas en el armario luego de la comida. Lidia, mi compañera oficial de baile en la bresh. Marc, por ayudarme a entender el mundo de la bioinformatica y el fitness. Y también agradecer a Eva, María, Marlene, Gemma, Macarena, Miriam, Joel.

Otra parte importante de los pasajeros en este viaje no pertenecían al Nb4D pero hicieron que el camino fuera inmejorable. Gracias Luqui, por transitar esta última etapa al lado mío apoyando, escuchando, compartiendo y aprendiendo juntos. A Sofi, incondicional desde el primer día y como una hermana. Fran, por esa amistad que vino desde Rosario y nos dio tantos momentos, viajes y mil anécdotas. Ric, por tu amistad y tantas historias y momentos compartidos. Kari y Juan, grandes compañeros y amigos en este viaje. La lista de pasajeros es muy grande y a cada uno también una mención especial, Palo, Lizy, Ale, Mati, Cami y seguro me olvido de algunos, espero sepan disculpar.

Mirando hacia atrás hoy puedo decir que gracias a todas estas personas no solo logre llegar al destino, sino también disfrutar de cada momento del largo viaje que culmina en esta tesis doctoral. ¡Muchas gracias!

Julian

THESIS ABSTRACT

Upcoming trends in diagnostic and screening applications are being determined by the establishment of bioanalytical techniques that feature multiplexed, high-throughput configurations. Microarray technology has emerged as a suitable platform for integrating miniaturized, low-cost, and site-specific detection of biochemical interactions for a variety of purposes. In the present work, the production and characterization of two multiplexed and universal microarray systems was examined within the framework of two different research projects.

The first section was focused on developing a multiplexed screening platform based on DNA-directed immobilization (DDI) techniques for identifying antibiotic residues in cow's milk in accordance with the European Union's regulations. For this, three in house produced class-selective monoclonal antibodies against tylosin, sulfonamides, and fluoroquinolones were used in an indirect competitive immunoassay format, reaching detectability's in the order of parts per billion (ppb's). The signal of each hapten-antibody pair was site-encoded utilizing oligonucleotide strains linked to hapten molecules, that were subsequently identified using secondary labelled antibodies. The identification of 18 veterinary residues in a single sample, with a system processing capacity of 180 samples simultaneously in less than 90 minutes, encourage a pre-validation study to evaluate the novel platform's performance in spiked commercial milk under blind conditions. In line with this, a portable and user-friendly biosensor based on imaging surface plasmon resonance (iSPR) incorporating smartphone readout was utilized to evaluate the antibody-hapten binding in a label-free format as a proof-of-concept.

The goal of the second project was to create point-of-care assays for fast detection of SARS-CoV-2 in an emerging pandemic scenario. Particularly our research proposal involved the production of a microarray chip based on SARS-CoV-2 peptides and proteins for customized COVID-19 immunodiagnostic. Initially, a rational design of potentially immunogenic linear peptides derived from the virus's S and N proteins was established. Through the use of computational prediction models and literature reports evidencing structural immunogenicity, a total of 28 peptide sequences were chosen and synthesized. Once established, the *Immuno*-μSARS2 chip was defined as a multiplexed and high-throughput hybrid microarray chip comprised of full-length viral proteins

and selected peptide sequences. This microarray enabled simultaneous IgG and IgM customized profiling against the selected panel of epitopes with minimal sample needs, resulting in an inexpensive and simple-to-implement diagnostic tool. The *Immuno*-µSARS2 chip worked effectively in over 750 human serum samples, with 98 % clinical sensitivity and 91 % clinical specificity when compared to RT-PCR. To maximize the chip's properties, artificial intelligence was integrated for data analysis to establish immunological signatures based on IgG response for prediction of disease severity utilizing samples categorized according to COVID-19 clinical outcomes. Our technology was able to distinguish patients going towards irreversible illness conditions (*Exitus*) with an 81 % accuracy, followed by 70 % accuracy for those admitted to ICU and 66 % accuracy for those requiring hospitalization from asymptomatic disease progression. Simultaneously, some peptide sequences were identified to possess promising immunodiagnostic features that might potentially replace the use of full-length proteins in future serodiagnostic tools.

The methodologies presented in this experimental work can readily applicable for a variety of other relevant scenarios. Universal DDI chips can be created by attaching different biomolecules to the complementary oligonucleotide chains utilized, and distinct immunogenic peptides can be rationally designed to address various pathogens or even study different immune-related disorders with multiplexed and cost-effective universal platforms.

TABLE OF CONTENTS

1 MULITPLEXED AND MINIATURIZED IMMUNOCHEMICAL PLATFORMS

1.1 BIOANALYTICAL TOOLS

A growing demand for cost effective and user-friendly bioanalytical tools is currently emerging for a wide range of applications like patient health monitoring, environmental control or even food safety. In an attempt to avoid sophisticated, time consuming and complex protocols, different approaches have been successfully implemented by integrating biological recognition elements to different transducers in order to detect the presence of specific analytes. On the other side, the main limitations found across diagnostic and monitoring platforms includes miniaturization, reproducibility, automation and multiplexing capacity [1].

Bioanalytical tools are characterized by three main components. In first place a bioreceptor or biomolecule (proteins, DNA, lipids, cells or even viruses) in charge of the selective recognition of the analyte, followed by a transducing system or a reporter which is required to translate the biological signal in a measurable output data and finally a readout system capable to interpret and display the results [2]. In this context, the biological components consist on natural, synthetic or semi-synthetic molecules with distinctive binding properties like antibodies, aptamers, nucleic acids or enzymes that provide robust and versatile alternatives to implement in novel bio-detection systems. Depending on the biological nature, these elements are generally characterized by high selectivity and relatively fast recognition of the target analyte in complex environments. However, the challenging aspects are found on the adequate selection of the most suitable receptor for a given application considering the stability, the level of sensitivity achieved, the transducing principle utilized as other features [3].

Recent progress has been focused on the improvement of aforementioned limitations, employing molecular biology techniques to increase bioreagents stability, working on the efficiency of novel transducers or signal amplification techniques and exploring further automatization processes [4]. As already mentioned, transducing systems are essential components of biosensing platforms, in charge of recognize a biological response and generate a measurable output. Although various transducers have been described in

biosensing applications during the last decades, electrochemical, optical, thermal and acoustic ones are the most frequently reported [5].

A different group of bioanalytical applications, that are not strictly defined as biosensors, require the presence of "reporters" to evidence the binding event. Including elements like enzymes to generate redox species or catalyze colorimetric reactions using chromogenic molecules as well as fluorescent and chemiluminescent dyes attached to selective biomolecules to detect the presence of the analyte [6].

In this scenario, a vast majority of bioanalytical tools rely on optical detection techniques under different configurations due to the robustness and versatility demonstrated. The most conventional approaches measure changes in the colorimetric signal directly affected by the presence of the analyte, visually monitored with lateral flow tests or for quantitative purposes in ELISA or microarray platforms, using spectrophotometers or fluorescent readers. Future bio detection systems are working on the improvement of miniaturized and user-friendly interfaces. In this regard, smartphones have become promising optical readout systems making use of optical components such as high-resolutions cameras, lenses and photodetectors to make colorimetric, chemiluminescent and fluorescent determinations offering a wide scope of applications in the biosensing area [7].

1.2 MULTIPLEXED BIOANALYTICAL PLATFORMS

An additional feature that began to be pursued through bioanalytical developments is the potential detection of more than one target analyte at a time. With the unprecedented progress of the technological field and molecular biology understanding, multiplexed bio detection is no longer a limitation. Next generation diagnostic and monitoring tools are promoting the use of multiparameter sensing systems integrating biological signals with computational analysis. In this context, multiplexation allows the simultaneous

detection and quantification of different target molecules in a reliable and reproducible manner [8, 9].

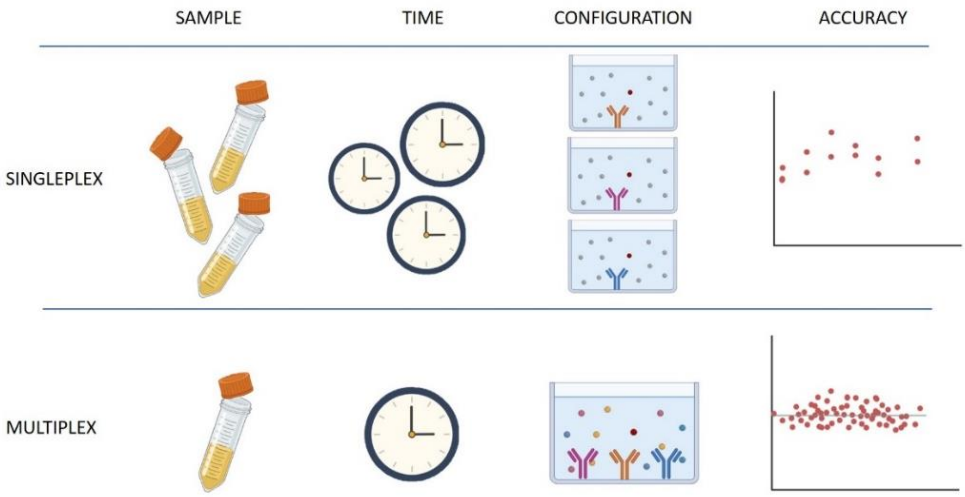

Figure 1.1 Graphical representation comparing singleplexed and multiplex assays configurations, highlighting relevant features across both bioanalytical detection approaches. Adapted from [10].

Multiplexed systems are characterized by minimum sample consumption and short time to answer response in contrast with monoplexed methods that are performed separately, thus resulting in the increase of handing errors as well as cost-per-assay. On the other hand, the development and characterization of multiparametric systems entails a hard challenge and should be carefully defined in order to achieve reliable and accurate determinations (see Figure 1.1).

With origin in genomic and proteomic analysis, high-throughput technologies have evolved during the past two decades establishing a new era for diagnostics, biomarkers identification, environmental applications and food safety monitoring [11]. Results inevitable to think that multiplex assays will replace sooner or later most of the monoplex approaches owing to significant advantages already mentioned. Furthermore, multi-analyte detection contributes to a deeper understanding of the complexity behind most of biological responses at different levels in diagnostics, research purposes and monitoring [12].

1.2.1 ADVANTAGES OF MULTIPLEXED DETECTION

Over the last few years, numerous multiplexed assays have been developed. For instance, protein arrays [13] and antibody arrays [14] demonstrated effective performance over applications involving autoantigen and autoantibody monitorization, biomarkers discovery and proteomic analysis. However, the bottleneck behind the rapid approval of novel diagnostic tools by regulatory agencies is generally associated to technical, methodological and regulatory issues. Some of the key advantages that emerge from the use of multiplexed approaches are:

Cost and assay duration: The use of multiplexed formats over single-analyte tests is a consequence of the significant reduction in cost per assay. The challenge consists on reaching robust and reliable performance increasing the number of analytes simultaneously determined considering the complexity of integrated responses to save time and costs [15].

Labour reduction: From a technical perspective, multi analyte detection systems are consider challenging developments, but the investment required throughout the initial characterization is translated in significant work reduction while performing simultaneous determinations in the final device also minimizing handling errors.

Sample volume and processing: Major interest arise on the potential detection of multiple analytes in a considerable small volume and without sample pre-treatment. This aspect is considered as a limitation due to the intrinsic differences found over the despaired abundance of certain analytes in the sample, for instance when two targets differ in the range of detectability (from mg mL^{-1} or µg mL^{-1}).

The main portion of multiplexed bioanalytical applications like diagnostic, infectious disease testing, food safety controls or environmental monitoring are still performed under semi or manually operated ELISA titter plates. These approaches require trained personnel, involve several incubation steps and do not always allow easy to implement multiplexed formats. On the contrary, several examples of multiplexed automated technological solutions integrating biological elements are available nowadays (see Figure 1.2) such as flow cytometry requiring fluorescently labelled antibodies [16], polymerase chain reaction making use of oligonucleotides and active enzymes [17], protein or DNA microarrays [18], aptamer-based biosensors [19] and immunoassays [20].

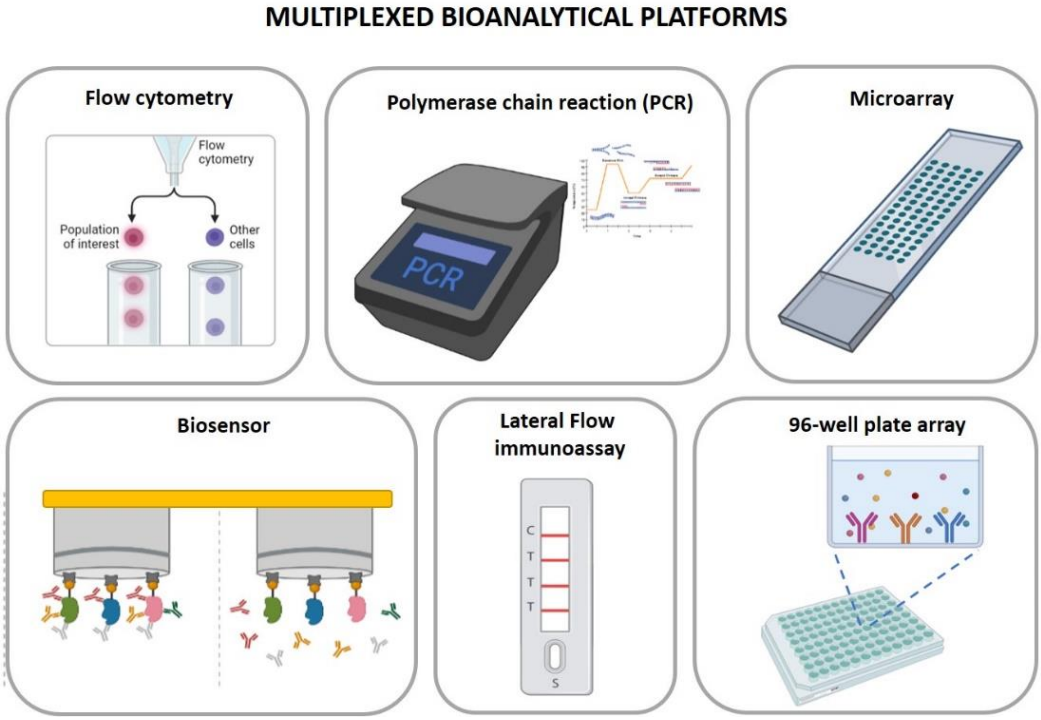

Figure 1.2 Summary of the most representative multiplexed bioanalytical platforms and techniques available at laboratory scale, with diverse biological detection purposes.

As can be seen, a wide variety of bioanalytical solutions were adapted at laboratory scale, although a common restriction is evidenced behind the lack of integration of bioreceptors with different chemical nature (like DNA and proteins) in the same platform imposing a significant challenge for biosensors developers.

1.2.2 LIMITATIONS OVER MULTIPLEXED DETECTION SYSTEMS

The coordinated incorporation of multiple elements (bioreceptors or target molecules) in a single analysis is always assumed as a challenging task due to methodological limitations and complex signal interpretation. In the first case, the experimental difficulty of integrate several bioreceptors simultaneously contemplate differences in stability, binding affinity, time to response, immobilization conditions, signal to noise ratio or cross reactivity [21]. While the detection of different analytes needs to consider the chemical nature of the target, bearing in mind different solubilities or additives required as well as comparable range of concentrations in the matrix analysed [22].

Furthermore, monoplexeded assays should be well characterized in order to perform adequately under strict regulatory guidelines, meanwhile multiplexed approaches face this characterization at individual and collective format considerably increasing the work needed. For that reason, it is assumed that the complexity results directly proportional to the amount of bioreceptors implemented in the system, considering individual and combined characterization of reagents and admitting possible modifications in the final assay format [23].

Additionally, a second limitation towards an easy implementation of multiplexed platforms is found on the complex signal interpretation. Different transducing systems have become accessible in recent years. Where the binding event mediated by the bioreceptor, generates a measurable signal that can be either directly or indirectly detected and translated into a digital output [24]. While a single receptor provides a unique and specific signal that can be simply monitored, multiple receptors contribute to increase the degree of complexity towards the generation of different signals and computational tools are required to interpret those responses. Despite the advantages of the multiplexed a approaches and their promising potential the need of using bioinformatics to develop appropriate algorithms for reliable interpretation of the data recorded still is contemplated as a barrier for the implementation [25].

Another significant consideration towards the development of mutli-analyte bioreceptor based devices is found on the wide concentration range of different target analytes. Several biological examples have been described were distinct biomarkers or even contaminants differ considerably on their relative abundance across the sample interfering with the detectability of less concentrated analytes. For instance, human serum is a well characterized matrix of analysis were several proteins are found in the range of mg mL^{-1} like albumins, while other components are detectable at ng mL^{-1} or even pg mL^{-1} for cytokines, making their simultaneous detection even more challenging in a single device [26]. The development of multiplexed systems paradoxically depends on the collaborative effort of multi-disciplinary teams in order to promote innovative solutions with feasible applications. Scientists working with engineers, informatics and healthcare specialist or even supported by regulatory authorities trying to tackle urgent necessities among different fields involving diagnostics, food safety and environmental monitoring.

1.3 MULTIPLEXED MICROARRAY PLATFORMS

Unquestionably, one of the most well-established high-throughput techniques for clinical monitoring and diagnostics is the microarray technology. Microarrays are defined as a two-dimensional arrangement of biological elements discreetly deposited in microscopic spots over a solid support. These platforms address the use of different biomolecules like (antibodies, DNA, aptamers, carbohydrates, membrane receptors, enzymes, cells, or molecularly imprinted polymers) over generally glass slides or other solid substrates (e.g., polymer-coated glass, plastics, nitrocellulose) [27].

This concept was introduced by Roger P. Ekins in 1989 for the first time, behind the development of a multi-analyte immunoassay [28], aiming to miniaturize several assays in a single support. The initial steps in microarray developments, were dedicated to explore DNA arrays for the assessment of genetic implications, mRNA transcription and profiling. Major limitations were found on signal analysis and interpretation, together with the lack of correlation between mRNA expression levels and real protein expression. Some years later, protein

microarrays were proposed to detect measurable levels of protein products offering a most accurate and robust response to multi parametric analysis [29].

The recent emergence of research areas dedicated to the large-scale analysis of biological molecules known as “omics” have helped to redefine the use of multiplexed microarray technologies. With the possibility to analyze a complete genome in the field of genomics or to detect a whole set of proteins expressed in a single cell and in more complex organisms with proteomics [30].

1.3.1 NON-PLANAR ARRAY PLATFORMS

Non-planar arrays, also known as bead-based assays, emerged as versatile and powerful tools to enable simultaneous analysis of multiple targets with high sensitivity and throughput in solution. This type of assays makes use of solid beads in a range in of 0.02 to 0.6 μm functionalized with specific capture molecules (oligonucleotides, antibodies, receptors) to selectively bind to the analyte in solution. Capture elements can be either covalently immobilized or adsorbed to the surface of the beads depending on the application [31].

The number of analytes adsorbed on the surface is restricted by the bead size and to the level of immobilization of the bioreceptor. The detection can occur through intrinsic bead characteristics like quantum dots (QD), fluorescent beads, magnetic beads or gold nanoparticles. The coupling chemistry will be associated to the type of bead employed and multiplexation is possible through the association of a bioreceptor to the signal produced of a specific bead property generally associated to the optical detection and size related response [32]. By combining a large number of bead types, several analytes can be monitored simultaneously in a single experiment obtaining fast and reliable results compared with standard ELISA assays [33; 34].

During the last decades several applications have been described making use of bead-assays in proteomics, genomics [35] screening of biomarkers [36], diagnosis and monitoring procedures [37]. In parallel, the improvement over novel bead chemistries, enhanced surface functionalization techniques or

detection methods were critical towards a straightforward integration of these assay formats in microfluidic systems, increasing automation, precise control, sensitivity and repeatability using beads arrays. In this regard, several readout technologies were also explored such as mass spectrometry, fluorescence, and next generation sequencing [38 ; 39].

In an attempt to compare potential features across slide, plate or non-planar-assays, the following graph represents key elements considered during the development of bioanalytical tools. Ranging from precision to multiplexation capacity, including automation, stability and specificity as essential features described along the three types of assays based on literature reports [40].

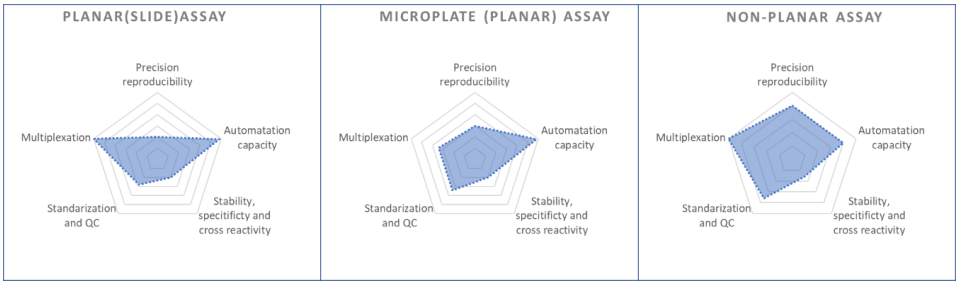

Figure 1.3 Analytical performance comparison between planar, microplate and non-planar-based assays. Adapted from [40].

As evidenced in Figure 1.3, each assay configuration is characterized by a distinctive performance that should be considered before embracing the development of multiplexed bioanalytical platforms. Planar or slide based assays allow high degree of multiplexation as well as automation, while microplate assays provide easier standardization and automation procedures. Finally, bead assays (non-planar) are versatile alternatives mainly increasing precision and multiplexation as well as standardization procedures, but stability and cross reactivity are often a problem.

1.3.2 PLANAR ARRAY PLATFORMS

Across typical microarray platforms a common feature is found on the generation matrices of micro spots (100-400 µm diameter) constituted by

selective probes or ligands (protein/peptide/aptamer/tissue) immobilized onto a solid support and separated by a few microns from each spot even in some cases allowing the arrangement of more than 1.000 spots/cm^2 [41, 42].

In this regard, a clear distinction can be established depending on the class of biomolecules or probes printed over the supporting material. Primarily identifying DNA and protein microarrays as well as alternative biomolecules such as enzymes [43], carbohydrates [44], small molecules [45] or aptamers [46] demonstrating the versatility behind this platform.

1.3.2.1 Optical array detection

Detection methods of planar arrays are mainly optical techniques based on colorimetric, chemiluminescent of fluorescent dyes that bind to DNA molecules, antibodies or receptors and allow their spatial localization over the surface for subsequent quantification. In the case of protein arrays, secondary labelled antibodies or enzymes labelled are used to evidence the binding event and promote a measurable signal. For methods using antibodies and fluorescent readout, the most common approaches include secondary anti IgG's antibodies coupled to fluorophores like TRITC, FITC, Alexa, Cy3 or Cy5. Microarray scanners are equipped with lasers and detectors capable to promote the excitation of respective dyes at specific wavelengths mostly around 450 to 650 nm [47]. Other examples include well plate arrays based on colorimetric detection, exploiting the use of enzymes as reporters (like HRP-conjugated monoclonal antibodies) that in the presence of a chromogenic analyte lead to the precipitation of this compound over the spot, to be quantified in a well plate microarray scanner [48].

1.4 MICROARRAY BASED ON AFFINITY BINDERS

As already mentioned, considering the chemical nature of the immobilized probe, microarrays can be differentiated. In the following section DNA and proteins arrays including antibody arrays will be discussed taking into account

the extended in most of current applications in contrast with the rest of bioreagents (see Figure 1.4).

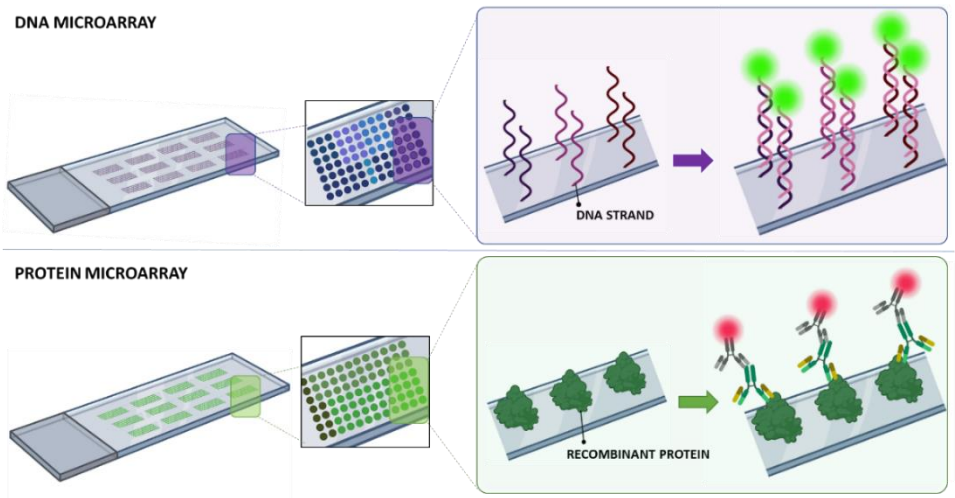

Figure 1.4 Schematic representation of universal DNA and protein microarray platforms combining various oligonucleotide strands or immobilizing recombinant proteins. Complementary oligonucleotides labelled with a fluorophore can be used in DNA arrays detection while secondary labelled antibodies are employed in protein arrays.

1.4.1 PROTEIN MICROARRAYS

Broadly, proteomics aims to understand the complex scene of protein expression profiles generated by a genome to determine the role in the organism. Protein quantification was historically assessed by 2D gel-based approaches. These methods provide differential response in regard of protein levels and physiological conditions. As new challenges require to understand complex protein environments and their interactions, protein microarrays evolved as massive analysis tools. Together with mass spectrometry are current strategies for protein characterization [49].

Principles on DNA and protein microarrays share some similarities but are differed basically by the chemical nature of those biomolecules. For instance, protein stability is more restricted and the biological function rely on the preservation of the three-dimensional structure. Therefore, sample preparation and deposition onto glass slides requires more control than DNA arrays.

Furthermore, protein quantification in multiplexed arrays has been addressed as a major limitation due to the heterogenous concentrations found in the samples as well as the lack of amplification techniques like PCR applied for nucleic acids determination. Nevertheless, protein microarrays have demonstrated great performance in the analysis of protein function and expression [50].

Alternative applications combining nucleic acid programmable protein array (NAPPA) principle were reported, making use cDNA templates to generate high-density and self-assembling protein microarrays [51]. Through this method, more than 1000 cDNA sequences were printed to then transcript, translate and capture a thousand of protein in the surface with significant reproducibility. Besides protein and DNA arrays other biological elements such as cells [52], tissues [53] or carbohydrates have been successfully immobilized under this assay configurations to potentially characterize biomolecular interactions. The wide range of applications derived from the use of a universal platform such as microarrays evidence the versatility towards novel technological approaches.

1.4.1.1 Peptide arrays

Nowadays, peptide arrays have emerged as a promising sub category of array platforms derived from protein arrays. Generally employed towards the identification and analysis of epitope mapping for antibody binding, as well as peptides that regulate cell adhesion, substrate screening for enzymes and profiling enzyme activity. These platforms are constituted by high numbers of peptide sequences arranged onto a solid support to allow simultaneous determinations in a single sample. Amongst the most common limitations, the incompatibility with complex matrixes and frequent false-positive and false-negative rates have been described as the result of differences over immobilization techniques, surface densities or unspecific interactions. On the other hand, in situ synthesis is generally used to create high density arrays at affordable costs and self-assembly monolayers were also implemented to control surface density and avoid unspecific adsorptions [54].

1.4.2 DNA MICROARRAYS

DNA microarrays are generally used to determine gene expression levels. They offer detailed information regarding specific gene regulation allowing comparative analysis of physiological response of the organisms to the environment. The isolated genetic material (DNA or RNA) from the sample is analyzed through PCR and tagged with a fluorescent dye. Later on, samples are incubated over the DNA array and through hybridization, those sequences present in the sample will bind to their counterparts on the array forming a double stranded structure that can be detected. The intensity of each spot is directly related to the amount of nucleic acids attached to the surface, allowing simultaneous assessment of several sequences in parallel [55, 56].

The genetic profile obtained from mRNA analysis is essential to understand how these molecular pathways are linked to an increase or decay in transcript production associated to a biological outcome. Indeed, the central dogma of molecular biology contemplates how DNA is transcribed into RNA that is further translated into functional proteins and microarrays allows some interpretation from these complex tasks. Moreover, protein arrays can be considered as complements of genetic arrays and correlation between both approaches provide a better understanding of molecular processes directing changes in protein levels [57].

1.4.3 ARRAY IMMOBILIZATION STRATEGIES

The immobilization of different biomolecules over distinct surfaces impose a complex task towards the development of planar microarray systems, in order to attach in a covalent or non-covalent format, give specific orientation to the ligands as well as considering surface regeneration conditions. Three major categories can be identified across planar array immobilization as physical, chemical and biological strategies. The first is based on physical adsorption over hydrophobic and positively charged surfaces (nitrocellulose, polylysine, polystyrene) rather than covalent coupling due to inexpensive and simple protocols. However, in most of the cases the biomolecules are randomly

distributed on the surface, leading to loss of activity if the binidng site is blocked or not accessible for the analyte [58].

On the other hand, covalent coupling provides more stable and regenerable conditions but also rely on the surface pretreatment protocols. In fact, different surface chemistries allow the interaction with specific residues naturally found in the biomolecules which usually requires the implementation of crosslinkers [59]. As standard coupling examples, the amino groups (-NH_2) generally present over Lysine residues in proteins or synthesized in different biomolecules, can be covalently attached with carboxylic acid, epoxy, aldehyde and active ester coated surfaces [60]. Alternatively, thiol residues (-SH_2) are commonly coupled to maleimide, vinyl sulfones and pyridyl disulfide derivatized surfaces. Moreover, ligands containing carboxylic acid residues (-COOH) can bind to surfaces coated with amines and hydroxyl groups (-OH) or even epoxy residues [61]. More recent developments exploit click chemistry protocols based on azide or alkyne functional groups to immobilize different probes under controlled conditions [62]. The following Figure 1.5, highlights a standard workflow associated to planar array production, as can be seen surface conditioning is the first step followed by the selection of the corresponding bioreceptor that will be incubated with the sample to finally perform the readout.

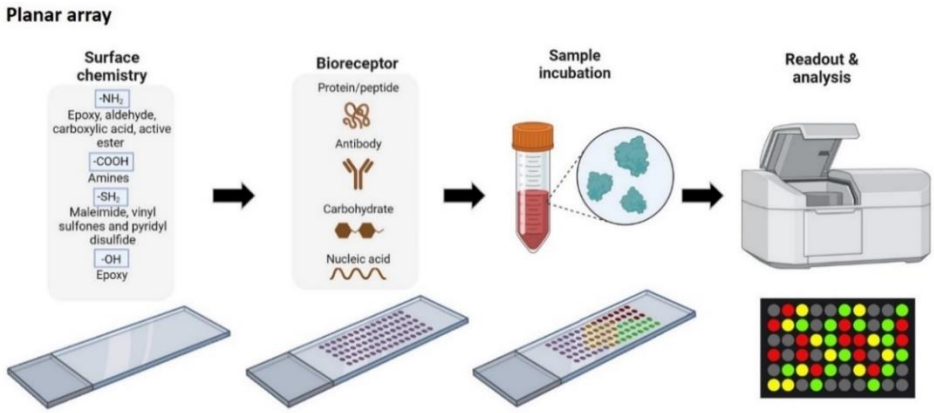

Figure 1.5 Steps involved towards planar microarray platforms development, starting from immobilization conditions determination, to then perform the biofunctionalization in an array format. Followed by sample incubation and data analysis.

1.4.3.1 Affinity protein immobilization

Alternative biofunctionalization strategies include the use of affinity proteins like streptavidin, lectins, protein G or antibodies against the Fc-portions as coating agents offering specific orientation and producing regenerable surfaces. Streptavidin is often immobilized onto microarray through covalent attachment or physical adsorption. This protein acts as a universal linker to capture biotinylated molecules, such as biotinylated DNA, RNA, peptides and proteins. The use of protein G was also implemented in microarray format to capture IgG antibodies from the sample. In addition, Anti-Fc antibodies recognize the Fc portion of immunoglobulins allowing their immobilization with specific orientation and homogenous coating conditions [63]. On the other hand, lectins are a class of glycoproteins with the ability to bind to carbohydrate structures and have been reported as affinity coating elements to capture and detect glycans present on different molecules [64 ; 65].

As previously discussed, the selection of the most adequate surface chemistry will directly influence the spot quality, assay specificity and potential unspecific interactions. The minimum background is expected aiming to maximize signal-to-noise ratio and enhance assay sensitivity. During spot quantification, microarray analysis software generally allows the depletion of background noise surrounding the spot in order to favor the signal detected.

1.4.3.2 DNA directed immobilization

On the other hand, DNA directed immobilization consists on the utilization of oligonucleotide probes, composed of 15 to 40 nucleotides to site encode covalently attached (bio)molecules to a discrete location of the surface. For these means, a “lower” strand is primarily immobilized onto a solid support (glass or gold layer, metal nanoparticle, nitrocellulose strip). Meanwhile, the complementary chain or upper oligonucleotide that was previously conjugated to a specific bioreceptor (antibody, aptamer, enzyme or even small molecules) is incorporated to the system to promote the spontaneous hybridization with the complementary strand functionalized [65].

The original description and potential applications of DDI were proposed by Niemeyer *et al* [66] through the development of multiplexed assay utilizing different pairs of oligonucleotides for distinct ligands incorporated. Moreover, the implementation of DDI also provides specific biomolecules orientation and regenerable surfaces based on hybridization and des-hybridization reaction that, for some applications like SPR sensing, may significantly reduce the cost per analysis. A summary of the main advantages associated to the use of DDI strategies in contrast with standard protein immobilization are described:

High stability: linear oligonucleotides are considered highly stable macromolecules compared to recombinant proteins. In this sense, nucleic acids may withstand more extreme environmental conditions like significant changes in temperature, pH or even long storage periods while proteins structural requirements may lead to easier denaturation.

Homogeneous immobilization: unlike proteins can be extremely diverse regarding chemical structure and biological properties, nucleic acids are relatively homogeneous in terms of structural and electrostatic properties. Because of this reason, manufacturing of DNA microarrays for genomic studies has been well standardized by important companies (Agilent Technologies, Roche, Affymetrix) using different immobilization approaches. With this scenario, DDI allows to make of DNA microarrays, universal platforms to immobilize distinct biomolecules using the same chemical approach, which would facilitate mass-scale production of microarrays with any other molecules.

High multiplexed potential: oligonucleotides offers the possibility to design probes with an almost unlimited diversity of sequences. Combined with the manufacturing DNA microarrays using light-induced in situ solid-phase synthesis [67], it may be possible to manufacture high-density microarray chips of any other molecules different from DNA.

Controlled orientation: Different chemical strategies can be proposed for directed coupling of the upper oligonucleotide to the bioreceptor selected (protein, aptamer, hapten or antibody). Once the lower strand is immobilized through the 3’ or 5’ end, the complementary upper sequence will hybridize

conferring a specific orientation to the biomolecule. Through this method, the active site of the ligand can be easily exposed thus facilitating the interaction with target analytes. Although accurate control of the preparation of ideally 1:1 oligonucleotide tagged proteins is challenging, site-specific labeling strategies have been reported.

Competitive step in solution: In most of protein-based assays, the coating antigen or antibody is coupled to the surface limiting the competitive step to the well. Through, this approach the pre-incubation of the sample containing the analyte, with the bioreceptor conjugated to DNA, allow this step directly in the sample. The probability of interaction increases when the reactants remain in solution, while in some cases repulsive effects or even nonspecific interaction can occur as a result of surface conditions. Afterwards, the ligand with the corresponding analyte are site directed over the complementary sequence for identification [68].

Taking a look back, Niemeyer was pioneer over the implementation of DNA directed immobilization strategies, assessing the use of oligonucleotide strands as templates of protein microarrays. In the first reported approach, streptavidin molecules were conjugated to short nucleic acid sequences to bind biotinylated antibodies translating a DNA array into a protein chip [66]. This precedent was essential for further developments making use of the stability and relatively simple chemistry behind DNA-protein conjugates. Along the literature, different molecules apart from antibodies were successfully coupled like aptamers [69] enzyme reactors [70], glycans [71], small molecules [72], and even whole cells [73]. Furthermore, this technique was utilized under different sensing principles like plasmonic modes decorating nanoparticles [74], electrochemical sensors [75] and functionalizing microarrays [76]. In a step further, DNA nanopatches were created using DNA-directed immobilization and atomic force microscopy nanografting claiming that the implementation at nanoscale will be highly valuable over multiplexed biomolecular recognition developments and single-cell proteomics [77].

1.4.3.3 Conventional printing techniques

In addition to the immobilization strategies, another relevant parameter in the production of planar microarrays rely on the printing technique utilized. The method selected for this purpose, will have direct impact on the quality, density and morphology of spots as well as the duration of the printing process and batch to batch variabilty. Depending on how deposition is performed, several techniques can be identified such as contact printing, non-contact methods, lithography techniques and cell free methods [78]. The first case was described as the initial strategy reported over array developments and consisted on the physical contact between a pin loaded with the target to the supporting material generating a spot. Alternative modes derived from this approach are pin printing or microstamping. Contact printing offers high reproducibility and minimum maintenance, but the major inconvenience is found on the extensive periods required for the printing process, limiting their mass production. Through this method, low-density arrays are preferably obtained and highly viscous fluids are tolerated, while the clean-up procedures for solid pins are simplest than other printing techniques [79].

Innovative solutions have emerged with non-contact printing techniques such as inject printing or piezo-dispense deposition. The main differences are found on the lack of physical contact between the pin and the surface. These methods rely on sophisticated robotics that enable faster, precise and automated array production promoting higher quality of spots and more reproducible deposition. Some of the challenges to still improving include possible interferences from satellite drops or partial denaturization of biological components as well as the costs of the equipment's, that sometimes are not feasible at the level of research laboratories [80]. Additionally, photolithography, laser writing or electron beam belongs to the group of lithographic techniques that uses light (generally UV) to transfer a pattern from a photomask to a photoresist chemical that is light-sensitive on the substrate. Finally, for the development of protein arrays, cell free methods allow the generation and immobilization of protein products obtained from precursor DNA arrays [80]. During microarray fabrication, additional parameters could directly affect the final performance of these platforms if they are not strictly monitored. On one side, humidity, results crucial during spot density, morphology and homogeneity determination. Protein

arrays, generally requires relative humidity between 45-60% while, nucleic acids deposition is recommended at 55 to 65% of humidity to minimize evaporation rates once the droplets are printed [81]. In this regard, undesirable phenomena can occur at spot level like the well described coffee ring effect, as a result of capillary flow pushing the solution from the centre to the border during droplet evaporation leading to higher probe concentrations at the edges of the spot. Hydrophobic surfaces can enhance such effect and therefore well controlled dispensing conditions are required [82].

1.4.4 BIOLOGICAL PROBE CHARACTERISTICS AND SELECTION

Depending on the analyte to be determined and the matrix of interest, the selection and characterization of the biological probe is a crucial step in the development of reliable multiplexed protein immunoassays and microarrays. The type of chemistry selected during immobilization should consider the chemical composition of the ligand and the surface in order to promote covalent or non-covalent interactions. In the following table 1.1, a comparative analysis of probe characteristics and the implementation in microarray platforms is proposed. Antibodies, peptides and oligonucleotides are compared as the most frequently reported probes implemented in planar arrays.

Table 1.1 Characteristic features of standard biological probes in microarray implementation

Features	Antibodies	Oligonucleotides	Peptides
Surface chemistry	Standard (NH_2; SH)	Standard (NH_2; SH)	Standard (NH_2; SH)
Target molecule	small molecules, proteins, peptides, polysaccharides, nucleic acids, virus, bacteria, cells	Complementary strain (RNA, DNA)	Peptide binder (antibody or receptor)
Amplification	No	Yes, thorough PCR	No
Stability	Medium, denaturization out of standard conditions	High, wide range of temperatures and pH's	High, more than proteins
3D structure and size	Required to be functional, size 150kDa	linear (unless aptamers or molecular beacons), between 10 to 50 nt	Linear, or conformational peptides, between 10 to 30 aa size
Regenerable surface	Generally single use, based on binding affinity	Allow regeneration, dehybridiation reaction	Generally single use, possible weaker binder

The use of the most adequate biorecognition element will be essentially defined by the assay configuration, smaple compostion and the target molecule. Therefore, the features discussed in the previous table will be determinant factors in assay performance and should be contrasted before the final selection.

1.5 ANTIBODY BASED MICROARRAYS

Constituting a specific sub-group derived from protein arrays, antibody arrays exploit the use of these selective biorecognition elements for specific analyte determination (a small molecule, protein, microorganisms, toxins, etc) or as target molecules in serological determinations for instance, binding to antigens immobilized onto a solid support (proteins, peptides, microorganisms) [83].

1.5.1 ANTIBODIES AND THEIR USE IN DIAGNOSTIC

Antibodies or immunoglobulins consist on a specific type of glycoproteins generated by lymphoid cells known as B lymphocytes with the ability to bind to an antigenic element promoting its degradation by other immune cells. These selective proteins are distinguished by their functional and physical characteristics into several isotypes like IgG's, IgM's, IgA's or IgE's. From these group, IgG's are the most abundant isotypes in serum reaching almost 80 % of its content. They are characterized by a typical Y shaped structure (150 kDa) constituted by two heavy and two light chains. The target region recognized by the antibody is defined as epitope and the pocket located in the variable fraction of the immunoglobulin interacting with the epitope is known as paratope. The detection of several molecules that naturally elicit an immune response can be achieved with antibodies, although alternative strategies have been developed to generate antibodies against not immunogenic elements like small molecules or short peptide fractions.

Apart from their original purpose as immune mediators, antibodies have been widely implemented in several applications promoting their use as bioreceptors in multiple fields with diagnostics, therapeutics, monitoring and screening purposes. Across the literature, the extensive use of antibodies has demonstrated effective performance towards multiple biomarkers like proteins, bacteria, viruses, nucleic acids and even small molecules. Another relevant aspect is found on the outstanding binding properties behind these biological elements, reaching sensitivities in the order of the nM to pM range [84]. For instance, a remarkable example reports the use of antibodies in a multiplexed chemiluminescent array achieving attomolar sensitivity against different cytokines [85]. On the other hand, nucleic acids and aptamers also present good sensitivities generally around the µM or even pM level, while enzymes are in a comparable range too. Recent progress in molecular biology and diagnostic tools, had led to considerable improvements related to their scalable production and characterization as well as implementation as bioreceptors even by non-expert users.

Some highlights on the history of immunoassays include the development of the ELISA method in 1970 [86] currently consider as a gold standard technique for

protein quantification reaching limits of detectability in the order of pg mL^{-1}, but requiring considerable incubation periods. In order to shorten the time of analysis, costs and trained personnel, lateral flow immunoassays (LFIA) emerged as fasters alternatives offering semi-quantitative information of specific biomarker outside the laboratory with generally less sensitivity than ELISA [87]. In an attempt to reach multiplexed determinations other approaches such as Luminex technology [88] and Quansys™ multiplexed ELISAs [89] were developed making use of these bioreceptos.

Additional applications involving the use of antibodies have been proposed such as, radioimmunoassay's using radioactively labelled molecules and immunohistochemistry to visualize specific antigens in tissues. On the other hand, immunochromatographic methods for selective separation of target analytes as well as chemiluminescent immunoassays (CLIA) requiring chemiluminescent substrates for detection were also generated. While, immunoturbidimetry allowed to evidence antigen-antibody complex formation in solution, also immunosensors coupling antibodies with different transducers serve to distinguish this binding event. Additionally, flow cytometry contributes to cell sorting applications based on labelled antibodies targeting surface cell receptors. Undoubtedly, the versatility behind these biological elements results unquestionable after the wide diversity of applications already discussed [90].

1.5.2 IMMUNOASSAY CONFIGURATIONS

Novel bio-detection systems must harmonize certain requirements in order to succeed in the bioanalytical field, considering smaller sample volumes, shorter time-to-answer response and affordable costs with outstanding detection properties. In light of this complex scenario, immunoassays and immunosensors arise as promising tools to commit to such demand. These biorecognition leaded strategies are based on the extraordinarily specificity of polyclonal (PAb's) and monoclonal antibodies (MAb's) towards particular antigenic structures or epitopes. On one side, PAb's consist on pooled serum immunoglobulins with the ability to recognize multiple epitopes of the same target obtained after repeated immunizations of the animal model, generally rabbits, rodents and chickens. On

the other hand, MAb's are antibodies of a single B lymphocyte clone generated through hybridoma technique targeting a unique epitope [91]

A detailed representation of all possible immunochemical assay configurations is shown in Figure 1.6 using ELISA, as reference platform for this case but applicable also to lateral flow assays, microarray systems and immunosensors too.

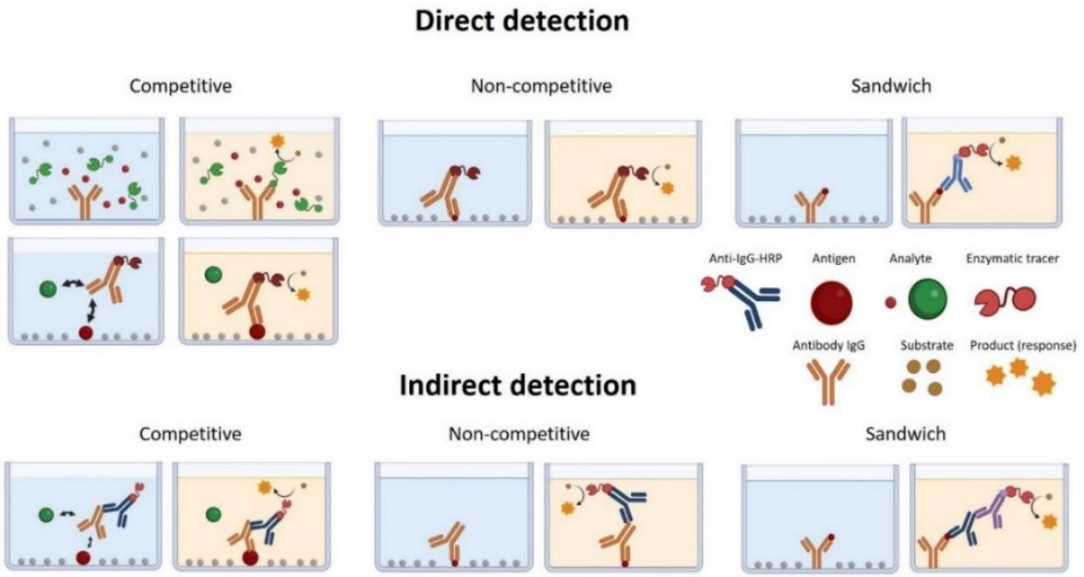

Figure 1.6 Schematic representation of ELISA formats, grouped in direct and indirect detection based on the need of a secondary label for indirect determinations. Competitive format is first represented requiring a competitor antigen either immobilized or in solution competing with the analyte. Then non-competitive formats coat the antigen and measure the amount of antibody bound and sandwich assays require a capture and detection antibody to detect a common analyte by different epitopes.

As can be seen, the distribution of the immunoreagents on the plate and the requirement of secondary labeled molecules acting as reporters during signal acquisition will define the type of assay format. In this regard, a clear distinction is established if the detection is performed in a direct or indirect way. Although, the antibody can be either immobilized in a support or remain free in solution, direct assays make use of an enzymatic tracer conjugated to an analogue target molecule or coupled to the primary antibody to catalyze a colorimetric or chemiluminescent reaction or tagged with a fluorescent dye [92]. This means that the response is directly obtained from the immunoreagents interacting in the binding event. On the other hand, indirect detection occurs when the signal

obtained is not directly acquired from the reagents forming the antigen-antibody complex and a secondary labeled antibody, that binds to the constant fraction of the primary one, is used to generate the measurable signal. Furthermore, depending on the distribution and behavior of the reagents as well as the type of analyte detected, a different classification is utilized to identify the type of assay under the following groups.

1.**Non-competitive format:** This are the simplest type of assay and basically consist on the immobilization of the target or epitopes to estimate the amount of antibodies in the sample. This format applies to serological assays aiming to define the level of antibodies against that molecule of interest.

2.**Competitive format:** consists on the use of a molecule mimicking the analyte that compete with the real analyte in the sample to bind the antibody. This competitor is always added at a fixed concentration allowing the correlation of the changes in the signal to the level of analyte in the sample. In this kind of assays is important to select compounds with similar affinity for the antibody, slightly favoring the displacement of the equilibrium to the formation of the antibody towards the real analyte in order to reach enough sensibility.

3**.Sandwich format:** typically used to detect large target analytes, such as full-length proteins or domains providing the highest specificity among the assays available due to the need of two different antibodies. Initially, a capture antibody is coated over the surface at high concentrations, followed by the addition of the samples and after a washing step, a detection antibody is incorporated targeting a different epitope of the analyte. These assays can be more expensive due to the need of two antibodies against non-related epitopes in contrast with formats that only require one.

The affinity of an antibody for a specific antigen set the basis of any immunochemical analysis. A label is generally required to evidence the immunorecognition event between both species (antigen-antibody) in standard assay.However, a growing number of label-free biosensors have been developed in the last decades, based on distinct real time transducing principles like SPR,

impedance, surface enhanced raman spectroscopy (SERS) or specific grating couplers [93].

Nevertheless, enzymatic tracers like horseradish peroxidase (HRP) or alkaline phosphatase are still among the most commonly utilized labels. These enzymes catalyze colorimetric reactions from chromogenic molecules like tetramethylbenzidine (TMB), that can be quantified with a spectrophotometer. Alternatively, chemiluminescent and fluorescent dyes emerged as excellent labels applied in all kind of immunoassays formats such as microplate-based ELISA, nitrocellulose strips and microarrays offering multiplexing potential due to the variety of dyes available [94]. A relevant aspect behind the use of colorimetric or chemiluminescent enzymatic tracers is found on the signal amplification procedure obtained with the use of this reagents favoring analytical sensitivity.

1.5.2.1 Calibration curve fitting in ligand binding assays

On the other hand, both label-free and labelled immunochemical techniques are typically affected by additional factors such as target size, affinity of reagents or characteristics of the matrix that limit their use in certain assays formats. As already discussed, each type of assay present strengths and limitations but considering the biological and chemical nature of the target analyte, the most suitable approaches can be selected. For instance, in the case of small molecules detection, a sandwich format is not preferred due to lack of two independent and accessible epitopes while a competitive format requiring the use of an analogue molecule at a fixed concentration will allow the determination of the target. In competitive assays, the analyte concentration and the colorimetric signal are inversely correlated (see Figure 1.7). The standard representation of the calibration curve consists in a sigmoidal inhibition curve, produced by plotting the logarithm of the analyte concentration against the signal detected. This curve, which was fitted to a four-parameter equation, will provide the assay's features such as hill slope, limit of detection (LOD) and IC_{50}. The Figure 1.7, indicates a standard ELISA inhibition curve and its fitted equation. Where A_{max} represents maximum absorbance, A_{min} minimum absorbance, and Hillslope: slope of the linear portion of the curve. IC_{50}: half maximal inhibitory

concentration and IC_{90} indicates the amount of a substance that inhibits in a 90% a particular biological activity. The LOD can be estimated by identifying the concentration at which the inhibition percentage reaches 90% on the inhibition curve [95].

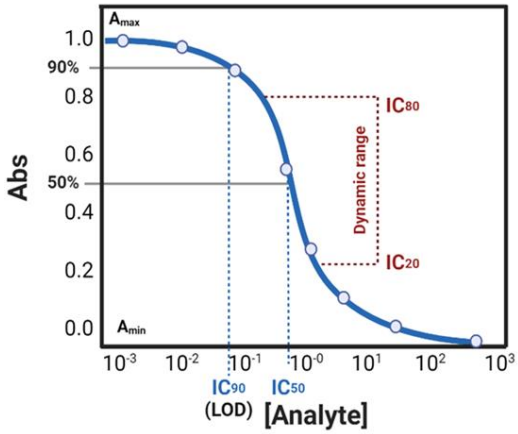

$$f(x) = A_{max} - \frac{(A_{min} - A_{max})}{(1 - \left(\frac{x}{IC_{50}}\right)^{Hillslope}}$$

Figure 1.7 Inhibition curve of the competitive ELISA and its fitted to the following equation. Where IC50: half maximal inhibitory concentration, A_{max}: maximum absorbance, A_{min}: minimum absorbance, hill slope: slope of the linear part of the curve. Adapted from [95].

In order to ensure reproducible performance using antibodies for analytical determinations, additional optimization steps need to be carefully studied. For instance, the influence of different blocking agents, duration of incubation periods, pH conditions, tolerance to organic solvents and temperature can also be determinant factors in the final assay behaviour.

1.5.3 CURRENT SCENARIO IN MULTIPLEXED IMMUNOASSAYS

Throuhg the last 20 years an exponential growth in the number of publications involving multiplexed immunoassays has been observed. This trend can be correlated with the progress in technological areas and bioinformatics incorporating sophisticated robotics to even artificial intelligence in the development of these platforms. Considering the search of “multiplexed

immunoassay" in PubMed repository from 1985 to early 2023, the amount of reports available in this field had shown a remarkable increase.

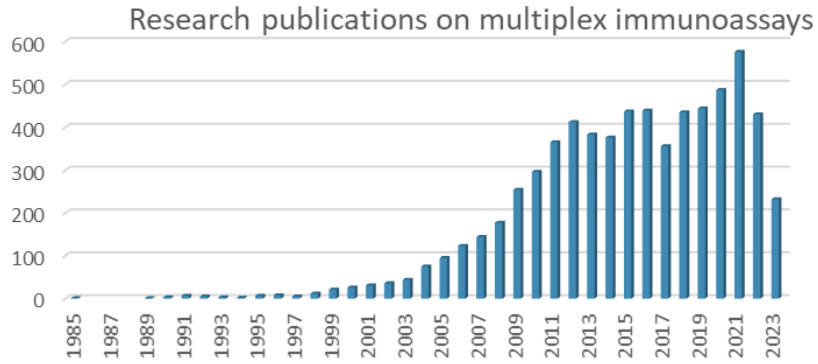

Figure 1.8 Number of publications related to multiplexed immunoassays available in the PubMed database by year (sampling 1985–2023).

Initial descriptions around multiplexed immunoassays started to emerge by late 90's accompanied with the standardization of antibody production techniques (seeFigure 1.8). In 2000's an average of 40 publications per year were registered and only ten years later the productivity was 10-folds higher elucidating the potential around these bioanalytical approaches. Current challenges across multiplexed assays include complex data sets interpretation and analysis aiming to extend their application towards profile-based determinations.

1.5.3.1 Considerations for the development of multiplexed immunoassays

In terms of applications, results essential to guarantee the system intra- and inter-assay repeatability either using commercially available multiplexed platforms or working with in-house developed ones. For the majority of ELISA-based systems, it is possible to assume inter-assay coefficient of variation (CVs) up to a 20 % but generally 10 % is achievable and this expectation should be shared by all tests under multiplex configuration independently. On the other hand, intra-assay CVs should be less than 15 %, and typically 10 %; however, some commercial assays make this assessment difficult since they lack of replicates for each target in the multiplexed matrix (i.e. if only duplicate features

are used for each target). Inter-assay CVs between 2.8 and 10 % are feasible but according to studies comparing bead and planar multiplex immunoassays they rely on the target analyte and the matrix of interest, interfering with the final determination [96].

Focusing on planar multiplexed microarrays development [97], the immobilization area allows unrestricted spot distribution. This is due to the small size of spots and the simplicity with which arrays can be resized depending on the necessities. For each target or control inside the multiplex matrix triplicate, quadruplicate or even higher numbers of repetitions are predominantly used. This goes well beyond the standard ELISA procedure, which involves processing triplicates or occasionally duplicate wells of each sample increasing volumes required and reducing throughput capacity. The following list summarizes specific concerns to keep in mind while using such multiplexed assays considering:

(I) Standardization of the assay design and quality control (calibration curves and quantification limits).

(II) Stability, specificity, matrix effect, and cross-reactivity assessment for all the reagents.

(III) Degree of automation and development of algorithms for row data interpretation.

(IV) Implementation in real matrix, following guidelines available for the corresponding validation [40].

1.5.4 IMMUNOARRAYS FOR MULTIPLEXED PROTEIN MEASUREMENT

Since the original description of a multianalyte ELISA by Ekins [28], high-throughput multiplex immunoassays became significant tools towards the determination of several target molecules in complex biological matrices ranging

from contaminants detection, monitorization of drugs of abuse, discovery of novel biomarkers in cancer or even in diagnostic applications [85, 98, 99]. In this context, main limitations associated to traditional immunoassays are found on the requirement of large sample volumes if multiple analytes need to be determined separately. In an attempt to overcome such difficulties, immunoarray platforms arise as promising candidates offering miniaturized and easy to multiplex formats. Comparably to the already described microarray configurations, multiplexed immunoarrays can be either classified as planar immunoarrays or non-planar (bead) immunoarrays.

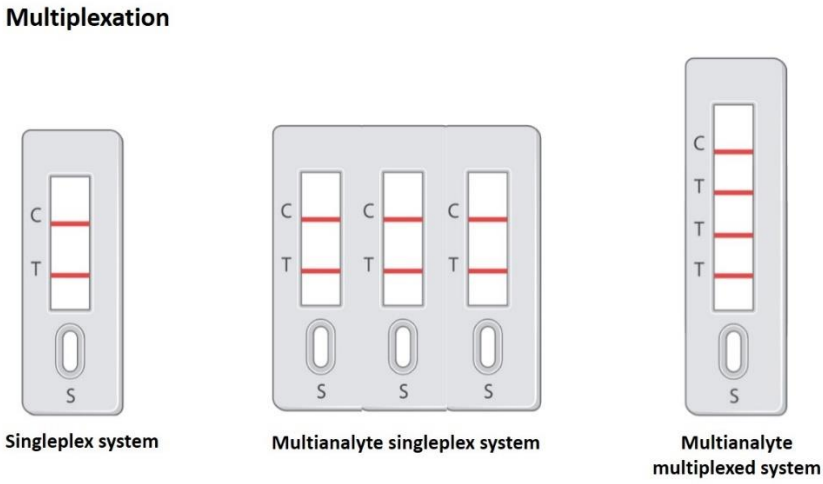

Figure 1.9 Graphical representation of singlepex, multianalyte singleplex and multiplexed platforms. Where, T is referred to the Test line and C as Control line constituting LFIA as model in this case.

On the other hand, a common misconception behind multiplexed platforms definition is described in the previous image. Some authors claim for multiplexed systems when they truly are multianalyte singleplex devices [100]. This general assumption is associated to the possibility to perform simultaneous determinations of more than one analyte in a single platform. However, from a technological perspective, they constitute independent assays and allow simpler optimization compared to real multiplex systems in which all the reagents are confined to the same space [101].

1.5.4.1 Limiting factors in multiplexed antibody-based platforms

Although, emerging multi-analyte detection using microarrays has been considered a cutting-edge research issue in analytical chemistry [102]. A general concern behind antibody-array data is attributed to the intrinsic variability in the results and complex signal interpretation required. Additionally, cross-reactivity also emerge as a potential drawback in this kind of platforms, consisting on the unspecific binding of the antibody towards a different target analyte, which is frequently observed when numerous detection antibodies are combined mainly in sandwich format [103]. As alternative solution, the work performed by Pla-Roca *et al.* described an antibody co-localization microarray (ACM) consisting on the immobilization of the capture antibody with a spotter, followed by the incubation of the chip with the sample to then place it again in the printing system for the specific deposition of the detection antibody showing sensitive and robust response [104].

1.5.4.2 Characterization of the analytical performance

Prior to clinical implementation, the analytical performance of multiplexed immunoassays should be characterized. The proposed criteria to assess those capabilities must include the establishment of limits of detection and quantification, range of linearity, analytical specificity, robustness, precision and accuracy. Moreover, if possible, comparison to the gold standard technique, is required for a complete validation demonstrating the considerable improvement respecting from the already available method. Additionally, the coefficient of variation, used to describe measurement variance, should be calculated using several sample replicates. If possible, intra- and inter-assay variability would be also evaluated to estimate imprecisions attributed to the platform and protocol reproducibility. Immunoassays contain inherent variability, thus is recommendable to test the same sample multiple times during platform characterization. By tweaking the assay or running replicated specimens and averaging the results, these effects can be considerably reduced [31]. Pilot studies could be helpful in figuring out the validity and reliability of tests [105, 106]. Although robustness and reproducibility are necessary in multi-bioanalytical determinations, the lack well-developed quality controls (QC) are

limiting their use [107] and therefore single-analyte quality controls are applied at laboratory levels [31].

Regarding microarray platforms, the lowest theoretical LOD for an array spot was reported to be 1 fg mL^{-1} [108], although such sensitivity is not often easy to achieve due to the intrinsic limitation in the affinity of the biorecognition elements like antibodies and also due to the lack of signal amplification techniques. However, the applications in personalized medicine mostly require low limits of detectability and microarrays for early cancer biomarkers detection have demonstrated successful performance detecting analytes in the range of pg mL^{-1} [109].

1.5.4.1 Multiplex immunoarray platforms in the market

Nowadays, an increasing number of commercial multiplexed immunoassays are available for comparative screening and diagnostic purposes. The imminent necessity to commit to the requirements established by regulatory agencies in different fields (food safety, diagnostic and environmental control) is highlighted expecting to develop competitive tools [102].

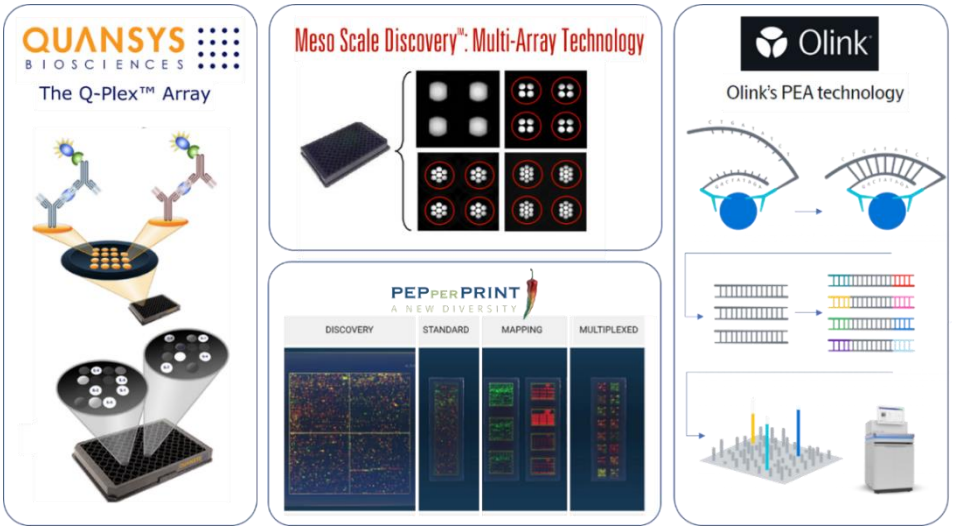

Figure 1.10 Multiplexed systems commercially available. Main technological approaches delivering multiparametric analytical tools for immunodiagnostic applications.

Some of the most relevant multiplexed immunoarray systems found in the market are represented in the previous figure. Such as, Mesoscale Discovery (MSD™) on solid supports presenting multi-array technology that uses electrochemiluminescence and array printing methods for rapid quantification of multiple analytes in a single sample. Then, Quansy´s Biosciences Ltd, with Q-Plex™ ELISA arrays provide quantitative solutions with chemiluminescent multiplexed arrays over ELISA plates against different panel of biomarkers with pre-defined kits or even customizable ones. On the other hand, Arrayit Corp. is well known due to the extensive portfolio of consumables for microarray development and immobilized protein and DNA chips. Focusing on peptide arrays, PEPperPRINT® is recognized for the generation high density peptide arrays used for epitope mapping purposes mainly. More innovative approaches emerged with Olink®'s proximity extension technology combining specificity of antibodies coupled to DNA oligos subsequently amplified by PCR techniques to increase multiplexing capacity and simultaneous determinations of different analytes [110]. Finally, in the case of beads immunoassays commercially available, Luminex® technology had revolutionized multiplexed diagnostic reaching several applications, even in flow cytometry [111]. As exposed, the growing interest for simultaneous analytical determinations in miniaturized and multiparametric systems is evidecend at industrial scale.

1.5.5 FUTURE PERSPECTIVES IN PROTEOMICS AND IN VITRO DIAGNOSTIC:

Most recent proteomics technologies applied in research fields consist on surface enhanced laser desorption/ionization-couple to time of flight mass spectrometry (SELDI-TOF MS), MALDI-TOF and protein array techniques. Expecting to may soon be adopted in clinical laboratories as standard tools for protein analysis some improvements are still required in regard of automation, cost of productions and throughput processing [112]. However, it has been proposed that multiparameter profiling techniques or pattern signatures will play a key role in next generation protein In vitro diagnostic (IVD's) revolutionizing current IVD limitations with the routinely implementation of such technologies in the clinical field [113]. In this sense, probably the most significant developments will be related to big data analysis and signal interpretation.

A wide variety of examples across the literature investigate the advantages of integrate bioinformatic tools with microarray signal handling and acquisition [114]. Deep learning and similar bioinformatic techniques have been effectively used in a number of fields, including the detection of cancer biomarkers mainly [115, 116] or sepsis monitoring [117]. Also, in aging related diseases like Alzheimer's [118] or Parkinson [119] have been addressed with bioinformatic methods to anticipate clinical and irreversible symptoms with considerable accuracy.

In light of this, while larger data sets are generated, novel bioinformatic approaches are required to understand the complexity behind those determinations. Additionally, future microarray developments will be positively influenced by automation capacity not only considering robotics required to generate those microscale arrays but also over readout and signal analysis using computational approaches [120]. Novel proposals aim to combine artificial intelligence to predict disease progression based on early profiles of response against multiple biomarkers [121]. In this regard, the identification of eight different proteins at nM concentration with high efficiency was reported after integrating machine learning techniques with biofunctionalized carbon dots in an array sensor demonstrating the potential improvements resulting from this type of synergy in future developments [122].

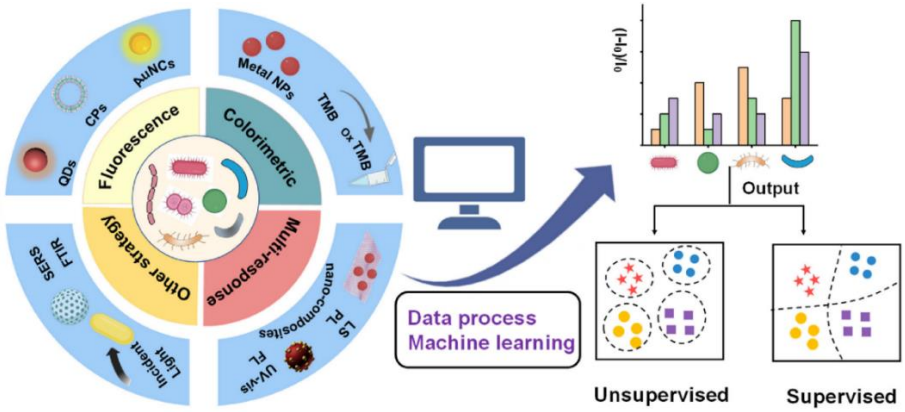

Figure 1.11 Scheme highlighting nanomaterials available for array sensors generation integrating machine learning techniques. Extracted with corresponding permission from [123].

Moreover, a recent literature review summarizes different machine learning algorithms implemented towards the detection of several microorganisms based on optical nanosensor-array data. As the previous Figure 1.11 shows, a variety of strategies are available with nanotechnology (functionalized gold or carbon nanoparticles, quantum dots, chromogenic molecules, nanocomposites) to couple with different optical detection methods (fluorescence, spectroscopy, localized surface plasmon resonance) that after adequate data processing lead to the identification of common features facilitating multiplexed analysis interpretation [123].

1.6 BIOSENSORS

Several attempts to create biochemical approaches integrating particular recognition elements with electronic components have been conducted in the last few years. Apart from microarray platforms, biosensors demonstrated to be highly compatible tools towards multiplexed formats providing miniaturized and easy to use configurations.

Biosensors are considered self-integrated analytical devices constituted by a biological recognition element in close contact with a transducer which converts the biorecognition event into a quantitative or semiquantitative output of a sample composition [124]. The basic configuration of every biosensor should include three essential units. In first place the biorecognition element, which is in direct contact with the target analyte and the sensing surface. Then a transducer, in charge to convert the biological signal produced by the receptor-target interaction into a measurable output value, and finally a read-out system capable to interpret and display the final data. According to IUPAC definition, biosensors are **"***devices that uses specific biochemical reactions mediated by isolated enzymes, immunosystems, tissues, organelles or whole cells to detect chemical compounds usually by electrical, thermal or optical signals*" [125]. Essentially, the biorecognition element is responsible for the specific binding event while different transducers allow the conversion into a measurable quantity through the use of potentiometric, amperometric, conductimetric, impedimetric, optical, acoustic or mechanical interfaces.

1.6.1 TYPES OF BIOSENSORS

Current trends in biosensing approaches look for user friendly, accurate and cost-effective alternatives to complex standard chromatographic techniques for analytical determinations. As consequence, biosensors and immunosensors emerged to potentially monitor the presence of several target analytes across different fields. From the methodological point of view, research in biosensors generally aimed to exploit miniaturized configurations, eliminating the need of sample pretreatments and allowing multiplexation capacity.

A broad classification of biosensors can be established considering the type of bioreceptor or transducer to be implemented. In the first case, catalytic biosensors exploit the catalytical properties of active enzymes. These bioreceptors allows monitoring the formation or inhibition of a product of reaction. According to the response expected for a given target molecule, the amount of analyte can be calculated considering the specific activity of the enzyme [126].

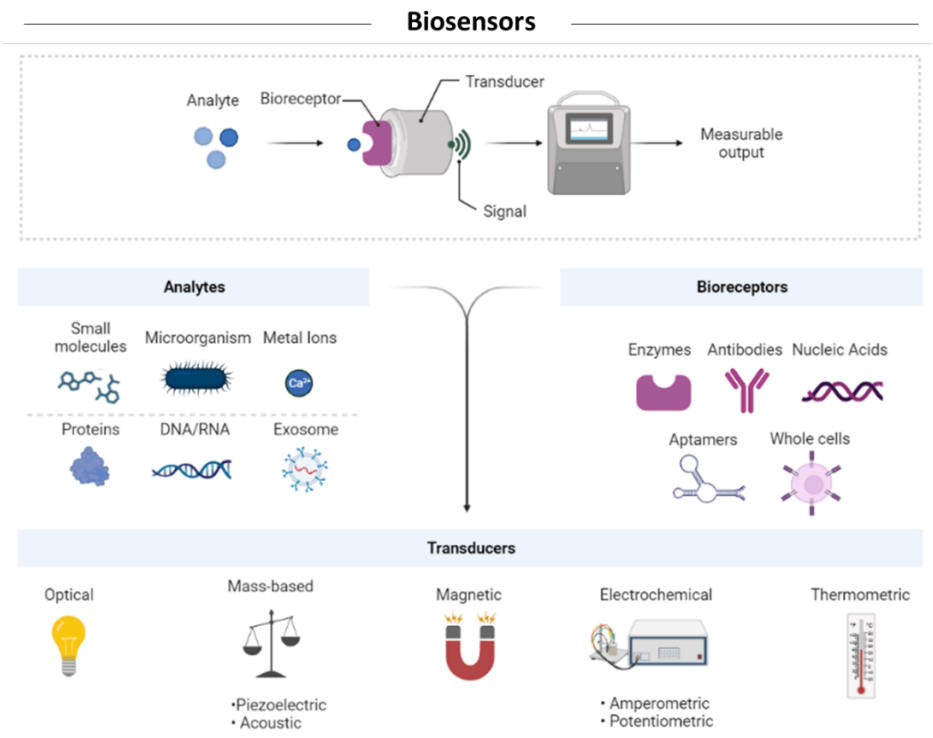

Figure 1.12 General description of biosensors and main components available in the literature including different target analytes, bioreceptors and transducers most commonly used.

Separately, affinity biosensors rely on the interaction of the analyte for the receptor towards the formation of a complex (analyte-receptor) in an equilibrium reaction. These types of receptors include, nucleic acids, proteins, cells, microorganisms and even tissues (see Figure 1.12). Particularly for antibodies, a sub-category along affinity biosensors can be established as immunosensors, characterized by the formation of a complex between the antibody and the antigen that allows analyte detection. Several immunosensor formats can be applied to detect a wide range of analytes including small molecules such as antibiotic residues, pesticides or even toxins [127].

On the other hand, considering the type of transducer utilized, biosensors are classified in:

- **Electrochemical biosensors**, measure electric signal fluctuations as a result of the interaction between the analyte and the receptor in contact with the surface of an electrode [128]. Different electric properties can be monitored like difference in potential, impedance or conductivity. Amperometric measurements rely on the use of redox compounds as makers when using enzymes [129].
- **Piezoelectric biosensors**, allow monitorization of changes in the frequency of a piezo element, provided by the biorecognition event. They include, bulk acoustic wave sensors or crystal quartz microbalances and surface acoustic waves. Also, as part of physical transducers thermometric sensors measure slight changes in temperature generated by the binding between the analyte and bioreceptor [130].
- **Optical biosensors** measure photons, particularly detecting changes in light properties as a consequence of the interaction of these photons with bioreceptors from biological, chemical or physical responses [131]. Some light characteristics generally evaluated in these systems include variations in intensity, wavelength, frequency shifts, decay time, positional changes (angle dependence) and so on. Main optical principles consist in evanescent wave (EW), surface enhanced raman spectroscopy (SERS), fluorescence (i.e. TIRF) , infrared (IR) or even plasmonic (SPR, LSPR) methods. As can be seen, several light properties are available to integrate across portable biosensing systems.

1.6.2 FUNDAMENTALS ON PLASMONIC SENSING

As part of optical sensing principles, the collective oscillation of surface electrons of noble metals surrounded by a dielectric media, give origin to the recognized surface plasmon resonance (SPR) phenomena [132]. The interaction of photons from the incident beam light with the external layer of electrons from the thin metal film, generates an evanescent electromagnetic field highly dependent to variations in refractive index (RI). Fluctuations along this evanescent field will serve to characterize the binding interactions taking place over the sensor surface, detected

from the reflected light under different acquisition modes depending on the SPR configuration.

In this context, nanophotonic emerged to underline the principles behind confined electromagnetic fields as a product of light interaction. Considering the plasmonic behavior, two characteristic modes can be distinguished based on the propagating or either localized nature of the surface plasmon. On one hand, sensors based on propagating SPR over metallic films or gratings, are generated through the excitation on surface electrons in a metal-dielectric interface. The most common coupling modes described to work under such conditions include prism coupling, grating coupling and waveguide coupling methods [133]. In the next Figure 1.13, the principle behind SPR sensing technique is described, after illuminating with polarized light the gold surface through a glass prism to promote the excitation of surface electrons generating the propagating plasmon. Then, the ligands will interact with the analyte in solution changing the RI of the surface resulting in a shift of the reflected light used to monitor real time and label free binding events.

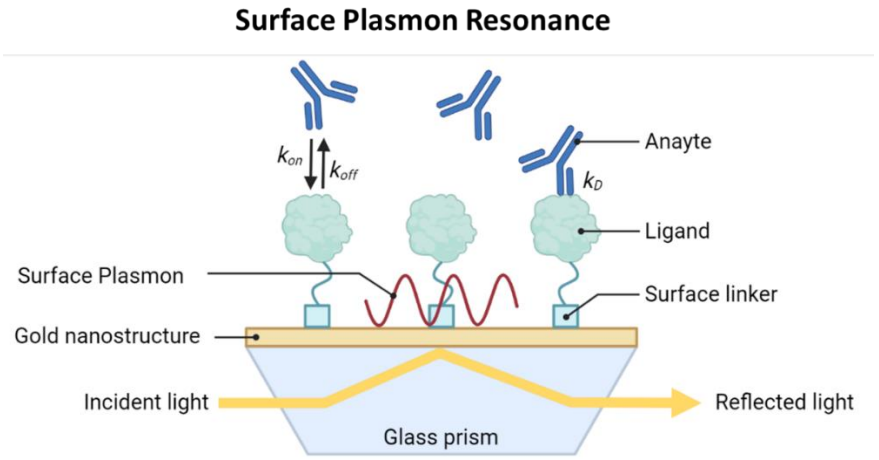

Figure 1.13 Representation of the basic configuration of SPR sensing platform coupling the ligand to the gold surface in contact with the prism to monitor analyte binding in real time through the reflected light.

On the other hand, alternative sensing options utilize metallic nanostructures such as nanoparticles, nanorods or nanostars instead of thin layers working under localized plasmonic conditions and are characterized by a distinctive resonant frequency. This optical effect known as localized surface plasmon resonance (LSPR)

shows increased surface area compared to planar arrangements theoretically enhancing systems sensitivity. The particles used typically range in size from 10 to 100 nm and the absorption spectra results highly dependent of size, composition, shape, and dielectric environment of the nanoparticles facilitating multiplexed configurations [134].

SPR and LSPR sensing approaches are generally described as label free strategies, allowing real time monitoring and potential surface regeneration conditions. In a typical SPR experiment, the immobilization of a ligand (receptor) over the sensing surface (thin layer or nanoparticle) is initially required, followed by the direct incubation (microfluidic chambers or in suspension) with the matrix of interest containing the analyte. The complex formation of ligand and the analyte will induce a change over the sensor surface that can be detected in real time. If the binding event is reversible, a regeneration step can be included to re-use the biosensing surface preserving the biological activity of the ligands covalently attached to the sensor.

1.6.2.1 Kinetic determination using SPR methods

A key feature over plasmonic based platforms is the possibility to asses kinetic characterization of the ligand-analyte interaction. Depending on the association (K_a) and dissociation (K_d) rates defined over the components under evaluation, kinetic studies help to characterize the binding profile between different molecular species establishing stronger and weaker binders as well as faster or lower biorecognition events [135]. For a simple 1:1 interaction, the chemical equation that express this behaviour is represented as follows:

$$\mathbf{A} + \mathbf{B} \underset{K_d}{\overset{K_a}{\rightleftharpoons}} \mathbf{AB}$$

where the components A and B interact to create the AB complex coexisting in equilibrium. The constants k_a and k_d define the association and dissociation rates, respectively.

The following Figure 1.14, describes the principal stages characterizing a typical binding curve. Once the analyte gets in contact with the receptor, the association phase occurs until the system reaches the steady state (equilibrium) over the surface. Afterwards, the analyte addition is restricted (buffer injection) and the dissociation phase takes place to finally perform a regeneration step to remove stronger interactions and re-use the biosensor in a different sample without losing activity.

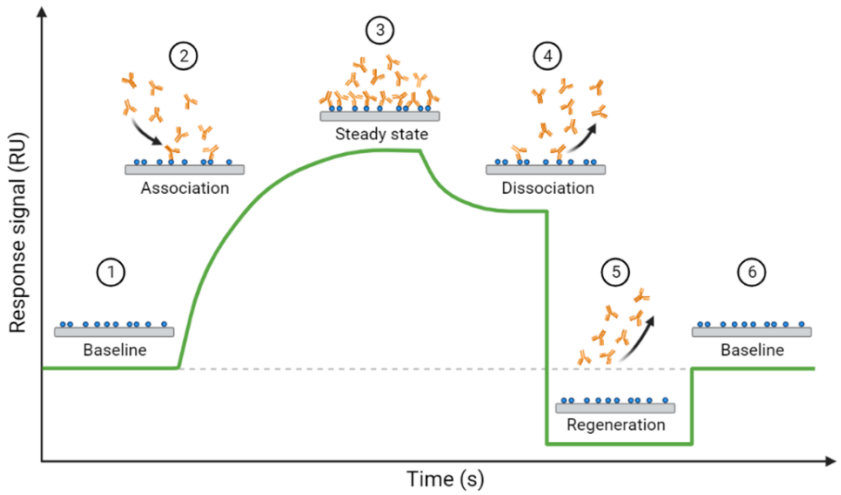

Figure 1.14 Representative view of a standard sensogram. Several steps registered during signal acquisition are detailed (1) Baseline, (2) Association, (3) Steady-state, (4) Dissociation, (5) Regeneration. RU represents resonance units.

The equilibrium dissociation constant (K_D) is the ratio between K_a and K_d, inversely related with the affinity (M^{-1}). The K_D value serve as indicator of the binding strength but do not describe the kinetic behavior of the components evaluated. The greater the interaction, the smaller the KD.

$$K_D = \frac{k_a}{k_d} = \frac{\mathbf{[A][B]}}{\mathbf{[AB]}}$$

Simultaneously, k_a and k_d represent the velocity of association and dissociation phases for a given ligand and target analyte. For this reason, different bio-elements can have the same global K_D meaning similar affinity but different k_a and k_d values indicating distinct kinetic behaviour [135].

Overall, the relevance of plasmonic immunosensors toward more sensitive, label-free, and multiplexed detection systems results promising. Some of the most innovative alternatives are focusing on the integration of these optical principles with smartphone detection due to the relevant compatibility evidenced. With the final aim to extend bioanalytical determinations to non-expert users for multiple purposes in biomedical research, diagnostics, food safety and environmental monitoring.

1.7 BIBLIOGRAPHY

1. Liu, D., et al., *Trends in miniaturized biosensors for point-of-care testing.* TrAC Trends in Analytical Chemistry, 2020. **122**: p. 115701.
2. Cui, F., et al., *Advancing biosensors with machine learning.* ACS sensors, 2020. **5**(11): p. 3346-3364.
3. Naresh, V. and N. Lee, *A review on biosensors and recent development of nanostructured materials-enabled biosensors.* Sensors, 2021. **21**(4): p. 1109.
4. Dkhar, D.S., et al., *Antibody-receptor bioengineering and its implications in designing bioelectronic devices.* International Journal of Biological Macromolecules, 2022.
5. Karunakaran, C., R. Rajkumar, and K. Bhargava, *Introduction to biosensors*, in *Biosensors and bioelectronics*. 2015, Elsevier. p. 1-68.
6. Hempen, C. and U. Karst, *Labeling strategies for bioassays.* Analytical and bioanalytical chemistry, 2006. **384**(3): p. 572-583.
7. Seo, S.E., et al., *Smartphone with optical, physical, and electrochemical nanobiosensors.* Journal of Industrial and Engineering Chemistry, 2019. **77**: p. 1-11.
8. Yokus, M.A., et al., *Wearable multiplexed biosensor system toward continuous monitoring of metabolites.* Biosensors and Bioelectronics, 2020. **153**: p. 112038.
9. Anfossi, L., et al., *Multiplex lateral flow immunoassay: An overview of strategies towards high-throughput point-of-need testing.* Biosensors, 2018. **9**(1): p. 2.
10. Rosa, B.G., et al., *Multiplexed immunosensors for point-of-care diagnostic applications.* Biosensors and Bioelectronics, 2022. **203**: p. 114050.
11. Chen, R. and M. Snyder, *Promise of personalized omics to precision medicine.* Wiley Interdisciplinary Reviews: Systems Biology and Medicine, 2013. **5**(1): p. 73-82.
12. Cheng, M.M.-C., et al., *Nanotechnologies for biomolecular detection and medical diagnostics.* Current opinion in chemical biology, 2006. **10**(1): p. 11-19.
13. Li, S., et al., *Applications of protein microarrays in biomarker discovery for autoimmune diseases.* Frontiers in immunology, 2021. **12**: p. 645632.
14. Yang, L. and J. Wang, *Antibody Arrays: Barcode Technology.* Antibody Arrays: Methods and Protocols, 2021: p. 93-102.
15. Jarockyte, G., et al., *Multiplexed nanobiosensors: current trends in early diagnostics.* Sensors, 2020. **20**(23): p. 6890.
16. Adan, A., et al., *Flow cytometry: basic principles and applications.* Critical reviews in biotechnology, 2017. **37**(2): p. 163-176.
17. Valasek, M.A. and J.J. Repa, *The power of real-time PCR.* Advances in physiology education, 2005. **29**(3): p. 151-159.
18. Zhu, H. and M. Snyder, *Protein arrays and microarrays.* Current opinion in chemical biology, 2001. **5**(1): p. 40-45.
19. Zhou, W., et al., *Aptamer-based biosensors for biomedical diagnostics.* Analyst, 2014. **139**(11): p. 2627-2640.
20. Dincer, C., et al., *Multiplexed point-of-care testing–xPOCT.* Trends in biotechnology, 2017. **35**(8): p. 728-742.

21. Mohd Hanafiah, K., et al., *Development of multiplexed infectious disease lateral flow assays: challenges and opportunities.* Diagnostics, 2017. **7**(3): p. 51.
22. Bollella, P. and E. Katz, *Biosensors—Recent advances and future challenges.* Sensors, 2020. **20**(22): p. 6645.
23. Cohen, L. and D.R. Walt, *Highly sensitive and multiplexed protein measurements.* Chemical reviews, 2018. **119**(1): p. 293-321.
24. Kaur, B., S. Kumar, and B.K. Kaushik, *Recent advancements in optical biosensors for cancer detection.* Biosensors and Bioelectronics, 2022. **197**: p. 113805.
25. Van Herck, Y., et al., *Multiplexed immunohistochemistry and digital pathology as the foundation for next-generation pathology in melanoma: methodological comparison and future clinical applications.* Frontiers in oncology, 2021. **11**: p. 636681.
26. Ray, S., et al., *Proteomic technologies for the identification of disease biomarkers in serum: advances and challenges ahead.* Proteomics, 2011. **11**(11): p. 2139-2161.
27. Aparna, G. and K.K. Tetala, *Recent Progress in Development and Application of DNA, Protein, Peptide, Glycan, Antibody, and Aptamer Microarrays.* Biomolecules, 2023. **13**(4): p. 602.
28. Ekins, R.P., *Multi-analyte immunoassay.* Journal of pharmaceutical and biomedical analysis, 1989. **7**(2): p. 155-168.
29. Call, D.R., *Challenges and opportunities for pathogen detection using DNA microarrays.* Critical reviews in microbiology, 2005. **31**(2): p. 91-99.
30. Song, Y., et al., *Machine learning-based cytokine microarray digital immunoassay analysis.* Biosensors and Bioelectronics, 2021. **180**: p. 113088.
31. Ellington, A.A., et al., *Antibody-Based Protein Multiplex Platforms: Technical and Operational Challenges.* Clinical Chemistry, 2010. **56**(2): p. 186-193.
32. Jia, X.-X., et al., *The role of suspension array technology in rapid detection of foodborne pollutants: Applications and future challenges.* Critical Reviews in Analytical Chemistry, 2022. **52**(6): p. 1408-1421.
33. Tang, D., Y. Cui, and G. Chen, *Nanoparticle-based immunoassays in the biomedical field.* Analyst, 2013. **138**(4): p. 981-990.
34. Elshal, M.F. and J.P. McCoy, *Multiplex bead array assays: performance evaluation and comparison of sensitivity to ELISA.* Methods, 2006. **38**(4): p. 317-323.
35. Bendes, A., et al., *Bead-based assays for validating proteomic profiles in body fluids.* Protein Microarrays for Disease Analysis: Methods and Protocols, 2021: p. 65-78.
36. Kim, B.K., et al., *The multiplex bead array approach to identifying serum biomarkers associated with breast cancer.* Breast Cancer Research, 2009. **11**: p. 1-12.
37. Wang, X., et al., *Nanoparticle-based immunosensors and immunoassays for aflatoxins.* Analytica chimica acta, 2016. **912**: p. 10-23.
38. Zhang, J., et al., *Improving the Accuracy, Robustness, and Dynamic Range of Digital Bead Assays.* Analytical Chemistry, 2023.
39. Van Dijk, E.L., et al., *Ten years of next-generation sequencing technology.* Trends in genetics, 2014. **30**(9): p. 418-426.

40. Tighe, P.J., et al., *ELISA in the multiplex era: potentials and pitfalls.* PROTEOMICS–Clinical Applications, 2015. **9**(3-4): p. 406-422.
41. Bertone, P. and M. Snyder, *Advances in functional protein microarray technology.* The FEBS journal, 2005. **272**(21): p. 5400-5411.
42. Gonzalez-Gonzalez, M., et al., *Nanotechniques in proteomics: protein microarrays and novel detection platforms.* European Journal of Pharmaceutical Sciences, 2012. **45**(4): p. 499-506.
43. Chen, J., et al., *Efficient and sustainable preparation of cinnamic acid flavor esters by immobilized lipase microarray.* LWT, 2023. **173**: p. 114322.
44. Liu, C., et al., *Carbohydrate microarrays fabricated on poly (2-methylacrylic acid)-based substrates for analysis of carbohydrate–protein interactions.* New Journal of Chemistry, 2022. **46**(9): p. 4300-4306.
45. Li, J., et al., *Highly sensitive simultaneous detection of multiple mycotoxins using a protein microarray on a tio2-modified porous silicon surface.* Journal of Agricultural and Food Chemistry, 2020. **69**(1): p. 528-536.
46. Wang, X., et al., *High-throughput aptamer microarrays for fluorescent detection of multiple organophosphorus pesticides in food.* Analytical Chemistry, 2022. **94**(7): p. 3173-3179.
47. Dadfar, S.M.M., et al., *Protein Microarray Immobilization via Epoxide Ring-Opening by Thiol, Amine, and Azide.* Advanced Materials Interfaces, 2021. **8**(10): p. 2002117.
48. Gehring, A., et al., *A high-throughput, precipitating colorimetric sandwich ELISA microarray for shiga toxins.* Toxins, 2014. **6**(6): p. 1855-1872.
49. Templin, M.F., et al., *Protein microarrays: promising tools for proteomic research.* Proteomics, 2003. **3**(11): p. 2155-2166.
50. Kingsmore, S.F., *Multiplexed protein measurement: technologies and applications of protein and antibody arrays.* Nature reviews Drug discovery, 2006. **5**(4): p. 310-321.
51. Ramachandran, N., et al., *Next-generation high-density self-assembling functional protein arrays.* Nature methods, 2008. **5**(6): p. 535-538.
52. Yu, N., et al., *Hierarchical hydrogel microarrays fabricated based on a microfluidic printing platform for high-throughput screening of stem cell lineage specification.* Acta Biomaterialia, 2023. **161**: p. 144-153.
53. Shrestha, S., et al., *Recent advances in microarray 3D bioprinting for high-throughput spheroid and tissue culture and analysis.* Essays in biochemistry, 2021. **65**(3): p. 481-489.
54. Szymczak, L.C., H.-Y. Kuo, and M. Mrksich, *Peptide arrays: development and application.* Analytical chemistry, 2018. **90**(1): p. 266.
55. Kumar, A., S.C. Pandey, and M. Samant, *DNA-based microarray studies in visceral leishmaniasis: identification of biomarkers for diagnostic, prognostic and drug target for treatment.* Acta tropica, 2020. **208**: p. 105512.
56. Bumgarner, R., *Overview of DNA microarrays: types, applications, and their future.* Current protocols in molecular biology, 2013. **101**(1): p. 22.1. 1-22.1. 11.
57. Caplan, M., et al., *Multi-omics reveals mitochondrial metabolism proteins susceptible for drug discovery in AML.* Leukemia, 2022. **36**(5): p. 1296-1305.

58. Rusmini, F., Z. Zhong, and J. Feijen, *Protein immobilization strategies for protein biochips.* Biomacromolecules, 2007. **8**(6): p. 1775-1789.
59. Chiu, S.-K., et al., *Synergistic effects of epoxy-and amine-silanes on microarray DNA immobilization and hybridization.* Biochemical Journal, 2003. **374**(3): p. 625-632.
60. Mateo, C., et al., *Epoxy-amino groups: a new tool for improved immobilization of proteins by the epoxy method.* Biomacromolecules, 2003. **4**(3): p. 772-777.
61. González-González, M., et al., *Evaluation of homo-and hetero-functionally activated glass surfaces for optimized antibody arrays.* Analytical biochemistry, 2014. **450**: p. 37-45.
62. Uszczyńska, B., et al., *Application of click chemistry to the production of DNA microarrays.* Lab on a Chip, 2012. **12**(6): p. 1151-1156.
63. Peluso, P., et al., *Optimizing antibody immobilization strategies for the construction of protein microarrays.* Analytical biochemistry, 2003. **312**(2): p. 113-124.
64. Hirabayashi, J., et al., *Lectin microarrays: concept, principle and applications.* Chemical Society Reviews, 2013. **42**(10): p. 4443-4458.
65. Meyer, R., et al., *Advances in DNA-directed immobilization.* Current Opinion in Chemical Biology, 2014. **18**: p. 8-15.
66. Niemeyer, C.M., et al., *Oligonucleotide-directed self-assembly of proteins: semisynthetic DNA—streptavidin hybrid molecules as connectors for the generation of macroscopic arrays and the construction of supramolecular bioconjugates.* Nucleic Acids Research, 1994. **22**(25): p. 5530-5539.
67. Sack, M., et al., *Express photolithographic DNA microarray synthesis with optimized chemistry and high-efficiency photolabile groups.* Journal of Nanobiotechnology, 2016. **14**(1): p. 1-13.
68. Ng, J.K., et al., *Spatially addressable protein array: ssDNA-directed assembly for antibody microarray.* Electrophoresis, 2007. **28**(24): p. 4638-4644.
69. Yang, Z., et al., *Community sewage sensors towards evaluation of drug use trends: detection of cocaine in wastewater with DNA-directed immobilization aptamer sensors.* Scientific reports, 2016. **6**(1): p. 21024.
70. Li, M., et al., *Controllable and high-performance immobilized enzyme reactor: DNA-directed immobilization of multienzyme in polyamidoamine dendrimer-functionalized capillaries.* Electrophoresis, 2020. **41**(5-6): p. 335-344.
71. Chevolot, Y., et al., *DNA directed immobilization glycocluster array: applications and perspectives.* Current opinion in chemical biology, 2014. **18**: p. 46-54.
72. Zuo, P. and B.-C. Ye, *A novel immobilization strategy using oligonucleotide as linker for small molecule microarrays construction.* Biosensors and Bioelectronics, 2008. **23**(11): p. 1694-1700.
73. Schroeder, H., et al., *Generation of Live-Cell Microarrays by Means of DNA-Directed Immobilization of Specific Cell-Surface Ligands.* Angewandte Chemie International Edition, 2007. **46**(22): p. 4180-4183.
74. Alsadig, A., et al., *DNA-Directed Protein Anchoring on Oligo/Alkanethiol-Coated Gold Nanoparticles: A Versatile Platform for Biosensing Applications.* Nanomaterials, 2022. **13**(1): p. 78.

75. Fruk, L., et al., *DNA-Directed Immobilization of Horseradish Peroxidase–DNA Conjugates on Microelectrode Arrays: Towards Electrochemical Screening of Enzyme Libraries.* Chemistry–A European Journal, 2007. **13**(18): p. 5223-5231.
76. Brambilla, D., L. Sola, and M. Chiari, *Advantageous antibody microarray fabrication through DNA-directed immobilization: A step toward use of extracellular vesicles in diagnostics.* Talanta, 2021. **222**: p. 121542.
77. Bano, F., et al., *Toward multiprotein nanoarrays using nanografting and DNA directed immobilization of proteins.* Nano letters, 2009. **9**(7): p. 2614-2618.
78. Fuentes, M., P. Díez, and J. Casado-Vela, *Nanotechnology in the fabrication of protein microarrays.* Microarray Technology: Methods and Applications, 2016: p. 197-208.
79. Barbulovic-Nad, I., et al., *Bio-microarray fabrication techniques—A review.* Critical reviews in biotechnology, 2006. **26**(4): p. 237-259.
80. Romanov, V., et al., *A critical comparison of protein microarray fabrication technologies.* Analyst, 2014. **139**(6): p. 1303-1326.
81. Mujawar, L.H., et al., *Influence of the relative humidity on the morphology of inkjet printed spots of IgG on a non-porous substrate.* RSC advances, 2014. **4**(37): p. 19380-19388.
82. Yang, M., et al., *The application of coffee-ring effect in analytical chemistry.* TrAC Trends in Analytical Chemistry, 2022: p. 116752.
83. Levy, S., et al., *FLU-LISA (fluorescence-linked immunosorbent assay): high-throughput antibody profiling using antigen microarrays.* Immunology and Cell Biology, 2023. **101**(3): p. 231-248.
84. Peltomaa, R., et al., *Recombinant antibodies and their use for food immunoanalysis.* Analytical and Bioanalytical Chemistry, 2022. **414**(1): p. 193-217.
85. Tobos, C.I., et al., *Customizable multiplex antibody array immunoassays with attomolar sensitivities.* Analytical chemistry, 2020. **92**(7): p. 5613-5619.
86. Hosseini, S., et al., *Fundamentals and history of ELISA: The evolution of the immunoassays until invention of ELISA*, in *Enzyme-linked Immunosorbent Assay (ELISA)*. 2018, Springer. p. 1-18.
87. Koczula, K.M. and A. Gallotta, *Lateral flow assays.* Essays in biochemistry, 2016. **60**(1): p. 111-120.
88. Wang, K., et al., *Validation and comparison of luminex multiplex cytokine analysis kits with ELISA: determinations of a panel of nine cytokines in clinical sample culture supernatants.* Journal of reproductive immunology, 2005. **66**(2): p. 175-191.
89. Rosser, C.J., et al., *Simultaneous multi-analyte urinary protein assay for bladder cancer detection.* BMC biotechnology, 2014. **14**(1): p. 1-6.
90. Vashist, S.K. and J.H. Luong, *Immunoassays: an overview.* Handbook of Immunoassay Technologies, 2018: p. 1-18.
91. Bayer, V. *An overview of monoclonal antibodies*. in *Seminars in oncology nursing*. 2019. Elsevier.
92. Grandke, J., et al., *Quality assurance in immunoassay performance—comparison of different enzyme immunoassays for the determination of caffeine*

in consumer products. Analytical and bioanalytical chemistry, 2013. **405**: p. 1601-1611.
93. Samuel, V.R. and K.J. Rao, *A review on label free biosensors.* Biosensors and Bioelectronics: X, 2022: p. 100216.
94. Fu, L., et al., *Fluorescence-based quantitative platform for ultrasensitive food allergen detection: From immunoassays to DNA sensors.* Comprehensive Reviews in Food Science and Food Safety, 2020. **19**(6): p. 3343-3364.
95. Van Emon, J.M., *Immunoassay and other bioanalytical techniques*. 2016: CRC Press.
96. Findlay, J.W., et al., *Validation of immunoassays for bioanalysis: a pharmaceutical industry perspective.* Journal of pharmaceutical and biomedical analysis, 2000. **21**(6): p. 1249-1273.
97. Angenendt, P., et al., *Toward optimized antibody microarrays: a comparison of current microarray support materials.* Analytical biochemistry, 2002. **309**(2): p. 253-260.
98. Marin, S.J., M. Merrell, and G.A. McMillin, *Drugs of abuse detection in meconium: a comparison between ELISA and biochip microarray.* Journal of analytical toxicology, 2011. **35**(1): p. 40-45.
99. He, X.-P., et al., *Multiplexed photoluminescent sensors: towards improved disease diagnostics.* Chemical Society Reviews, 2017. **46**(22): p. 6687-6696.
100. Fenton, E.M., et al., *Multiplex lateral-flow test strips fabricated by two-dimensional shaping.* ACS applied materials & interfaces, 2009. **1**(1): p. 124-129.
101. Peng, J., et al., *Multiplex lateral flow immunoassay for five antibiotics detection based on gold nanoparticle aggregations.* RSC advances, 2016. **6**(10): p. 7798-7805.
102. Jones, A., et al., *Multiplexed immunosensors and immunoarrays.* Analytical chemistry, 2019. **92**(1): p. 345-362.
103. Juncker, D., et al., *Cross-reactivity in antibody microarrays and multiplexed sandwich assays: shedding light on the dark side of multiplexing.* Current opinion in chemical biology, 2014. **18**: p. 29-37.
104. Pla-Roca, M., et al., *Antibody colocalization microarray: a scalable technology for multiplex protein analysis in complex samples.* Molecular & Cellular Proteomics, 2012. **11**(4).
105. Liew, M., et al., *Validating a custom multiplex ELISA against individual commercial immunoassays using clinical samples.* Biotechniques, 2007. **42**(3): p. 327-333.
106. Urbanowska, T., et al., *Protein microarray platform for the multiplex analysis of biomarkers in human sera.* Journal of immunological methods, 2006. **316**(1-2): p. 1-7.
107. Kricka, L.J. and S.R. Master, *Validation and quality control of protein microarray-based analytical methods.* Molecular biotechnology, 2008. **38**(1): p. 19-31.
108. Lee, Y., et al., *ProteoChip: A highly sensitive protein microarray prepared by a novel method of protein immobilization for application of protein-protein interaction studies.* Proteomics, 2003. **3**(12): p. 2289-2304.
109. Wu, D., et al., *Serum biomarker panels for the diagnosis of gastric cancer.* Cancer medicine, 2019. **8**(4): p. 1576-1583.

110. Assarsson, E., et al., *Homogenous 96-plex PEA immunoassay exhibiting high sensitivity, specificity, and excellent scalability.* PloS one, 2014. **9**(4): p. e95192.
111. Tait, B.D., et al., *Luminex technology for HLA antibody detection in organ transplantation.* Nephrology, 2009. **14**(2): p. 247-254.
112. Ortea, I., G. O'Connor, and A. Maquet, *Review on proteomics for food authentication.* Proteomics for Food Authentication, 2020: p. 3-36.
113. Syu, G.-D., J. Dunn, and H. Zhu, *Developments and applications of functional protein microarrays.* Molecular & Cellular Proteomics, 2020. **19**(6): p. 916-927.
114. Mahendran, N., et al., *Machine learning based computational gene selection models: a survey, performance evaluation, open issues, and future research directions.* Frontiers in genetics, 2020. **11**: p. 603808.
115. Shah, S.H., et al., *Optimized gene selection and classification of cancer from microarray gene expression data using deep learning.* Neural Computing and Applications, 2020: p. 1-12.
116. Basavegowda, H.S. and G. Dagnew, *Deep learning approach for microarray cancer data classification.* CAAI Transactions on Intelligence Technology, 2020. **5**(1): p. 22-33.
117. Schaack, D., M.A. Weigand, and F. Uhle, *Comparison of machine-learning methodologies for accurate diagnosis of sepsis using microarray gene expression data.* PloS one, 2021. **16**(5): p. e0251800.
118. Zafeiris, D., S. Rutella, and G.R. Ball, *An artificial neural network integrated pipeline for biomarker discovery using Alzheimer's disease as a case study.* Computational and Structural Biotechnology Journal, 2018. **16**: p. 77-87.
119. Zhang, J., et al., *Diagnostic AI Modeling and Pseudo Time Series Profiling of AD and PD Based on Individualized Serum Proteome Data.* Frontiers in Bioinformatics, 2021. **1**: p. 764497.
120. Balakrishnan, K. and R. Dhanalakshmi, *Feature selection techniques for microarray datasets: a comprehensive review, taxonomy, and future directions.* Frontiers of Information Technology & Electronic Engineering, 2022. **23**(10): p. 1451-1478.
121. Zhu, J.S., et al., *Deep-learning artificial intelligence analysis of clinical variables predicts mortality in COVID-19 patients.* Journal of the American College of Emergency Physicians Open, 2020. **1**(6): p. 1364-1373.
122. Pandit, S., et al., *Machine learning-assisted array-based biomolecular sensing using surface-functionalized carbon dots.* ACS sensors, 2019. **4**(10): p. 2730-2737.
123. Yang, J., et al., *Machine learning-assisted optical nano-sensor arrays in microorganism analysis.* TrAC Trends in Analytical Chemistry, 2023: p. 116945.
124. Huang, C.-W., et al., *A review of biosensor for environmental monitoring: principle, application, and corresponding achievement of sustainable development goals.* Bioengineered, 2023. **14**(1): p. 58-80.
125. Nagel, B., H. Dellweg, and L. Gierasch, *Glossary for chemists of terms used in biotechnology (IUPAC Recommendations 1992).* Pure and Applied Chemistry, 1992. **64**(1): p. 143-168.
126. Wu, Y., D.C. Darland, and J.X. Zhao, *Nanozymes—Hitting the biosensing "target".* Sensors, 2021. **21**(15): p. 5201.

127. Mathai, T., et al., *Portable biosensor for the detection of Enrofloxacin and Ciprofloxacin antibiotic residues in food, body fluids, environmental and wastewater samples.* Biosensors and Bioelectronics, 2023: p. 115478.
128. Cotchim, S., et al., *Multiplexed label-free electrochemical immunosensor for breast cancer precision medicine.* Analytica Chimica Acta, 2020. **1130**: p. 60-71.
129. Ranjan, P., et al., *Rapid diagnosis of SARS-CoV-2 using potential point-of-care electrochemical immunosensor: Toward the future prospects.* International Reviews of Immunology, 2021. **40**(1-2): p. 126-142.
130. Narita, F., et al., *A review of piezoelectric and magnetostrictive biosensor materials for detection of COVID-19 and other viruses.* Advanced Materials, 2021. **33**(1): p. 2005448.
131. Singh, A.K., et al., *Optical biosensors: A decade in review.* Alexandria Engineering Journal, 2023. **67**: p. 673-691.
132. Homola, J., *Present and future of surface plasmon resonance biosensors.* Analytical and bioanalytical chemistry, 2003. **377**: p. 528-539.
133. Uniyal, A., et al., *Recent advances in optical biosensors for sensing applications: a review.* Plasmonics, 2023. **18**(2): p. 735-750.
134. Kim, D.M., et al., *Biosensing applications using nanostructure-based localized surface plasmon resonance sensors.* Sensors, 2021. **21**(9): p. 3191.
135. Capelli, D., V. Scognamiglio, and R. Montanari, *Surface plasmon resonance technology: Recent advances, applications and experimental cases.* TrAC Trends in Analytical Chemistry, 2023: p. 117079.

2 CONTEXT SCENARIO, OBJECTIVES AND THESIS STRUCTURE

THESIS FRAMEWORK

The present doctoral thesis has been developed within the framework of two different research projects:

FoodSmartphone Project

The FoodSmartphone (H2020-MSCA-ITN2016-720325): proposes the development of smartphone-based (bio)analytical sensing and diagnostics tools for simplified on-site rapid pre-screening of food quality and safety parameters and wireless data transfer to servers of relevant stakeholders. The network involved comprises 7 Training Sites, 2 partner organizations and 11 PhD candidates working on different subjects to deliver, through high level training, (bio)analytical solutions into a common supra-disciplinary goal in food safety. Specifically, this thesis is enclosed in the subproject entitled "DNA addressable arrays for multiplexed ligand binding assays with optical smartphone readout", focusing on the development of a rapid screening tool for the multiplexed detection of antibiotic residues in cow's milk samples. Web page: www.foodsmartphone.eu

PoC4Cov project

The PoC4CoV project was granted during the initial period of the COVID-19 pandemic with the aim to develop Point-of-Care (POC) devices for the rapid and inexpensive *in vitro* diagnosis of SARS-COV-2 infection making use of already available technological approaches to reach immediate application. In this regard, the main scope was focused on combine PoC diagnostic platforms (optical and electrochemical) with specific and selective capture biomolecules and nanoprobes (enzyme bioconjugates, oligonucleotides, peptides and bifunctional plasmonic and magnetic nanoparticles), allowing the simultaneous determination of different biomarkers (viral RNA and antigens, IgM and IgG levels) related to COVID-19 disease. Particularly, in the context of this thesis,

main interest was focused on the development of a multi-epitope serological array including rationally designed peptides and selected viral proteins towards IgG and IgM determination in human serum samples. (CSIC Ayudas Extraordinarias a proyectos de Investigación del COVID-19, Ref CSIC-COV19-041).

GENERAL THESIS OBJECTIVES

The general objective of this thesis has been to investigate the use of high-throughput immunoarray platforms aiming to offer versatile bioanalytical solutions in the context of food safety screening applications and immunodiagnostics for respiratory infections. The specific objectives associated to each research project will be described at the end of the sections identified as PART I and PART II respectively.

THESIS STRUCTURE

The present thesis is structured following the scheme presented in the figure 2.1. The state of the art related to the development and use of multiplexed microarray diagnostic platforms (Chapter 1) is followed by the description of the framework of the research work performed in the PhD thesis, the general objectives (Chapter 2). Because the two different scenarios to which the multiplexed technologies are addressed, the thesis has been divided in two parts. Every experimental chapter contains an independent material and methods section.

PART I is dedicated to the food safety context. It describes the research performed towards the implementation of multiplexed bioanalytical technologies coupled to smartphones for the determination of antibiotic residues in milk. Each chapter is organized according to the logic evolution of the research performed, starting from the immunoreagents characterization (Chapter 3), followed by their implementation in a multiplexed microarray format using DNA directed immobilization DDI (Chapter 4), to finally explore the potential application in a portable iSPR platform integrating smartphone detection as proof of concept (Chapter 5).

PART II provides a wide overview of SARS-CoV-2 emergence, focused on the role of the host immunological response during infection as well as the state of the art regarding serodiagnostic platforms. After the general introduction two experimental sections are chronologically presented. The development of a first version of the *immuno*-µSARS2 chip V1.0 at an early phase of the pandemic with only a limited number of peptides (10 sequences) is initially described (Chapter 6), followed by the description of the research performed towards the consecution of the the immunoarray chip version 2.0, including new viral epitopes and integrating biostatistical tools for data analysis defining system accuracy, as well as predictive capacity towards clinical outcomes.

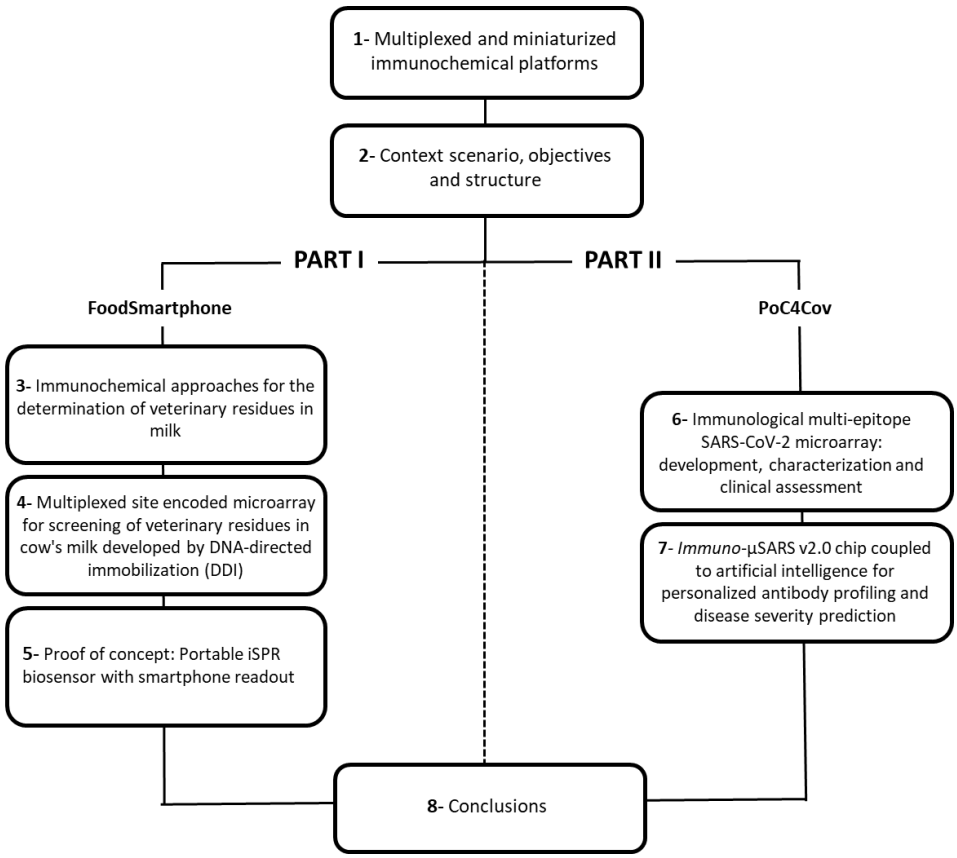

Figure 2.1 Schematic representation of chapter distribution through the thesis.

PART I: CURRENT SCENARIO IN FOOD SAFETY TARGETING VETERINARY RESIDUES IN MILK

I. FOODSAFETY CONTEXT AND DAILY IMPLICATIONS

Food is an essential component in animal's daily life and every human being should have access to safe food worldwide in order to guarantee one of the basic needs established by the WHO [1]. The way we obtain nutrients from food defines an important aspect of our health, and food safety is strictly related to the promotion of a healthy lifestyle. Consuming food that do not accomplish preventative or safety measures, can impose high risk for consumers at different levels like planting, harvesting, packaging, cooking and storing food [2]. Many variables may affect the way we eat, the type of food we like or even the food products available in our nearby markets depending on the geographical region, culture, economical possibilities and also dietary restrictions.

Nevertheless, the safety behind food products consumption must be ensured by the competent authorities and food producers in charge of this essential duty. While there are disparities in food access across the globe, concerns about the safety of different food products also need to be taken into consideration. Besides providing nutrition and satisfaction, food also serves as a means of spreading potential hazards, illness and even death if proper controls are not applied along the food chain. Perhaps one of the most imperceptible diseases facing humanity today are food-borne illness or food related diseases and infections, while on the other hand, food related disorders like obesity, malnutrition, diabetes, anorexia, allergies can also contribute significantly to lower economic productivity [3].

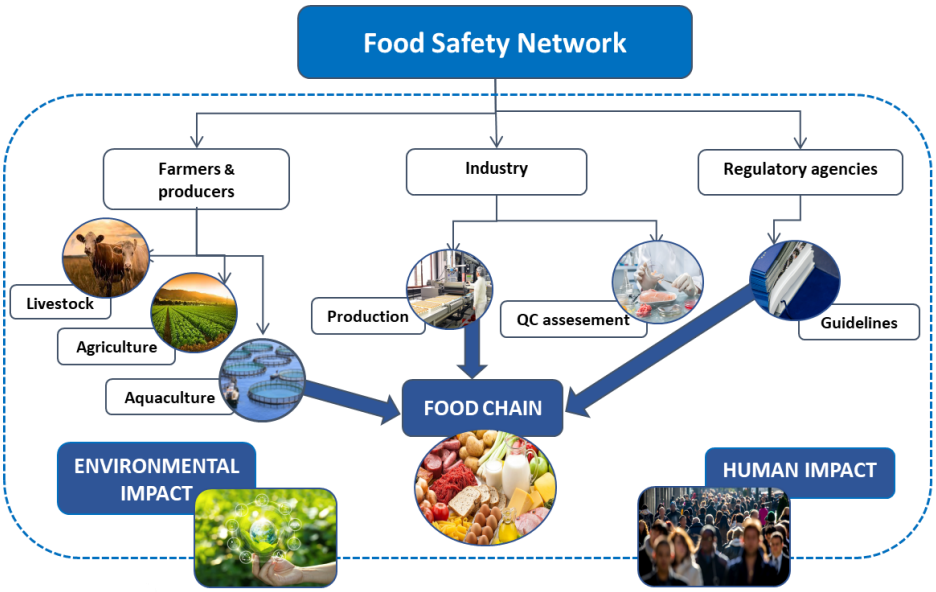

Figure I.I Schematic representation including different stakeholders involved in the food safety network. Including farmers and producers, industry and regulatory agencies. The role assumed by each part will have a direct impact in the environment and society.

A complex environment give origin to the food safety network, as expressed in the previous scheme, farmers and producers as well as the industry or regulatory agencies play essential roles among the food chain as we know it today. The contribution of each sector will have a direct impact on the environment and the society afterwards. Therefore, the emergence of versatile solutions to facilitate the work at each level is highly required.

In agreement with the WHO, more than 200 different diseases, ranging from diarrhoea to more severe pathologies, can be attributed to contaminated food containing dangerous bacteria, viruses, parasites or hazard chemicals. Every year, almost 600 million individuals, or what is equivalent 1 in 10 people, are affected after consuming unsafe food, leading to more than 420 000 deaths worldwide [4]. From an economical perspective, food safety plays a pivotal role in terms of preventing medical care and promoting sustainable production. It is estimated that contaminated food causes 110 billion dollars in annual productivity losses and medical costs in low- and middle-income nations. Therefore, its implementation and regulation result mandatory to prevent health problems at consumers level and also avoid economical losses [5].

II. REGULATORY AFFAIRS IN FOOD SECURITY ACROSS EUROPE

Every country is responsible of the food quality and safety for their consumers according to the guidelines adopted by competent organisms. Even though, the WHO aims to promote inclusive actions to mitigate possible causes affecting food safety worldwide, a substantial effort to unify these criteria is needed. Therefore, the local authorities must ensure the correct implementation at regulatory and monitoring scale. The legal framework in food safety regulations around EU is underlined by articles 168 TFEU (ex Article 152 EC) related to public health and 169 in charge of consumer protection mainly on the European Commission. All regulations and legal updates are regularly published by respective organisms responding to emerging risks and giving the alarm under threatening conditions [6].

Consumer protection should be one of the biggest concerns over food safety policies establishment. The term "from farm to fork" was adopted by EU authorities with the idea of include all the stakeholders involved in the food chain production, considering EU laws, guidelines and regulations which applies to the "one health" philosophy. This last proposal aims to conceive human health as a result of the balanced integration of environmental factors, animal welfare, food safety and many others aspects as equal partners promoting a globalized one human health. At the same time, it is assumed that each of these areas requires continuous monitorization to anticipate potential health threats in the near future to take preventive actions [7]. However, the food safety topic encompasses several steps involved in the process to guarantee its effective implementation such as primary manufacturing, ensuring hygienic conditions during food processing, packaging, labelling and consider official regulations making the scenario even more complex to oversee.

Aiming to guarantee secure food production, animal welfare, plant health and to prevent contamination from external agents like pesticides, antibiotics or toxins, the EU has adopted a number of different criteria. Every step in the food safety chain is rigorously controlled and even imported food must adhere to the same standards and undergo the same inspections as food produced in the EU territory.

III. RISK ASSESSMENT FOR DISTINCT FOOD CONTAMINANTS

Several hazards related to food integrity are annually reported around the globe and particularly in Europe. In this regard, four main categories can be distinguished to classify the causing agents giving origin to the most common food risks:

In first place, microbiological hazards emerge as food illnesses related threats, including microorganisms like bacteria, fungi, viruses and yeast as potential agents contaminating food. If hygiene and sanitation controls as well as questionable handling or packaging conditions are not adequately performed, the emergence of some of these microorganisms results inevitable. In fact, the best way to reduce microbiological threats rely on good consumer practices like washing and cocking fruits, vegetables and meat or paying attention to expiration and correct preservation conditions. Another relevant food risk is associated to chemical hazards. This category considers potentially harmful substances like pesticides, veterinary residues, toxins, biocides and even food additives. Some of these chemical components are applied over the food as preventive strategies in plague control for the case of pesticides or during bacterial infection in food producing animals referring to antibiotics. Others arise as sub-products generated from microorganisms during crops storage like mycotoxins which may impose high risks for consumers even in some cases associated with certain types of cancer [8].

As part of the third group, physical hazards are identified. This category mainly considers packaging and food preservation conditions, such as the use of glass reservoirs to transport food. Although they are not as frequent as the other two groups, need a different classification and therefore a distinct treatment. Finally, allergens are considered potential hazards too, affecting consumers exposed to an excessive immune response triggered by a foreign substance present in the food. The principal cause is related to the lack of information regarding to the presence or absence of potential allergenic components in the labels. Strict controls should be performed from producers and manufacturers in order to guarantee the exact composition of the products in the market [9].

Every food product available is exposed to a certain degree of contamination at different levels. The actions adopted to prevent this to happened must be

preestablished and should be performed across food chain till reach the final consumer. Considering the food matrix composition (liquid, solid, viscous), origin (plant based, food derivate product, fermented sub product) and storage conditions (tank, silos, bottles, box) several risks can be addressed and therefore preventive measures are required for each case [10].

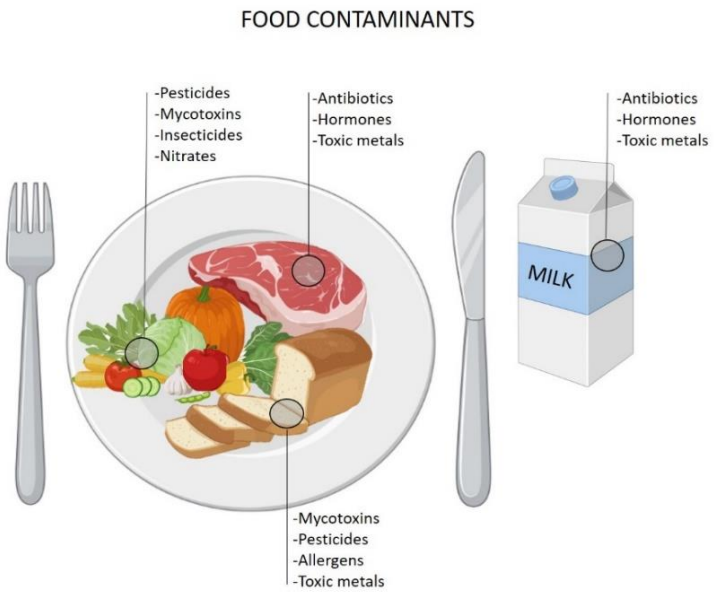

Figure I.II Main contaminants generally found in daily food. Ranging from crops and vegetables exposed to pesticides, mycotoxins and insecticides or animal derivate products containing traces of antibiotics, hormones and even toxic metals.

The image shows, some of the most representative contaminants in different food products like pesticides or mycotoxins in grains and vegetables or antibiotics and hormones in animal derived food stuff like meat and milk. Amongst all the potentially harmful substances described, during the last years special attention was directed towards food producing animals. The lack of strict controls has been directly associated to increased levels of contamination over meat, milk and dairy products with the presence of small molecules like antibiotics. The strict monitorization of these molecules results challenging due to the difficulty to identify them in complex matrixes with fast, accurate and affordable tools.

IV. ANTIBIOTICS RESIDUES CONTROL AND MONITORIZATION

Antibiotics are chemical, natural or semi-synthetic molecules with potential activity against bacterial proliferation. These group of small compounds are able to selectively alter bacteria life cycle interfering with DNA replication, protein synthesis or membrane integrity when are administered to humans and animals without damaging the host cells. Nowadays, antibiotics make possible medicine as we know it, dealing with several infections, surgical interventions, dental procedures and even birth.

During the last decades, authorities, scientist and medical personnel began to warn about the importance of strict controls behind antibiotics administration owing to the upward trends reporting the emergence of antimicrobial resistant bacteria [11 , 12]. The misuse of antibiotics is one of the leading causes of antimicrobial resistance according to the WHO, being recognized as one of the biggest public health threats of the present time.

Respecting to this, the overuse of antimicrobial substances in food producing animals has gained special attention during the last decades due to its direct relationship promoting the development of resistant strains [13]. In addition to treat and prevent diseases, since their discovery, antibiotics have also been used for non-medicinal purposes as feed efficiency enhancers and growth promoters in the livestock and poultry industries for meat production and other animal products. Farmers know that when antibiotics are used at subtherapeutic levels in feeds, the growth rate increases, the mortality and morbidity is reduced, and reproductive performance is improved [14]. The use of antibiotics as growth promoters and feed enhancers during the past years, particularly in the US, has largely resulted in economic gains [15]; however, this also entails significant risks to public health due to the enrichment of resistant microorganisms. Further, antibiotic residues constitute a threat to human health by entering the food supply chain and the environment. Hence, traces of antibiotic residues in meat or animal derivate products like milk are significant hazards for consumers.

According to the WHO, the unprescribed consumption of antimicrobials without proper schemes of administration for human and veterinary purposes added to the lack of sanitation in hospitals and farms are probably the most concerning aspects leading to resistance. When antibiotics reach the bacterial population,

the most susceptible ones are quickly eliminated, resulting in the proliferation of the most resistant bacterial phenotypes [16, 17]. Concerningly, the development of novel antibiotics has slowed down dramatically in recent years, owing to the lack of exclusive targets available in bacteria. On the other side, pharmaceutical companies have lost interest on the development of new antibiotics since, even if they were to be successful, should be kept as a last treatment choice to avoid resistance, without immediate financial rewards given the investment required [18].

Several public agencies and organizations worldwide dedicate resources to monitor and report the current use and consumption of antimicrobial agents as a major concern in healthcare and food safety fields. The Table I.I, shows some of the most relevant entities promoting responsible use of antimicrobials along the food chain to minimize potential resistance strains developments. The corresponding web pages offer reliable and updated information regarding the state of use of antimicrobials and current scenario through official reports, infographics, experts advise and even formats for non-experts such as podcasts.

Table I.I Summary of the most relevant organizations actively reporting antibiotic resistance emergence:

Organization	Website
World Health Organization (WHO)	www.who.int
European Commission (EC)	www.ec.europa.eu
European Medicines Agency (EMEA)	www.emea.europa.eu
European Food Safety Authority (EFSA)	www.efsa.europa.eu
International Federation for Animal Health (IFAH)	www.ifahsec.org
Centres for Disease Control and Prevention (CDC)	www.cdc.gov
Food and Drug Administration (FDA)	www.fda.gov
US Environmental Protection Agency (USEPA)	www.epa.gov

Originally, the development of antibiotics was directed to disrupt different bacterial mechanisms in order to specifically generate an inhibitory action towards the targeted pathogen with minimum side effects. Depending on the mechanism of action and the specificity generated, several families of antibiotics are available nowadays, sharing common structural similarities and adding slight chemical modifications to enhance the therapeutic efficacy for different purposes. Furthermore, due to the threatening antibiotic resistance, dual

antibiotic prescription is more frequent at clinical levels to mitigate the loss of efficacy behind these compounds showing synergic effects. In this context, some of the most relevant antibiotics described in the veterinary field include tetracyclines, β-lactams, aminoglycosides and also sulfonamides, macrolides and fluoroquinolones based on their prevalence in samples derived from food producing animals [19].

Sulfonamides

General description: This group of antimicrobials are structural competitors of p-aminobenzoic acid characterized by a similar 4-aminobenzene sulfonamide backbone. They are generally applied in veterinary schemes, human health, agriculture and aquaculture interfering with the enzymatic synthesis of dihydrofolic acid playing a role in different bacterial functions. These antimicrobials have a bacteriostatic effect rather than a bactericidal activity, which implies that they restrict bacterial replication and growth. The target enzyme, dihydropteroate synthase (DHPS), is in charge of the production of dihydropteroic acid (DHPA), a precursor of folic acid, purine and deoxyribonucleic acid (DNA) synthesis, in bacteria and some eukaryotic cells, conferring specific selectivity considering that humans don't synthesize folic acid, thus is incorporated through the diet.

The SA's family is constituted for 20 different congeners characterized by several chemical substituents. SA's are rapidly removed from the organism in almost 60 to 85%, typically as the original substance or as bioactive metabolites. These polar compounds have significantly enough water-solubility and can ionize depending on the pH of the matrix (SAs pKa values from 6.36 to 7.99). HPLC MS/MS methods have been developed in order to monitor the presence of these substances in milk [20].

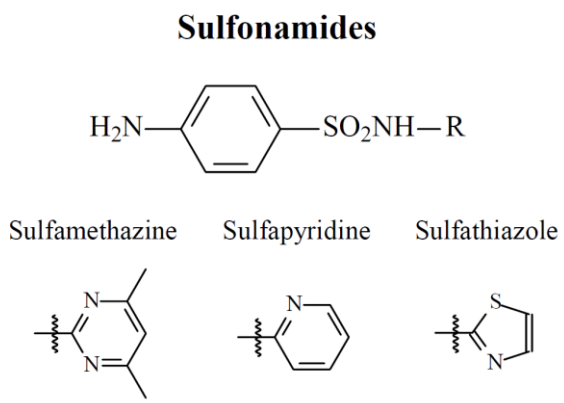

Figure I. III Common chemical structure among SA's antibiotics and three of the most representative congeners.

Regarding the consumption of this group of antibiotics, a joint report published by the ECDC (European Centre for Disease Prevention and Control), EFSA (European Food Safety Authority) and EMA (European Medicines Agency) specifies that SA's were one of the highest selling classes utilized in food producing animals [21]. Thus, the risk of antimicrobial resistance development is remarkable. Further information around the extensive use of these compounds in animals is described in the following section 82VII.

On the other hand, in the last EFSA report from 2021 the presence of non-compliant samples for SA's content was detected in honey from Croatia. As a result of pig samples monitorization several cases were reported showing limits above the regulations in Belgium, Germany, Spain, Denmark, Netherlands, France and Italy. While positive bovine samples were also reported in Italy and Germany for SA's presence [19]. As can be seen, the high consumption of such antimicrobials directly influences the amount of non-compliant specimens detected in EU.

Macrolides

General description: Depending on the size of the macrocyclic lactone ring ranging from 13 to 16 atoms, macrolides can be classified into different classes.

These molecules interfere with protein synthesis by reversibly interacting with the ribosome's 50S subunits, inhibiting transpeptidation and translocation which results in the premature separation of incomplete polypeptide chains [22]. These antibiotics are naturally produced by *Streptomyces* strains and some others are semi-synthetically generated showing special activity over gram positive aerobic bacteria, being *Clostridium* and *Campylobacter* generally highly susceptible to them. Once administered, a considerable portion is released as inactive metabolites while other relevant amount is excreted on its active form to the environment. Some of the most relevant examples of macrolides include erythromycin, spiramycin, tilmicosin, tylosin, azithromycin. Particularly tylosins (TYL's) belongs to naturally produced 16 membered ring of macrolides, isolated from *Streptomyces fradia.* Also *c*onsidered as a weak base (pKa 7.1) is highly lipid soluble and showed remarkable activity against *Mycoplasma spp*.[22].

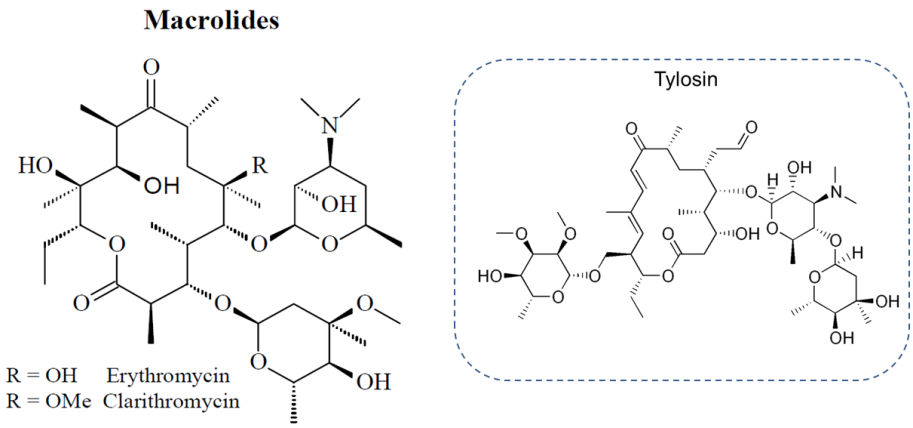

Figure I.IV Chemical structure of macrolides with different substituents and separately the tylosin structure is represented.

The consumption of macrolides for human and veterinary purposes was reported around 7.8 and 11.4 mg per kg of estimated biomass in 2014 [21]. In the same document a positive correlation between the over-use of these compounds in food-producing animals was proposed as causative agent propagating resistant *E. Coli* strains. See more in section VII.

In accordance to the document published by the European Public Health Alliance (EPHA) of January 2022, macrolide resistant *Campylobacter jejuni* strains were found significantly correlated to the consumption of poultry by humans [23]. Furthermore, bovine samples were found non-compliant for tylosin presence in

France as well as honey samples from Romania as expressed in the last EFSA report [19].

Fluoroquinolones

General description: Fluoroquinolones (FQ's) are selective bactericidal compounds, with a suppressive activity against DNA gyrase (in gram negatives) and topoisomerases IV (in gram positive) involved in bacterial replication. These compounds interfere with bacterial DNA synthesis and are used to deal with urinary, cystitis, respiratory, dermal and soft tissue infections [24]. Characterized by an exocyclic oxygen at position 4 and the carboxylic acid side chain at position 3, these moieties are responsible for the interaction with the DNA gyrase. In addition, all FQ's also present a fluorine atom defining the chemical structure of these residues. After administration, they can be released as the original compounds or conjugated, hydroxylated, decarboxylated, alkylated products.

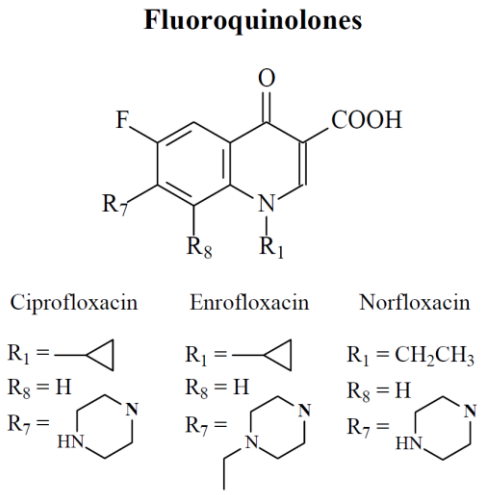

Figure I.V Chemical structure of the most representative FQ's and family of residues.

The overall consumption of FQ's in animals by 2014 was reported to be 3.5 mg per kg of estimated biomass slightly below the amount consumed for human medicine. These compounds are listed by the WHO as critically important antimicrobials also due to the relevant emergence of resistant strains [21].

According to the report from the EPHA on 2022, the presence of FQ's resistant *E. coli*, *Salmonella spp*. and *Campylobacter jejuni* strains were found in food producing animals (Cows, pigs, poultry) as a result of antibiotic administration with veterinary purposes [23]. On the other hand, based on the EFSA monitoring report, enrofloxacin and ciprofloxacin content in bovine samples was detected above the regulatory limits in Italy and Spain. Also, non-compliant levels in eggs from Poland and pig meat from Spain were pointed out. In this regard, relevant data highlights the importance of continuous assessment of these families of antimicrobial residues in animal derived products to reduce the emergence of novel resistant strains.

V. FROM FARM TO GLASS: ANTIBITIOC RESIDUES IN COWS MILK

Cows are producers par excellence of the most consumed type of milk worldwide. This emulsion of fat in water is composed of an 86 % of water, 4.5 % of triglycerides (Palmitic acid, stearic acid, oleic acids), 4.3 % of casein and whey proteins forming micelles in suspension with another portion of lactose and minerals [25]. Nowadays, cow's milk production is driven by a multi-billion-dollar industry worldwide. With almost 160 million tonnes of milk generated in 2021, the European Union is considered as one of the largest producers worldwide with the US and India, followed by China [26]. Although milk is widely consumed by humans during early phases to late adulthood, the added value of cow's milk arises as a result of dairy products derived from milk supplies like cheese, yogurts, ice cream, butter and many others.

On the other hand, this food source is exposed to several hazards before reaching the market, therefore adequate regulatory framework is needed to guarantee the safe commercialization. Heat treatment was initially implemented by 1880 as preventive measure to avoid microorganism's growth and contamination. Some years later with pasteurization, industrialized nations adopted this requirement as a standard procedure during milk production laying the foundations of current sterilization, preservation and hygiene practices [27]. According to the US Food and Drug Administration, a maximum limit of 100.000 cfu ml^{-1} for bacteria in raw cow's milk and 20.000 $cfu.ml^{-1}$ for pasteurized is tolerable [28].

Several contaminants have been reported in cow's milk like heavy metals [29, Zhou, 2019 #26] or mycotoxins [30] but one of the most concerning threats among milk contaminants are unboundedly associated to the presence of veterinary residues. Main reports evidence the presence of these small molecules in meat of pigs, cattle, chickens, turkeys as well as products obtained from them like cows, goat or sheep milk [16]. The presence of antibiotics residues in milk is considered a serious threat due to its contribution to antimicrobial resistance as already discussed. Furthermore, the unregulated consumption of these substances even at low levels, has implications for human health, leading to allergies, teratogenicity, hypoplasia, aplasia, and increased cancer risks [31]. It is estimated that at least an 80 % of cattle worldwide has been exposed to antibiotic treatment once in their lives.

Nowadays in Europe, the majority of reported cases prescribing the use of antibiotics in milk producing cows are referred to bacterial infections like mastitis, consisting on the inflammation of the breast tissue causing abnormal milk production. In order to combat such infections, veterinaries should prescribe antibiotics and depending on the dose and method of administration, the volume of milk produced, the severity of mammary illness and the interval between treatment and milking, cows will excrete differently those antibiotics and their metabolites through the milk. Different routes of administration will influence the time required to fully clear a treated animal from antibiotics and in case of mastitis the intra-mammal application is generally preferred over oral, intramuscular or intravenous administration due to significant differences in costs and doses, interfering with a rapid clearance [31]. If withdrawal periods are not adequately respected, veterinary residues and their metabolites will be imminently present in the milk obtained from these animals. Common storage conditions in refrigerated tanks with daily or weekly production will be exposed to contaminated samples to then be transferred directly to the dairy. In the best of cases, a confirmatory analysis as part of the quality control procedures will reveal the contamination prior the commercialization (see Figure I.VI). Therefore, the identification of traces of antibiotics in milk above regulatory limits will impose huge economic losses for farmers and dairy industries, emphasizing on the need of controls at farm level.

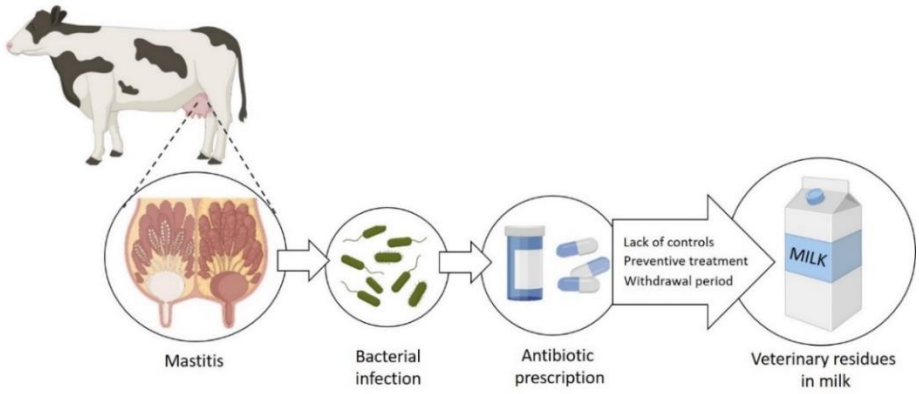

Figure I.VI Scheme indicating one of the main causes leading to the presence of antibiotic residues in cow's milk. If a dairy cow suffers bacterial infection in the mammary gland and is prescribed with antibiotics, the lack of effective monitoring could end up in the contamination of milk samples.

In comparison with pasteurization methods used to eliminate potentially dangerous microorganisms across milk production chain, some interesting approaches propose alternative milk treatments to remove antibiotics residues. This is the case of the application of gamma radiation to get rid of amoxicillin, ciprofloxacin, doxycycline. These radiations provoke water radiolysis that result in the oxidation of hydroxyl radicals and has been successfully implemented in matrixes with high water content like milk or eggs instead of meat for instance [32]**.** Alternatively, Alsager, *et al.* demonstrated that ozonisation induce the decomposition of amoxicillin, doxycycline, ciprofloxacin and sulfadiazine most efficiently in milk samples than in aqueous solutions. They claim that is possible to reach to a 95 % of removal over tested antibiotics with an ozone dose as low as 75 mg L^{-1} [33].

In order to prevent this to happen, new strategies are focusing on the development of novel screening methods to be implemented at farm level expecting to monitor single cow production before reaching common reservoirs. Most promising applications should allow real time monitoring of veterinary residues clearence from previously treated cows to shorten the rest days (ranging from 4 to 7) depending on the animal as a preventive strategy [34].

VI. REGULATORY FRAMEWORK FOR VETERINARY RESIDUES IN MILK ACROSS THE EU

Due to the implementation of new regulations restricting the use of antibiotics without veterinary consent, the amount of antibiotics employed in the EU with veterinary purposes has dramatically decreased over the last years.

Additionally, the European Commission has established several directives, regulations and decisions in order to monitor the use of veterinary products reasonability over the european space and for the products commercialized there [35]. Some directives are oriented to the regulation on additives for use in animal nutrition (Regulation 1831/2003), others banning the use of growth promoting agents in food-producing animals (Directive 96/22/EC and 97/6/EC). Particularly the use of veterinary drugs is laid by the European Regulation 2377/90/EC, that define general procedures for the establishment of the maximum residue limits (MRL) allowed for each veterinary residue in animal derivate products like meat, eggs and milk. Throughout this document and the correspondent annexes, limits of veterinary residues in each matrix are available and any product in the market must adhere to this regulation. Alternatively, Decision 2002/657/EC, defines MRPL (minimum required performance limit) as the *"minimum content of an analyte in a sample, which to be detected and confirmed*", while Commission Directive 2005/34/EC states the MRPLs values for some veterinary residues. On the other hand, the Commission Regulation (EU) Nº37/2010 summarizes the MRL values for allowed antibiotics in different food derivate products [36]. In order to visualize the MRL's for some the most relevant compounds belonging to the three families of antimicrobials already discussed in milk, the following table collects the EU regulatory levels to be accomplished.

Table I.II MRL values established for three prevalent antibiotic families commonly detected in milk

FQ's		SA's		Macrolides	
Compound	MRL*	Compound	MRL*	Compound	MRL*
Enrofloxacin	100	Sulfamethazine	100	Tylosin A	50
Ciprofloxacin	100	Sulfathiazole	100	Erythromycin	40
Danofloxacin	30	Sulfapyridine	100	Spiramycin	200
Flumequine	50	Sulfamethoxine	100	Tilmicosin	50
Marbofloxacin	75	Sulfamerazine	100		

*MRL values are expressed in μg kg^{-1}. [a] The sum of enrofloxacin and ciprofloxacin should not exceed μg kg^{-1} in cow's milk samples. [b] For sulfonamides group the MRL established is 100 μg kg^{-1} considering combined residues. Adapted from [36]

Results interesting to emphasize that each country is responsible of defining their own regulations and therefore in a globalized economy the commercialization of these kind of products should commit to the guidelines of the importing country. The lack of consensus among the food chain at different countries is another limitation towards an effective monitorization and control of antimicrobial resistance, considering that some regions will fulfil to the requirements when other regions will induce resistant strains that can be spread worldwide. General actions should be taken to mitigate the risk of antimicrobial resistance development at global level considering veterinary residues in food as a healthcare problem [37].

VII. PREVALENCE AND SURVEILLANCE OF ANTIMICROBIALS IN MILK

As a result of the continuous monitoring campaigns, the number of non-compliant milk samples for veterinary residues in the EU is still evidencing the urgent need of screening tools offering rapid and accurate on-site detection. From 366 raw cow's milk samples analyzed in Germany by 2019, a 7.7% were found positive for Methicillin-resistant *Staphylococcus aureus* (MRSA) [38]. Particularly FQ's often constitute the first-line treatment for invasive salmonellosis in humans being relevant the direct association based on evidence, of zoonotic infection, originating from animals [39]. Additionally, a recent study assessed the presence of resistant bacteria in cow's milk over 100 samples utilizing antibiograms as detection techniques but also showing a significant incidence of tolerant microorganisms in this matrix [40].

Furthermore, the European Commission defines the number of samples that should be taken in regard of the annual production by each country. It's established that at least 1 sample must be analysed per 15000 tons of milk produced or a minimum of 300 hundred samples if production is lower. In the last report available, most of the regions do accomplish this procedure but countries like France, Germany and Portugal did not achieve the first 1/15000 tones requirement while Finland and Hungary not even reached the minimum of 300 samples tested. From a regulatory perspective, this leads to an ineffective monitoring plan and also evidence the lack of reliable information from the real scenario to influence political decisions and define future action plans [41].

From a positive side, recent trends in antimicrobial sales around Europe have considerably decreased in the last years. Several actions were taken in order to promote the responsible use of antimicrobials, and as consequence the imminent reduction on the emergence of resistant strains should be expected if they are correctly applied. As the following graph shows, the total amount of antimicrobial sales in recent years slowed down over the EU. In agreement with the data, after the announcement of strict regulatory policies a direct impact is evidenced in the total consumption of these products [42].

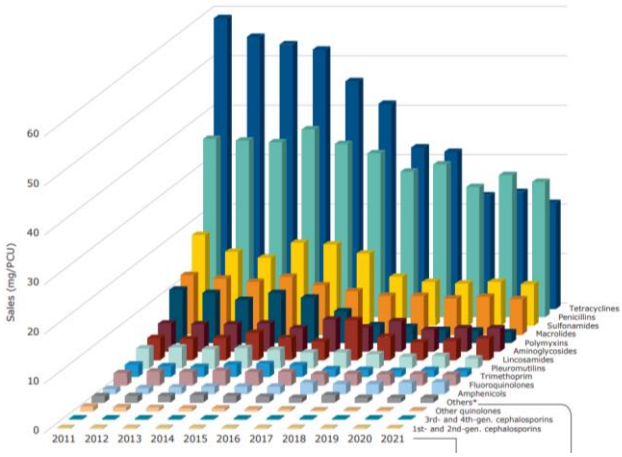

Figure I. VII Antimicrobial sales (in mg/PCU) distribution per year and family of compound. Adapted from [42].

On the other hand, a recent report from the EPHA, evidenced the emergence of resistant bacterial strains by direct association of antimicrobial consumption in

humans and food producing animals showing statistically significant results. As examples, *E. Coli* and *Salmonella Spp.* resistant to FQ's strains are reported as a result of antimicrobial use in food producing animals. *C. Jejuni* resistant to macrolides were detected in poultry and significant association to human infection due to poultry consumption is postulated. Based on the growing evidence, several actions should be taken in order to prevent further antimicrobial resistant strains development in food producing animals [23]. As part of the innovative programmes adopted to mitigate antibiotics demand across Europe, the EU from Farm to Fork plan is an ambitious proposal aiming to cut total sales of antibiotics for use in animals and aquaculture by 50 % by 2030 referring to 2018. The European Commission (EC) created the Farm to Fork Strategy as an instrument of transition to a more sustainable agricultural and farming system [43].

VIII. CONSIDERATIONS FOR ANALYTICAL DETERMINATION OF VETERINARY RESIDUES IN MILK

According to EU regulations, two methodological categories are defined to monitor the presence of potential contaminants in food products, like antibiotics in cow's milk. In this regard the Decision 2002/657/EC [44], categorizes analytical procedures into "screening" and "confirmatory" methods and gives generic validation guidelines that are applicable to any type of detection technique.

There are numerous performance characteristics that must be considered during the validation of a novel bioanalytical techniques but as can be expected, differ for screening and confirmatory analysis mainly on the quantification capacity. Some of these features include the establishment of the method detection capability (CCβ) defined as the lowest amount of analyte that can be detected or identified with an error probability of β. While the estimation of the technique precision and recovery are decisive during the characterization of screening methods.

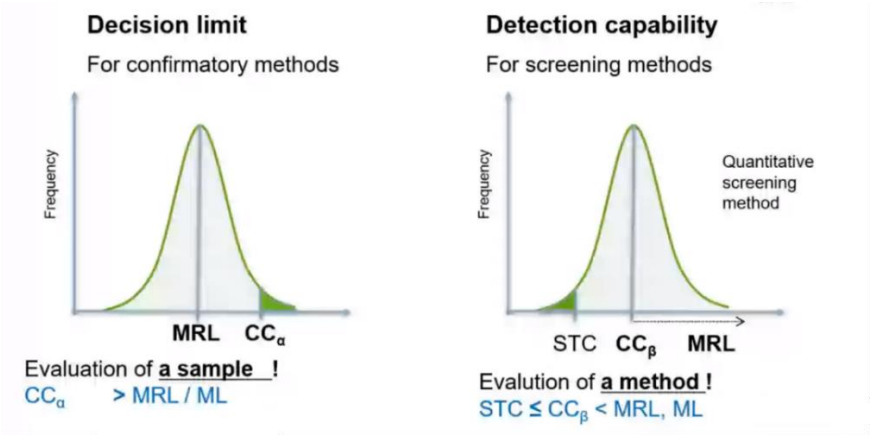

Figure I.VIII Graphic representation of the definition of decision limit (CCα) and detection capability (CCβ) according to EU guidelines.

On the other hand, a recent commission implementing regulation (EU) 2021/808, establish a clear distinction of the decision limit (CCα) in confirmatory methods from the detection capability (CCβ) applicable to screening methods, as expressed in the Figure I.VIII. Thus, indicating that the use of CCα, should be restricted to sample analysis while the CCβ allows method evaluation and this value should be higher than the screening target concentration (STC) and lower than the MRL for quantitative screening techniques. Moreover, validation protocols are critical and laborious procedures since they proof that a technique will work as intended by the law. Several guidelines emphasizing on the type of analyte that aims to be detected were created by European Union Reference Laboratories (EURL) and the Directorate-General for Health and Food Safety (DG SANTE) as well as particular rules for qualitative and semi-quantitative methods developments according to Regulation 519/2014 on validation of screening techniques [45].

Recent changes have been established for milk sampling collection replacing Directives 96/23/EC and 97/747/EC, for commission regulations 2022/1644 on the requirements needed to correctly perform veterinary residues monitoring and regulation 2022/1646 propose practical suggestions just like the minimum number of samples required to obtain representative results considering the amount of milk produced and also the sampling frequency recommended by country. Following the classification between confirmatory and screening methods for the assessment of contaminants (pesticides, antibiotics, mycotoxins) in food products (fruits, milk, eggs, grains) [46]. Confirmatory

methods rely on chromatographic techniques generally coupled to mass detectors. These methods should provide information of the structural chemical composition of the sample and for authorized substances, the CCα shall be higher and as close as possible to the MRL [47]. However, some drawbacks arise with the use of these techniques like extended sample to answer response or the necessity of sophisticated equipment as well as trained personnel. These aspects limit the implementation of confirmatory techniques at farm level and that's why they are only performed at industrial or laboratory scale [48].

IX. STATE OF THE ART OVER SCREENING METHODS FOR ANTIBIOTIC RESIDUES IN MILK

In a different group, screening methods arise as attractive solutions to detect particular contaminants at the level of interest under rapid, easy to implement and cost-effective configurations to assess high number of samples in parallel. The state of the art on screening methods for the detection of antimicrobials in food sources like milk, involve a broad range of applications. In first place, plate or tube based microbiological inhibition assays, constitute one of the most widely used approaches due to their inexpensive and simple configuration. These types of assay generally promote a visible change in the culture media or plate, correlated with the presence of antimicrobial compounds interfering with bacterial growth rate. Despite their relatively low cost these assays generally lack of sensitivity and may require long incubation periods to provide a qualitative response [49]. As an alternative strategy, enzymatic assays make use of the potential inhibition capacity of certain contaminants over the catalytical activity of an enzyme. The presence of the target analyte can be evidenced as a result of the interference in the colorimetric or chemiluminescent response detected.

Apart from enzymes, several other bioreceptors were successfully implemented towards antibiotics identification in milk like aptamers [50, 51], molecularly imprinted polymers (MIP's) [52] and the biorecognition elements by excellence that are the antibodies, due to their robustness and specificity in complex matrixes. These glycoproteins have been carefully designed to detect a complete family of antibiotics or even a single congener among other veterinary residues. Their implementation in ELISA formats over 96 or 384 well plates [53], along with LFIA over nitrocellulose membranes, and even coupled to optical or

electrochemical transducers [54] to generate biosensing interfaces demonstrates the potential use of these immunoglobulins for divers screening purposes as shown in Figure I.IX.

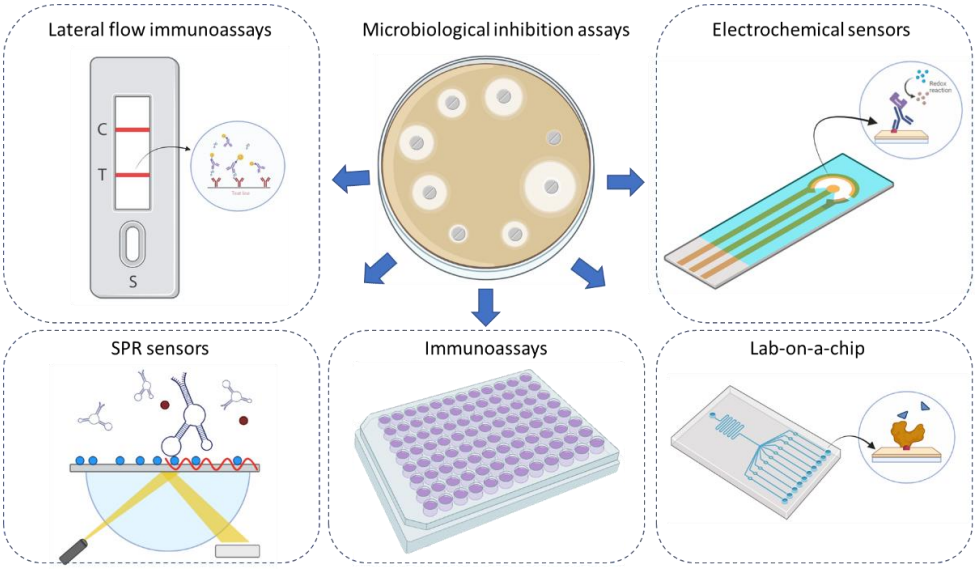

Figure I.IX Alternative screening methods reported for antibiotics in milk detection against conventional microbiological inhibition assays.

On the other hand, the main limitation over the use of immunoglobulins for screening purposes is found on the exclusive dependence of laboratory animals to develop high-quality antibodies [55]. Currently, european policies aim to improve the already mentioned production techniques moving towards animal free protocols [56]. Another example to promote an extensive use of these macromolecules propose the modification of pre-existent antibodies through molecular biology techniques to reach higher sensitivities and increase stability after exposure to organic solvents [57].

Recent trends in bioanalytical techniques make use of different sensing principles and bioreceptors to determine antibiotic residues in milk. For instance, an electrochemical platform to detect chloramphenicol through amperometric signal was reported [58], by using reduced graphene oxide and silver nanoparticles as transducers coupled to a selective aptamer as bioreceptor**.** A different group of authors, employed differential pulse voltammetry (DPV) to detect the presence of thiamphenicol in milk samples using a carbon nanotube-

silver nanoparticle composite [59]. Alternatively, a bi-plexed electrochemical aptasensor for kanamycin and streptomycin was implemented on a screen-printed electrode with outstanding sensibility of 87.3 pM and 45.0 pM, respectively in spiked milk samples [60].

On the other hand, optical sensors have also been proposed for the screening of veterinary residues in milk exploiting different light properties. The most common approaches involve the use of decorated AuNP's coated with antibodies [61] or aptamers [62] reaching low sensitivity and relatively easy detection formats. While plate based colorimetric immunoassays [63] or lateral flow tests [64] have demonstrated great efficacy towards antibiotics determination and are currently considered as reference methods. In a different category, a multiplexed and label free SPR biosensor was implemented for antibiotics in milk [65] and a different SPR study was conducted in a Biacore^{TM} 3000 platform using nano MIP's for vancomycin determination [66].

Exploiting a different optical technique, a fluorescent aptasensor to detect florfenicol was developed. In this case, the principle of detection consisted on fluorescence quenching of the aptamer by a graphene oxide substrate in absence of analyte. If the system was exposed to positive florfenicol samples, a conformational change on the aptamer supresses the quenching effect displaying a fluorescent signal [67]. Another report, demonstrates the potential use of a fluorescent immunoassay over paper substrate for the detection of norfloxacin in milk at picogram levels. In this case the low sensibility was mainly attributed to the use of high-quality monoclonal antibodies coupled to quantum dots to maximize signal emission [68]

In order to accomplish higher throughput capacity, a multi-analyte fluorescent immunoassay based on quantum dots has been used to monitor the presence of streptomycin, tetracycline and penicillin G in milk samples. The main limitation behind this platform was found on the use of 96 well plates to perform separate determinations over each well, instead of using a single well for the detection in an array format reducing sample size, reagents consumption and handling errors [69]. Consistent experimental evidence highlights the potential implementation of bioanalytical screening platforms to detect veterinary residues in cow's milk, making use of different receptors like antibodies, enzymes or aptamers while exploiting alternative sensing principles. Future trends in the development of

screening methods integrating bioreceptors in food safety should consider the incorporation of user-friendly interfaces like smartphones for rapid data acquisition and interpretation as well as increasing multiplexing capacity to favour high-throughput performance.

GENERAL AND SPECIFIC THESIS OBJECTIVES: FOODSMARTPHONE PROJECT

The general objective of this thesis has been to investigate the use of high-throughput immunoarray platforms aiming to offer versatile bioanalytical solutions in food safety screening applications and immunodiagnostics for respiratory infections.

In the context of food safety applications, the final objective of this research has been achieving a portable optical immunoarray coupled to a smartphone acquisition system for the detection of antibiotics residues in milk samples. To overcome the limitations derived from the high scale manufacturing of non-DNA microarrays or the difficulties to regenerate and reuse immunoassay chips, we have also addressed the objective of using DNA-directed immobilization (DDI) strategies. Hence the following specific objectives were proposed:

1. Evaluating the performance of a selected panel of immunoreagents towards the detection of veterinary antibiotic residues in cows' milk.

2. Establishing a standardized procedure for the preparation of well-defined and characterized oligonucleotide-hapten conjugates to be used for the manufacturing of the microarray chip.

3. Developing a reusable multiplexed microarray chip for antibiotic residues determination making use of DNA directed hapten immobilization strategy.

4. To characterize the analytical performance of the multiplexed microarray platform within the regulatory guidelines established by food safety authorities.

5. Addressing the technological transition of the hapten-DDI immunoarray over a portable and label free iSPR surface plasmon resonance system integrating smartphone detection for *on-site* screening.

X. BIBLIOGRAPHY

1. Control, C.f.D. and Prevention, *Challenges in Food Safety*. 2020, Centers for Disease Control and Prevention. https://www. cdc. gov/foodsafety ….
2. Uyttendaele, M., E. Franz, and O. Schlüter, *Food safety, a global challenge*. 2016, MDPI. p. 67.
3. Flynn, K., et al., *An introduction to current food safety needs.* Trends in Food Science & Technology, 2019. **84**: p. 1-3.
4. Organization, W.H. *Food safety*. 2023.
5. Antle, J.M., *Economic analysis of food safety.* Handbook of agricultural economics, 2001. **1**: p. 1083-1136.
6. Commission, E. *Food Safety*. 2023.
7. Authority, E.F.S., et al., *Food safety regulatory research needs 2030.* EFSA Journal, 2019. **17**(7).
8. Li, C., et al., *Chemical food contaminants during food processing: sources and control.* Critical Reviews in Food Science and Nutrition, 2021. **61**(9): p. 1545-1555.
9. Nerin, C., M. Aznar, and D. Carrizo, *Food contamination during food process.* Trends in food science & technology, 2016. **48**: p. 63-68.
10. Marriott, N.G., et al., *Food contamination sources.* Principles of Food Sanitation, 2018: p. 83-91.
11. Roca, I., et al., *The global threat of antimicrobial resistance: science for intervention.* New microbes and new infections, 2015. **6**: p. 22-29.
12. Use, E.C.f.M.P.f.V., et al., *EMA and EFSA Joint Scientific Opinion on measures to reduce the need to use antimicrobial agents in animal husbandry in the European Union, and the resulting impacts on food safety (RONAFA).* EFSA Journal, 2017. **15**(1): p. e04666.
13. Larsson, D.J. and C.-F. Flach, *Antibiotic resistance in the environment.* Nature Reviews Microbiology, 2022. **20**(5): p. 257-269.
14. Kasimanickam, V., M. Kasimanickam, and R. Kasimanickam, *Antibiotics use in food animal production: escalation of antimicrobial resistance: where are we now in combating AMR?* Medical Sciences, 2021. **9**(1): p. 14.
15. Durso, L.M. and K.L. Cook, *Impacts of antibiotic use in agriculture: what are the benefits and risks?* Current opinion in microbiology, 2014. **19**: p. 37-44.
16. Ma, F., et al., *Use of antimicrobials in food animals and impact of transmission of antimicrobial resistance on humans.* Biosafety and Health, 2021.**3**(01):32-38.
17. Chokshi, A., et al., *Global contributors to antibiotic resistance.* Journal of global infectious diseases, 2019. **11**(1): p. 36.
18. Lewis, K., *The science of antibiotic discovery.* Cell, 2020. **181**(1): p. 29-45.
19. Authority, E.F.S., D. Brocca, and S. Salvatore, *Report for 2021 on the results from the monitoring of veterinary medicinal product residues and other substances in live animals and animal products*. 2023, Wiley Online Library.
20. Białk-Bielińska, A., et al., *Optimization of multiple reaction monitoring mode for the trace analysis of veterinary sulfonamides by LC–MS/MS.* Talanta, 2009. **80**(2): p. 947-953.

21. Prevention, E.C.f.D., et al., *ECDC/EFSA/EMA second joint report on the integrated analysis of the consumption of antimicrobial agents and occurrence of antimicrobial resistance in bacteria from humans and food-producing animals: Joint Interagency Antimicrobial Consumption and Resistance Analysis (JIACRA) Report.* EFSA Journal, 2017. **15**(7): p. e04872.
22. Gaynor, M. and A.S. Mankin, *Macrolide antibiotics: binding site, mechanism of action, resistance.* Current topics in medicinal chemistry, 2003. **3**(9): p. 949-960.
23. Nunan, C., *Ending Routine Farm Antibiotic Use in Europe.* Achieving Responsible Farm Antibiotic Use through Improving Animal Health and Welfare in Pig and Poultry Production, 2022.
24. Blondeau, J.M., *Fluoroquinolones: mechanism of action, classification, and development of resistance.* Survey of ophthalmology, 2004. **49**(2): p. S73-S78.
25. Foroutan, A., et al., *Chemical composition of commercial cow's milk.* Journal of agricultural and food chemistry, 2019. **67**(17): p. 4897-4914.
26. Shahbandeh, M. *Leading producers of cow milk worldwide 2022, by country*. 2023.
27. Claeys, W.L., et al., *Raw or heated cow milk consumption: Review of risks and benefits.* Food control, 2013. **31**(1): p. 251-262.
28. Hayes, M., et al., *Identification and characterization of elevated microbial counts in bulk tank raw milk.* Journal of dairy science, 2001. **84**(1): p. 292-298.
29. Malhat, F., et al., *Contamination of cows milk by heavy metal in Egypt.* Bulletin of environmental contamination and toxicology, 2012. **88**(4): p. 611-613.
30. Milićević, D.R., et al., *A review of the current situation of aflatoxin M1 in cow's milk in Serbia: risk assessment and regulatory aspects.* Food Additives & Contaminants: Part A, 2017. **34**(9): p. 1617-1631.
31. Calahorrano-Moreno, M.B., et al., *Contaminants in the cow's milk we consume? Pasteurization and other technologies in the elimination of contaminants.* F1000Research, 2022. **11**.
32. Ye, Q., et al., *Heterogeneous irradiation system: enhanced degradation of methylene blue by electron beam irradiation combined with graphite carbon nitride/carbon nanodots.* Environmental Science and Pollution Research, 2022: p. 1-11.
33. Mohammadi, I., S. Ghorbanidehkordi, and A. Hallajisani, *Assessment of ionic liquid-based aqueous two-phase system abilities to remove sulfonamide antibiotics from the aquatic environment.* International Journal of Environmental Science and Technology, 2022. **19**(11): p. 11291-11300.
34. Anika, T.T., et al., *Time dependent screening of antibiotic residues in milk of antibiotics treated cows.* Journal of Advanced Veterinary and Animal Research, 2019. **6**(4): p. 516.
35. Tsagkaris, A.S., et al., *Critical assessment of recent trends related to screening and confirmatory analytical methods for selected food contaminants and allergens.* TrAC Trends in Analytical Chemistry, 2019. **121**: p. 115688.
36. Commission, E., *Commission Regulation (EU) No 37/2010 of 22 December 2009 on pharmacologically active substances and their classification regarding maximum residue limits in foodstuffs of animal origin.* Off J Eur Union, 2010. **15**(2377): p. 1-72.

37. Landers, T.F., et al., *A review of antibiotic use in food animals: perspective, policy, and potential.* Public health reports, 2012. **127**(1): p. 4-22.
38. Authority, E.F.S., E.C.f.D. Prevention, and Control, *The European Union Summary Report on Antimicrobial Resistance in zoonotic and indicator bacteria from humans, animals and food in 2018/2019.* EFSA Journal,2021,**19**(4):p. e06490.
39. Authority, E.F.S., *The European Union Summary Report on Antimicrobial Resistance in zoonotic and indicator bacteria from humans, animals and food in 2019–2020.* EFSA Journal, 2022. **20**(3).
40. Hassani, S., et al., *High prevalence of antibiotic resistance in pathogenic foodborne bacteria isolated from bovine milk.* Scientific Reports, 2022 **12**: 1-10.
41. Authority, E.F.S., *Report for 2019 on the results from the monitoring of veterinary medicinal product residues and other substances in live animals and animal products*. 2021, Wiley Online Library.
42. Agency, E.M., *Sales of veterinary antimicrobial agents in 31 European countries in 2019 and 2020.* European Surveillance of Veterinary Antimicrobial Consumption, 2021.
43. Health, E.P.o.A., et al., *Methodological guidance for the development of animal welfare mandates in the context of the Farm to Fork Strategy.* EFSA Journal, 2022. **20**(7): p. e07403.
44. Commission, E., *Commission Decision 2002/657/EC of 12 August 2002 implementing Council Directive 96/23/EC concerning the performance of analytical methods and the interpretation of results.* Official Journal of the European Communities, 2002. **50**: p. 8-36.
45. Commission, E., *Commission Regulation (EU) No 519/2014 of 16 May 2014 amending Regulation (EC) No 401/2006 as regards methods of sampling of large lots, spices and food supplements, performance criteria for T-2, HT-2 toxin and citrinin and screening methods of analysis.* Off. J. Eur. Union, 2014. **147**:p.29-43.
46. Gentili, A., D. Perret, and S. Marchese, *Liquid chromatography-tandem mass spectrometry for performing confirmatory analysis of veterinary drugs in animal-food products.*TrAC Trends in Analytical Chemistry,2005.**24**(7):704-733.
47. Jank, L., et al., *High-throughput method for macrolides and lincosamides antibiotics residues analysis in milk and muscle using a simple liquid–liquid extraction technique and liquid chromatography–electrospray–tandem mass spectrometry analysis (LC–MS/MS).* Talanta, 2015. **144**: p. 686-695.
48. Cháfer-Pericás, C., A. Maquieira, and R. Puchades, *Fast screening methods to detect antibiotic residues in food samples.* TrAC Trends in Analytical Chemistry, 2010. **29**(9): p. 1038-1049.
49. Ribeiro, B.V., L.F. Ferreira, and D.L. Franco, *Advances in biosensor development for the determination of antibiotics in cow's milk-a review.* Talanta Open, 2022: p. 100145.
50. Zhou, N., J. Zhang, and Y. Tian, *Aptamer-based spectrophotometric detection of kanamycin in milk.* Analytical Methods, 2014. **6**(5): p. 1569-1574.
51. Zhang, Y., et al., *Dual triple helix-aptamer probes for mix-and-read detecting antibiotics in fish and milk.* Journal of Agricultural and Food Chemistry, 2020. **68**(35): p. 9524-9529.

52. Amiripour, F., S. Ghasemi, and S.N. Azizi, *Design of turn-on luminescent sensor based on nanostructured molecularly imprinted polymer-coated zirconium metal–organic framework for selective detection of chloramphenicol residues in milk and honey.* Food Chemistry, 2021. **347**: p. 129034.
53. Du, B., et al., *Presence of tetracyclines, quinolones, lincomycin and streptomycin in milk.* Food Control, 2019. **100**: p. 171-175.
54. Liu, X., et al., *Electrochemical immunosensor based on the chitosan-magnetic nanoparticles for detection of tetracycline.* Food analytical methods, 2016. **9**: p. 2972-2978.
55. Gonzalez-Fernandez, A., et al., *Non-animal-derived monoclonal antibodies are not ready to substitute current hybridoma technology.* Nature Methods, 2020. **17**(11): p. 1069-1070.
56. Gray, A.C., et al., *Animal-derived-antibody generation faces strict reform in accordance with European Union policy on animal use.* Nature methods, 2020. **17**(8): p. 755-756.
57. Li, C., et al., *Engineering of organic solvent-tolerant antibody to sulfonamides by CDR grafting for analytical purposes.* Analytical Chemistry, 2021. **93**(15): p. 6008-6012.
58. Liu, S., et al., *Amperometric aptasensing of chloramphenicol at a glassy carbon electrode modified with a nanocomposite consisting of graphene and silver nanoparticles.* Microchimica Acta, 2017. **184**: p. 1445-1451.
59. Muhammad, A., et al., *A screen printed carbon electrode modified with carbon nanotubes and gold nanoparticles as a sensitive electrochemical sensor for determination of thiamphenicol residue in milk.* RSC advances, 2018. **8**(5): p. 2714-2722.
60. Li, F., et al., *Multiplex electrochemical aptasensor for detecting multiple antibiotics residues based on carbon fiber and mesoporous carbon-gold nanoparticles.* Sensors and Actuators B: Chemical, 2018. **265**: p. 217-226.
61. Du, B., et al., *Evaluation of an ELISA-based visualization microarray chip technique for the detection of veterinary antibiotics in milk.* Food Control, 2019. **106**: p. 106713.
62. He, L., et al., *Colorimetric sensing of tetracyclines in milk based on the assembly of cationic conjugated polymer-aggregated gold nanoparticles.* Food Analytical Methods, 2013. **6**: p. 1704-1711.
63. Adrian, J., et al., *A multianalyte ELISA for immunochemical screening of sulfonamide, fluoroquinolone and ß-lactam antibiotics in milk samples using class-selective bioreceptors.* Analytical and bioanalytical chemistry, 2008. **391**: p. 1703-1712.
64. Alhammadi, M., et al., *A highly sensitive lateral flow immunoassay for the rapid and on-site detection of enrofloxacin in milk.* Frontiers in Nutrition, 2022. **9**.
65. Fernández, F., et al., *A label-free and portable multichannel surface plasmon resonance immunosensor for on site analysis of antibiotics in milk samples.* Biosensors and Bioelectronics, 2010. **26**(4): p. 1231-1238.
66. Altintas, Z., *Surface plasmon resonance based sensor for the detection of glycopeptide antibiotics in milk using rationally designed nanoMIPs.* Scientific reports, 2018. **8**(1): p. 11222.

67. Sadeghi, A.S., et al., *Development and characterization of DNA aptamers against florfenicol: fabrication of a sensitive fluorescent aptasensor for specific detection of florfenicol in milk.* Talanta, 2018. **182**: p. 193-201.
68. Zong, L., et al., *based fluorescent immunoassay for highly sensitive and selective detection of norfloxacin in milk at picogram level.* Talanta, 2019. **195**: p. 333-338.
69. Song, E., et al., *Multi-color quantum dot-based fluorescence immunoassay array for simultaneous visual detection of multiple antibiotic residues in milk.* Biosensors and Bioelectronics, 2015. **72**: p. 320-325.

3 IMMUNOCHEMICAL APPROACHES FOR THE DETERMINATION OF VETERINARY RESIDUES IN MILK

3.1. SUMMARY

This chapter aimed to develop two immunochemical approaches making use of the same immunoreagents, to compare the analytical performance and potential transition from the reference ELISA to microarray platforms for the determination of traces of veterinary residues in cow's milk. For these means, an indirect competitive immunoassay format was selected, making use of haptenized BSA molecules as coating antigens and monoclonal antibodies (MAb's) for relevant antibiotics used in veterinary medicine. During this section the preparation of hapten-BSA bioconjugates and subsequent characterization is described. In addition, a comparative study between both bioanalytical platforms in respect to detectability's in buffer and milk as well as potential multiplexation is explored. The initial characterization of the immunoreagents was proposed using BSA-hapten conjugates as reference, to facilitate the use of the same haptens and MAb's in a DNA directed immobilization (DDI) microarray, described in the following chapter.

Classification of types of bioanalytical platforms:

Bioassay: tools employed to measure biological activity or quantify a discreet analyte, based on the use of recognition elements like cells, tissues, bacteria.

Biochemical assays: methods that rely on a biorecognition element such as enzyme, oligonucleotide, antibody or other protein interacting with a target analyte under stoichiometric conditions.

Biosensor: device composed of a biorecognition element (enzyme, oligonucleotide, antibody) in close contact with the transducing system that are responsible to translate the biorecognition event into a measurable output).

3.2. INTRODUCTION

3.2.1. IMMUNOREAGENTS AND PRECEDENTS FROM OUR GROUP

The immunoreagents, including antibodies, haptens and bioconjugates implemented in the subsequent sections have been originally developed in the Nanotechnology for Diagnostic group in the framework of different projects. The first immunoreagents for FQ's antibiotics were developed by Daniel G. Pinacho, who designed a suitable immunizing hapten based on theoretic and molecular modeling studies [2]. The generation of immunoreagents against SA's was possible through the collaboration of Hector Font and Javier Adrian [3, 4]. Finally, the work carried out towards the development of TYL's immunoreagents was performed by Salvador Petanas. The antibodies developed on a first stage were polyclonal (PAb), produced in rabbit, and were used to develop highly sensitive competitive microplate-based ELISAs. The analytical parameters obtained with the corresponding reagents are summarized in the following table 3.1 reaching considerably low detectability's (IC_{50}) in the three cases

Table 3.1 Analytical parameters obtained with PAb's under indirect competitive ELISA for the detection of enrofloxacin, sulfapyridine and tylosin B in buffer.

PAb's ELISA	As172/PrEDA-BSA	As155/SA2-OVA	As241/hTB-BSA
A_{max}	1.67	1.07	1.75
A_{min}	0.07	0.04	0.09
Slope	-1.08	-0.73	-0.80
IC_{50}[a]	0.35	2.35	1.31
R^2	0.99	0.99	0.99
LOD[b]	0.12	0.15	0.30

[a] values expressed in μg Kg^{-1}. [b] values expressed in nM

Owing to the excellent analytical performance achieved with the PAb's in ELISA reaching sensitivities in the low nM range; the implementation in label free biosensing approaches was feasible. SPR was utilized to detect FQ's in milk [5], while wavelength interrogated allowed multi residues determinations including SA's, β-lactams and tetracyclines [6]. Furthermore, electrochemical modes were also explored developing disposable immunosensors [7] and exploiting amperometric detection of SA's [8].

Further on, the generation of the corresponding MAb's was also accomplished using the same immunizing haptens and employing well designed screening technologies, to isolate the most appropriate antibody producer cell clones. Another remarkable feature behind these MAb's is that they were produced as class selective antibodies with the objective of recognizing a significant number of antibiotic congeners used in the veterinary field. For this, the chemical structure of the three immunizing haptens was designed making use of prediction models and theoretical calculations [2] to mimic FQ's, SA's and TYL's common moieties for the generic recognition of structurally related compounds using one antibody for each family.

3.3. RESULTS AND DISCUSSION

The following chapter discusses the development and characterization of three independent indirect competitive immunoassays for the detection of veterinary residues in ELISA and microarray format. Analytical performance is compared among both platforms as well as implemented in cow's milk matrix. In order to facilitate the identification of the corresponding reagents utilized in this work, the next table summarizes the nomenclature attributed to each bioconjugate and MAb employed.

Table 3.2 Identification of immunoreagents utilized in the development of the immunochemical platforms

Target Analytes	MAb's	Clon N°	Bioconjugate	Hapten
FQ's	MAb-FQ	FQ1109C2.2	PrEDA-BSA	PrEDA
SA's	MAb-SA	8E5-16085E	SA2-BSA	SA2
TYL's	MAb-Tyl	C6.23.4.2	hTB-BSA	hTB

As expressed, each bioconjugate takes the name of the hapten molecule conjugated followed by BSA in order to identify them from the single haptens. Considering the competitive step, the MAb's utilized are named according to the target molecules required for quantification through ELISA or microarray.

3.3.1. PREPARATION AND CHARACTERIZATION OF BSA-HAPTEN CONJUGATES

The generation of functional and highly selective antibodies against small molecules like pesticides, antibiotics, anabolic steroids or mycotoxins is considered as a challenging procedure, because they are not able to naturally elicit an immune response in the host organism. For this purpose, hapten molecules based on the structure of the target need to be covalently attached to larger immunogenic proteins like horseshoe crab hemocyanin (HCH) or keyhole limpet hemocyanin (KLH). After that, subsequent immunization with the bioconjugates (hapten and carrier protein) will induce the production of antibodies in the animal, offering a wide response against the epitopes of the molecule of interest and the immunogenic protein. A decisive aspect towards

the development of high-quality antibodies against small molecules consists on the rational design of the immunizing hapten as well as the screening procedure to avoid unspecific epitopes.

3.3.1.1. Hapten bioconjugation to BSA

The first step, towards the immunoassay standardization consisted on the covalent bioconjugation of each hapten to the carrier BSA to produce the coating antigens required for the competitive assay. Bioconjugate competitors for the three analytes of interest were prepared using the haptens previously synthesized by the Nb4D group members and already described [1, 9].

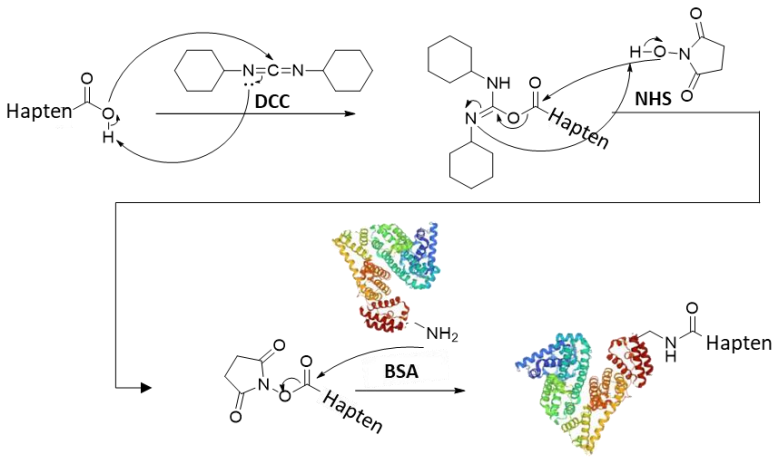

Figure 3.1 Scheme of reaction for active ester method utilizing DCC and NHS for BSA conjugation.

SA2 and hTB haptens were conjugated through the active ester method using carbodiimide and N-hydroxysuccinimide to activate the carboxyl group of the hapten. The active esters allowed the covalent reaction of the haptens with the amine groups from lysin residues of the BSA as shown in the Figure 3.1.

On the other hand, the bioconjugation of the PrEDA hapten was made using a (homo)bifunctional cross-linker known as dimethyl-pimelimidate (DMP, see Figure 3.2). The hapten:lys molar ratios were slightly adapted in order to achieve optimum hapten densities for each molecule. After purification through dialysis, each bioconjugate was characterized by MALDI-TOF-MS and their functional performance was evaluated in titration assays.

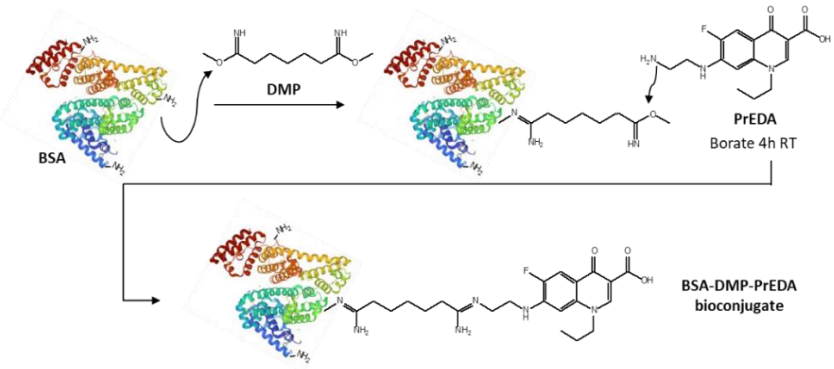

Figure 3.2 Reaction scheme for PrEDA conjugation to BSA through the use of dimethyl pimelimidate (DMP) crosslinker.

In the next graph, a representative example of the MALDI-TOF-MS spectra for a PrEDA-BSA conjugate is displayed (see Figure 3.3) using non-conjugated BSA (as control at 66.5 KDa). All three bioconjugates showed a peak at higher m/z ratio depending of molecular weight (MW) of the hapten, and eventually the crosslinker used, estimating the hapten density achieved. Hapten density was calculated with this formula, δ hapten= [MW(BSA-hapten $_{conjugate}$)MW(BSA)]/ [MW(hapten)]. In the case of PrEDA, the hapten MW is 307.32 Da and the crosslinker was also considered, leading to a hapten density of 4. The hapten SA2, presents a MW of 386.3 Da, and achived a hapten density of 10 follwing the protocol described. Finally, hTB hapten with a MW of 771.94 Da reached a density of 8, meaning that 8 hapten molecules were covalently attached per molecule of BSA.

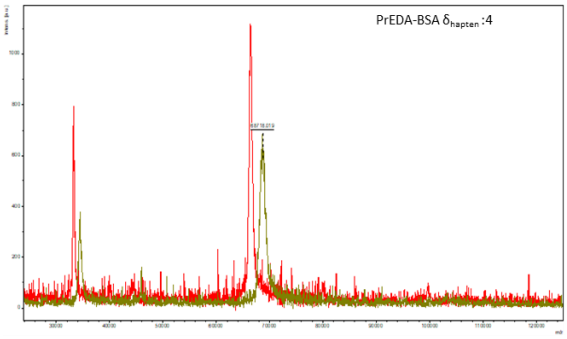

Table 3.3 hapten density of BSA-bioconjugates

Bioconjugate	Batch	Hapten δ
PrEDA-BSA	2	4
SA2-BSA	1	10
hTB-BSA	2	8

Figure 3.3 Representative MALDI-TOF spectra comparing reference BSA and BSA-PrEDA conjugates produced through chemical synthesis and table expressing hapten densities obtained for the rest of bioconjugates.

Using the active ester method, comparable hapten densities were reached for SA2 and hTB bioconjugates with 10 and 8 hapten molecules per BSA protein, respectively. On the contrary, a reduced hapten density was achieved for PrEDA-BSA conjugate, and this can be attributed to the poor solubility of PrEDA hapten in solution, requiring heating conditions to be properly dissolved.

3.3.2. ESTABLISHMENT OF THREE IMMUNOCHEMICAL ELISA PROTOCOLS FOR FLUOROQUINOLONES, SULFONAMIDES AND TYLOSIN DETECTION

An extensive description of the structural characteristics of immunizing haptens and competitors utilized to generate these antibodies can be found in the already published experimental work [2]. Afterwards, the most suitable immobilization concentrations were defined to work at 80 % of saturation while the antibody dilutions were established to reach a maximum signal around 1.5-2 absorbance units under selected conditions. Bearing in mind that the same assay was expected to be implemented in milk samples, this is not assumed as a major inconvenience because skimmed milk and BSA are well known blocking agents and therefore could induce a reduction in the maximum signal due to a blocking effect described in previous reports [10].

The first step towards immunoreagents (haptens + MAb's) characterization consisted on the preparation of individual calibration curves in buffer to assess the recognition of each target analyte. Because of the small MW of the targets, the most suitable assay configuration was an indirect competitive immunoassay format generated by coating the plates with the corresponding hapten-BSA conjugates and incubating them with the analyte and the MAb's to measure dose dependent response. The higher the signal, the lower the concentration of the target in the sample. The dose-response can be fitted to a sigmoidal curve using the four-parameter logistic equation (see Figure 3.4).

Based on previous studies, the SA and TYL immunoreagents were characterized by establishing ELISAs using PBST 10 mM while on the other hand, the FQ immunoreagents were optimized using PBST-Ca^{2+} ($CaCl_2$ 1mM) as assay buffer. Both, the PrEDA hapten and the target FQ analytes are able to chelate divalent cations such as Ca^{2+} [11]. Therefore, the antibodies produced recognize with

higher affinity the hapten structure and the analyte complexed to divalent cations as it was demonstrated by Gonzalez-Pinacho *et al.* [2]. In this regard, the IC_{50} for ERFX (enrofloxacin) in absence of Ca^{2+} was estimated in 3.75 nM and after addition of the divalent cation in the assay buffer diminished to 0.65 nM. Moreover, the incorporation of Ca^{2+} to the buffer was preferred because the assay was addressed to be performed in milk samples where this cation is present at significant higher concentrations (~1-4 mM depending on the method used) [12], than for example is Mg^{+2}, which has been reported to be only 10 % of Ca^{+2} content [13].

In view of the objective of developing a multiplexed platform, it was necessary to set common assay conditions for all three analytes. Therefore, a direct comparison after adding 1mM $CaCl_2$ in the assay buffer was evaluated against standardized conditions in PBST 10mM using the MAb's and hapten conjugates. For this purpose, independent calibration curves were generated in buffer with and without Ca^{2+}, incubated with respective MAb's and afterwards the colorimetric determinations were obtained at each point of the curve and are expressed in the following graph.

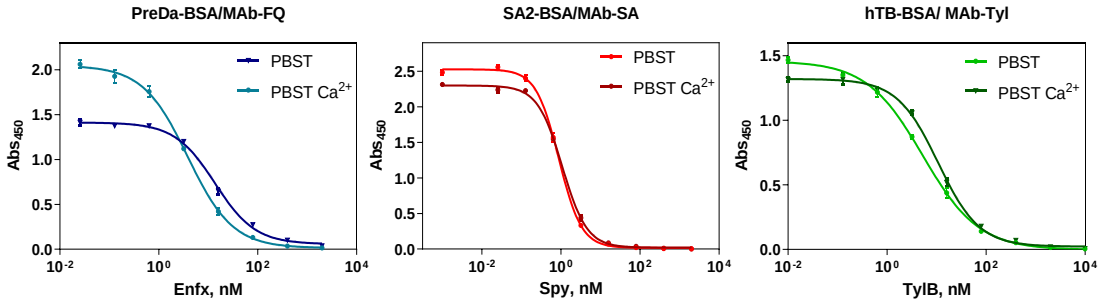

Figure 3.4 Calibration curves of the microplate ELISAs developed against three families of antibiotics selected in absence and presence of 1mM $CaCl_2$.in the assay buffer The results correspond to independent assays peformed on different ELISA microplates against referecne analytes. Each point shown is the average and standard deviation of three well replicates. Results on the analytical parameters are shown in table 3.4 Performance of single-analyte ELISA's in absence and presence of Ca^{2+}.

Table 3.4 Influence of Ca^{2+} in ELISA's analytical performance

Features	FQ ELISA		SA ELISA		TYL ELISA	
Buffer	**PBST**	**PBST Ca^{2+}**	**PBST**	**PBST Ca^{2+}**	**PBST**	**PBST Ca^{2+}**
A_{max}	1.42	2.04	2.52	2.29	1.45	1.32
A_{min}	0.05	0.01	0.01	0.01	0.01	0.02
Slope	-1.06	-0.95	-1.509	-1.38	-0.76	-1.048
IC_{50}[a]	13.73±0.03	3.85±0.03	0.88±0.01	1.08±0.02	5.25±0.03	10.7± 0.02
R^2	0.99	0.99	0.99	0.998	0.99	0.99

[a] concentrations are expressed in µg Kg^{-1}

The previous table, shows the analytical parameters of the three ELISAs developed in PBST and PBST Ca^{2+}, extracted from the logistic equation used to fit the standard curve. The results shown correspond to the average and standard deviation of two different assays. On each assay the standard curve was build using three well-replicates

Based on the results obtained is possible to deduce that only the FQ ELISA is considerably affected by the presence of this cation, improving the A_{max} and slope, which translates in a lower IC_{50} as was previously demonstrated by Pinacho and collaborators [2]. Furthermore, no remarkable differences were observed over the detectability of SA's and TYL assays, although a slight increase over the IC_{50} in the last mentioned can be observed, but this is not assumed as a limitation considering that is still under the MRL. In this regard, the use of PBST Ca^{2+} as a common buffer is encouraged for the multiplexed format without affecting the determination of the other target analytes.

An additional consideration is that through this experimental procedure it was possible to reach comparable detectability to the originally reported using PAb's under indirect competitive ELISA format (see table 3.3). Only with the exception of TYLB determination with the MAb, that in presence of Ca^{2+} displayed an $IC_{50.}$ around 10 µg Kg^{-1} in contrast with the PAb at 1.31 µg Kg^{-1}. On the other hand, the rest of assays showed similar performance and even in most of the cases PAb's reached lower IC_{50} and more robustness in comparison with MAb's as evidenced in Table 3.5.

As a general assumption, MAb's are preferred over PAb's in different fields, attributing standardized production methods, well characterized binding properties and excellent reproducibly in addition to the potential implementation in therapeutic approaches if are humanized. However, for diagnostic applications sometimes the real value of PAb's is underestimated, missing out the importance of clonal and biophysical diversity. These means that PAb's are able to bind to multiple antigenic determinants on the target, increasing sensitivity under some assay formats targeting multiple biological elements (proteins, cells). In addition to this, as PAb's are constituted by a diverse population of antibodies with different biophysical properties, higher stability against restrictive conditions is observed, such as changes in the matrix of analysis, pH's, temperatures or even dealing with target protein mutations that may became undetectable with MAb's against those epitopes [14]. On the other hand, a main drawback is attributed to the limited source of PAb's for long term applications, based on the amount of serum extracted from the immunized animal mostly applicable to mice or rabbits. Alternative solutions propose the immunization of larger animals, like goats or sheep leading to higher yields and being completely functionals under proper storage conditions.

Table 3.5 Comparison of single-analyte ELISA performance using PAb's and MAb's for antibiotics determination

Parameters	**FQ ELISA**		**SA ELISA**		**TYL ELISA**	
Antibody	**PAb's**	**MAb's**	**PAb's**	**MAb's**	**PAb's**	**MAb's**
A_{max}	1.67	2.047	1.07	2.52	1.75	1.459
A_{min}	0.07	0.01	0.04	0.016	0.09	0.01
Slope	-1.08	-0.95	-0.73	-1.509	-0.80	-0.76
IC_{50} [a]	0.35	3.85	2.35	0.88	1.31	5.25
R^2	0.99	0.99	0.99	0.99	0.99	0.99

[a] values are expressed in μg $Kg^{-1.}$ The table compares the analytical parameters of the three ELISAs developed using PAb's and MAb's.The results were extracted from the logistic equation used to fit the standard curve and correspond to the average and standard deviation of two different assays. On each assay the standard curve was build using three well-replicates.

The previous table shows the analytical parameters of the three ELISAs developed using PAb's and MAb's for the same target analytes. Based on the experimental observations from previously discussed PAb's and currently implemented MAb's through ELISA using the same haptens and bioconjugates, is interesting to highlight the similarities achieved in buffer. In terms of A_{max} the MAb's displayed higher signals but this is attributed to the optimization

experiments affected by the amount of reagents or incubation times, while absorbance units around 1 are preferred like is the case of PAb's. Regarding IC_{50} the PAb's evidenced lower detectability but it was still in the range of MAb's for the purpose established. Indistinct use of both types of antibodies is evidencend for quantification of veterinary residues according to this comparative analysis. As additional consideration, PAb's production is much faster and less laborious than MAb's production and this is not a minor aspect in diagnostic tools developments.

3.3.2.1. Matrix effect studies

The remarkable difference between the detectability reached with the assays in buffer and the MRL's values established by the european authorities in cow's milk (TYL's 50 µg Kg^{-1} and 100 µg Kg^{-1} for SA's and FQ's, excepting danofloxacin at 30 µg Kg^{-1}) encouraged the assessment of matrix effect studies. Respecting to this, in some cases the regulatory limits are determined as the sum of two different congeners like ERFX detection considering as marker residues either CIP and ERFX, or for sulfonamides that are restricted to the quantity detected from all the congeners indistinctly [15].

In addition to that, the proposed strategy wanted to detect the presence of these compounds avoiding the need of complex sample pretreatments that could induce time consuming and laborious protocols increasing handling errors in the final assay format. For this reason, several dilutions of commercial milk samples were prepared in PBST Ca^{+2} following the next order: undiluted, 1/2, 1/5, 1/10, 1/20 and independent calibration curves were generated using those dilutions for each analyte.

Interestingly by looking at the Figure 3.5, FQ's assay showed an unexpected response at higher milk dilutions 1/10 and 1/20, where the maximum signal obtained was above the reference calibration curve prepared in buffer. This effect can be attributed to the natural presence of Ca^{2+} ions in the milk that at high dilutions improve the binding between the MAb-FQ and the coating antigen increasing the signal detected, while the assay in buffer was optimized to reach a standard A_{max}. On the other hand, the opposite effect is evidenced at smaller sample dilutions 1/2 or undiluted milk, because the contribution of the matrix as blocking agents is more relevant reducing the maximum signal detected. In this

case, several proteins like albumins or caseins present in the milk at higher concentrations can interfere with the binding of the antibodies to the coating antigens reaching lower A_{max}. Although this hypothesis should be experimentally corroborated, based on the results obtained could explained the phenomena described.

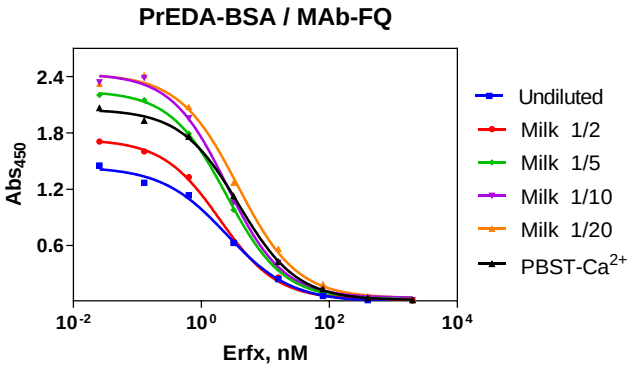

Figure 3.5 Matrix effect of FQ ELISA. Different milk dilutions were assessed by spiking the corresponding samples with ERFX to generate calibrations curves coating the plates with PrEDA-BSA and using MAb-FQ under indirect competitive formats. On each assay the standard curve was build using three well-replicates. The table 3.6 expresses the analytical parameters for each condition evaluated and SD are estimated form replicate wells.

Table 3.6 Analytical parameters of FQ's ELISA at different milk dilutions

ERFX	PBST Ca^{2+}	Undiluted	Milk 1/2	Milk 1/5	Milk 1/10	Milk 1/20
A_{max}	2.05	1.44	1.73	2.25	2.43	2.42
A_{min}	0.01	0.01	0.02	0.03	0.04	0.04
Slope	-0.95	-0.86	-0.96	-0.98	-0.99	-0.94
IC_{50a}	3.83±0.03	2.47±0.05	1.95±0.04	2.71±0.01	2.20±0.03	3.73±0.03
R^2	0.99	0.99	0.99	0.99	0.99	0.99

[a] Concentrations expressed in µg Kg^{-1} The table 3.6 compares the analytical parameters of FQ ELISAs at different milk dilutions in buffer. On each assay the standard curve was build using three well-replicates.

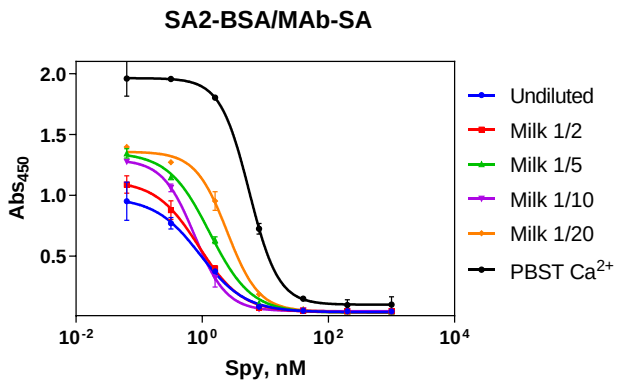

Figure 3.6 Matrix effect of SA ELISA. Different milk dilutions were assessed by spiking the corresponding samples with SPY to generate calibrations curves coating the plates with SA2-BSA and using MAb-SA under indirect competitive formats. On each assay the standard curve was build using three well-replicates. The table 3.7 expresses the analytical parameters for each condition evaluated and SD are estimated form replicate wells.

Table 3.7 Analytical parameters for SA's ELISA at different milk dilutions

SPY	PBST Ca^{2+}	Undiluted	Milk 1/2	Milk 1/5	Milk 1/10	Milk 1/20
A_{max}	1.96	0.98	1.12	1.35	1.29	1.36
A_{min}	0.11	0.04	0.04	0.03	0.05	0.04
Slope	-1.89	-1.212	-1.27	-1.32	-1.71	-1.72
IC_{50}[a]	5.56±0.08	0.93±0.04	0.88±0.02	1.31±0.02	0.75±0.02	2.48±0.02
R^2	0.99	0.98	0.99	0.99	0.99	0.99

[a] Concentrations in µg kg^{-1} The table 3.7 compares the analytical parameters of SA ELISAs at different milk dilutions. On each assay the standard curve was build using three well-replicates.

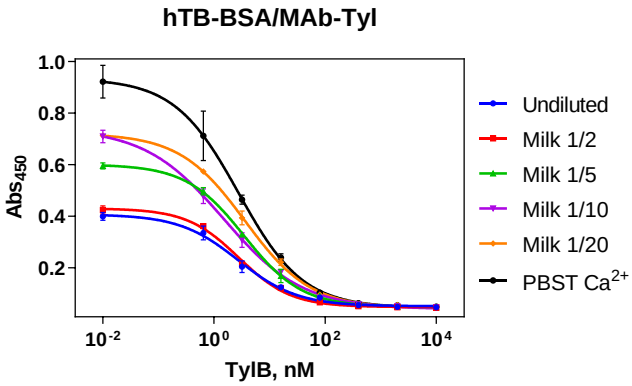

Figure 3.7 Matrix effect of TYL ELISA. Different milk dilutions were assessed by spiking the corresponding samples with TYLB to generate calibrations curves coating the plates with hTB-BSA and using MAb-TYL under indirect competitive formats. On each assay the standard curve was build using three well-replicates. The table 3.8 expresses the analytical parameters for each condition evaluated and SD are estimated form replicate wells.

Table 3.8 Analytical parameters for TYL's ELISA at different milk dilutions

TYLB	PBST Ca^{2+}	Undiluted	Milk 1/2	Milk 1/5	Milk 1/10	Milk 1/20
A_{max}	0.93	0.41	0.43	0.60	0.74	0.72
A_{min}	0.05	0.05	0.04	0.05	0.04	0.04
Slope	-0.75	-0.82	-0.92	-0.84	-0.61	-0.73
IC_{50a}	2.78±0.06	2.73±0.03	2.80±0.02	3.45±0.05	1.48±0.02	3.61±0.06
R^2	0.99	0.99	0.99	0.99	0.99	0.99

[a] Concentrations in µg. Kg^{-1}. The table 3.8 compares the analytical parameters of TYL ELISA's at different milk dilutions. On each assay the standard curve was build using three well-replicates.

On the contrary, for the SA and TYL assays a dilution factor dependence in the signal was observed, demonstrating no considerable interferences in the analytical performance. Although smaller dilutions (undiluted and milk diluted 1/2) generally present lower signal (A_{max}), this is due to the blocking effect already mentioned, attributed to the milk. Remarkably, in most of the cases the IC_{50} remains stable showing that the even without sample pretreatment, assay detectability is not affected. The results obtained across this characterization prove that is possible to work with the corresponding immunoreagents by simply diluting the sample 5 times in the assay buffer and performing the corresponding calibration curve in the same matrix, without additional steps. In all of the cases

the detectability of the assays were significantly below the MRL's established by european authorities.

3.3.2.2. Selectivity studies

Considering the precedents in the group, the development of class-selective antibodies has been a major motivation behind PAb's production with the ability to recognize other structurally related antibiotics with different affinity. Consistently, the MAb's available were also generated as class selective reagents, thus the characterization of the recognition profile against the main congeners was proposed. For this, cross reactivity studies were conducted using as reference the three target analytes (ERFX, SPY and TLYB) and performing the determination of structurally related and non-related compounds (see Table 3.9).

In the case of TYL's assay, cross reactivity was assessed against TYLB and TYLA showing good profile of recognition with higher sensitivity for the precursor TYLA. While penicillin's, FQ's, tetracyclines and SA's were also evaluated without showing cross recognition. On the other hand, for the SA's ELISA, SPY was initially selected as reference analyte but the immunoreagents showed cross recognition for other structurally related compounds like Sulfathiazole, Sulfamethazine, Sulfamerazine, Sulfametoxipirydazine or Sulfadiazine. In fact, the proposed immunoassay was able to selectively discriminate six SA's without presenting cross reactivity for other antibiotic families like TYL's, penicillin's, tetracyclines or FQ's.

Particularly for case of MAb-FQ, a previous characterization has been reported by Tufa *et al*.[1]. Based on these results the corresponding antibody was able to selectively bind to at least eight FQ's evaluated (enrofloxacin, ciprofloxacin, sarafloxacin, difloxacin, ofloxacin, danofloxacin, norfloxacin and marbofloxacin). On the other hand, through this section the specificity determined over SA and TYL assays using MAb's was addressed for the first time. In the following table, the cross-reactivity values obtained for each immunoassay are summarized.

Table 3.9 Cross-reactivity profile for each MAb against structurally related and non-related antibiotic residues

FQ ELISA[a]	IC_{50} [b]	% CR	SA ELISA	IC_{50} [b]	% CR	TYL ELISA	IC_{50} [b]	% CR
Enrofloxacin	**16.3**	**100**	**Sulfapyridine**	**0.28**	**100**	**Tylosin B**	**10.25**	**100**
Ciprofloxacin	**10.3**	**157.9**	**Sulfathiazole**	**5.71**	**5.1**	**Tylosin A**	**1.44**	**1140**
Sarafloxacin	**42**	**38.7**	**Sulfamethazine**	**0.44**	**69.4**	Amoxicillin	-	<1.7
Difloxacin	**41**	**39.7**	**Sulfamerazine**	**0.55**	**54.0**	Ampicillin	-	<1.7
Ofloxacin	**-**	**-**	**Sulfametoxipirydazine**	**0.78**	**40.2**	PenicillinG	-	<1.7
Danofloxacin	**33.9**	**48**	**Sulfadiazine**	**6**	**4.7**	Ciprofloxacin	-	<1.7
Norfloxacin	**32.2**	**74.8**	Tylosine B	-	<0.11	Emrofloxacin	-	<1.7
Marbofloxacin	**21.7**	**50.5**	Tylosin A	-	<0.11	Sarafloxacin	-	<1.7
Tylosin A	-	<0.15	Amoxicillin	-	<0.11	Difloxacin	-	<1.7
Tylosin B	-	<0.15	Ampicillin	-	<0.11	Ofloxacin	-	<1.7
Ampicillin	-	<0.15	Penicillin G	-	<0.11	Danofloxacin	-	<1.7
Penicillin G	-	<0.15	Ciprofloxacin	-	<0.11	Norfloxacin	-	<1.7
Tetracycline	-	<0.15	Emrofloxacin	-	<0.11	Tetracycline	-	<1.7
Sulfapiridine	-	<0.15	Sarafloxacin	-	<0.11	Sulfapiridine	-	<1.7
Sulfathiazole	-	<0.15	Difloxacin	-	<0.11	Sulfathiazole	-	<1.7
Sulfamethazine	-	<0.15	Ofloxacin	-	<0.11	Sulfamethazine	-	<1.7
Sulfamerazine	-	<0.15	Danofloxacin	-	<0.11	Sulfamerazine	-	<1.7
Sulfametoxipirydazine	-	<0.15	Norfloxacin	-	<0.11	Sulfametoxipirydazine	-	<1.7
Sulfadiazine	-	<0.15	Tetracycline	-	<0.11	Sulfadiazine	-	<1.7

[a] FQ's cross reactivity studies were performed by Tufa et al.[1]. [b] represents values expressed in µg kg^{-1}. The values determined are obtained from three replicate wells. Cross-reactivity is expressed as a percent of the IC_{50} (nM) of the reference analyte divided by the IC_{50} (nM) of the other compounds tested.

Remarkably, the use of a single antibody for the determination of multiple congeners with no cross-reactivity towards others species considerably improves the screening capacity of the platform under development. Based on the previous results, the implementation of the already described immunoreagents to the analysis of real samples was encouraged due to the selective recognition demonstrated under ELISA format. In addition, the lack of cross-reactivity evidenced between the main families of antibiotics tested supports their use in multiplexed platforms with potential implementation as screening tools in the

food safety field. To asses this, microarray technology was proposed combining high-throughput performance with miniaturization capacity to allow a relatively easier multiplexation.

3.3.3. ESTABLISHMENT OF SINGLE-ANALYTE MICROARRAY IMMUNOASSAYS FOR FQ', SA'S AND TYL'S

3.3.3.1. Implementation of BSA bioconjugates in monoplexed microarray format

The aim of this section was oriented to assess the influence of the assay format on the detectability and bioanalytical performance of the immunoassays for FQ's, SA's and TYL's. Hence, here we attempt to implement the immunoassays developed on a microarray chip.

On a first instance, three independent microarray chips were developed for each family of antibiotic residues. For this purpose, suitable concentrations of each pair of immunoreagents were selected by performing 2D experiments in which increasing concentrations of each BSA conjugate (solutions 12.5, 25, 50 and 100 µg mL^{-1} in PBS buffer) were spotted on the individual chips with a matrix of 2x5. Subsequently, three concentrations of the corresponding MAb solutions (0.1, 1 and 10 µg mL^{-1}) were tested to select those concentrations that provided a fluorescence response of 15.000-20.000 relative fluorescence units (RFU) while working at conditions around 20 % below saturation.

Main methodological differences among microplate ELISA and microarrays are found on the nature of the support and the chemical approach used to immobilize the bioconjugates. In the first case, 96-well plates consist on flat bottom, solid polystyrene plates that bind the coating antigen through adsorption, mainly due to hydrophobic interactions. On the other hand, for this type of microarray glass slides were used, and a chemical derivatization protocol was required. Methodologically, ELISA's were coated by simply incubating 100 µl of the bioconjugate solution in coating buffer overnight while microarrays require activation of the surface to introduce chemical functional groups suitable for covalently attach the bioconjugates. Drop deposition of the immunoreagents

is performed with the aid of a high-precision robot. Finally, while in ELISA an additional enzymatic reaction takes place due to the use of anti-mouse IgG-HRP, in microarray a fluorescent labelled anti-mouse IgG was necessary, lacking of the signal amplification step. In this case we used tetramethylrhodamine (TRITC) as label

Hence, on a first instance the clean slides were activated with 10 % NaOH to generate a significant number of alkoxy groups, that subsequently were made to react treated with an alkyloxy silane reagent provided of epoxy groups at the other end of the molecules (see Figure 3.8). Due to the ring strain, epoxides are reactive functional groups that in the presence of nucleophiles, such as it could be the amino group of the lysine residues of the proteins, is able to react through the electrophilic C of the C-O bond, resulting in opening of the ring through a S_N2 reaction. Reactive nucleophiles usually attack the less hindered C position providing in this case a secondary alcohol. For this purpose, the bioconjugates are printed with the assistance of the automated micro-spotter as described in the experimental section. Deposition of five drops on every spot (300 pL per drop or a total of 1500 pL per spot) was found to be suitable for the microarray we were attempting to develop. The biofunctionalized slides were kept dry at 4 ºC for at least one night before use. In our hands the biofunctionalized slide were stable and could be used, stored under these conditions.

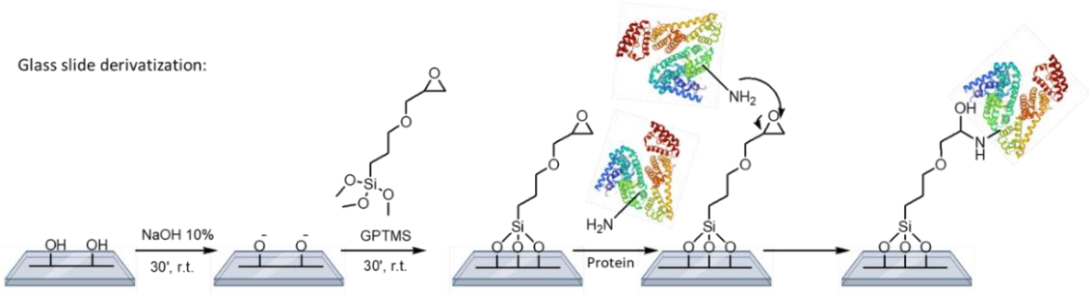

Figure 3.8 Schematic representation of standard derivatization protocol applied over bare glass slides utilizing GPTMS to generate epoxy reactive groups for covalent coupling with BSA conjugates.

The fluorescent immunoassay was performed on top of the slides with the aid of a hardware that defines precise zones for independent sub-microarrays. In our case, the holder configuration consists of 8 rows and 3 columns on a single glass slide, allowing to run several assays in parallel. The individual calibration curves obtained (see Figure 3.9) for each target analyte were assessed in PBST Ca^{2+}. The

microarray chips probed to be robust with very low inter-spot variability (SD <10%), and for this experiment a matrix of 2 x 5 was utilized for each bioconjugate with 10 replicate spots.

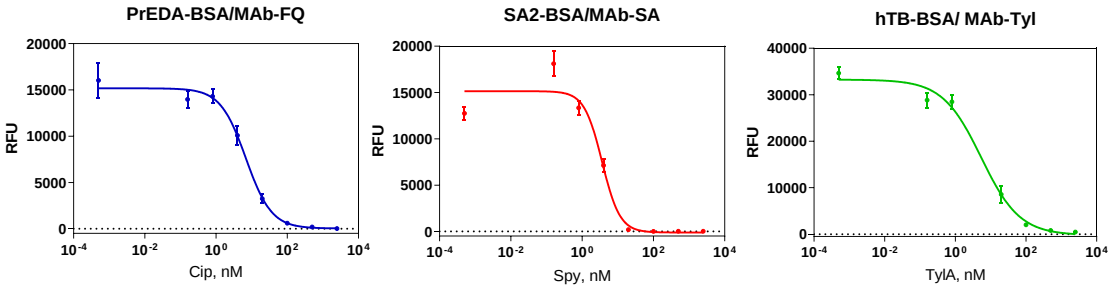

Figure 3.9 Single-analyte indirect competitive microarray. Calibration curves were obtained for single analyte microarray determinations, using a matrix of 2x5 including ten replicate spots of each bioconjugate in independent wells. SD corresponds to single determinations from two different wells.

Table 3.8 Analytical comparison of single-analyte immunoassays under ELISA and microarray format buffer**.**

Target	**FQ's**		**SA's**		**TYL's**	
Assay	Microarray[c]	ELISA	Microarray	ELISA	Microarray	ELISA
S_{max}[b]	15173	2.25	15144	2.60	33255	1.46
S_{min}[b]	32.32	0.02	-115.1	0.03	-228	-0.01
Slope	-1.20	-0.93	-1.73	-1.42	-0.79	-0.77
IC_{50}[a]	6.92±0.07	3.45±0.04	3.64±0.14	0.95±0.02	5.40±0.17	5.21±0.7
R^2	0.99	0.99	0.99	0.998	0.99	0.99

[a] concentration expressed in µg kg^{-1} [b] S, refers to the signal detected with both methods expressed in relative fluorescent units (RFU) for microarray and absorbance units (A) for ELISA-[c] in this experiment CIP was used as representant of the FQ family. The table, shows the analytical parameters of the three immunoassays comparing ELISA and microarray platforms in buffer conditions extracted from the logistic equation employed to fit the standard curve. The results shown correspond to the average and standard deviation of at least two well replicates.

Although both systems exploit optical detection mechanisms, the signal obtained in each case is not strictly comparable due the intrinsic nature of the colorimetric and fluorescent response. However, the analytical features extracted from the logistic equation following an indirect competitive format can be contrasted. Regarding the IC_{50} (assumed as detectability) the differences observed were negligible, despite the lack of the enzymatic amplification in

microarray compared to ELISA. In both cases the determinations achieved for all the analytes where in compliance with the EU regulations in respect to the MRLs established, just for SPY, the IC_{50} reached through ELISA was lower. Slopes were consistent among both assay formats, bearing in mind that specific optimizations were required over each platform, emphasizing on the high reproducibility obtained with the well characterized MAb's. Previous reports from our group also demonstrated that comparable performance to ELISAs was achived with multiplexed protein arrays for environmental pollutants detection [16]. However, the degree of multiplexation provided by microarray technology is considerably higher in contrast with conventional 96-well plate type of assays.

3.3.3.2. Matrix effect of commercial cow's milk in the microarray

Supported by the results obtained in ELISA, the effect of cow's milk in the microarray was assessed only selecting a 1/5 dilution. For this purpose, calibrations curves were prepared for each reference analyte in this matrix and in the assay buffer to then be measured in monoplexed arrays printing 10 replicate spots (2x5 matrix). Comparably to ELISA; the data showed in the Figure 3.10 evidenced that the use of milk during the analysis does not significantly interfere with the microarray detectability or the analytical performance at the dilution selected, thus eliminating the need of sample pretreatment to facilitate the final assay protocol.

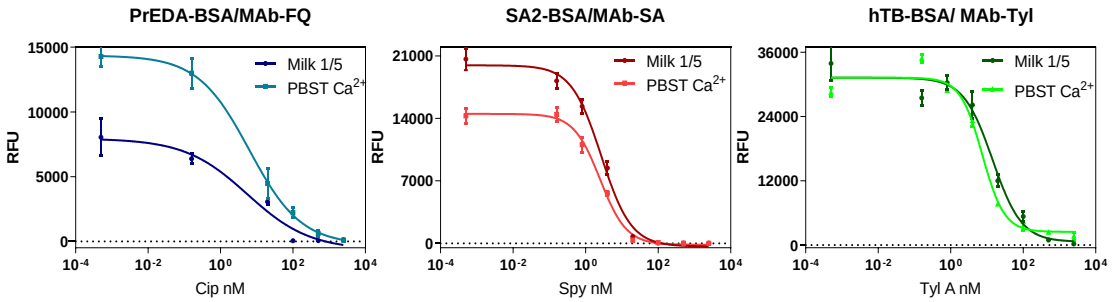

Figure 3.10 Matrix effect studies. Individual calibration curves of the reference target analytes were generated in milk diluted 1/5 and in the assay buffer under microarray configuration. The signals are expressed in relative fluorescence units and standard deviations are estimated from ten replicate spots for each point.

Interestingly, only in the case of FQ's assay, the maximum signal (RFU_{max}) in milk 1/5 was reduced at half to one detected in buffer assuming the blocking capacity

of milk at this dilution, also observed in ELISA. While in the other two examples, the RFU_{max} was similar and even increased in SA's assay. Regarding IC_{50}, in most of the assays remains the same, unless towards the detection of TYLA, that seems to perform better in buffer than in milk. The remarkable aspect is that the array system allows direct detection after sample dilution 1/5 without affecting detectability.

In the following table 3.11, the analytical performance of the assays carried out in ELISA and microarray format in buffer and milk 1/5 conditions are summarized. According to our results, comparable analytical properties were achieved with both immunoassay platforms, encouraging the indistinct use without evidencing variations in the detectability mediated by highly selective antibodies. Although several methodological aspects differ in both approaches, the reagents in common evidenced robust and reproducible behavior validating their use in more complex technological approaches.

Table 3.11 Summary of analytical performances obtained for individual immunoassays under ELISA and microarray format in buffer and milk diluted 1/5.

Assay	**FQ (MAb-FQ/PrEDA-BSA)**				**SA (MAb-SA/SA2-BSA)**				**TYL (MAb-TYL/hTB-BSA)**			
Format	ELISA		Microarray		ELISA		Microarray		ELISA		Microarray	
Matrix	Buffer	Milk[b]	Buffer	Milk[b]	Buffer	Milk[b]	Buffer	Milk[b]	Buffer	Milk[b]	Buffer	Milk[b]
S_{max}[a]	2.05	2.25	14359	7944	2.29	1.35	14662	19946	1.03	0.60	31270	31258
S_{min}	0.01	0.03	-266.3	660.2	0.019	0.03	-158.5	-350.3	0.02	0.047	2477	615.2
Slope	-0.95	-0.98	-0.60	-0.50	-1.38	-1.32	-1.19	-1.05	-1.048	-0.83	-1.42	-1.08
IC_{50}[c]	3.85± 0.03	2.47± 0.01	6.29 ± 0.04	5.52± 0.54	1.08± 0.02	1.31± 0.02	2.5 ± 0.16	2.70± 0.07	10.7± 0.02	3.45± 0.05	7.46± 0.12	14.3± 0.13
R^2	0.99	0.99	0.99	0.97	0.998	0.99	0.99	0.99	0.99	0.99	0.99	0.98

[a] **S_{max}** and **S_{min}** corresponds to the maximum signal expressed in absorbance units for ELISA and RFU for microarray [b] Milk was used diluted 5 times in the assay buffer. [c] the concentration is expressed in μg Kg^{-1}. The results were extracted from the logistic equation used to fit the standard curve and correspond to the average and standard deviation of three replicate wells in ELISA and ten replicate spots in microarray.

Through the comparison showed in the previous table, results interesting to emphasize on the high degree of reproducibility achieved in both immunoassay formats. The next challenges may address the potential implementation of

immunoreagents in a multiplexed configuration using microarray technology. For this reason, the deposition of the three coating antigens in a single matrix was proposed and will be discussed in the following section.

3.3.4. ESTABLISHMENT OF A MULTIPLEXED HAPTEN BIOCONJUGATE MICROARRAY FOR ANTIBIOTIC RESIDUES

In this occasion, a single matrix of 5 columns per 3 rows was generated immobilizing the three bioconjugates in 5 replicate spots, over previously silanized glass slides. As mentioned, one of the key features of microarray technology relies on the possibility to include several spots for analyzing different substances, in this case the three bioconjugates in the same well minimizing sample requirements and independent assay procedures (Figure 3.11). However, one of the main challenges when accomplishing quantitative microarrays is to know the cross-reactivity profile of the individual assays and ensure lack of cooperative phenomena (antibodies of one assay recognizing spots printed with bioconjugates from other assays), to guarantee that the response recorded on each spot is due to the target analytes we want to determine. The cross-reactivity profile of the MAb's was already reported (see table 3.9) and the following experiments described were addressed to demonstrate microarray reliability and the absence of cooperative phenomena.

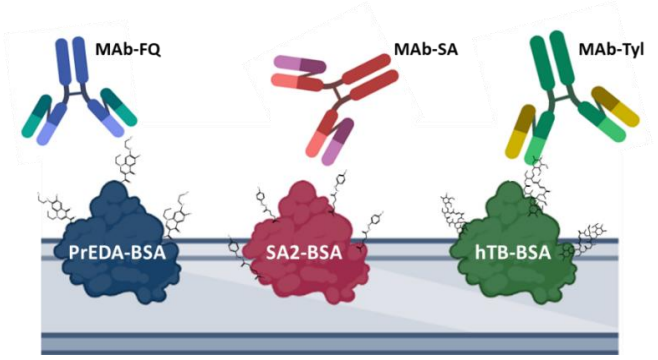

Figure 3.11 Graphic representation of a single well in absence of analyte, where the cocktail of monoclonal antibodies is utilized and each one binds to their corresponding site encoded bioconjugate under multiplexed format.

To ensure absence of interferences caused by the combination of immunoreagents, an experiment was designed in which single-analyte calibration curves prepared in the assay buffer were measured in the microarray but using a "cocktail" of the three MAb's. The same concentration of MAb's employed for the individual assays was used for the mixutre. As can be seen, in Figure 3.12 each assay performed adequately under these conditions, without displaying a significant variation in the analytical parameters of the calibration curve, bearing in mind that in this case all BSA bioconjugates and MAb's were present in the same microarray well. Only the respective MAb's did bind to the corresponding target analyte and bioconjugate competitors, evidencing no shared-reactivity effects. Remarkably, the antibodies against the other analytes present in the cocktail did bound to their corresponding bioconjugate reaching in those spots the maximum signal as is observed in the graphs with CV% values below 15 % in all the cases. In the same figure, the calibration curves obtained under monoplexed conditions (Figure 3.9) are included (in grey) to represent the level of reproducibility achieved either using the reagents separately or combined.

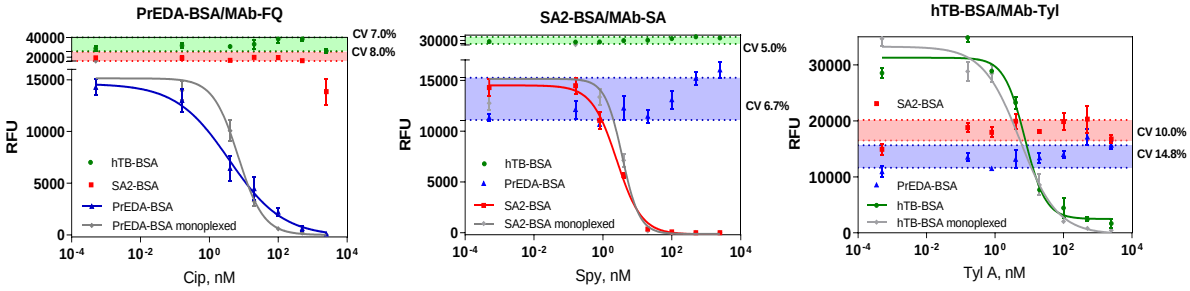

Figure 3.12 Shared reactivity studies. Individual calibration curves were generated utilizing the cocktail of antibodies in the multiplexed array. Each assay calibration curve was performed on a different column of the slide holder. Each point of the data shown in the graphs correspond to 5 replicate-spots inside each microarray chip. For every graph, the curve generated under monoplexed conditions is represented in grey. For non-selective immunoreagents, the CV % is expressed independently.

Table 3.12 Analytical parameters obtained for three analytes under multiplexed conditions in assay buffer

Multiplexed	FQ	SA	TYL
RFU_{max}	14625	14504	31270
RFU_{min}	-134	-158.5	2477
Slope	-0.56	-1.194	-1.42
IC_{50}[a]	3.79	2.51	7.47
R^2	0.99	0.94	0.98
CV % PrEDA	-	8.7	14.8
CV % SA2	8.0	-	10.0
CV % hTB	7.0	6.0	-

[a] Concentration expressed in µg kg^{-1} The results were extracted from the logistic equation used to fit the standard curve and correspond to the average and standard deviation of ten replicate spots in microarray.

In agreement with the data showed in table 3.12 the maximum signals (RFU_{max}) obtained were around 15.000 RFU's for the case of CIP and SPY determination and 30.000 RFU's in TYLB assay. In TYL's assay, almost the same intensity values were observed among different assessed conditions like individual assay format, individual assay in milk diluted 1/5 and finally in the multiplexed approach, evidencing a robust response. Considering the IC_{50} values, the three immunoassays reached sufficient detectability, being comparable to the ones obtained under individual assay conditions, and no remarkable differences were attributed to the incorporation of the three immunoreagents in the same well.

After this study, a successful integration of the three bioconjugates in a single matrix using the cocktail of antibodies was demonstrated, validating the multiplexing capacity of the system. From this result, is possible to ensure that the reagents perform comparably under ELISA and microarray format, with the potential of multiplexation in the last mentioned. At this point it is also expected that the insignificant cross-reactivity evidenced in ELISA is also maintained under the array format. Throughout the work performed in this section, the use of the well characterized immunoreagents is strongly suggested for reliable and robust immunochemical developments in the frame of food safety applications.

Taking a look at the literature available, a comparable system consisting on a multiplexed colorimetric 96-well plate array for the determination of quinolones, tetracycline, lincomycin and streptomycin antibiotics in milk was reported [17]. In this case, a commercial test kit was utilized to evaluate simultaneous quantification of the target analytes, due to the similarities with standard ELISA

conditions and the benefit of multiplexed arrays in well plate. Compared to our system, an indirect competitive format is also employed mainly, differing on the target analytes identified, only sharing FQ's detection with similar limits of quantification (LOQ's) between 8 and 11 μg Kg^{-1}, slightly above the values detected with our microarray. The main limitation compared to our platform is found on the need of milk sample pre-treatment with trichloroacetic acid and centrifugation prior veterinary residues determination. This can lead to increase handling errors and extend analysis periods during the screening of several samples. Moreover, the authors evaluate the selectivity of the method against only 6 non-structurally related compounds, but never demonstrate class selectivity of the immunoreagents towards the family of antibiotics apart from the ones used as reference.

Alternatively, an aptasensor was proposed for selective detection of three veterinary residues by fluorescence resonance energy transfer (FRET) strategy using DNase I-assisted cyclic enzymatic signal amplification (CESA) [18]. In this case, selective aptamers were immobilized over graphene oxide substrates to target sulfadimethoxine, kanamycin, and ampicillin reaching LOD's around 2 μg Kg^{-1}, assuming comparable performance to our array. However, during the experimental procedure a sample pre-treatment through extraction with ethyl acetate was necessary, also a step of centrifugation and incubation at 37^{o}C were described, highlighting the user-friendly protocol achieved in our determination. Besides, three different fluorophores were conjugated to the aptamers for multiplexed identification (Cy3, FAM, and Cy5) requiring a more complex detection system able to distinguish three wavelengths, instead of site-encode the signal to a discrete spot as was proposed in our case utilizing a single fluorophore as common label during the signal acquisition.

Recently, another report proposed the use of suspension array platform constituted by agarose-silica microbeads functionalized with BSA bioconjugates (coating antigens) to determine four antibiotics (chloramphenicol, sulfamethoxazole, metronidazole and amoxicillin) [19]**.** Comparably, an indirect competitive assay format was selected and in presence of the target the antibodies were not bound to the microbeads, while in absence of analyte, the antibodies were interacting with the coating antigen in the particles. After the addition of a secondary MAb fluorescently labeled, each microbead population was identified by a characteristic reflection peak reaching limits of detection

between 0.9 to 0.8 ng mL^{-1} and exhibiting good linear ranges in tap water. Selectivity studies revealed CR% against ampicillin (26 %) and tinidazole (37 %) and in contrast with our system, were not implemented in milk samples attributing a potential interference of the matrix obstructing the cavities on the microbeads that may lead to considerable signal reductions.

As discussed, the multiplexation capacity over the BSA-hapten microarray make this approach more competitive than conventional ELISA, reaching comparable performance. The possibility to detect three analytes in the same well is pointed out as a significant advantage in the development of screening platforms. Nevertheless, a critical aspect working with protein arrays is found on large scale manufacturing conditions, concerning to protein stability and functionalization conditions as well as increased batch to batch variations. On the other hand, protein microarrays are usually more expensive than DNA arrays, considering laborious recombinant protein production [20]. Although the surface chemistry was not assumed as a limiting factor due to the use of BSA as common support for the haptens, the final aim of this project intended to develop a portable iSPR system. Owing to this, no further analytical characterization was considered for the multiplexed protein array and instead the utilization of a DNA directed immobilization (DDI) strategy was suggested to allow surface regeneration with the SPR biosensor. As a preliminary step, in the following chapter a DDI microarray platform was explored for the multiplexed detection of antibiotic residues under indirect competitive assay format with the aim of characterizing the reagents performance in a reference system for the transition to the portable iSPR device in a straightforward manner discussed in chapter 5.

3.4. CHAPTER CONTRIBUTIONS

- The comparative study of the analytical performance of polyclonal and monoclonal antibodies targeting antibiotic residues revealed similar outcomes and slightly improved polyclonal detectability in an indirect competitive ELISA format.
- The incorporation of Ca^{2+} ions to the assay buffer notably improved FQ's detection without affecting the analytical features of the other immunoassays.

- ELISA and microarray proven to be highly compatible immunochemical platforms allowing straightforward transition of single-analyte colorimetric detection in 96-well plates to multiplexed fluorescent readout with microscope glass slides in the second case, without compromising assay detectability in buffer and in milk diluted.
- The hapten-BSA microarray showed equivalent performance either designed as a singleplex or multiplex chip, increasing throughput capacity for screening purposes. In addition, the lack of cross interaction demonstrated between immunoreagents could allow the recognition of the 16 congeners evaluated in a single sample.

3.5. MATERIALS AND METHODS

3.5.1. REAGENTS, MATERIALS AND EQUIPMENT.

The immunoreagents utilized in this work for SA's, FQ's and TYL's detection were produced in our facilities and some of them have been already described in previous reports [1, 9]. In the case of TYL immunoreagents, will be published elsewhere. The preparation of the bioconjugate competitors (hapten-BSA, hapten density 8-10) and the production of MAb's has been performed with the support of the U2 of the ICTS "NANBIOSIS", more specifically by the Custom Antibody Service (CAbS, CIBER-BBN, IQAC-CSIC). The rest of immunochemical reagents were purchased at Sigma-Aldrich (St. Louis, MO, USA). N,N'-Dicyclohexylcarbodiimide 99% (DCC) and N-hydroxysuccinimide (NHS) were purchased from Sigma- Aldrich (St. Louis, MO, USA) and the working aliquots were prepared in anhydrous DMF (dimthylformamide). DMP (dimethyl pimelimidate) crosslinker was acquired from Sigma Aldrich.

The target analytes under study, Sulfapyridine (SPY) Sulfatiazole (STZ), Sulfametoxypiridazine (SMPZ), Sulfamerazine (SRZ), Sulfamethazine (SMT), Sulfadiazine (SDZ), Enrofloxacin (ERFX), Ofloxacin (OFX), Ciprofloxacin (CPX), Sarafloxacin (SFX), Danofloxacin (DNFX), Difloxacin (DFX), Norfloxacin (NFX), Marbofloxacin (MFX), Tylosin A (TYLA), Tylosin B (TYLB) were delivered from Sigma-Aldrich and Honeywell. SA's and TYL's stock solutions were prepared at 10 mM concentration in DMSO, but quinolones were dissolved in 0.1M NaOH. All of them, stored at 4^{o}C for a maximum period of one month.

Commercial milk samples from "Letona" (Barcelona, Spain) were lyophilized (LyoQuest, Telstar) and stored at -40^{o}C, once needed were resuspended with H_2O ultrapure and stirred at 37^{o}C, considering density of 124.8 g/L.

The matrix-assisted laser desorption ionization time-of-flight mass spectrometer (MALDI-TOF-MS) was a Bruker autoflex III Smartbeam spectrometer (Billerica, Massachusetts). Polystyrene microtiter plates were purchased from Nunc (Maxisorp, Roskilde, Denmark). Dilution plates were purchased from Nirco (Barberà del Vallés, Spain). Washing steps were performed on a Biotek ELx405 (Biotek Inc.). Absorbances were read on Multiskan™ GO Microplate

Spectrophotometer (Thermo Scientific™, Massachusetts, USA). Competitive curves were analyzed with a four-parameter logistic equation using GraphPad Prism 7.03 (GraphPad Software Inc., San Diego, CA, USA).

3.5.2. BUFFERS AND EQUIPMENT.

Unless otherwise indicated, phosphate buffer saline (PBS) was 0.01 M phosphate buffer (1.48 mM KH_2PO_4 and 8.3 mM Na_2HPO_4) in a 0.8% saline solution (137 mmol/L NaCl, 2.7 mmol/L KCl), at pH 7.5. PBST is PBS previously described with 0.05% Tween 20. The solution of PBST-Ca^{2+} corresponds to a 10mM PBST pH 7.5 solution that contains 1mM $CaCl_2$. Borate buffer is 0.2 M boric acid/sodium borate, pH 8.7. Coating buffer is a 0.05 M carbonate-bicarbonate buffer pH 9.6. Citrate buffer is 0.04 M sodium citrate, pH 5.5. The pH and the conductivity of all buffers and solutions were measured with a pH-meter pH 540 GLP and a conductimeter LF 340, respectively (WTW, Weilheim, Germany).

3.5.3. PREDA-BSA, SA2-BSA, HTB-BSA BIOCONJUGATES PREPARATION

3.5.3.1. SA2-BSA, hTB-BSA conjugation. Active ester method

Each hapten (10 µmols SA2 and hTB) were dissolved in 100 µL DMF anh. A solution of N, N'-dicyclohexylcarbodiimide (DCC) (50 µmols) in 50 µL DMF and a solution of N-hydroxysuccinimide (NHS) (25 µmols) in 60 µL DMF were added sequentially. The mixture was stirred for 3 hours for each case, or until a white precipitate appeared. The suspension was centrifuged at 10000 rpm for 10 min. The supernatant was added dropwise to a solution of 10 mg of albumin from bovine serum (BSA) in 1.8 mL borate buffer. The reaction mixture was gently stirred for 4 hours at room temperature and kept O.N. at 4^{o}C.

3.5.3.2. PrEDA-BSA conjugation. DMP method

For the preparation of the other bioconjugate, the BSA (10 mg) was dissolved in 1mL 0.2 M sodium borate pH 8.6. In parallel, PrEDA hapten (2.5 mg) and DMP (2 mg) were dissolved in hot anhydrous DMF (100 µL) and 0.5 mL 0.2 M sodium borate pH 8.6, respectively. At the same time, 100 µL of PrEDA and 40 µL of DMP solutions were added immediately to the dissolved BSA. The whole mixture was stirred overnight at room temperature.

The following day, the bioconjugates were purified by dialysis using Spectra/Por membranes from Spectrumlabs (Piraeus, Greece, EU) with molecular weight cut-off of 12-14 kDa. Starting with 0.5 mM PBS (4 × 5 L) and ultrapure water (1 × 5 L) then frozen at -80^{o}C and lyophilized (Telstar, LyoQuest). If not indicated, working aliquots were stored at 4 °C in 10 mM PBS at 1 mg mL^{-1}. For the characterization of the conjugate's, matrix-assisted laser desorption ionization time-of-flight (MALDI-TOF) was used on the products of reaction. MALDI spectra were obtained by mixing 2 µL of the freshly prepared matrix (trans-3,5-dimethoxy-4-hydroxycinnamic acid, 10 mg mL^{-1} in ACN/H_2O 70:30, 0.1% TFA) with 2 µL of a solution of the conjugates or proteins (10 mg mL^{-1} in ACN/H_2O 70:30, 0.1% TFA). The hapten densities (δ hapten) were calculated according to the following equation: [MW(conjugate)-MW(protein)]/MW(hapten).

3.5.4. TITRATION ASSAYS

The optimum concentrations of coating antigens (PrEDA-BSA, SA2-BSA and hTB-BSA) and MAb's were evaluated. Initially, two-dimensional titration assays (2D-assay) were carried out assessing several dilutions of coating antigens in the plate (1 µg mL^{-1} to 0.01 µg mL^{-1} , and zero in coating buffer; 100 µL $well^{-1}$) with serial dilutions of the MAb (by 1/2 dilutions starting at 1µg mL^{-1} to 0.015 µg mL^{-1} and zero for TYL's, FQ's, SA's assay in PBST Ca^{2+} and PBST) . From these experiments, optimum concentrations for coating antigens and MAb's dilutions were chosen to obtain maximum signals around 1-1.8 units of absorbance.

3.5.5. ELISA ASSAYS FOR FQ, SA AND TYL

Three individual indirect competitive immunoassays were developed for the determination of ERFX, SPY and TYL B. Initially, the microtiter well plates were coated with PrEDA-BSA (0.5 μg mL^{-1}), hTB-BSA (0.0625 μg mL^{-1}) and SA2-BSA (0.125 μg mL^{-1}) in coating buffer (100 μl/well), incubated overnight 4ºC. The following day, the microplates were washed four times with 300 μL/well of PBST. Then, calibration curves for each analyte were prepared from 5 μM to 0.5 nM after 1/5 dilutions, in PBST and PBST-Ca^{2+} for the three analytes. After a washing step, 100 μl of a solution of anti-mouse IgG HRP (1/6000) in PBST was added and left for 30 min. The next step consisted on the addition 100μl of the substrate solution (citrate solution, 0.0004% H_2O_2 and 0. 375 μg mL^{-1} TMB) covered from light for 30 min. Finally, 50 μl of 4M H_2SO_4 per well was used to stop colorimetric reaction on each well and absorbance was measured at 450nm. The standard curves were fitted to a four-parameter equation according to the formula: Y = [(A - B)/1 -(x/C)D̂] + B, where A is the maximal absorbance, B is the minimum absorbance, C is the concentration producing 50% of the maximal absorbance, and D is the slope at the inflection point of the sigmoid curve.

3.5.5.1. Specificity studies

Stock solutions of the veterinary residues assessed were prepared at 10mM concentration. Then, the stocks were utilized to prepare calibration curves in the range of from 5 μM to 0.5 nM in buffer, for subsequently addition in the coated well plates. The same protocol established for each target antibiotic (EFX, SPY and TYLB) in ELISA was individually performed incubating the different analytes prepared in the calibration curves. Three replicate wells were utilized for each curve dilution and the average intensity of the three wells plotted. Taking as reference the calibration curve corresponding to the analyte initially selected as reference target. The cross-reactivity (CR) values were calculated according to the following equation: IC_{50} [nM] (Reference analyte)/ IC_{50} [nM] (cross-reactant) × 100 through ELISA.

The analytes evaluated in this study were, Sulfapyridine (SPY) Sulfatiazole (STZ), Sulfametoxypiridazine (SMPZ), Sulfamerazine (SRZ), Sulfamethazine (SMT), Sulfadiazine (SDZ), Enrofloxacin (ERFX), Ofloxacin (OFX), Ciprofloxacin (CPX),

Sarafloxacin (SFX), Danofloxacin (DNFX), Difloxacin (DFX), Norfloxacin (NFX), Marbofloxacin (MFX), Tylosin A (TYLA), Tylosin B (TYLB). And other non-strucutrally related compounds like Ampicillin, Amoxicillin, Penicillin G or Tetracycline.

3.5.5.2. Matrix effect studies

Lyophilized commercial milk samples "La letona" were resuspended in assay buffer according to the density expressed by producers (124.8 g/L.). In order to evaluate such effect, calibration curves (from 5 µM to 0.5 nM of reference target analytes) were prepared at different milk dilutions in PBST Ca^{2+} (1/1, 1/2, 1/5, 1/10 and 1/20) and the respective assays were carried out under the already mentioned conditions for ELISA determination in buffer of the same analytes. After quantification, each dilution factor generates a sigmoidal curve that was plotted in a single graph to evidence contribution of matrix content in the detectability of the assay.

3.5.6. MULTIPLXED FLUORESCENT PROTEIN MICROARRAY

3.5.6.1. Immunoarray printing

Microscope slides (75 × 25 mm) were purchased from Corning Inc (Corning, NY, USA). A derivatization protocol to functionalize the glass surface with epoxy groups was carried out and was already reported in previous works from our group [16]. The BSA conjugates were spotted onto the glass slides. Spotting concentration: PrEDA-BSA 50 µg mL^{-1}, SA2-BSA 100 µg mL^{-1} and hTB-BSA 12.5 µg mL^{-1} in printing buffer. The printing was performed using an automated piezo-driven SciflexArrayer S3 (Scienion AG, Berlin, Germany). A piezo dispense capillary (PDC) 70 type 4 was employed, the voltage was set at 82V and the pulse width 49µs. 5 drops of 350pL were deposited per spot and the temperature set at 25^{o}C with humidity at 60%, allowing slides to dry for 1 hour after printing process in the spotting chamber and then kept at 4^{o}C until use for a maximum of five days. For the monoplexed conditions, matrix used as 2x5 for 10 replicate spots. For the assessment of the cooperative phenomena the matrix employed

was 5x3 array (five spots per row, and a single row per conjugate, with a total of 5 replicate spots) following the dimensions to fit with the ArrayIt® holder (Arrayit Corp, Sunnyvale, CA, USA) utilized for the assays that generates 24 independent arrays in a single slide.

3.5.6.2. Microarray signal acquisition

Microarray measurements were acquired on a Two-Color Microarray Scanner InnoScan 710 (Innopsys, Carbonne, France) with an optical filter with 10-µm resolution. The laser power and photomultiplier tube (PMT) gain were set to 95% and 80%, respectively. The spots were measured by deducting the mean TRITC background intensity to the mean of TRITC foreground intensity using Mapix - Microarray image acquisition and analysis software (Innopsys, Carbonne, France). Calibration Curves are obtained from the RFU (Relative Fluorescence Units) generated in each group of spots (Average of at least 3, replicate spot) for a defined analyte. The curves were analyzed using the software GraphPad Prism v 6 (GraphPad Software Inc., San Diego, CA, USA). The standard curves were fitted to a four-parameter equation according to the following formula: $Y = [(A-B)/1-(x/C).D] + B$, where A is the maximal fluorescence, B the minimum fluorescence, C the concentration producing 50% of the difference between A and B (or IC_{50}), and D the slope at the inflection point of the sigmoid curve. The limit of detection (LOD) was defined as the concentration producing 90% of the maximal fluorescence (IC_{90}).

3.5.6.3. Individual microarray based on BSA-conjugates:

Indirect competitive assays were proposed for the individual quantification of selected target antibiotic residues, calibrations curves in PBST Ca^{2+}, and dilutions of reconstituted milk samples in the same buffer (1/5) were generated in a range of 0.5 nM to 5 µM. Matrix containing 10 replicate spots of the same bioconjugate were applied in separate sub-arrays in a 2x5 distribution (PrEDA-BSA 100 µg mL^{-1}, SA2-BSA 50 µg mL^{-1}, hTB-BSA 12.5 µg mL^{-1}). Once spotted, the slides are dry at room temperature for 1 hour and then stored at 4º O.N. The following day, the slides mounted in the ArrayIt holder and washed with PBST 10mM three times. Then were incubated with the analyte in buffer and in milk diluted 1/5 in PBST-Ca^{2+}, together with the corresponding MAb's (MAb-FQ 1 µg mL^{-1}, MAb-SA 1 µg

mL^{-1}; MAb-Tyl 0.75 µg mL^{-1} in PBST Ca^{2+}). After 30 minutes, an additional washing step was performed and the array was incubated with a secondary antibody labeled Anti-IgG-TRITC (Abcam) 1/250 in PBST 10mM buffer. A final wash with 10mM PBST and MiliQ H_2O was carried out and slides were dried with N_2 stream to be processed in the fluorescent scanner.

3.5.6.4. Multiplexed microarray based on BSA-conjugates

For this purpose, the matrix chip designed was composed of 5 columns per 3rows, and the row 1 was spotted with PrEDA-BSA, the row 2 with SA2-BSA and remaining 3 with hTB-BSA to define the spatial distribution of the spots at the same concentrations optimized for individual arrays. Once printed and dry, calibration curves were prepared in PBST Ca^{2+} buffer ranging from 0.5nM to 5µM of target analyte, and incubated with the "cockatil" of Mab's. The cocktail of MAbs corresponds to the combination of the three antibodies at the concentrations already established for individual assays (MAb-FQ 1 µg mL^{-1}, MAb-SA 1 µg mL^{-1}; MAb-Tyl 0.75 µg mL^{-1} in PBST Ca^{2+}). The subsequent steps were identical to the already mentioned in the protocol for individual determinations.

3.6. BIBLIOGRAPHY

1. Tufa, R.A., et al., *Development and validation of an enzyme linked immunosorbent assay for fluoroquinolones in animal feeds.* Food Control, 2015. **57**: p. 195-201.
2. Pinacho, D.G., F. Sanchez-Baeza, and M.-P. Marco, *Molecular modeling assisted hapten design to produce broad selectivity antibodies for fluoroquinolone antibiotics.* Analytical chemistry, 2012. **84**(10): p. 4527-4534.
3. Adrian, J., et al., *Generation of broad specificity antibodies for sulfonamide antibiotics and development of an enzyme-linked immunosorbent assay (ELISA) for the analysis of milk samples.* Journal of Agricultural and Food Chemistry, 2009. **57**(2): p. 385-394.
4. Font, H., et al., *Immunochemical assays for direct sulfonamide antibiotic detection in milk and hair samples using antibody derivatized magnetic nanoparticles.* Journal of agricultural and food chemistry, 2008. **56**(3): p. 736-743.
5. Fernandez, F., et al., *Portable surface plasmon resonance immunosensor for the detection of fluoroquinolone antibiotic residues in milk.* Journal of agricultural and food chemistry, 2011. **59**(9): p. 5036-5043.
6. Adrian, J., et al., *Wavelength-interrogated optical biosensor for multi-analyte screening of sulfonamide, fluoroquinolone, β-lactam and tetracycline antibiotics in milk.* TrAC Trends in Analytical Chemistry, 2009. **28**(6): p. 769-777.
7. Conzuelo, F., et al., *Integrated disposable electrochemical immunosensors for the simultaneous determination of sulfonamide and tetracycline antibiotics residues in milk.* Biosensors and Bioelectronics, 2013. **50**: p. 100-105.
8. Conzuelo, F., et al., *Disposable and integrated amperometric immunosensor for direct determination of sulfonamide antibiotics in milk.* Biosensors and Bioelectronics, 2012. **36**(1): p. 81-88.
9. Jimenez, V., et al., *Validation of an enzyme-linked immunosorbent assay for detecting sulfonamides in feed resources.* Journal of agricultural and food chemistry, 2010. **58**(13): p. 7526-7531.
10. Xiao, Y. and S.N. Isaacs, *Enzyme-linked immunosorbent assay (ELISA) and blocking with bovine serum albumin (BSA)—not all BSAs are alike.* Journal of immunological methods, 2012. **384**(1-2): p. 148-151.
11. Cuprys, A., et al., *Fluoroquinolones metal complexation and its environmental impacts.* Coordination Chemistry Reviews, 2018. **376**: p. 46-61.
12. Tsioulpas, A., M.J. Lewis, and A.S. Grandison, *Effect of minerals on casein micelle stability of cows' milk.* Journal of Dairy Research, 2007. **74**(2): p. 167-173.
13. On-Nom, N., A. Grandison, and M. Lewis, *Measurement of ionic calcium, pH, and soluble divalent cations in milk at high temperature.* Journal of Dairy Science, 2010. **93**(2): p. 515-523.
14. Ascoli, C.A. and B. Aggeler, *Overlooked benefits of using polyclonal antibodies.* Biotechniques, 2018. **65**(3): p. 127-136.
15. Commission, E., *Commission Regulation (EU) No 37/2010 of 22 December 2009 on pharmacologically active substances and their classification regarding*

maximum residue limits in foodstuffs of animal origin. Off J Eur Union, 2010. **15**(2377): p. 1-72.

16. Sanchis, A., et al., *Fluorescent microarray for multiplexed quantification of environmental contaminants in seawater samples.* Talanta, 2018. **184**: p. 499-506.
17. Du, B., et al., *Evaluation of an ELISA-based visualization microarray chip technique for the detection of veterinary antibiotics in milk.* Food Control, 2019. **106**: p. 106713.
18. Youn, H., et al., *Aptasensor for multiplex detection of antibiotics based on FRET strategy combined with aptamer/graphene oxide complex.* Scientific reports, 2019. **9**(1): p. 7659.
19. Wang, X., et al., *Sensitive and multiplexed detection of antibiotics using a suspension array platform based on silica-agarose hybrid microbeads.* Journal of hazardous materials, 2019. **373**: p. 115-121.
20. Syu, G.-D., J. Dunn, and H. Zhu, *Developments and applications of functional protein microarrays.* Molecular & Cellular Proteomics, 2020. **19**(6): p. 916-927.

4 A MULTIPLEXED SITE ENCODED MICROARRAY FOR SCREENING OF VETERINARY RESIDUES IN COW'S MILK DEVELOPED BY DNA-DIRECTED IMMOBILIZATION (DDI)

4.1. SUMMARY

In the following chapter the implementation of the previously characterized immunoreagents through ELISA and protein microarray (see section 3.3) is proposed utilizing DNA-directed immobilization (DDI) strategies to generate a multiplexed and high-throughput DDI microarray platform. The motivation behind this experimental section aims to corroborate the adequate performance of the immunoassay under the innovative DDI configuration to translate the experience in microarray format to a portable iSPR system integrating smartphone detection. For this purpose, the initial steps consisted on the haptens conjugation to oligonucleotide strands, to then explore the analytical performance in an indirect competitive assay format for the detection of FQ's, SA's and TYL's in cow's milk. Moreover, the fluorescent DDI microarray can be considered as a relevant screening tool in the food safety field reaching adequate analytical performance under EU regulatory guidelines.

4.2. DNA DIRECTED IMMOBILIZATION (DDI)

4.2.1.1. Literature on DDI and potential applications

A great number of experimental approaches making use of DDI are available in the literature mainly implemented as alternative immobilization strategies for ligands such as antibodies, enzymes, glycans or even nanoparticles. In the following scheme some of the already described systems are represented evidencing the universal application of oligonucleotide driven immobilization techniques to multiple purposes (see Figure 4.1).

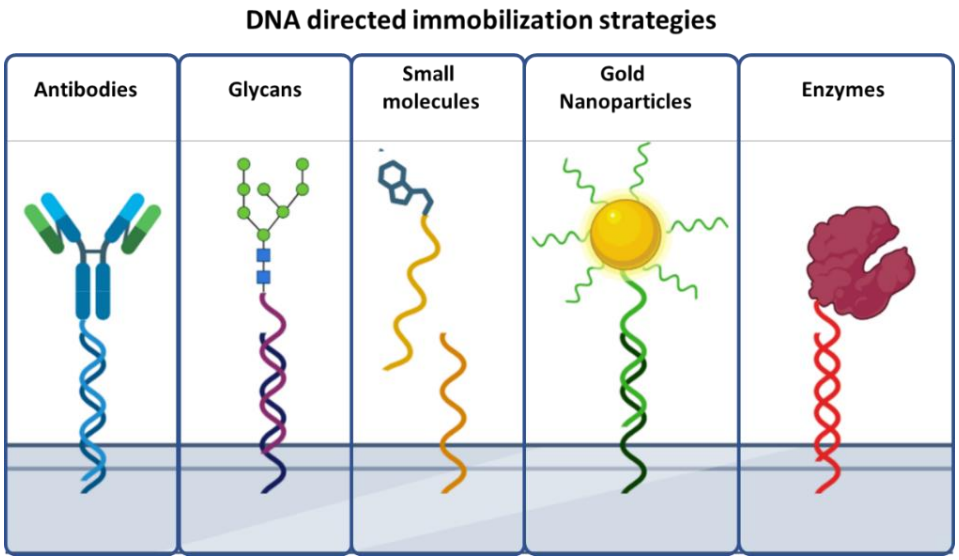

Figure 4.1 Schematic representation of the most commonly reported probes making use of DDI across the literature. From left to right, antibodies, glycans, small molecules, nanoparticles and enzymes are found.

Conventional applications employ oligonucleotide coupled antibodies to provide specific ligand orientation and enhance active binding sites available to even create regenerable surfaces. An interesting example, propose the use of DDI under microarray format to conjugate oligonucleotides with antibodies for extracellular vesicles (EV) detection [1]. In addition, a standard coupling protocol and a silicon immobilization procedure are detailed in the manuscript demonstrating the use of DDI-antibody microarrays to detect these novel biomarkers. In a different proposal, DDI was used to functionalized polydopamine magnetic nanoparticles with trypsin, in order to evaluate enzymatic performance after several uses as well as potential regeneration. The authors state that trypsin preserves up to 55 % of initial activity after 70 cycles of regeneration also showing almost 5 times more specificity than free enzyme immobilized. In agreement with these findings, the use of DDI seems to be promising towards the reusability of reagents in systems exploiting regeneration conditions [2].

In another report, the modular activity of DNA biohybrid molecules was explored by the generation of DNA–protein (or gatekeeper) conjugates that were selectively cleaved by matrix metalloproteases (MMPs) for cargo release (Figure

4.2). These protein-DNA constructs were immobilized on top of mesoporous silica nanoparticles (MSN) through DDI and at the same time, the nanoparticles were directed using a different oligonucleotide onto a solid support acting as substrates for cell adhesion. Once the MMPs were present, the selective release MSN-bound gatekeeper proteins and the encapsulated cargo peptide occurs [3]. This approach extends the use of DDI for drug delivery, tissue engineering or distinct biomedical applications rather than exclusive biofunctionalization.

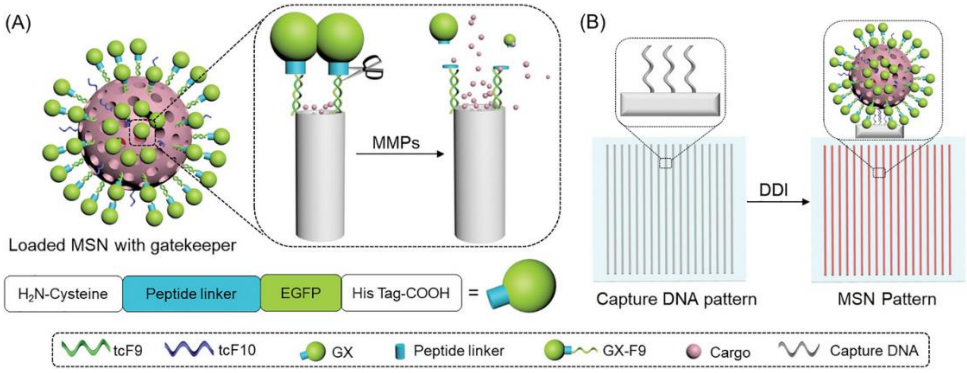

Figure 4.2 Schematic illustration of MSNs bearing DNA–protein conjugates as A) a proteinase-responsive gatekeeper and B) the DNA-directed immobilization (DDI) of MSNs. The gatekeeper is bound on the MSN surface by one of two orthogonal DNA sequences (green), while the other (blue) one can be used for DDI of the MSN construct on surfaces patterned with complementary capture oligonucleotides. The scheme below (A) indicates the design of the recombinant gatekeeper protein. Reprinted from [3].

In addition to this, the multiplexation capacity behind DDI relies on the correct design of the oligonucleotide sequences, to minimize cross-reactivity during simultaneous hybridization reactions. An interesting application report the use of photolithography and DDI immobilization for the multiplexed discrimination of cell subpopulations using selective antibodies conjugated to oligonucleotides. Through this approach two applications are described, the first reported for cell line separation and the second consisting on the immobilization of three antibodies against E-cadherin, N-cadherin, and β-integrin to perform label-free screening of three breast epithelial cells types based on surface markers [4]. As can be seen, multiplexed determinations are feasible with the application of DDI technology. Moreover, the use of multi-parametric bioanalytical systems involves considerable advantages like reduction in assay time and cost per analysis, minimizing sample size and reagents required [5]. In this regard, DNA directed immobilization (DDI) and microarray technology emerged as highly

compatible tools to easily implement multiplexed detection systems, site encoding the desired bioreceptors in a specific region over the sensing surface offering site dependent signalling [6].

Another recent example, implemented DDI for multienzyme immobilization to bind glucose oxidase and horseradish peroxidase into a polyamidation dendrimer functionalized capillary. Enzymatic activity was demonstrated towards the determination of glucose with a LOD of 0.39 mM allowing controlled co-deposition of enzymes conjugated to the DNA chains by optimizing the DNA ratio of each strand [7]. On the other hand, a single-particle interferometric reflectance imaging sensor was used to monitor vesicular stomatitis virus with antibodies conjugated to oligonucleotide strains. An improvement in sensibility is indicated while detectability with DNA conjugated antibodies is compared with direct antibodies showing LODs of 500 PFU/mL (plaque forming units) in the first case and 8.000 PFU/mL for the single antibody [8].Alternatively, DNA strains were conjugated to carbohydrates to develop glycoarrays [9].

As summarized, distinct perspectives to exploit DDI principles are still available in the nanobiotechnological field. Although a wide scenario is accessible to implement these versatile site encoded DNA strategies, multiplexation should be considered as the major motivation promoting novel developments and future applications.

4.2.1.2. Precedents using DDI in our group

In the context of our research group, DDI strategies have been successfully employed for the multiplexed screening of Anabolic Androgenic Steroids (AAS) under different assay formats. Hence, *Tort et al.* reported the detection of these small molecules using DDI describing for the first time the development of a hapten microarray using hapten-oligonucleotide probes [10]. The combination of MAb's allowed simultaneous determination of stanozolol, boldenone and tetrahydrogestrinone on a microarray chip, as Figure 4.3 shows. Following, an extensive analytical characterization, the robustness as well as selectivity of the DDI platform reached to limits of detection between 0.14 and 0.48 $\mu g\ L^{-1}$ in buffer [11]. The same DNA-hapten bioconjugates were later utilized in a label free SPR immunosensor monitoring the binding of selective antibodies against the

bioconjugates under a multiplexed format [10], reaching comparable analytical performance.

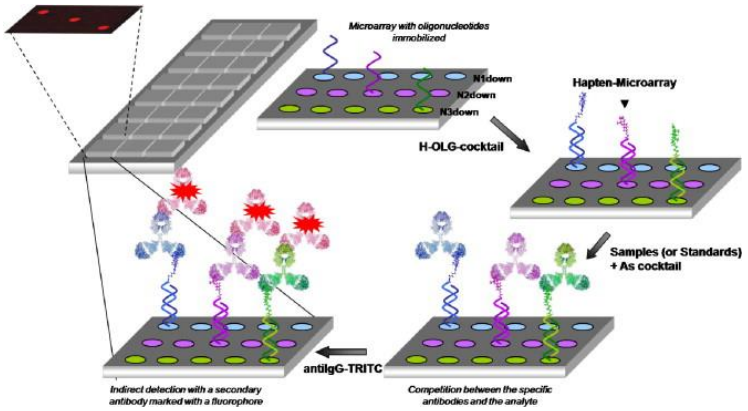

Figure 4.3 Scheme of the DNA directed immobilization microarray using of haptens conjugated to oligonucleotides towards the determination of anabolic androgenic steroids with selective monoclonal antibodies and fluorescent detection.

The success achieved on the use of such approach prompted the research team to demonstrate that the same strategy could be used to manufacture localized SPR (LSPR) chips using DDI instead of the usual more expensive advanced lithographic technologies. Thus, multimodal plasmonic nanostructures were achieved by using DNA directed strategies to immobilize on a glass substrate gold nanoparticle with different optical properties. To accomplish such kind of LSPR biosensor, each nanoparticle was biofunctionalized with two different oligonucleotide strands, named N_{up} and $N_{down,}$ see Figure 4.4. The first one allowed guiding the nanoparticle to right spot of the microarray containing the matching oligonucleotide sequence. The remaining strand in the particle, N_{down}, was used to hybridize with the complementary hapten-oligonucleotide probe This innovative approach was used, as proof of concept, to detect stanozolol and tetrahydrogestrinone in the nM range with sufficient analytical sensitivity according to the WADA (world anti-doping agency) and the EC for food safety purposes [12].

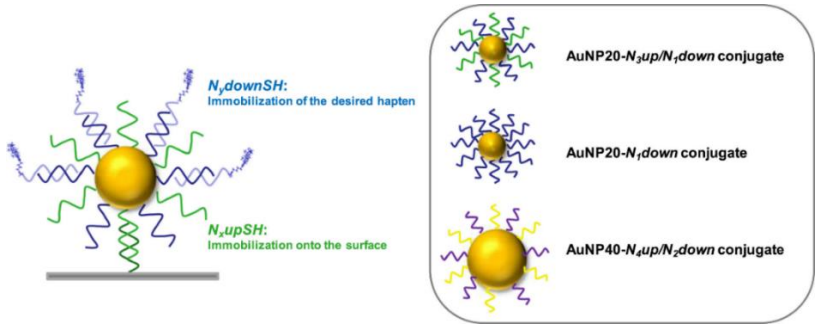

Figure 4.4 Schematic representation of multimodal gold nanoparticles coated with different oligonucleotide to direct through hybridization the immobilization over the microarray and cover the particles with hapten-oligonucleotide conjugates for the subsequent quantification in an indirect competitive immunoassay format.

At the light of these successful precedents in the group, and aiming at finally developing a smartphone coupled portable SPR, we decided to assess the possibility to also use DDI on the final SPR chip with the aim to reduce analysis cost. Hence, on a first instance, we addressed the development of DDI microarray chips on glass surfaces with the objective to evaluate if the analytical parameters could remain in compliance with the EC regulations when using this strategy.

4.3. RESULTS AND DISCUSSION

4.3.1. EXPERIMENTAL STRATEGY

The platform under development was intended to be used as a multiplexed screening tool in the food safety area. Therefore, simultaneous detection of at least three target analytes in the same assay was required as well as high-throughput format to allow processing of large number of samples. Bearing this in mind, the DDI based microarray was adapted to fit in a commercial slide gasket used to confine 24 incubation chambers in a single glass slide for independent determinations. With this system, a total of eight slides can be processed in parallel, each one containing 23 wells available for samples and the remaining as control, with the added value of a multiplexed detection of three main families of antibiotic residues per well.

The following scheme (Figure 4.5) describes the assay protocol required for the DDI microarray chip. First consisting on the immobilization of the lower oligonucleotides (N_{down}), to then allow the hybridization with the complementary strands (N_{up}) conjugated to the haptens, and finally the biorecognition event in a competitive format with cocktail of MAb's (described in section 3.3.4) to monitor the presence of the target analytes in milk samples according to the EC regulations.

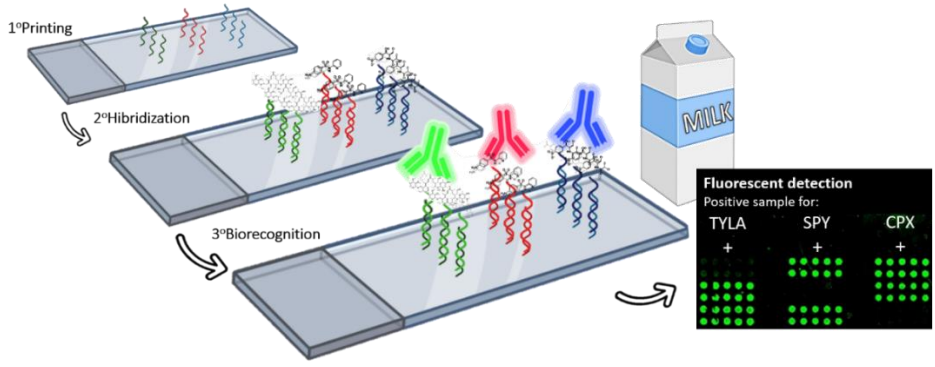

Figure 4.5 Antibody fluorescent microarray based on DDI. The figure shows the main steps involved in the immunoassay. First, the printing of the oligonucleotide N4-6 $_{down}$ probe over the glass slide, followed by an incubation with a complementary strand conjugated to the hapten and finally the selective recognition using monoclonal antibodies and fluorescent quantification.

4.3.2. OLIGO-HAPTEN CONJUGATION AND CHARACTERIZATION

Initially, the design of three oligonucleotide pairs was required to ensure adequate performance without cross interference between the sequences. Through this work, the identification of the oligonucleotide pairs (up/down) was possible after assigning a different number as $N4_{down/up}$, $N5_{down/up}$ and $N6_{down/up}$ respectively. A similar G/C content, of around 50% (purines/pyrimidines), was considered during sequence generation to reach comparable hybridization performances amongst them. The sequence selection was carried out in collaboration with by Prof. Ramon Eritja, expert in in nucleic acid synthesis. For this, the three down sequences (N4-6_{down}) were constituted by 20 nucleotides and a carbon chain spacer of six atoms with an amino group (-NH_2) in the 5' end for their covalent attachment to the epoxy-silanized glass surface. Furthermore, similar criteria was used for the design of the upper oligonucleotides N4-6_{up}, addressed to be linked to the antibiotic- hapten molecules through their carboxylic or amino groups. All the oligonucleotides sequences were purchased from Merck (KGaA, Germany).

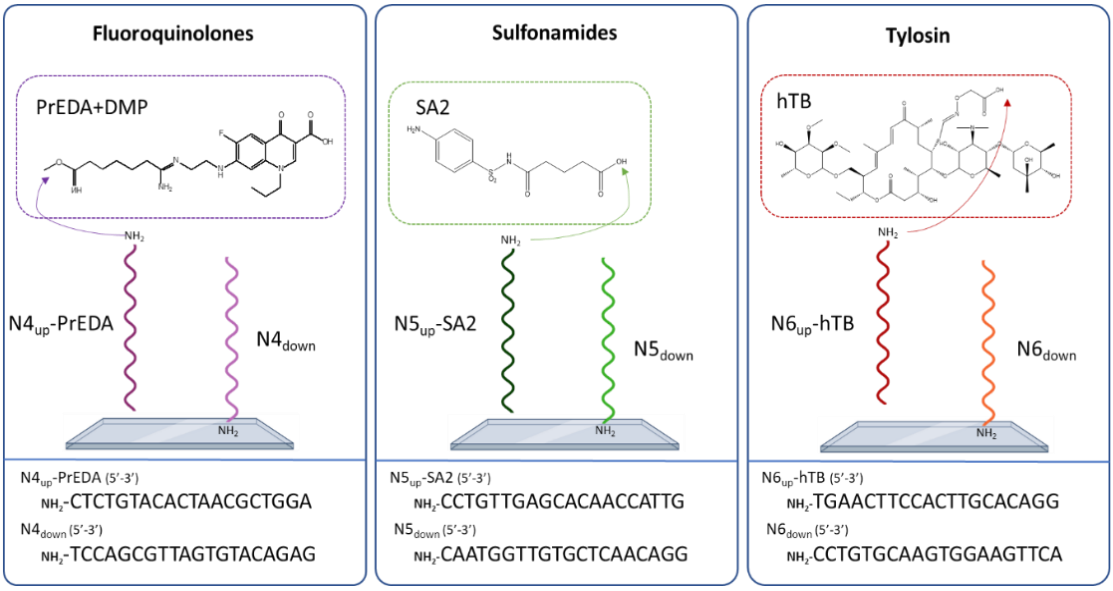

Figure 4.6 Schematic representation of the oligonucleotide sequences used for DDI immobilization and the conjugation of the corresponding haptens for the three types antibiotic families (FQ's, SA's and TYL's). The spatial distribution of the oligonucleotide probes on the DDI microarray is also described.

The corresponding oligonucleotides $N4_{up}$, $N5_{up}$ and $N6_{up}$ were successfully conjugated to the haptens (PrEDA, SA2 and hTB) as represented in Figure 4.6. For these means, the conjugation of SA2 and hTB molecules was based on the active ester method in aqueous solution, consisting on the activation of the carboxylic acid group of the haptens using DCC and NHS, following the procedure employed by Tort. et al [11] with slight modifications. While PrEDA hapten conjugation required the use of DMP as homobifunctional crosslinker, reaction described in the previous chapter for BSA coupling. Afterwards, all bioconjugates were purified using HPLC and characterized by MALDI-TOF-MS.

The verification of the functional activity was performed with the microarray platform following the scheme shown in Figure 4.5, under non-competitive conditions. The results corroborate that all three bioconjugates worked accordingly as they were binding the respective MAb's. In the following figure 4.7, the MALDI spectra and the HPLC chromatogram obtained after the conjugation of hTB-$N6_{up}$, evidence the shift of the MW to a higher mass (MW: 7086.6) attributed to the covalent coupling of the $N6_{up}$ oligo (MW: 6295.7) to the hapten (MW: 771.9). In addition, the HPLC chromatograms recorded during the purification also shows the difference in the retention time between the single $N6_{up}$ oligonucleotide and the product of the reaction oligonucleotide probe, hTB-$N6_{up}$

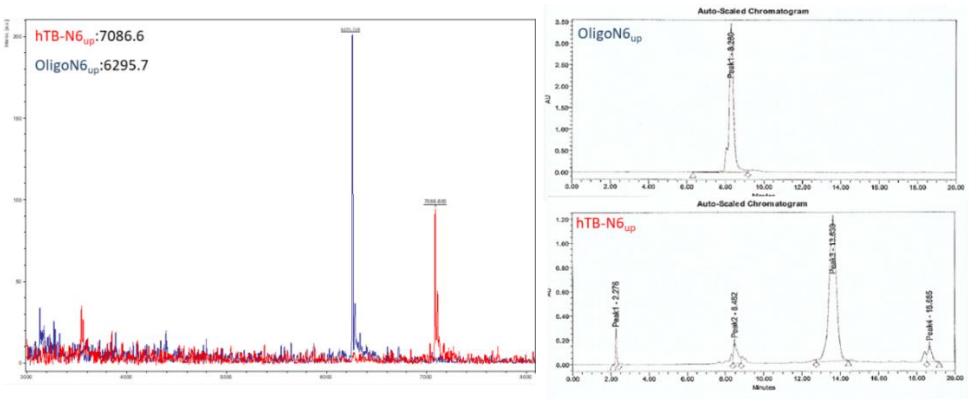

Figure 4.7 MALDI-TOF-MS spectra obtained after conjugation of $OligoN6_{up}$ with hTB hapten (7086.6 MW) using non-conjugated Oligo $N6_{up}$ as control (6295.7 MW). And HPLC chromatogram for the reference (blue) and the product of reaction (red).

In the following table the features of all the oligonucleotides designed are shown, indicating the melting point of each strand as well as their MW, before and after bioconjugation according to MALDI-TOF-MS.

Table 4.1 Features of oligonucleotide strands, including melting temperature and molecular weight (MW)

Oligonucleotide	Melting Temp (°C)	Theoretical MW	Estimated MW	MW conjugate
$N4_{down}$	58.1	6336.25	-	-
$N4_{up}$	58.1	6256.21	6284.09	6812.62
$N5_{down}$	64.2	6336.25	-	-
$N5_{up}$	64.2	6256.21	6254.15	6532.02
$N6_{down}$	64.0	6336.25	-	-
$N6_{up}$	64.0	6256.21	6259.13	7086.60

Theoretical MW: based on the nucleotide sequence. Estimated MW: experimentally determined by MALDI-TOF-MS. MW bioconjugate: experimentally determined by MALDI-TOF-MS after conjugation.

4.3.3. ESTABLISHMENT OF INDIVIDUAL DDI FLUORESCENT ANTIBODY MICROARRAY

4.3.3.1. Indirect competitive single analyte detection in assay buffer

Suitable concentrations for all the species of this DDI microarray assay (oligonucleotides N4-6_{down}, hapten-oligonucleotide N4-6_{up} bioconjugates and MAb's) were selected by performing titration experiments under noncompetitive conditions. For this purpose, distinct concentrations (200, 100, 50 and 25 µg mL^{-1}) of the oligonucleotides N4-6_{down} were spotted (5 drops/spot) on the epoxy-silanized glass (see Figure 4.8). Further on, the binding of three dilutions (0.1, 1, 10 µg mL^{-1}) of the hapten-oligonucleotide N4-6_{up}-bioconjugates was evaluated after incubation with serial 1/2 dilutions of respective MAb's starting at 1 µg mL^{-1}. The criteria used to define the most adequate bioconjugate immobilization condition was based on the analysis of saturation curves for concentrations reaching 80 % of saturation. Then, the antibody dilution was

selected in order to achieve a signal around 10.000-20.000 RFU's considering coating conditions previously established.

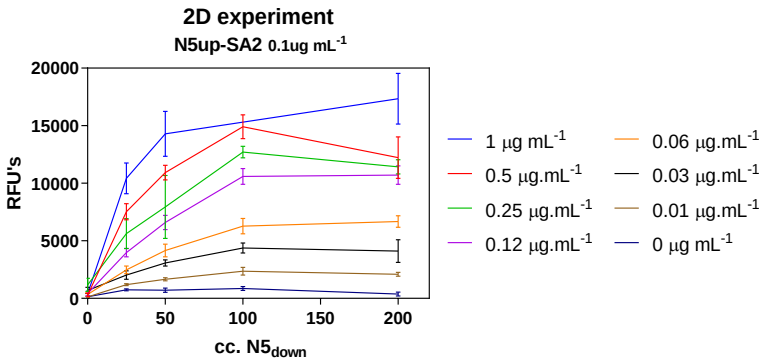

Figure 4.8 Non-competitive binding curves for $N5_{down/up}$ pair. Different coating concentrations of $N5_{down}$ were assessed (represented in x-axis), followed by the addition of 0.1 µg mL^{-1} of SA2-$N5_{up}$ solution. Finally, seven dilutions 1/2 of MAb-SA stock at 1 µg mL^{-1} were incubated with the hybridized array and are expressed with different colors showing a concentration dependent response. A microarray matrix of 5x5 was used for these experiments dedicating 5 replicate spots per lower oligonucleotide solution reporting the corresponding SD.

The previous experiments were performed in PBST Ca^{2+} with incubation steps of 30 min. Hence the total assay time was 90 min, considering the hybridization, competitive step and secondary labelled detection. The Table 4.2 shows the final concentrations of the immunoreagents for each group of antibiotics.

Table 4.2 Optimized assay conditions for single analyte determination in monoplexed format.

Assay target	$Oligo_{down}$[a]	$Oligo_{up\text{-}hapten}$[a].	MAb[a]
FQ's	100	0.1	1
SA's	0.25	0.1	0.25
TYL's	3.12	0.1	0.06

[a] Assay concentrations are expressed in µg mL^{-1}.

Afterwards, competitive DDI microarray experiments performed under these selected conditions for each group of antibiotics, using TYLA, SPY and CIP in PBST Ca^{2+}, as reference standards allowed to calibrate the single-analyte microarrays (see Figure 4.9 for the standard curves). The analytical parameters are shown in table 4.3. As it can be observed the detectability achieved was very good, comparable to that obtained in the protein microarray (see Figure 3.9 in page 116) and therefore, also in compliance with the EC regulations. Moreover, despite the greater complexity of the system the intra-assay %CV recorded for

the different spots was adecquate, as it can observed by the standard deviation of the points of the calibration curves. For comparative reasons, the CV for the three immunoassays formats was determined in the linear zone of the calibration curves performing with less than 10.3 % for ELISA, then 12.7 % for the protein microarray and 15.1 % for the DDI microarray. These results encourage us to pursuit in the direction to implement this DDI microarray to the analysis of milk samples, for which reason the effect of this matrix was evaluated.

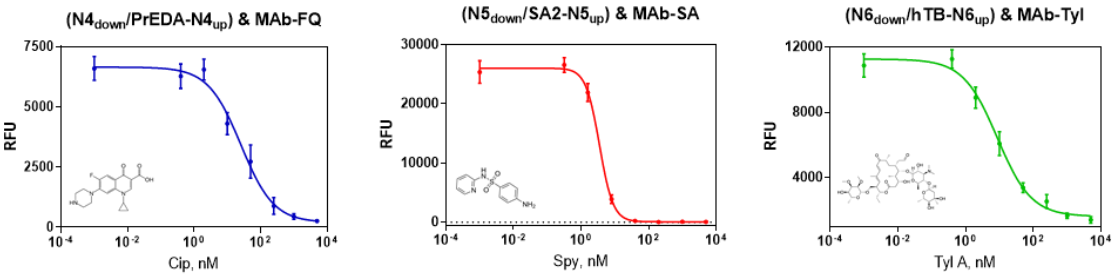

Figure 4.9 Single analyte indirect competitive DDI microarray in PBST Ca^{2+}. Calibration curves were obtained for the selected target analytes to estimate the analytical performance of the immunoassay in buffer. A matrix of 2 x 5 was printed in individual sub arrays, with a total of ten replicate spots for each oligonucleotide pair. The SD corresponds to the value defined with 2 independent wells.

4.3.3.2. Matrix effect of single-analyte DDI microarrays in cow's milk

For these experiments, slides in which microarray matrices of 6 x 5 (raw x columns) of the oligonucleotides N4-6down had been printed, were used. With this set-up, 10 spot-replicates were assigned to each oligonucleotide probe.

Based on the knowledge already acquired through the experiments described in chapter 3, assessment of the potential matrix interferences was performed by building standard curves (5 µM to 0.5 nM) in PBST $Ca^{2+}$and in milk diluted 1/5 in the same buffer. Both curves were measured with the DDI microarray approach following the standard assay procedure. Consisting in a first incubation of thirty minutes with the complementary upper oligonucleotide conjugated to the hapten at optimized conditions, to undergo through a washing step with 10 mM PBST and continue with the competitive step including the analyte and the MAb solutions for additional thirty minutes. Afterwards, a washing step takes place and the secondary labeled antibody is added to each well at the same

concentration for thirty minutes. A final wash is required to quantify the fluorescent signal from every spot using a microarray scanner.

The DDI microarray performs well also for the analysis of 1/5 diluted milk samples (see Figure 4.10), although there exists a slight matrix effect, if compared with the performance in buffer. In this case, the matrix effect of higher dilutions was assessed by ELISA reaching up to 1/20 without observing relevant analytical differences compared to the assays in buffer. Due to this, it was expected that if the DDI performs adequately in buffer and in milk diluted 1/5, will also do it in further dilutions.

Hence, the similar detectability (CIP) or even better than in buffer (SPY and TYLA) and the maximum signals are quite close, except for CYP that was lower in milk 1/5, may be due to the blocking effect already observed for this sample. In fact, the signal increase observed in the case of CIP (22.884 multiplexed vs 4.818 monoplexed RFU's) is explained due to the use of a higher concentration of PrEDA-$N4_{up}$ in the multiplexed format (table 4.3), without compromising the detectability. For the rest of the single-analyte microarrays diluting the milk did not produce any relevant variation of the analytical parameters, demonstrating the robustness of the assay.

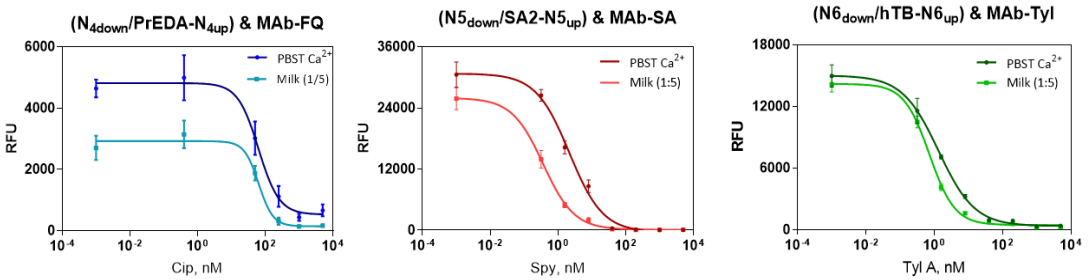

Figure 4.10 Matrix effect of milk 1/5 in the DDI microarray. The graphs show the calibration curves in buffer and 1/5 diluted milk (10mM PBST Ca^{2+}). The milk samples used in this study were commercial whole milk acquired on a grocery store, that was aliquoted and stored freeze-dried. Before use, it was reconstituted and diluted as required. Each data point is the average and standard deviation of 10 spot replicates of two microarray chips performed in two different days. See Table 4. for the analytical parameters of the calibration curves.

The limits of detections in buffer and in diluted milk, were in compliance with the EC regulation requirements despite the dilution applied to the matrix. Thus, the MRL's for the antibiotic residues under study are in the order of 30-100 µg Kg^{-1}

and the DDI microarray platform reached LOD's in the order of 1 to 5 µg Kg^{-1} demonstrating the real application of this technology for screening purposes.

Table 4.3 Analytical parameters of the three DDI microarrays in buffer and milk diluted under for singleplexed (S) or multiplexed (M) format for the selective determination of reference analytes from FQ´s, SA's and TYL's antibiotics

Assay features	FQ			SA[b]			TYL		
	S. PBST Ca^{2+}	**S. Milk 1/5**	**M. Milk 1/20**	**S. PBST Ca^{2+}**	**S. Milk 1/5**	**M. Milk 1/20**	**S. PBST Ca^{2+}**	**S. Milk 1/5**	**M. Milk 1/20**
RFU_{max}	4818 ±167	2921 ±155	22884 ±984	30755 ±1211	25970 ±345	20269 ±997	15017 ±217.3	14197 ±278.6	20515 ±878
RFU_{min}	526.3 ±201	144 ±90	1033.11 ±254	382.5 ±103	98.63 ±75	210.2 ±114	355.5 ±130	459.1 ±139	690.2 ±120
Slope	-1.41 ±0.41	-2.03 ±1.11	-1.27 ±0.24	-0.87 ±0.12	-0.94 ±0.05	-1.38 ±0.32	-0.82 ±0.04	-1.16 ±0.08	-1.72 ±0.13
IC_{50} [a]	4.08 ±0.18	3.99 ±0.24	1.91 ±0.83	5.43 ±1.78	1.28 ±0.97	2.43 ±0.23	13.56 ±3.56	4.95 ±1.32	4.79 ±0.92
LOD [a]	2.17 ±0.44	2.60 ±0.48	0.89 ±0.54	1.03 ±0.87	1.08 ±0.71	1.67 ±0.40	1.26 ±1.02	1.23 ±0.45	1.43 ±0.62
R^2	0.99 ±0.01	0.98 ±0.01	0.96 ±0.09	0.99 ±0.01	0.99 ±0.01	0.98 ±0.01	0.99 ±0.01	0.99 ±0.01	0.99 ±0.01

S= Singleplexed assay M=Multiplexed assay, [a] the concentrations are expressed in µg kg^{-1}.[b] SA's **S** assays were carried out using SPY as reference, and for **M** assay format, STZ was used as reference target. The SD was estimated from two different wells. The assay conditions for **M** format were re-adjusted in order to generate comparable response, mainly observed in the FQ assay RFU_{max}.

The high detectability achieved by the DDI microarray chip allows performing antibiotic determination in milk samples at even higher dilutions than 1/5 in order to ensure the absence of nonspecific interferences. In fact, for practical reasons, measurements with the multiplexed chip were performed using a unique sample dilution of 1/20. Besides, commercial milk should be diluted 20-fold in PBST Ca^{2+}, because SA´s immunoassay presented considerably low detectability in contrast with MRL. By diluting the sample, the range of detection for the immunoassay was the adequate to distinguish the presence of SA's at the level of interest and afterwards real concentration should be re-calculated in direct matrix 20 times more concentrated. According to the results displayed in Table 4.3, comparing different DDI assay formats, no relevant variability was attributed to the use of multiplexed or monoplexed configurations. Aditionally,

the milk dilutions evaluated (1/5 or 1/20) evidenced adequate analytical performance too. In spite of that, the assessment of cross-reactivity between oligonucleotides strand needed to be corroborated.

4.3.3.3. Assessment of cooperative phenomena on the DDI microarray

A series of experiments were performed in order to elucidate the specificity provided by DNA hybridization reaction. Microarray chips were printed with the three oligonucleotides N4-6$_{down}$ on a 6 x 5 (raw x column, in Figure 4.11) matrix configuration, in which two rows were dedicated for each lower oligonucleotide.

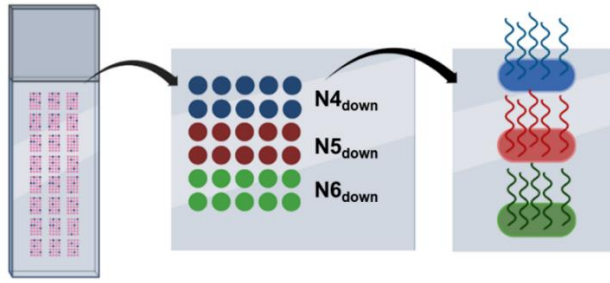

Figure 4.11 Magnified view of the multiplexed DDI microarray matrix, from a single glass slide patterned with 24 independent sub arrays, to the 6x5 matrix dedicating 10 replicate spots to the same N_{down} oligonucleotide sequence identified with different colors.

Subsequently, the chips were incubated with the pool of hapten-oligonucleotide conjugates for 30 minutes. Three sets of 8 hybridized microarray chips (*h*-DDI chips) were then used to measure, individually, standard curves (5.000-0.4 nM) for each group of antibiotics, but using also the pool of the three MAb's. At this point we assume that no cooperative phenomena between these antibodies should take place considering the previous characterization experiments.

As can be seen in Figure 4.12, the results demonstrated that the hybridization reaction was specific as well as the recognition of the mediated by the MAb's. Hence, each analyte can be properly detected and quantified, under this configuration despite having use mixtures of reagents on each chip. When adding the pool of oligonucleotides (haptens-N4-6$_{up}$), each probe did hybridize only with the corresponding complementary chain (N4-6$_{down}$), as it is evidenced by the fluorescence recorded on each spot of the different chips used, in the

following figure. Notice that maximum fluorescence is accomplished when there is no analyte, and since assays were run with a cocktail of antibodies, all three antibodies react with the immobilized hapten-oligonucleotide probes. A decrease in the spots signal was produced when the specific target analyte (CIP, STZ or TYLA) interacts with the corresponding antibodies (MAb-FQ/MAb-SA/MAb-Tyl), is only observed on those spots where the corresponding probe has been immobilized, without interfering with the binding of the other MAbs. From these experiments we can conclude that the hybridization reaction is specific and that no cooperative phenomena were observed between different oligo chains and MAb's.

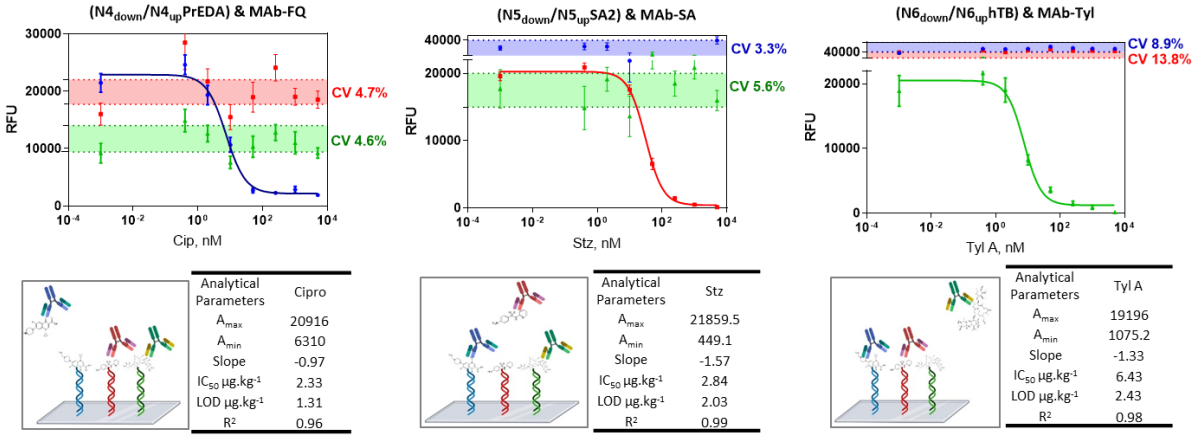

Figure 4.12. Cooperative phenomena studies. Single analyte calibration curves using the pool of haptenized oligos and the cocktail of MAb's for each analyte, showing the CV% of the maximum signal detected from non-specific reagents in each assay. Each data point in the graphs correspond to 5 replicate-spots inside each microarray chip Analytical performance of the assays was plotted in the tables, extracted from the logistic equation used to fit the standard curve. The results shown correspond to the average and standard deviation of two different wells and the schematic representation of the reagents behavior in each well is plotted.

The coefficient of variation (CV%) in the maximum signal (zero analyte) over non-selective reagents for each assay was calculated to corroborate the absence of potential interferences at increasing analyte concentrations combining the set of upper oligonucleotides and MAb's. For FQ multiplexed assay the CV for SA's reagents was 4.7 % and TYL 4.6 % demonstrating specific response. Similar behavior was observed in the case of SA's assay reaching CV's of 5.6 % for TYL and 3.3 % FQ reagents. While at increasing concentrations of TYLA, the signal fluctuations over the other reagents included in the same well were 8.9 % for FQ and 13.8 % for SA's reagents. Hence, these results validate the adequate

performance of the system under multiplexed format without evidencing shared reactivities between combined reagents, reaching limits of detections below the regulatory requirements.

4.3.4. PERFORMANCE OF THE MULTIPLEXED DDI MICROARRAY CHIP IN MILK SAMPLES

The influence of the milk matrix on the multiplexed microarray combining oligonucleotides and MAb's was evaluated in the following experiment. Along the table 4.4 and Figure 4.14, the analytical performance of the multiplexed DDI microarray was reported for each antibiotic family under milk diluted 1/20. Throughout the assay characterization, the pool of oligonucleotides and the cocktail of antibodies were utilized with different analytes prepared in diluted matrix reaching a LOD of 0.89 µg Kg^{-1} for CIP; 1.67 µg Kg^{-1} for STZ and 1.43 µg Kg^{-1} for TYLA, however the real concentration in undiluted matrix was 20 times higher. Baring this in mind, the minimum amount detected for each assay in direct matrix was 17.8 µg Kg^{-1} for CIP, 33.4 µg Kg^{-1} for STZ and 28.6 µg Kg^{-1} for TYLA, all of them below the MRL established by regulatory authorities.

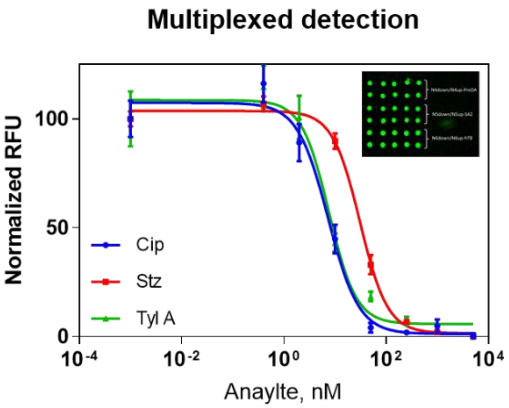

Table 4.41 Analytical parameters obtained using the multiplexed assay configuration

Parameters	CIP	STZ	TYLA
RFU_{max}	22884 ± 984	20269 ± 997	20515 ± 878
RFU_{min}	1033.11 ± 254	210.2± 114	690.2 ± 420
HillSlope	-1.27± 0.24	-1.38± 0.32	-1.72± 0.13
IC_{50}[a]	1.91± 0.83	2.43± 0.23	4.79± 0.92
LOD[a]	0.89±0.54	1.67± 0.40	1.43± 0.62
R^2	0.96 ± 0.09	0.98± 0.01	0.99± 0.01

[a]IC50 and LOD concentrations are expressed in µg Kg^{-1}

Figure 4.13 Multiplexed detection in diluted milk. The pool of oligonucleotides and the cocktail antibodies were implemented in commercial milk samples diluted 1/20. For this, different calibration curves were generated against selected analytes using a microarray of 6x5 as showed in the graph. The analytical performance is expressed in the table. Results are expressed in normalized relative fluorescence units. The SD corresponds to two well replicates performed in different days.

4.3.5. EVALUATION OF ANTIBODIES REACTIVITY PROFILE

The proposed platform makes use of three different immunoassays with intrinsic bioanalytical properties such as different LOD's, IC_{50} or linear range, therefore homogenous conditions should be selected to allow adequate performance for each determination like a unique sample dilution or assay buffer. In addition, a distinct MRL has been established for each veterinary residue at 50 µg Kg^{-1} for TYL's and 100 µg Kg^{-1} SA's and FQ's, with the exception of danofloxacin at 30 µg Kg^{-1} in milk. In the same line, the SA's assay experimentally showed the lowest detectability in contrast with FQ and TYL assays and we decided to take the compromise of applying a unique 20-fold milk sample dilution, in order to detect the three reference analytes at the MRL value. In other words, if a lower dilution (for instance 1/10) was utilized and a sample was contaminated closely below the MRL concentration (75 µg Kg^{-1} for SA's), the assay won't be suitable to discriminate that slight difference between positive or negative sample. This is because the content of analyte at the dilution selected is out of the working

range of the immunoassay and will be assigned as a positive sample in the lower plateau of the curve (high concentration range) although it was truly negative.

On the other hand, as class selective antibodies were employed for the development of this platform showing a broad recognition for structurally related compounds, the potential identification of more than three analytes is highlighted. In order to ensure that a representative amount of congeners were detectable with the DDI microarray at the level of interest, a discrete selection of some of the most prevalent analytes from each antibiotic family were evaluated, constituting a total of 18 different molecules (9 SA's, 8 FQ's and TYLA). In order to do this, form the panel of antibiotics analyzed in each family, the analyte with the worst detectability was selected as reference. This was carried out by measuring the same concentration (at MRL) of different related antibiotics, to look for the one producing the higher signal (less inhibition %) in the competitive format. By using this analyte as reference, the rest of molecules that were below that intensity will be detectable at the MRL concentration expecting to use the system for semi-quantitative purposes.

To demonstrate that the multiplexed DDI microarray was able to detect a wide variety of FQ's and SA's antibiotics in compliance with the EC regulations, milk samples were spiked at the level of interest (MRL) and above and below (2 times MRL or 0.5 times MRL). Then, the samples were diluted 20-times with the assay buffer and analyzed in the DDI microarray under multiplexed format using the pool of oligonucleotides and MAb's. The maximum fluorescence obtained over the zero-analyte concentration for each bioconjugate was referenced as 100 % of the RFU signal and normalized.

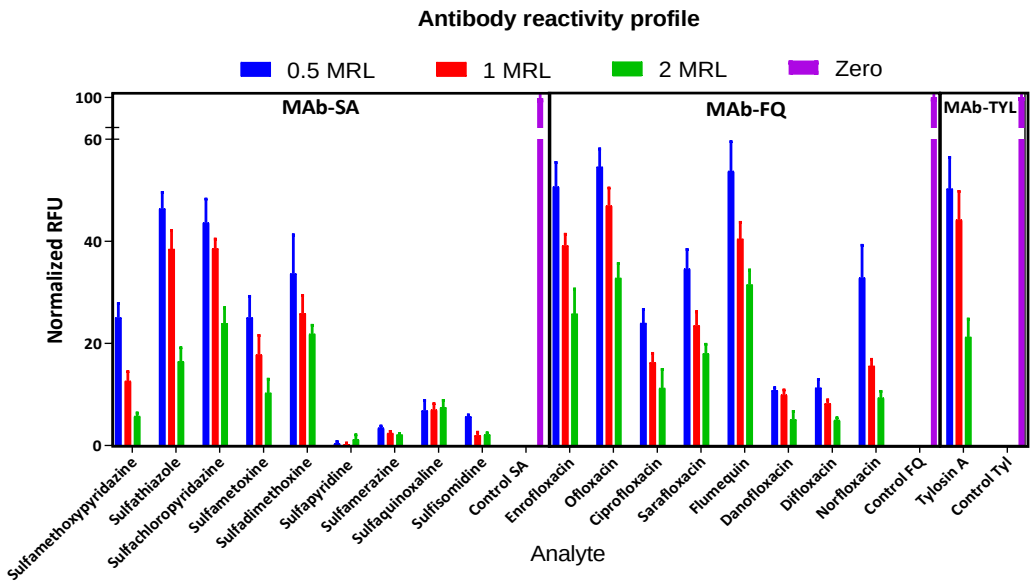

Figure 4.14 Reactivity profile of the class selective antibodies. Commercial milk samples were spiked at 2 MRL, 1 MRL and 0.5 MRL concentration depending on the antibiotic family to then be diluted in the assay buffer (1/20). The multiplexed DDI microarray of 6x5 was utilized, including the pool of oligonucleotides and the cocktail of MAb's. The standard deviation (SD) reported corresponds to two different well replicates with 10 identical spots each. In total, 9 SA's, 8 FQ's and TYLA were evaluated with this system. The signal is expressed in normalized RFU's.

As expressed in the previous graph, a dose dependent response considering 0.5, 1 and 2 MRL concentrations was observed for each antibiotic. Interestingly, clear response differences are detectable amongst distinct analytes and this behavior is attributed to the particular affinity of the MAb's for the corresponding antibiotic congeners. Because of the competitive nature of the DDI microarray, the lower the signal the better is the recognition. Considering these results (see Figure 4.14), SPY was the antibiotic SA congener better detected while STZ was the one that gave lower response but still produced 60 % of inhibition of the signal at MRL concentration. Selecting STZ as reference for calibration, it was possible to ensure reliable detection of the other eight SA's. The same study was applied to the family of FQ's, finding that CIP was the better detected and ERFX was the less selective antibiotic promoting the recognition of the rest of seven structurally related compounds evaluated at MRL value. For the case of TYL assay, the antibody was selective against TYLA and TYLB, keeping as reference the first mentioned.

Throughout this experiment the possibility to detect at least 18 different antibiotic residues from three prevalent families in cow's milk was demonstrated. Remarkably, more congeners can be evaluated in order to maximize the screening capacity of the platform for future applications. In accordance with the list of antimicrobial agents of veterinary importance published in June 2021 by the World Organization for Animal Health [13], in the case of bovines TYL's were indicated as veterinary critically important antimicrobial agents as well as FQ's. For this family, the eight compounds evaluated in the experiment were included in the list of second-generation quinolones, missing marbofloxacin and orbifloxacin from our analysis and considering flumequine (measured) as a quinolone first generation also critically important. Regarding SA's, sixteen congeners were described as critically important and eight of them were detectable with the DDI platform covering a 50 % of the relevant analytes for this class of substances.

From a different perspective, in the last EFSA report from 2021 [14], the presence of chloramphenicol in three milk samples from Malta was alarming. Although the use of this substance for veterinary purposes has been banned in EU since 1994, is still detected and this emphasize on the need of continuous monitoring even if are unauthorized antibiotics. Another relevant group of veterinary residues commonly detected were β-lactams including five positive samples (two for amoxycillin and three for penicillin G) in different countries, and one positive for tetracyclines in France. In agreement with this information, the incorporation of reagents targeting β-lactams, chloramphenicol and tetracycline antibiotics to the already developed multiplexed DDI microarray would cover main testing needs against residues commonly found in milk samples. As an additional fact, an oligonucleotide bioconjugate carrying a chloramphenicol hapten was prepared during the course of this thesis (data not showed) thanks to the availability of reagents in the group but not further characterization was carried out due to time limitations. Nevertheless, the addition of these reagents to the already generated microarray matrix could be considered in future applications without significant difficulties. To summarize, the 18 veterinary residues evaluated have demonstrated to be critically important in the food safety field and the proposed platform emerges as a promising screening tool towards some of the most relevant targets in cow's milk evidencing the application in the real scenario.

4.3.6. PLATFORM PRE-VALIDATION IN COMMERCIAL MILK SAMPLES

In order to assess the performance of the DDI microarray in real samples a pre-validation study was conducted. Twenty commercial milk samples were spiked at different levels above and below the MRL established for each analyte (see Figure 4.15). The unknown samples were prepared under blind conditions. Moreover negative (NEG) and MRL controls (spiked at the level of interest for the three analytes) were also simultaneously measured on each set of experiments. Samples were randomly distributed on the different wells of the ArrayIt® holder containing the glass slides with the microarray chips printed. Semi-quantitative results were obtained with fluorescent readout by comparing the signal with that of the controls.

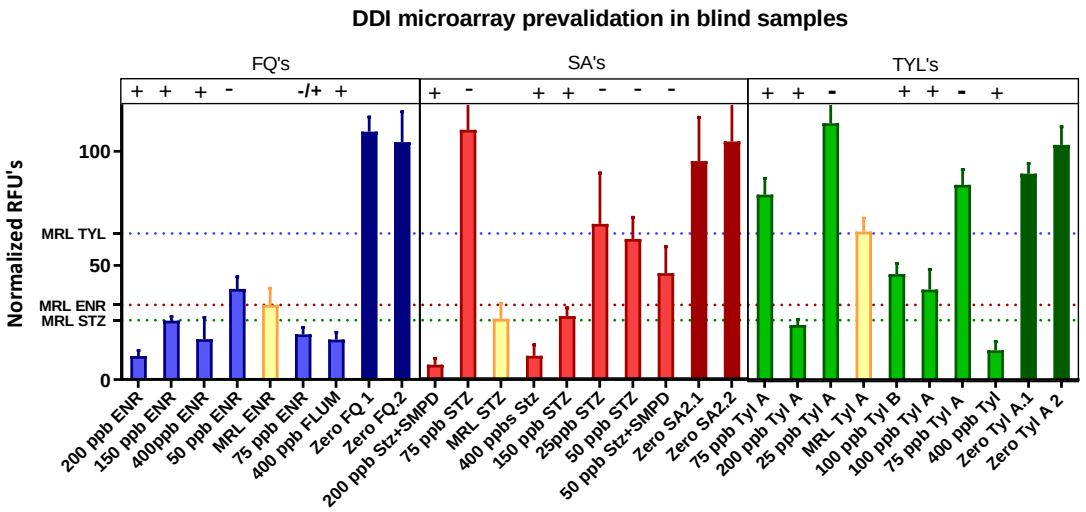

Figure 4.15 Pre-Validation studies. Commercial milk samples were spike at different levels above and below the MRL under blind conditions and diluted 1/20 in assay buffer. The multiplexed microarray of 6x5 was utilized combining the pool of oligonucleotides and MAb's for different analyte determinations. As negative control, samples with zero- content of analyte were used and for MRL controls the target analytes were ENR, STZ and TYLA respectively. All values below the MRL signal were assigned as positive for that antibiotic while samples with fluorescence above the MRL were considered negative correlating. Seventeen milk samples from the twenty evaluated, were correctly classified. The SD reported corresponds to ten replicate spots.

Table 4.5 Distribution of blind samples assigned using the DDI multiplexed microarray

Assay	Positive samples	Negative samples	False +	False -
FQ	3 (3)	3 (2)	1	0
SA	5(4)	4(4)	0	1
Tyl	3(2)	2(2)	0	1

Values between () corresponds to samples properly classified with the DDI microarray

Because of the great detectability achieved by the DDI microarray, the use of only 5 µl of commercial whole milk was necessary to perform these analyzes, reaching enough sensitivity according to regulations. As it is shown in table 4.5 from the total of twenty milk blind samples analyzed, seventeen were correctly assigned. Since positive results recorded by a screening method are usually followed by a confirmatory analysis, the occurrence of a low rate of false positives is not considered a major problem. However, a high % of false negatives samples would entail higher risk for consumers. In this case, the rate of false positives was 18 % (2 samples from 11), while the rate of false negatives was 11 % (1 from 9). For a complete system validation, the Commission Decisions 2002/657/EC [15] laid that screening methods intended for semiquantitative purposes should be assessed towards CCβ determination, specificity, stability and ruggedness. Although some of these features were discussed during this section, our platform couldn't commit to a β error < 5% under the conditions evaluated as established by the regulations [16] and due to time limitations only a pre-validation was conducted to demonstrate system implementation in samples. However, the extensive characterization performed supports the use of the DDI microarray as promising tool in alternative technological approaches or even for semiquantitative determinations of at least 18 veterinary residues in cow's milk feasible to be optimized with mimimum requirments.

4.3.7. EXPERIMENTAL SUMMARY

Across the development of the already described DDI microarray, the optimization and characterization of several assay parameters was achieved. In first place, the definition of standardized conditions for the bioconjugation of three hapten molecules with different oligonucleotides sequences was successfully accomplished. Followed by the implementation of such reagents in an indirect competitive immunoassay format in a DDI microarray combining the

MAb's previously characterized by ELISA and protein microarray. For the three analytes under assessment (FQ's, SA's and TYL's) the proposed platform was complying EU regulations in buffer and diluted milk, lacking of sample pretreatments.

In this work, single analyte determinations in buffer reached excellent detectability with LOD's around 1-2 ppb (μg Kg^{-1}), far below the MRL's and comparable to gold standard ELISA method. Moreover, these parameters were consistent when the assay was performed in diluted matrix (1/5) allowing direct detection without sample pretreatment in a singleplexed format. In the next step, a multiplexed assay configuration was explored combining oligonucleotides in the same well with the cocktail of antibodies, reaching LOD's of 0.89 μg Kg^{-1} for CIP, 1.67 μg Kg^{-1} for STZ and 1.43 μg Kg^{-1} for TYLA in a 20-fold milk dilution. No shared and cross reactivity events were evidenced while reagents were combined.

Although the use of a DDI microarray to selectively discriminate small molecules using immunochemical tools was not extensively approached thorough the literature, two relevant examples can be highlighted. The first consisting on the characterization of a DDI immunoarray coupling a selective Anti-caffeine antibody with a short 12-mer oligonucleotide sequence to immobilize through hybridization the bioconjugate on the surface of a glass slide. While, a more similar approach coupling haptenized molecules from anabolic androgenic steroids to three oligonucleotide sequences for indirect competitive detection of the target analytes was proposed by Tort *et al.* [11]. Up to our knowledge, the strategy followed in this chapter was never before implemented for antibiotics detection in cow's milk samples. In addition to this, the use of class selective antibodies under a multiplexed format allowed the identification of at least 18 different molecules belonging to the three families evaluated of concerning veterinary residues in the same well saving money, reagents and time.

Based on the evidence already discussed, we strongly propose the use of the DDI microarray as a screening tool for rapid and affordable analytical determination of suspected milk samples at dairy industry scale. The current platform allows semiquantitative analysis of 23 milk samples (5 μL each) per slide in less than 90 minutes and depending on the glass holder capacity, even up to 4 or 8 slides can be processed in parallel reaching more than 180 samples in a single run

evidencing the high-throughput property. Moreover, a system pre-validation in blind samples was conducted to demonstrate the real impact of these approach in the screening of veterinary residues contaminants for food safety applications.

4.4. CHAPTER CONTRIBUTIONS

- Two standardized methodologies for bioconjugation and characterization of three oligonucleotide strands to different hapten molecules derived from antibiotics were established.
- Single-analyte DDI microarrays in an indirect competitive format showed comparable analytical performance with gold standard ELISA and also with protein microarray in buffer and in milk diluted 1/5.
- Is the first time that a multiplexed fluorescent DDI microarray has been developed for selective identification of at least 18 antibiotic residues, constituted by 9 SA's, 8 FQ's and 2 TYL's in diluted cow's milk samples according to EU regulations without pretreatment steps.
- Platform pre-validation was conducted in 20 commercial milk blind samples spiked around the MRL value of the antibiotic family. Adequate semiquantitative determination was possible in 17 of the 20 evaluated samples, showing 11% of false positive rate and 18% of false negative rate.

4.5. MATERIALS AND METHODS

4.5.1. REAGENTS AND IMMUNOREAGENTS

The immunoreagents used in this work for FQ's, SA's and TYL's were produced in our facilities as described in the previous chapter. The oligonucleotides strands ($N4_{down/up\text{-}NH2}$, $N5_{down/up\text{-}NH2}$ and $N6_{down/up\text{-}NH2}$) were acquired from Merck (Merck KGaA, Darmstad, Germany) and the hapten-oligonucleotide conjugation (FQ: PrEDA-$N4_{up}$, SA's: SA2-$N5_{up}$, and Tyl: hTB-$N6_{up}$) will be described below. For the hapten conjugation to the oligonucleotides, N,N'-Dicyclohexylcarbodiimide 99% (DCC) and N-hydroxysuccinimide (NHS) were purchased from Sigma- Aldrich (St. Louis, MO, USA). and dimethyl pimelimidate (DMP) from Thermo Fisher Scientific (Massachusetts, USA) and the working aliquots were prepared in anhydrous DMF (dimthylformamide).

The target analytes under study, Sulfapyridine (SPY) Sulfatiazole (STZ), Sulfametoxypiridazine (SMPZ), Sulfatchloropiridazine (SCPZ), Sulfadimetoxine (SDMX), Sulfamethoxine (SMX), Sulfamerazine (SRZ), Sulfachinoxaline (SCX), Sulfisomidine (SSD), Enrofloxacin (ERFX), Ofloxacin (OFX), Ciprofloxacin (CPX), Sarafloxacin (SFX), Flumequin (FLUM), Danofloxacin (DNFX), Difloxacin (DFX), Norfloxacin (NFX), Tylosin A (TYLA), Tylosin B (TYLB) were delivered from Sigma-Aldrich and Honeywell. SA's and TYL's stock solutions were prepared at 10 mM concentration in DMSO, but quinolones were dissolved in NaOH 0.1M. All of them, stored at 4°C for a maximum period of one month. The secondary antibody, Anti-mouse IgG-TRITC was purchased from Sigma-Aldrich (St. Louis, MO, USA) and employed at 1/250 in PBST 10mM. Commercial milk samples "la letona", were lyophilized and stored at -40°C, once needed were resuspended with H_2O ultrapure by stirring at 40°C, considering density:124.8 g L^{-1}. Acetonitrile (ACN, HPLC gradient grade) was obtained from Panreac Quimica (Barcelona, Spain).

4.5.2. BUFFERS

PBS was 0.01 M phosphate buffer (1.48 mM KH_2PO_4 and 8.3 mM Na_2HPO_4) in a 0.8% saline solution (137 mmol L^{-1} NaCl, 2.7 mmol L^{-1} KCl), at pH 7.5. PBST is PBS

previously described with 0.05% Tween 20. The solution of PBSTCa^{2+} corresponds to a PBST 10mM pH 7.5 solution that contains 1mM $CaCl_2$. The printing buffer utilized for the deposition of oligonucleotides over the slide consisted in 150 mM di-sodium hydrogen phosphate (pH 8.5)/0.01% sodium dodecyl sulphate in H_2O ultrapure. Hybridization buffer is composed of 10 mM Tris, 1 mM EDTA, 1 M NaCl (pH 7.2). Borate buffer is 0.2 M boric acid/sodium borate, pH 8.7. The pH and the conductivity of all buffers and solutions were measured with a pH-meter pH 540 GLP and a conductimeter LF 340, respectively (WTW, Weilheim, Germany).

4.5.3. OLIGO-HAPTEN CONJUGATION PROTOCOLS

4.5.3.1. N_{4up}-PrEDA Oligo-hapten conjugate

The upper oligo N_{4up}-NH2 was dissolved in 25 µL of ultrapure water and mixed immediately with 75 µL mL of 0.2 M sodium borate pH 8.6. In parallel, PrEDA hapten (1 mg) and DMP (1 mg) were dissolved in hot anhydrous DMF (100 µL) and 0.2 mL 0.2 M sodium borate pH 8.6, respectively. At the same time, 40 µL of PrEDA and 5 µL of DMP solutions were added immediately to the dissolved oligonucleotide. The whole mixture was stirred overnight at room temperature. Finally, the desalting of oligonucleotide-hapten was carried out using NAP™-5 Columns Sephadex™ G-25 DNA grade columns from G&E HealthCare, eluted in water. All conjugates were purified by HPLC for further implementation on the bioassay. HPLC conditions: Nucleosil 120–10 C18 column (250 × 4 mm). Solvent A: 5 % ACN in 0.1 M aqueous TEAAc (triethylammonium acetate) pH: 7 and solvent B: 70 % ACN in 0.1 M aqueous TEAA (pH = 7). Flow rate: 1 mL/min. Conditions: 20 min linear gradient from 0% to 50% B. For the characterization of the conjugates Matrix-assisted laser desorption ionization time-of-flight (MALDI-TOF) was used on the products of oligo-hapten reaction. The conjugates were evaluated in a Bruker Autoflex III Smartbeam spectrometer (Billerica, Massachusetts). For this purpose, a mixture of 3-Hidroxypicolinic acid (3HPA)/ACN (1 % v/v) 50 mg mL^{-1} and a solution of diammonuym hydrogen citrate (AHC) (100 µg mL^{-1}) were prepared (10:1 v/v, HPA: AHC) and 1 µl applied onto the target plate. Once dried, 1 µL of solution containing the oligonucleotide purified (non-conjugated sequence and the product of reaction) in water at concentrations ranging from (0.25pmol µL^{-1} to 5pmol µL^{-1}) the mixture 1:1:1 of

THAP:CA:SAMPLE completely dry drop takes 25 min. Methods: LN_ProtMix.Par, Detection 3000-10.000Da, Processing:SC_Protein_Low, Laser Power:80%.

4.5.3.2. N_{5up}-SA2 and N_{6up}-hTB Oligo-hapten conjugate

The upper oligos (N_{5up} and N_{6up}) were dissolved in 0.2 mL of water, and mixed with 0.1 mL of 0.2 M sodium borate pH 8.6. In a separate vial the carboxylated haptens (SA2 and hTB, 10 molar excess) were dissolved each in 0.1 mL of DMF and mixed with NHS (25 molar excess) and DCC (50 molar excess). The mixture was left with magnetic stirring for 3 h at room temperature, until the solution became opaque due to the precipitation of the urea. Then, we centrifuge (10.000 rpm for 15 min) to remove the precipitate and the supernatant was added to the corresponding aqueous solution of the amino-oligonucleotide. The mixture was left stirring and kept O.N. at 4°C. The mixture was purified and characterized as described above.

4.5.4. PROTOCOL OF THE FLUORESCENT DDI MICROARRAY

4.5.4.1. DDI microarray printing conditons

Microscope slides (75 × 25 mm) were purchased from Corning Inc (Corning, NY, USA). A derivatization protocol with GPTMS to functionalize the glass surface with epoxy groups was carried out, already reported in previous works [17]. Oligonucleotides $N4_{down}$ to $N6_{down}$ were spotted onto the glass slides attaching the sequences through the amino group in the 5'-end. The spotting concentration: $N4_{down}$ 75 µg mL^{-1}, $N5_{down}$ 50 µg mL^{-1} and $N6_{down}$ 6.25 µg mL^{-1}in printing buffer. The printing was performed using an automated piezo-driven SciflexArrayer S3-Scienion AG (Scienion AG, Berlin, Germany). For these means a piezo dispense capillary (PDC) 70 type 1 was employed, setting the voltage at 98V and the pulse width 50 µs. 5 drops of 350 pL were deposited per spot and the temperature defined at 25°C with humidity at 65 %, allowing slides to dry for 1 hour after printing process in the spotting chamber and then kept at 4°C until use for a maximum of 7 days. Depending on the experiment performed the spot matrix was customized to match with the ArrayIt® holder (Arrayit® Corp, Sunnyvale, CA, USA) utilized for the assays.

4.5.4.2. Single analyte monoplexed DDI microarray procedure

In the case of individual indirect DDI based competitive assays, calibrations curves in PBST-Ca^{2+}, and dilutions of reconstituted milk samples in the same buffer (1/5) were generated in a range of 0.5 µM to 5 nM. Matrix containing 10 replicate spots of the same Oligo N*4-6*$_{down}$ were prepared in separate sub-microarrays ($N4_{down}$ 100 µg mL^{-1}, $N5_{down}$ 0.25 µg mL^{-1}, $N6_{down}$ 3.12 µg mL^{-1}). After careful optimization experiments the most suitable oligonucleotide pair concentrations were established. The following day, an initial washing step (3 times 200µL/well PBST 10mM) was performed and the incubation with complementary chains for 30 minutes at 0.1 µg mL^{-1} for the three oligonucleotide hapten conjugates (PrEDA-$N4_{up}$, SA2-$N5_{up}$, hTB-$N6_{up}$) took place. After incubation, other washing step was required to remove unbound oligo and reach the competitive step incubating the analyte (in PBST Ca^{2+} and separately in milk diluted 1/5 in the same buffer) with the corresponding MAb's (MAb-PrEDA 1 µg mL^{-1}, MAb-SA 0.25 µg mL^{-1}; MAb-Tyl 0.06 µg mL^{-1}). Following 30 min of incubation another washing step was performed and the microarray was incubated with a secondary antibody labelled Anti mouse-IgG-TRITC 1/250 in PBST 10mM buffer. Then a final wash with PBST and single was with 200 µl/well with MiliQ-H_20 took place and slides were dried with N_2 stream to be quantified in the fluorescent scanner.

4.5.4.3. Indirect competitive multiplexed DDI microarray conditions

All microarrays were performed using the aforementioned holder, generating 24 separate wells in a holder of 3 columns and 8 rows per slide using the spotting solutions from the monoplexed assays. After resting O.N. at 4°C, printed slides were washed with 200 µL of 10mM PBST and then incubated with the pool of oligonucleotides N4-6_{up}-hapten for 30 min at optimized concentrations to reach comparable signal respecting the single-analyte format (PrEDA-$N4_{up}$ 0.8 µg mL^{-1}, SA2-$N5_{up}$ 0.5 µg mL^{-1} and hTB-$N6_{up}$ at 0.2 µg mL^{-1}in Hybridization buffer, 100 µl per well). Then, a washing step was performed and standards solutions for every antibiotic ranging from 0.5 nM to 5 µM (CIP, STZ, TYLA) in buffer or milk diluted 1/20 in PBST Ca^{2+} where included with the ''Cocktail of Antibodies'' (50 µL/well), consisting on the combination of the three MAb's (MAb-FQ 0.8 µg mL^{-1}, MAb-SA

0.6 µg $mL^{-1}$and MAb-Tyl 0.42 µg mL^{-1}in in PBST Ca^{2+}) for 30 min at RT. An additional washing step took place, followed by the incubation for other 30 minutes with the secondary labelled Anti-mouse-IgG-TRITC 1/250 in PBST at RT covered from light. Each incubation was done under stirring conditions at 350 RPM. After this incubation a wash step with PBST 10mM was required and a final wash with MiliQ water. Then slides were dried with N2 stream and the signal acquired by the fluorescent scanner.

4.5.4.4. Fluorescent spot signal acquisition

Microarray measurements were acquired on a Two-Color Microarray Scanner InnoScan 710 (Innopsys, Carbonne, France) with an optical filter with 10-µm resolution. The laser power and photomultiplier tube (PMT) gain were set to 95% and 80%, respectively. The spots were measured by deducting the mean TRITC background intensity to the mean of TRITC foreground intensity using Mapix - Microarray image acquisition and analysis software (Innopsys, Carbonne, France). Calibration Curves are obtained from the RFU (Relative Fluorescence Units) generated in each group of spots (Average of 10 replicate spot) for a defined amount of analyte. The curves were analysed with a four-parameter logistic equation using the software GraphPad Prism v 6 (GraphPad Software Inc., San Diego, CA, USA)]. The standard curves were fitted to a four-parameter equation according to the following formula: Y = [(A-B)/1-(x/C) D] + B, where A is the maximal fluorescence, B the minimum fluorescence, C the concentration producing 50% of the difference between A and B (or IC_{50}), and D the slope at the inflection point of the sigmoid curve. The limit of detection (LOD) was defined as the concentration producing 90% of the maximal fluorescence (IC_{90}).

4.5.4.5. Shared reactivity studies

With the aim to ensure the selectivity of the antibodies for their corresponding hapten molecules, shared reactivity studies were performed incubating the cocktail of antibodies at different analyte concentrations in a range of 0.5 nM to 5 µM (CIP, STZ, TYLA) in milk diluted 1/20. Calibration curves were obtained for the desired target molecule while the non-specific antibodies were binding to the haptenized oligos on the slide showing always the maximum signal, evidencing no cross interaction.

4.5.5. ANTIBODIES REACTIVITY PROFILE UNDER DDI MICROARRAY

Standards solutions for every selected target antibiotic and their family of compounds were prepared at three different concentrations at 2 MRL, 1 MRL and 0.5 MRL in milk and then diluted 1/20 in PBST Ca^{2+} 10mM. From SA's: Sulfapyridine (SPY) Sulfatiazole (STZ), Sulfametoxypiridazine (SMPZ), Sulfatchloropiridazine (SCPZ), Sulfadimetoxine (SDMX), Sulfamethoxine (SMX), Sulfamerazine (SRZ), Sulfachinoxaline (SCX), Sulfisomidine (SSD) were assessed. From Fluorquinolones: Enrofloxacin (ERFX), Ofloxacin (OFX), Ciprofloxacin (CPX, Sarafloxacin (SFX), Flumequin (FLUM), Danofloxacin (DNFX), Difloxacin (DFX), Norfloxacin (NFX)were assessed and from macrolides: Tylosin A (TYLA), was evaluated. After the addition of the target analyte, the ''Cocktail of Antibodies'' was added and incubated for 30 min at RT. The slides were washed followed by the addition of anti-IgG TRITC solution (1/250 in PBST 10 mM, 100 µL/well). The last 30 min at RT incubation took place and slides were washed with MiliQ H_20 dried with N_2 and read with the fluorescent scanner.

4.5.6. PLATFORM PRE-VALIDATION

Samples were spiked considering the MRL established for the respective antibiotics as reference value. The blind samples were prepared spiking at different concentrations above and below the reference, then 5µl of spiked samples were added in 95 µl of buffer PBST Ca^{2+} 10mM in each well. Making use of the multi-analyte assay, the randomly distributed samples were measured following the protocol previously described. Negative or Zero, and positive control solutions with a concentration of the analyte at the level of interest (MRL in each case) were also measured on the same slide to define the threshold value for that analyte to compare with the rest of the samples. The fluorescence obtained from the zero sample was normalized as 100 % of the signal and the control sample was set as reference value. Following the indirect assay format, a sample was classified as positive if the signal was lower than the control value obtained at the MRL and, on the contrary, a negative sample will evidence a higher fluorescence in comparison with the control and less than the zero. RFU's values were normalized and the graph is expressed in normalized RFU's to avoid

differences in the maximum response among the three immunoassays. Throughout this approach is possible to perform a semi-quantitative analysis by referring the signal obtained with the unknown sample to the reference and considering the intensity as indicator of regulatory compliance or not.

4.6. BIBLIOGRAPHY

1. Brambilla, D., L. Sola, and M. Chiari, *Advantageous antibody microarray fabrication through DNA-directed immobilization: A step toward use of extracellular vesicles in diagnostics.* Talanta, 2021. **222**: p. 121542.
2. Yang, Y., et al., *Enhanced reusability and activity: DNA directed immobilization of enzyme on polydopamine modified magnetic nanoparticles.* Biochemical Engineering Journal, 2018. **137**: p. 108-115.
3. Sun, P., et al., *DNA-Directed Assembly of a Cell-Responsive Biohybrid Interface for Cargo Release.* Small Methods, 2021. **5**(7): p. 2001049.
4. Kozminsky, M., et al., *Multiplexed DNA-Directed Patterning of Antibodies for Applications in Cell Subpopulation Analysis.* ACS applied materials & interfaces, 2021. **13**(39): p. 46421-46430.
5. Li, J. and J. Macdonald, *Multiplexed lateral flow biosensors: Technological advances for radically improving point-of-care diagnoses.* Biosensors and Bioelectronics, 2016. **83**: p. 177-192.
6. Meyer, R., et al., *Advances in DNA-directed immobilization.* Current Opinion in Chemical Biology, 2014. **18**: p. 8-15.
7. Li, M., et al., *Controllable and high-performance immobilized enzyme reactor: DNA-directed immobilization of multienzyme in polyamidoamine dendrimer-functionalized capillaries.* Electrophoresis, 2020. **41**(5-6): p. 335-344.
8. Seymour, E., et al., *DNA-directed antibody immobilization for enhanced detection of single viral pathogens.* Analytical chemistry, 2015. **87**(20): p. 10505-10512.
9. Morvan, F., et al., *Glycoarray by DNA-directed immobilization.* Carbohydrate Microarrays: Methods and Protocols, 2012: p. 195-219.
10. Tort, N., et al., *Synthesis of steroid–oligonucleotide conjugates for a DNA site-encoded SPR immunosensor.* Bioconjugate Chemistry, 2012. **23**(11): p. 2183-2191.
11. Tort, N., et al., *Fluorescence site-encoded DNA addressable hapten microarray for anabolic androgenic steroids.* TrAC Trends in Analytical Chemistry, 2009. **28**(6): p. 718-728.
12. Tort, N., J.-P. Salvador, and M.-P. Marco, *Multimodal plasmonic biosensing nanostructures prepared by DNA-directed immobilization of multifunctional DNA-gold nanoparticles.* Biosensors and Bioelectronics, 2017. **90**: p. 13-22.
13. Health, W.O.f.A., *OIE List of Antimicrobial Agents of Veterinary Importance (June 2021).*
14. Authority, E.F.S., D. Brocca, and S. Salvatore, *Report for 2021 on the results from the monitoring of veterinary medicinal product residues and other substances in live animals and animal products*. 2023, Wiley Online Library.
15. Commission, E., *Commission Decision 2002/657/EC of 12 August 2002 implementing Council Directive 96/23/EC concerning the performance of analytical methods and the interpretation of results.* Official Journal of the European Communities, 2002. **50**: p. 8-36.

16. Commission, E., *Commission Implementing Regulation (EU) 2021/808 of 22 March 2021 on the performance of analytical methods for residues of pharmacologically active substances used in food-producing animals and on the interpretation of results as well as on the methods to.* Off J Eur Union, 2021. **180**: p. 84-109.
17. Sanchis, A., et al., *Fluorescent microarray for multiplexed quantification of environmental contaminants in seawater samples.* Talanta, 2018. **184**: p. 499-506.

5. PROOF OF CONCEPT: PORTABLE *I*SPR BIOSENSOR WITH SMARTPHONE READOUT

5.1. SUMMARY

This section describes the studies made towards the development a portable, cost effective and easy to use imaging surface plasmon resonance (iSPR) biosensor, integrating smartphone detection [1] and based on oligonucleotide biofunctionalized chips, for the analysis of veterinary drug residues in milk. The reasons behind the use of DNA chips were mainly three. First, the possibility to allow using the same chip for a variety of potential applications, reducing in that way the cost. As mentioned in Chapter 4, DDI microarrays can be contemplated as universal platforms, which could be used to immobilize any kind of bioreagents as soon as the corresponding complementary oligonucleotide probes are available. Hence, although in this thesis, the objective has been the detection of antibiotic residues, the same chip could be used to detect anabolic androgenic steroids, for which oligonucleotide probes and antibodies have been previously prepared in our group [2, 3] or any other target that could be considered of interest in the food safety, environmental o clinical fields.

Secondly, the SPR signal is strongly dependent of changes in the refractive index (RI) of the surface, and this is directly affected by the mass of the ligand immobilized and the target analyte interacting. Indeed, the relative mass ratio between the ligand and analyte determines the resolution in SPR [4, 5]. Therefore, it would be expected that the mass ratio between the hapten-oligonucleotide conjugate (1.2 KDa, hybridized strands) with the MAb (150 KDa) will be considerably higher to the hapten-BSA conjugate (67 KDa) interacting with the MAb, that will be translated in an increased resolution.

A third hypothesis for using DNA conjugates instead of proteins, is founded on the idea that functionalized sensors with hapten-oligonucleotide probes, may promote close proximity of reagents to the gold surface of the SPR chip, improving detectability due to the fact that the sensing electromagnetic field is confined to a length of almost 300 nm [6-8].

Part of the work discussed in this chapter, is the result of a collaboration with Linkoping University (LiU, Sweden), particularly with the Optical Devices Laboratory group headed by Prof. Daniel Filippini in the context of the FoodSmartphone project (ITN-Marie Curie Action) as part of a secondment to

receive mentoring and support in aspects related to the portable sensing devices.

5.2. INTRODUCTION TO BIOSENSING DEVICES

5.2.1. PLASMONIC SMART-SENSING: INTEGRATING SPR WITH SMARTPHONE DETECTION

The necessity of miniaturized, cost effective and easy to use on-site sensing platforms became highly desirable for analytical determinations. In this context, smartphones have evolved to reduce the gap between complex optical detection systems with familiar user interfaces. Furthermore, trends in smartphones developments are moving from communication purposes to the integration of sophisticated tools such as high-resolution cameras, global positioning systems, internet access, ambient light sensors or touch screens sensors to improve their performance and market competitivity [9]. On the other hand, optical detection methods and more precisely plasmonic approaches became feasible techniques to implement across portable analytical devices since new detection elements were incorporated to these hand-held devices, also favoured by user friendly interfaces. Remarkably, new alternatives to approach bioanalytical determinations into portable, cheaper and easier to use solutions emerge with promising impact in the market.

Driven by the idea of moving towards the improvement of user-friendly point-of-care (PoC) devices and bioanalytical platforms, numerous examples combined smartphones detection with lateral flow immunoassays [10], fluorescence [11], colorimetric assays [12]. On the other hand, SPR principle was coupled to smartphone technology takeing advantage of common elements such as light sources (LED's), CMOS detectors (camera) or even processing data capacity to address label free, re-usable and easy to perform bioanalytical determinations [13]. A schematic representation of SPR phenomena integrating smartphones is shown in Figure 5.1 making use of the camera as optical detector to translate a binding interaction in real time.

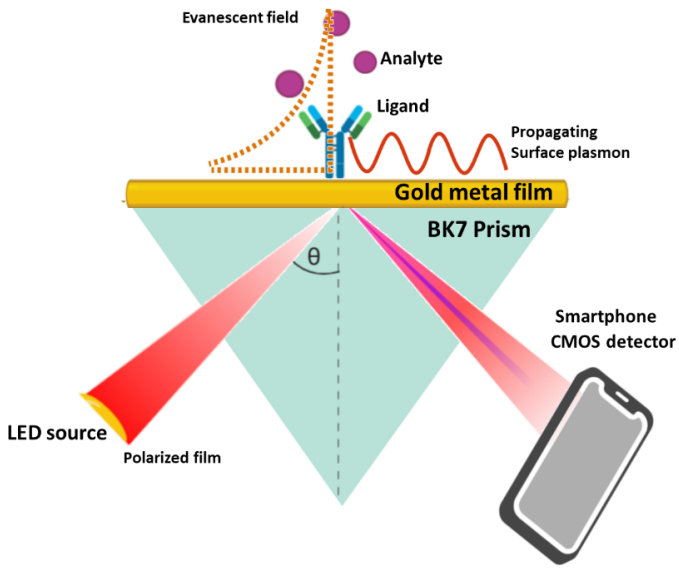

Figure 5.1 Principle of SPR technique integrating smartphone detection. The LED source and the polarizer film generates a p-polarized light beam that is conducted through the glass prism to the gold sensing surface. The interaction of photons from the light, excite surface electrons generating the evanescent field that allows monitoring in real time and label free the binding events. Interactions taking place at surface level will be evidenced in a change in the reflected light that is recorded with the smartphone camera for further analysis.

Commencing a decade ago, the group of Prof. Fillipini reported for the first time the development of a single use iSPR detection system to monitor β2 microglobulin (β2M) in serum and urine reaching limits of 0.1 mg mL^{-1} integrating an iPod touch/iPhone system as part of the detection [14]. Afterwards, different authors made use of a similar principle, to monitor the binding of immobilized mouse-IgG's with rabbit anti-mouse antibodies using a smartphone and reaching nanomolar detection levels [15]. Alternatively, a different plasmonic approach consisting on grating coupled SPR was successfully incorporated with smartphones to detect endotoxins in clinical injectable fluids [16]. The sensor surface was coated with a synthetic peptide receptor to provide specificity for the target molecule making use of the flash light and the camera to record the sensor response declaring a detectability of 32.5 ng mL^{-1} of lipopolysaccharides in water. In an attempt towards miniaturization, the properties of optical fibres were utilized to conduct light to the sensing surface using the SPR principle to measure IgG levels with considerable reproducibility. The advantage of this approach relies on the lack of complex and delicate optical components such as glass prims or grating elements [17]. As expressed, the potential integration of plasmonic techniques with smartphones has

been addressed by many authors evidencing successful results in different applications towards more robust and miniaturized components.

5.2.2. DESCRIPTION OF THE PORTABLE AND MINIATURIZED SMARTPHONE BASED ISPR BIOSENSOR

A smartphone based iSPR prototype was developed by the group of Prof. Fillipini (LiU, Sweden) based on their expertise on the fabrication of portable analytical devices [18], 3D printing technology, microfluidics and smartphone detection [19]. However, the innovative platform needed to be evaluated in terms of potential applications related with the bioanalytical field. As result of this collaboration within the context of the FoodSmartphone ITN-MCSA project we approached the possibility to use it for the determination of antibiotic residues detection in milk integrating the already characterized MAb's and hapten bioconjugates.

As a general description, the portable iSPR system basically contains a LED source covered with a polarizer to conduct the p-polarized light beam across the glass prism that is in contact with the gold sensor chip through a thin interface of immersion oil, see Figure 5.2. Immediately, the light interacts with the external layer of electrons from the 50 nm gold surface, producing an electromagnetic field (surface plasmon) that is sensitive to changes in refractive index in a confined region of 300 to 400 nm from the surface. Shortly after, the light reflected is guided through the prism in the opposite direction at a specific angle, that is slightly shifted if any event changing the RI takes place over the sensor, producing a label free and real time measurable response. The light beam finally impacts on a curved mirror, that will reflect this beam directly to the smartphone camera recording the real time data in video format. The shift of the intensity dip reflected is monitored by the video, as consequence of changes in RI on the sensing surface. The corresponding signal displacement recorded in pixels, can be quantified to estimate the (resonant units) RU's attributed to the interaction occurring over the sensor.

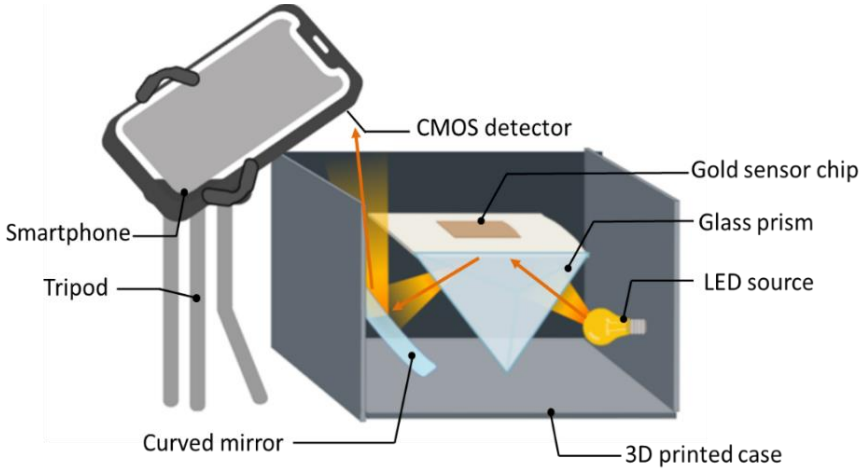

Figure 5.2 Portable smartphone based iSPR experimental setup Schematic representation of the portable iSPR system composed by an LED source that travels through the prism, impact on the sensor chip generating the propagating plasmon and the light is reflected in the curved mirror and recorded with the smartphone evidenced as a dip in the intensity recorded to monitor changes taking place at the sensor surface.

Following, a detailed description of the main components of the portable iSPR, the method of signal acquisition via smartphone and the post processing analysis developed by LiU partners is discussed [1].

5.2.2.1. Main components of the miniaturized iSPR prototype

The external attachment of the portable iSPR is a three-piece component generated through 3D printing technology, that allows the correct setting of the optical elements required for the SPR measurement. As the Figure 5.3 shows, a- ; b- and c-, sections represent the individual parts of the holder that are assembled in the section d- of the picture, containing the glass prism, mirror and LED. In the section e-, a rendered view of the device is available with the corresponding dimensions.

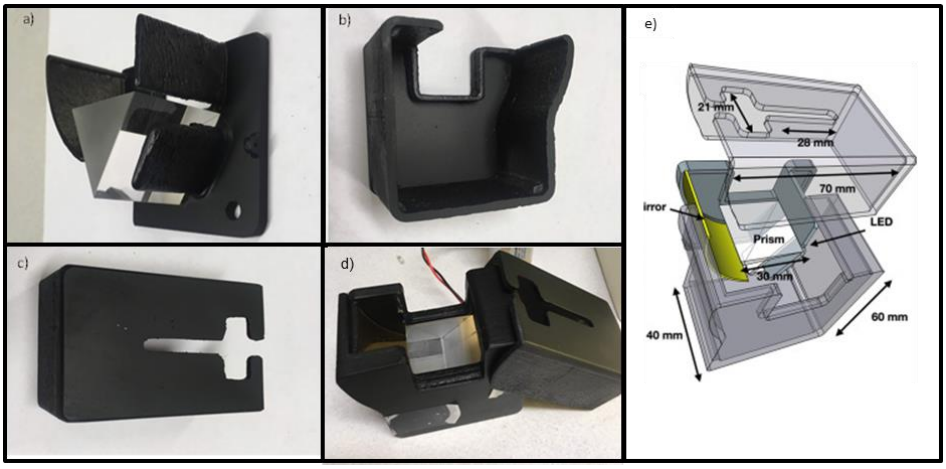

Figure 5.3 3D printed modules of the portable iSPR device. a) component holding the Prism, and curved mirror b) Lateral piece that fits with the component a and act as holder for the LED source and in picture c) device cover, to avoid light interference and guide smartphone position. d) top view of the final device assembled e) CAD rendered scheme of the miniaturized device extracted from [1].

In general, benchmark SPR devices are characterized by bulky and expensive equipment's limiting their implementation outside the laboratory. A substantial difference in size and cost is achieved with the portable iSPR compared to reference SPR systems like Biacore. Although the miniaturized platform also present certain limitation regarding automation, sensitivity and reproducibility at the same time provides a starting point to integrate real time and label free detection into user friendly and affordable alternatives.

5.2.2.2. PDMS microfluidic cell chips

The described system works under continuous flow mode, and for this purpose an inexpensive 3D printed PDMS microfluidic cell was designed. The cell is composed of a single 1 mm microfluidic that is adhered to the gold sensor chip with a double-sided tape to conduct the solutions injected (see Figure 5.4) On a-section, a scheme indicating cell dimensions is represented while next to it an image obtained using an optical microscope sealing the cell over a glass surface and flowing a blue solution to verify the absence of leakages is showed.

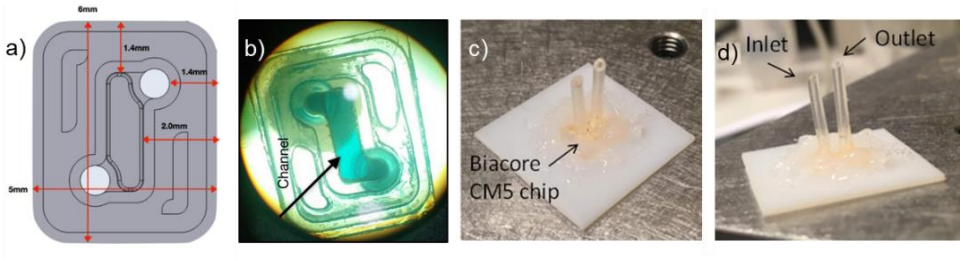

Figure 5.4 Microfluidic cell dimensions a) Computer aided design of the microfluidic cell and spatial distribution. b) optical microscope image of the sealed microfluidic chip over a glass surface after injecting coloured solution to evidence the absence of leakages. c)d) Mounted CM5 sensor and microfluidic cell. Inlet and outlet silicone tubes connected to the microfluidic cell.

Once the cell is completely sealed on the CM5 sensor chip, the inlet and outlet silicon tubes are placed in the corresponding holes to allow solutions injection and ejection from the surface (sections c- and d-). Afterwards, the mounted chip with the microfluidic is placed on top of an immersion oil drop over the glass prims to start the measurments.

5.2.2.3. Smartphone data acquisition

In the next step, the signal acquisition was carried out through a smartphone device and in this case a Google Pixel II was utilized. To standardize video recording conditions such as external illumination, exposure or ISO values the OpenCamera App was implemented. This App allows to fix the parameters required for the signal determination minimizing variability between measurements. In the following table, the main camera settings are described.

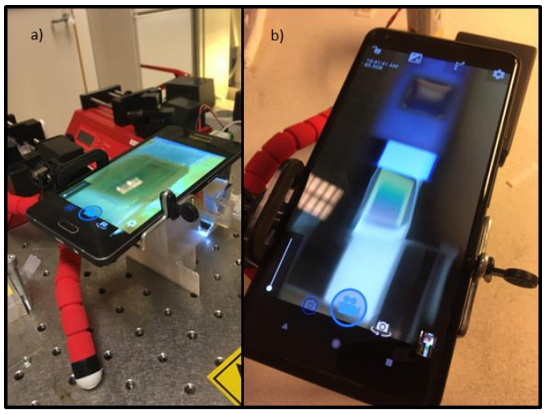

Table 5.1 Open Camera general settings

Feature	Setting used
Camera flash	off
Frames/sec	30 frames/sec
Time	15-30 min
ISO value	100-300
Zoom	X 2.4
Focus mode	Static
Exposure	Locked
Size	720 Mb
Format	MP4

Figure 5.5 Smartphone positioning on top of the portable iSPR system a) The view of the complete device connected to a syringe pump and tripod is observed. b) Front view of the Google pixel II screen during video recording of the plasmon band.

In order to place the smartphone camera over the curved mirror to evidence the plasmon signal (represented as a green band, in Figure 5.5), a tripod was utilized. The green section of the image corresponds to the plasmon generated over the sensor chip, and the displacement of that band during the measurement is directly correlated to changes in RI of the surface like ligand analyte interactions in real time.

5.2.2.4. Smartphone iSPR data post-processing

The measurements performed with the smartphone were saved as .MP4 format to then be transferred to a computer to proceed with the data analysis using an in-house Python software developed LiU partners, to extract the data points from the video to a .CVS file for further processing. The signal is basically obtained from the displacement of the intensity dip recorded as a green band on the video. This optical phenomenon is utilized to monitor refractive index changes over the gold surface with the smartphone camera. Afterwards, the computer software adjusts the selected frames to a polynomial function to obtain the characteristic dip, which is monitored at 30 frames per second (fps) to generate the sensogram.

On a first instance, it was necessary to define the section of the video to be used for recording the change in the refractive index (where the plasmon band was registered). For this, the user interface showed in Figure 5.6 allows the selection of a specific area, by establishing the X1 and Y1 values according to the frames processed of width, height and filter. By pressing "Apply Mask" button, the program automatically adjusts the predefined area to a polynomial function, showing the SPR signal as the characteristic dip. Then, by clicking the "Compute" button, the signal processing step occur, to finally obtain the sensogram displayed and ready to be exported as a .CSV file compatible with excel.

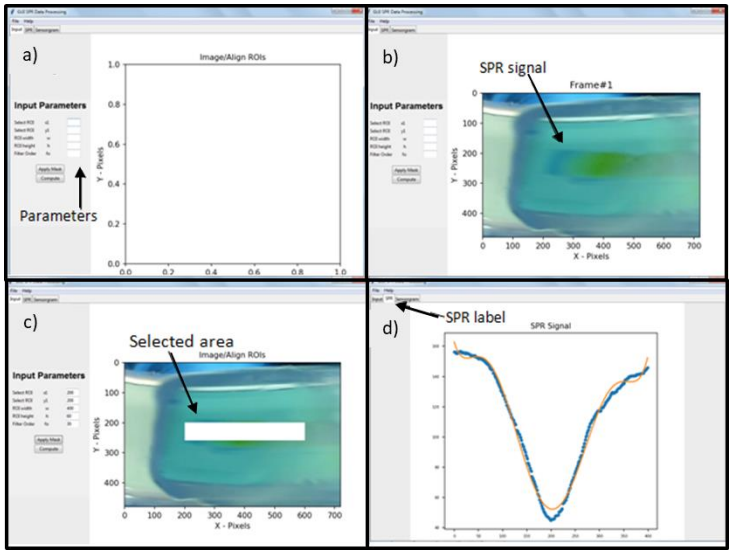

Figure 5.6 User interface and selection of the area of quantification a) Main menu without a selected file b) Image of the video with the plasmon band necessary to define for the analysis c) selected area for quantification d) SPR signal obtained from that selection.

The step by step sequence already described, is represented in the screenshots obtained during the analysis of a video recorded after buffer injections. Although the state of development of the device was not fully achieved by the time that the determinations in this chapter were performed, the final aim of LiU collaborators was to integrate the analysis software as a smartphone App to conduct the post-processing steps directly in the smartphone without the need of external computer.

5.2.3. FINAL PROTOCOL FOR THE USE OF SMARTPHONE ISPR SYSTEM

The final prototype of the smartphone iSPR system was expected to be used as a portable, cost effective and user-friendly screening tool for the determination of veterinary residues in milk at dairy farm or even at consumer levels. Due to this, the following schemes represent the desirable final device with potential application in the real field, bearing in mind that during this work, the measurements were performed under laboratory conditions. First the potential SPR test KIT components are described in the following image.

-Incubation vial: containing freeze dry immunoreagents (Hapten-oligonucleotides and MAb's) where the milk sample would be added to perform the competitive step in solution.

-Portable SPR module: to place the sensor and perform SPR determination

-Gold sensor and microfluidic cell: with already immobilized oligonucleotide strands (N_{down})

-Smartphone and computer software: for signal acquisition and processing

-Syringe Kit: containing the buffers needed to perform the assay

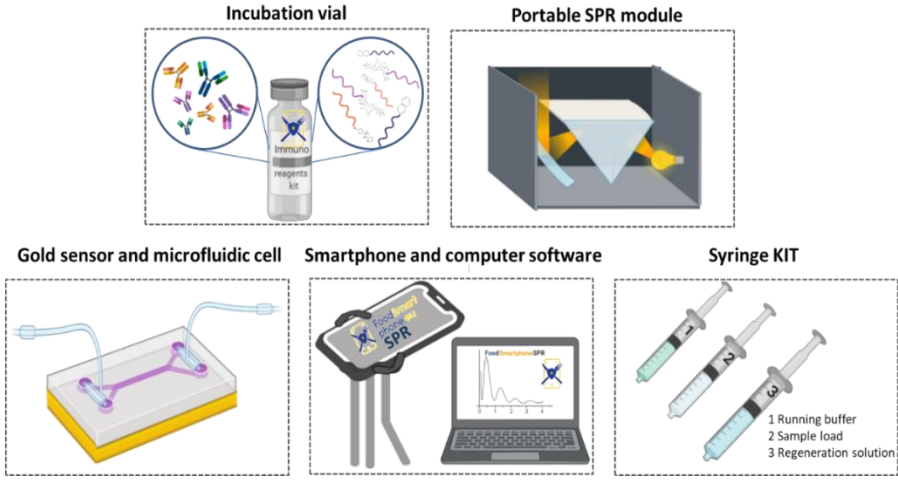

Figure 5.7 TEST Kit components for portable smartphone based iSPR detection of antibiotics in milk. the detailed description of the main components needed is represented in the picture including immunoreagents, the portable iSPR platform as well as the smartphone and computer for analysis.

After describing the system components, the proposed experimental workflow to determine traces of antibiotics with the iSPR system in real time is detailed in the following scheme in Figure 5.8:

Step 1: Add the milk sample to the incubation vial and wait for thirty minutes

Step 2: In parallel, mount the sensor chip with the microfluidic cell over the portable iSPR platform.

Step 3: After that, start recording with the smartphone and flowing running buffer through the sensor with the syringe 1 at a moderate flow rate for ten minutes to reach a stable base line. Avoid the formation of bubbles in the system. Next, take syringe 2 to inject the milk sample from the incubation vial through the microfluidic cell at low flow rate and wait 10 minutes. Finally, take syringe 3 for surface regeneration making a single injection for 5 minutes at low flow rate. Repeat the same cycle for every sample.

Step 4: Once sample injections are finished. Stop recording and transfer the data from the smartphone to the computer with the software of analysis. The sensogram will be processed

Step 5: Final test results from the iSPR analysis will be displayed in your smartphone.

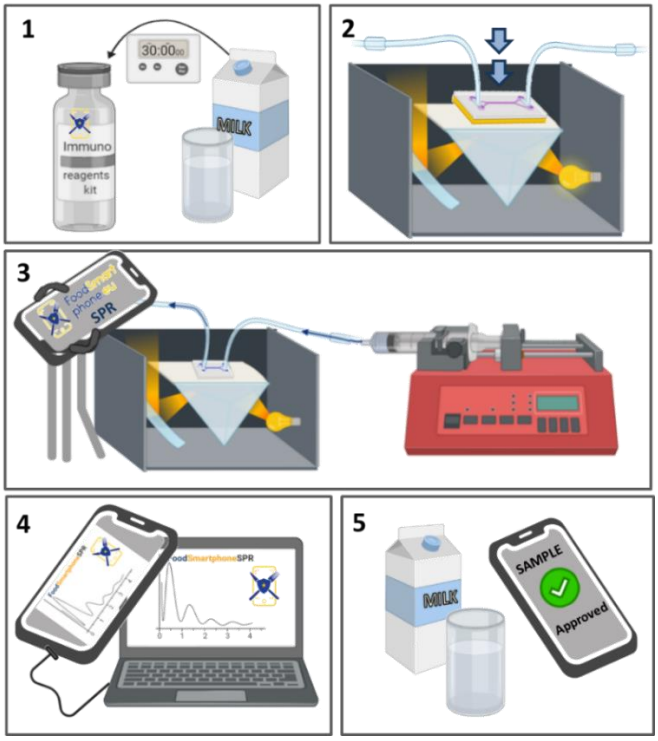

Figure 5.8 Step by step protocol for portable iSPR determination. The visual representation of every step taking place during sample detection is represented in the figure. Numbers are assigned to identify the order suggested to perform the analysis.

Assuming the limitations of the platform by the time that was implemented in this experimental work, the potential development of a commercial test kit is proposed if the bioanalytical performance is demonstrated and the system works as expected. In the biosensing field, the transition from laboratory-based technologies to real life applications is a major concern considering the high amount of novel developments and the limited number of devices that reach the market. In this regard, science requires the interest of third parties also involved in the scaling process with the corresponding financial support to reach an adequate technological maturation stage to be competitive with other platforms.

5.3. RESULTS AND DISCUSSION

5.3.1. IMMUNOREAGENTS EVALUATIONS WITH REFERENCE SPR TECHNIQUES

As prior step before proceeding with the development of a portable iSPR for food safety we considered relevant to evaluate the properties of the immunoreagents used in the thesis through a reference SPR system. These sets of experiments not only would provide data on the affinity of our antibodies, but also the sensograms obtained could be used as reference of the results recorded with the portable device, allowing to carry out a critical comparison and evaluation of the iSPR system. Hence, on first instance we used Biacore™ T200, as a benchmark and well-established SPR technology since 1990's when the first Biacore SPR instrument was commercially released. Biacore was founded by researchers from Pharmacia, Linkoping Institute of Technology and the Swedish National Research Agency on year 1984, and on year 1996 named Biacore AB Corporation to became a reference in respect to the measurement of biomolecular interactions. The company, that had great success became later on a brand of GE Healthcare Life Sciences and since year 2020 is Cytiva. On a second stage, we attempted to perform the same kind of measurements with an equipment available in our group based on the LSPR principle commercialized under the OpenSPR name from Nicoya (Ontario, Canada).

5.3.2. KINETIC CHARACTERIZATION OF THE MONOCLONAL ANTIBODIES WITH BIACORE™ T200

Kinetic and affinity studies were performed utilizing Biacore™ T200 SPR system, considered as reference method for ligand-analyte affinity characterization in solution [20], using a commercial gold chip grafted with a carboxymethyl-dextran hydrogel (CM5). Such hydrogels provide a biocompatible environment with the necessary biomolecule attachment sites (in this case carboxy groups), favours the use of a higher fraction of the evanescent field and prevents from nonspecific undesired adsorptions on the gold. Firstly, pH scouting experiments were conducted to define the most adequate immobilization condition to favour

electrostatic interactions between hapten-BSA conjugates (positively charged at a pH's below the isoelectric point of the protein) and the electronegative carboxylated dextran coating on the gold surface. As a result, 10 mM sodium acetate at pH 4.5 was selected as the preferred buffer for ligand immobilization. The CM5 sensor chips allow covalent coupling of biomolecules with amino groups (-NH_2) such as those present in our ligand (lysine residues from BSA protein) over the thin gold layer coated with dextran molecules containing carboxyl groups (-COOH) once have been activated with EDC/NHS chemistry in continuous flow (see Figure 5.9).

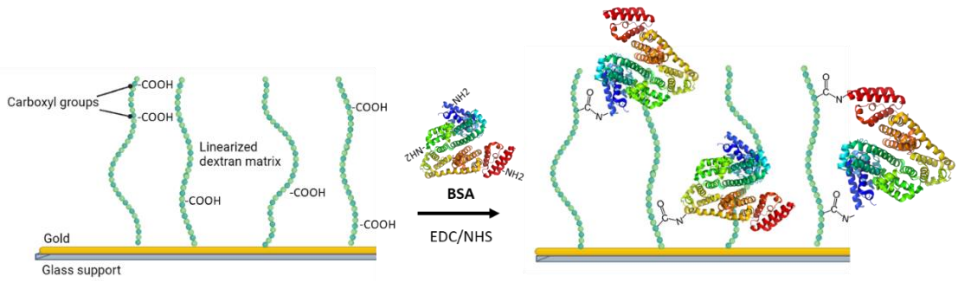

Figure 5.9 Schematic representation of the covalent immobilization of BSA molecules to the carboxymethylated dextran matrix using EDC/NHS chemistry.

During affinity experiments, the immobilization step had to ensure low surface density to avoid steric hindrance/aggregation, reduce mass transport limitation and to obtain a higher range of controlled binding. The Biacore™ T200 system is composed of a 4-channel microfluidic cell that allows independent immobilization over each channel and simultaneous chamber communication. Additionally, this tuneable format also admits to flow the desired matrix over all channels sequentially or separately. For the proposed experiment, the first channel was employed to covalently bind BSA as control of nonspecific adsorptions, the second was designated to immobilize PrEDA-BSA (50 µg mL^{-1}) bioconjugates defining the FQ's channel, then third channel contained SA2-BSA (50 µg mL^{-1}) for SA's detection and in the fourth microfluidic channel was dedicated to hTB-BSA (50 µg mL^{-1}) immobilization for TYL residues determination The final immobilization levels archived were in control BSA 166 RU's, PrEDA-BSA 304 RU's, SA2-BSA 71 RU's and hTB-BSA 236 RU's. A single CM5 sensor chip allowed simultaneous immobilization and characterization of all immunoreagents simultaneously.

Once the chips were prepared, single cycle kinetic experiments were performed to determine the affinity constants of hapten-BSA conjugates with the MAb's in assay buffer. According to the results from Figure 5.10, the pair that showed the strongest affinity (or lower KD value) was MAb-Tyl / hTB-BSA pair with a KD of $1.367x10^{-10}$ M, followed by MAb-FQ/ PrEDA-BSA with a KD of 7.14610^{-9} M and then the MAb-SA/ SA2-BSA with a KD of $1.098x10^{-8}$ M. The already described experiments were performed in 10mM PBST-Ca^{2+} as running buffer required for optimum detection of FQ's. This buffer was previously evaluated over the other immunoreagents demonstrating no significant changes in detectability under ELISA and microarray formats and because it would be needed on the multiplexed format. Afterwards, making use of the corresponding Biacore™ T200 evaluation software v1.1, the association(k_a) and dissociation (k_d) rates were calculated which can be found on the table 5.2.

Based on the experimental results recorded with the Biacore™ T-200, MAb-FQ showed fast association rate (10^{-4}) with relatively low dissociation value, offering a KD in between of the other two immunoreagents assessed. While on the other hand, MAb-SA and MAb-Tyl evidenced the faster association rates (10^{-5}), but the dissociation step occurred differently, affecting the final KD value. A fraction of MAb-SA was easily unbound in buffer, without applying a regeneration step which indicates weaker affinity if compared with MAb-Tyl that during dissociation step remained bound. Particularly, to dissociate MAb-Tyl/hTB-BSA complex, a different regeneration solution was required evidencing the strong interaction of the antibodies for the hapten also expressed in the low dissociation rate measured. Several dilutions of each MAb's were prepared in PBST Ca^{2+} buffer and single cycle kinetic experiments were performed acquiring replicates for each corresponding dilution.

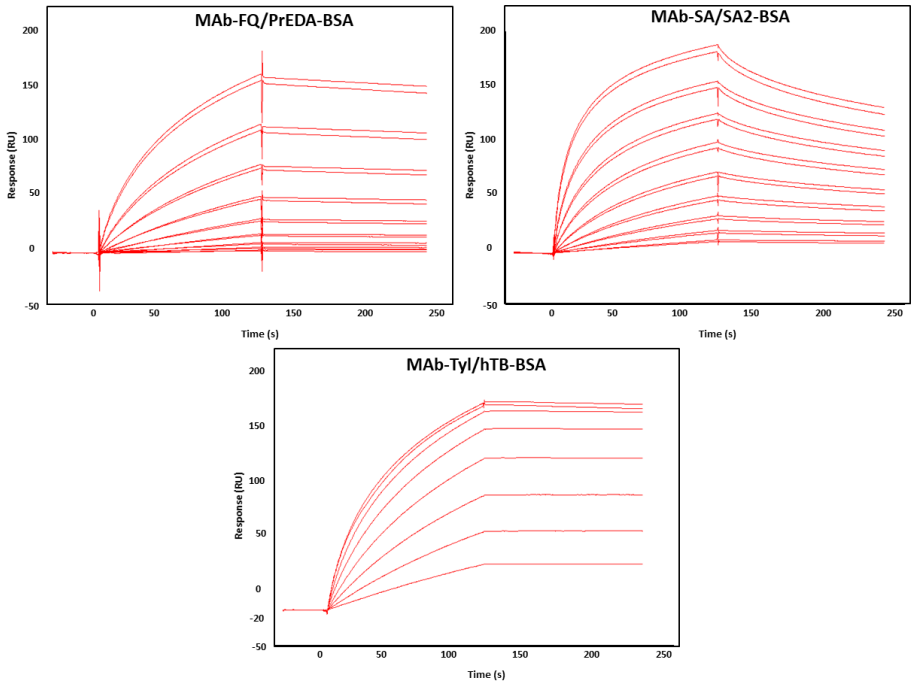

Figure 5.10 *Binding profile of MAb's and hapten-BSA conjugates. Binding curves under multicycle kinetic format were after immobilization of BSA-hapten conjugates with duplicate injections of MAb's serial dilutions in PBST Ca^{2+}. Regeneration was carried out with Gly-HCl 0.1M for FQ and SA reagents while10mM NaOH was used over TYL reagents.*

Duplicate injections of antibody solutions at different concentrations were flowed through the biofunctionalized CM5 sensor chip with the corresponding BSA conjugates with antibody dilutions ranging from 332 nM-2.6 nM Typical association and dissociation phases are observed for each antibody/conjugate pair in the sensogram showing differences in recognition profiles.

Table 5.2 Kinetic features of the three MAb 's and their respective bioconjugate pairs evaluated in Biacore™.

Kinetic parameters	MAb-FQ	MAb-SA	MAb-Tyl
ka ($M^{-1}.s^{-1}$)	$6.424x10^{+4}$	$2.505x10^{+5}$	$3.166x10^{+5}$
kd (s^{-1})	$4.590x10^{-4}$	0.002752	$4.328x10^{-5}$
KD *	**7.14610^{-9}**	**$1.098x10^{-8}$**	**$1.367x10^{-10}$**

*KD is expressed in M. Kinetic determinations were determined from duplcate injections of 8 serial MAb's dilutions each.

As can be seen in the, Figure 5.10 each antibody presents a distinctive binding behaviour, however the affinity estimated in these expermients corresponds to the interaction between the antibody and the hapten-BSA conjugate immobilized, that is not strictly equivalent to the analyte free in solution. Interestingly, MAb-Tyl presented the strongest affinity constant for the hapten-BSA conjugate and experimentally required more aggressive conditions (10 mM NaOH) for surface regeneration in comparison with the others bioconjugates using standard 0.1 M Gly-HCl as regeneration solution. Furthermore, if the equilibrium is shifted to the formation of antibody-hapten complex rather than the antibody-target analyte, a worst assay detectability can be expected as a result of the stronger interaction of the antibody for the competitor (hapten-BSA), thus careful assay optimization is highly recommendable at this point [21].

On the other hand, the MAb-SA showed weaker affinity for the BSA conjugate and unexpectedly when was used on the DDI microarray (Chapter 4) presented the lower detectability of the three assays. This can be partially explained by a stronger interaction of the MAb-SA for the analyte free in solution rather than the BSA-hapten conjugate, translated in a lower affinity constant detected in SPR. Contrarily, the same effect is observed in the case of MAb-Tyl with significant affinity for the hTB-BSA bioconjugate through SPR, while the detectability of the assay in ELISA or microarray was not the most remarkable of the three analytes evaluated. Although this hypothesis should be corroborated with additional experimental evidence, it may be useful to explain the behaviour evidenced under competitive assay formats.

From the developmental perspective, this type of characterization results essential to optimize immunosensors performance in the real field. For instance, in multiplexed approaches it would always be preferable to have immunoreagents with similar binding profiles to define a unique incubation time or sample dilution as well as achieving comparable detectability amongst the species involved. According to the results obtained, the MAb-SA offers a quick response, but if long incubation periods are required for other reagents, part of the analyte can be released underestimating the real content in the sample. Although the association phases are not strictly comparable among MAb-Tyl and MAb-FQ, due to the low dissociation rates estimated, both antibodies can be successfully implemented with a relatively long incubation period without affecting analyte determination in each case.

5.3.3. BINDING PROFILE CHARACTERIZATION OF TYLOSIN MONOCLONAL ANTIBODY USING THE OPENSPR™

In an attempt to compare the data recorded within the Biacore™ T-200 and a different plasmonic approach, the OpenSPR™ was used. This device is a benchtop LSPR instrument that allows binding kinetic determinations of ligand-analyte interactions in friendly assay formats. A characteristic feature of this platform is found on the sensor chip which consist on a micro-structured glass surface containing nanogold coated with a carboxylated dextran matrix, instead of the typical flat thin gold layer (SPR) of the Biacore™ T200 and other SPR systems.

To make comparable determinations between both platforms, TYL immunoreagents were used as reference, owing the excellent features evidenced by the Biacore™. Once again, the use of EDC (0.2 M)/NHS (0.05 M) chemistry was required for surface activation and protein immobilization (hTB-BSA conjugate) over the sensor chip, which in this case was used with dual channel injection mode. The OpenSPR™ system is composed of two independent flow channels allowing the simultaneous immobilization of hTB-BSA ligand (in blue, Figure 5.11) in channel A while channel B was kept as empty as reference (in red) for unspecific binding to the sensor surface, as the lack of interaction with BSA was demonstrated in the Biacore™ system. Comparably, the hTB-BSA (50 µg mL^{-1}) conjugate was injected in 10 mM sodium actetate at pH 4.5 to enhance electrostatic interactions. The running buffer for the MAb-Tyl dilutions was 10 mM PBS, without Ca^{2+}, since this MAb's did not required presence of divalent cations.

In the next Figure 5.11, the sensograms obtained during immobilization showed a response difference between the two channels attributed to the immobilization of hTB-BSA on channel A. After the injection of 1 M ethanolamine pH 8.5 to block remaining active carboxy groups, a total of 3.350 RU's (response units) were recorded, defining the immobilization level of this bioconjugate on the OpenSPR™ chips, using the associated analysis software (Trace Drawer).

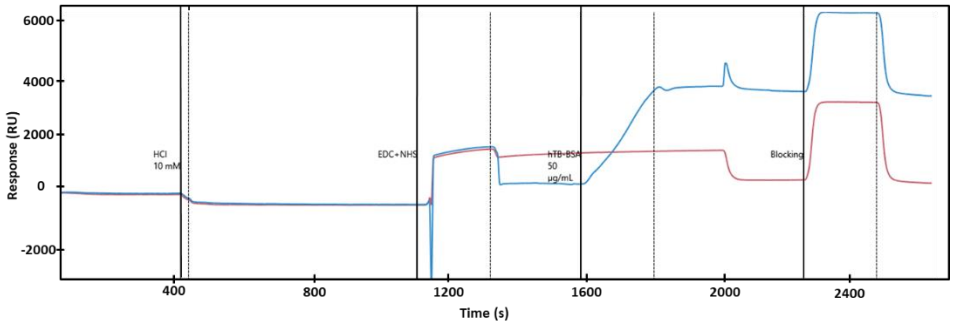

Figure 5.11 *Biofunctionalization of hTB-BSA. Sensogram recorded, when a stable baseline is achieved, the addition of the EDC/NHS mixture took place, followed by the injection of hTB-BSA conjugate evidencing the high immobilization level in the signal recorded in the channel A (blue) because of the covalent coupling of the bioconjugate while the channel B (red) remains the same. Finally, a blocking step with 1M ethanolamine was performed recovering the baseline.*

Subsequently, a dose dependent response was recorded after MAb-Tyl injections at different concentrations with a continuous flow rate of 25 µl min^{-1}, using what is known as multicycle kinetic experimental mode. This approach consists on the repeated additions of the binder (MAb) during the association phase, followed by a dissociation period in which the MAb injection is limited and only running buffer (10 mM PBS) is added to the system, to promote the release of weaker interactions to finally perform a regeneration step (10mM NaOH) to ensure complete removal of the binder from the surface allowing repeated injection cycles. In this case, a total of eight injections with increasing antibody concentrations were tested giving a specific response signal correlated to the amount of antibody interacting with the bioconjugate.

Probably one of the main limitations of multicycle kinetic approaches rely on the achievement of a complete surface regeneration without compromising the biological activity of the ligand immobilized. For this example, 10mM NaOH was utilized as regeneration solution as determined before in the Biacore™ experiments. A remarkable aspect behind regeneration is based on monitoring no drift in the baseline due to the loss of BSA conjugates or denaturation of the protein that could affect the biological activity after repeated uses of the sensor also interfering with an accurate estimation of the affinity constant. As can be seen in the sensogram (Figure 5.12) the baseline is recovered after each regeneration step validating adequate performance of the sensor under optimized conditions.

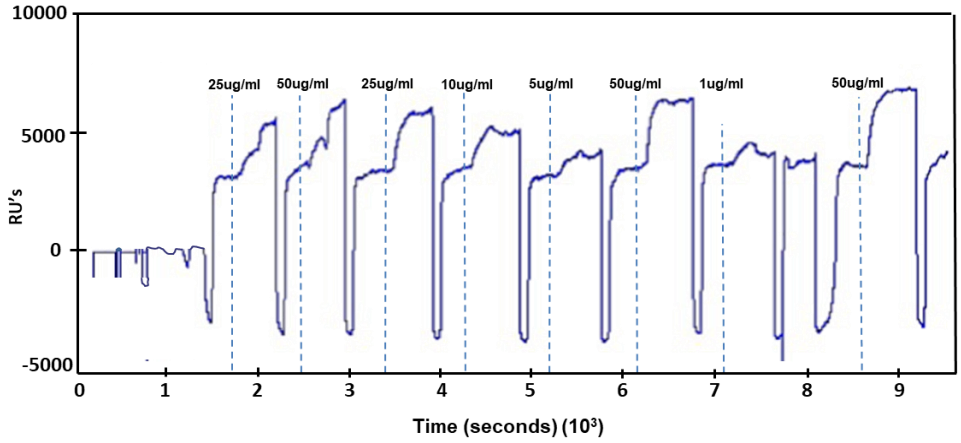

Figure 5.12 Multicycle Kinetic determination of MAb-Tyl over hTB-BSA conjugates affinity. The raw sensogram obtained after repeated cycles of MAb-Tyl injections and regenerations with 10mM NaOH are evidenced. The regeneration is observed as a characteristic dip in the response recorded due to the change in the RI of the surface.

Throughout this experiment, antibody concentrations ranging from 50 µg mL^{-1} to 1 µg mL^{-1} in 10mM PBS were injected and the sensor response acquired. Afterwards, binding curves were extracted from the raw sensogram analysis making use of the software to estimate the affinity constant (KD) and the kinetic parameters. As Figure 5.13 shows, experimental curves obtained from the sensogram were fitted to a 1:1 binding model, following Langmuir behaviour, defining association for 250 sec and dissociation phases for 250 sec, respectively to estimate k_a, k_d and the equilibrium constant (KD).

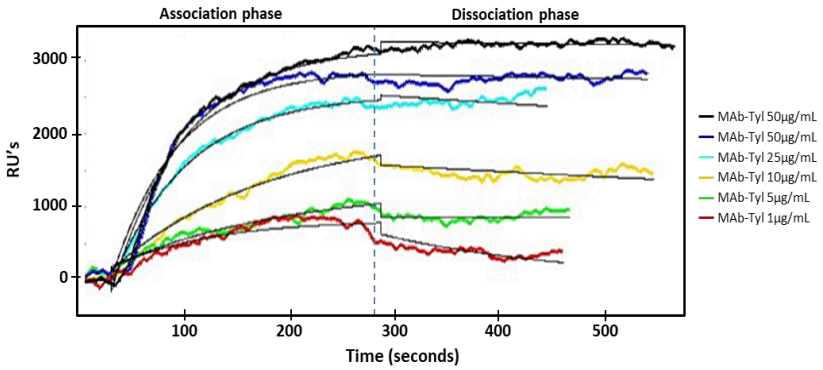

Figure 5.13 Binding curves experimentally obtained and fitted curves determined with TraceDrawer analysis software. Binding curves extracted from the sensogram generated following multicycle kinetic mode. Each curve corresponds to a single injection of MAb-Tyl at the corresponding concentration. Association and dissociation phases are discriminated.

Table 5.3 Kinetic parameters estimated with OpenSPR™ for single MAb-Tyl injections and global KD estimation.

MAb-Tyl cc.[a]	RU_{max}	K_a (1/(M*s))	K_d (1/s)	KD[b]	Global KD[b]
50	3353.24	$4.28x10^{4}$	$4.85x10^{-5}$	$1.13x10^{-9}$	$1.73x10^{-9}$
50	2870.88	$4.78x10^{4}$	$8.88x10^{-5}$	$1.86x10^{-9}$	
25	2669.89	$8.13x10^{4}$	$3.82x10^{-4}$	$4.71x10^{-9}$	
10	2041.97	$9.62x10^{4}$	$5.08x10^{-4}$	$5.28x10^{-9}$	
5	1101.04	$1.81x10^{5}$	$3.46x10^{-5}$	$1.92x10^{-10}$	
1	1356.09	$8.08x10^{5}$	$5.60x10^{-3}$	$6.93x10^{-9}$	

[a]The MAb-Tyl concentrations are expressed in µg mL^{-1} [b] KD values expressed in M.

As the Table 5.3 indicates, the KD for each antibody injection was estimated and in most of the cases successfully fitted to the nM range between 1 to 6 units, demonstrating reproducibility at different concentrations as well as a strong interaction of the immunoreagents. Furthermore, the global KD was also determined as the average value of all the injections performed defining an affinity constant of $1.73x10^{-9}$ M for the MAb-Tyl/hTB-BSA pair by LSPR. As shown above, the KD value recorded with the Biacore™ T200 system, was $1.367x10^{-10}$, one order of magnitude smaller.

Something to remark is that the KD for the injection of 5 µg mL^{-1} in the OpenSPR™ was in $1.92x10^{-10}$ M being comparable to the value obtained with Biacore™ device. A potential explanation for such effect, could be attributed to the intrinsic strong binding of the immunoreagents selected as models that under multicycle kinetic modes were difficult to determine due need of aggressive regeneration conditions. An alternative experimental procedure known as single cycle kinetic could have been used for this antibody-antigen pair. Consisting on at least five consecutive additions of increasing concentrations of antibody and a final dissociation step without regeneration to minimize variations arising from the difficult separation of the ligand and target in solution. Another aspect to contemplate would be the presence of Ca^{2+} in the running buffer, used for the Biacore™ studies and not applied in the OpenSPR experiments. Interestingly, the incorporation of Ca^{2+} ions in ELISA (see section 3.3.2) increased the IC_{50} of the assay, and this could explain a potentially higher affinity for the hapten bioconjugate in presence of Ca^{2+}, affecting the detectability of the target analyte in solution.

Another characteristic feature across kinetic estimations rely on the preference of low immobilization levels to minimize mass transport effects. In this regard, Biacore™ experiments showed lower immobilization level around 304 RU's compared to 3350 RU's for OpenSPR™, although the sensing principle differs, this could also explain the kinetic differences. Based on these results, we decided to pursuit with the implementation on the portable Smartphone iSPR biosensor of the same bioconjugate and MAb-Tyl as proof of concept of the potential of this device for food safety.

5.3.4. PORTABLE iSPR SMARTPHONE SENSOR

5.3.4.1. Sensor response characterization to RI changes with ethanol

Before the evaluation of the portable iSPR system with biological reagents and samples, we initially performed a characterization of the signal form the novel device to significant changes in the RI as consequence of ethanol (EtOH) additions. The present study aimed to estimate a response value from the sensor to significant changes in the RI, assuming that biological systems will provide lower response.

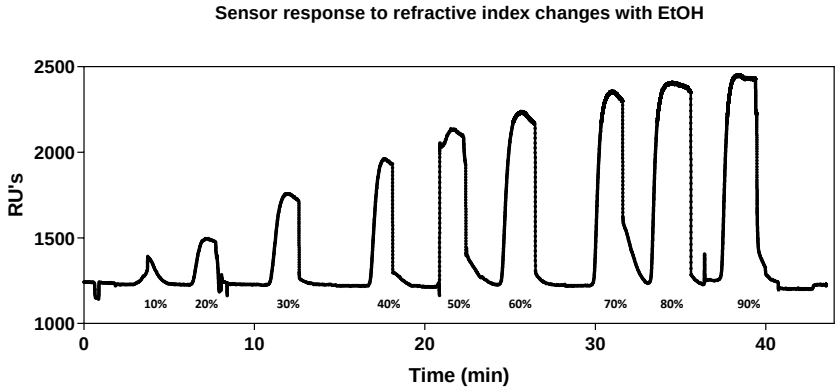

Figure 5.14 Raw sensogram obtained with the portable iSPR integrating smartphone detection after several injections of increasing concentrations of EtOH solutions, monitored as changes in RI of the gold chip. the response values (RU's) obtained were plotted against solutions with distinct EtOH content.

For these means, the base line was established using ultrapure H_2O. Afterwards, increasing EtOH/H_2O mixtures with RI ranging from 1.3330 (for 10% EtOH) to 1.3616 (for 90% EtOH) were measured over a bare gold CM5 surface. Based on the response detected with the system, a resolution of $3.1.10^{-4}$ RIU (refractive index units)/%EtOH was calculated. Moreover, platform sensitivity was estimated to be 3.792 10^5 RIU/RU with a low noise level of 0.581 (based on 3 standard deviations of baseline) in accordance with Xiao *et al.* [1], reaching a similar resolution to commercial SPR instruments.

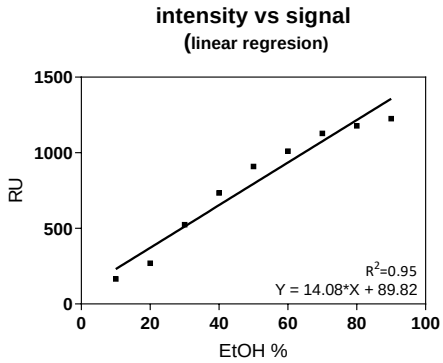

*Figure 5.15 Linear response to EtOH solutions injection. A linear fit was used to plot the dose dependant response obtained at increasing concentrations of EtOH. The linear regression equation Y=14.08*X+89.82 was obtained with a R^2 of 0.95.*

The shift recorded after EtOH/H_2O injections was corelated to a ΔRU (difference in response units) to estimate a change in the sensor response due to fluctuations in the RI. The experimental procedure commenced after injecting a mixture of 10 % EtOH in water, followed by alternate additions of 10 % increase EtOH content until reach 90 % of EtOH in water at the end of the run. As can be observed from the sensogram (see Figure 5.14) a concentration dependent response was demonstrated and the peaks detected after each individual injection correlate with increasing changes in the RI over the sensor. A different way to visualize that effect was representing the content of EtOH plotted against ΔRU (Figure 5.15). A difference of 0.004-0.005 in RIU's is measured with an increase of 150 ± 47 RU's in the sensor. Although, RI variations as consequence of water/EtOH solutions are significantly higher than the changes produced by biological elements, this study was utilized as reference to estimate the adequate performance of the system. Additional characterization was performed by our collaborators from Linkoping University using the updated

version of the portable iSPR device for the detection of β2-microglobulin, after surface functionalization with an Anti β2-microglobulin antibody, working in a linear range of 10-200 nM and reaching an LOD of 1.5 nM for the protein detection [1] validating the potential application using hTB-BSA and MAb-Tyl as proof of concept.

5.3.4.2. Immobilization of BSA-hTB conjugates over sensor chip

Immobilization of the BSA-hTB conjugate was made using the same procedures as those described for the Biacore™ T200 and OpenSPR™. It should be noticed that the chips used were the CM5, the same used with Biacore™ T200.

The Biacore™ CM5 sensor chip was docked to the 3D printed PDMS microfluidic cell with a double-sided adhesive tape. The response from the biofunctionalization step with the hTB-BSA bioconjugate is shown in Figure 5.16, describing the different additions performed during the process. First, the injection of running buffer took place until the baseline was stable. Surface activation was performed injecting a mixture of EDC/NHS for three minutes followed by the addition of the bioconjugate at 50 μg mL^{-1} in 10mM sodium acetate at pH 4.5 for eight min. to maximize surface-ligand interaction reaching good immobilization levels. The chip was finally passivated with 1M ethanolamine.

A remarkable aspect is that the determination of the immobilization level with this system was not strictly controlled in comparison with the other commercially available platforms. However, the change in the baseline before and after addition of BSA conjugate indicates that the biofunctionalization occurred to an extent equivalent to 300 RU's

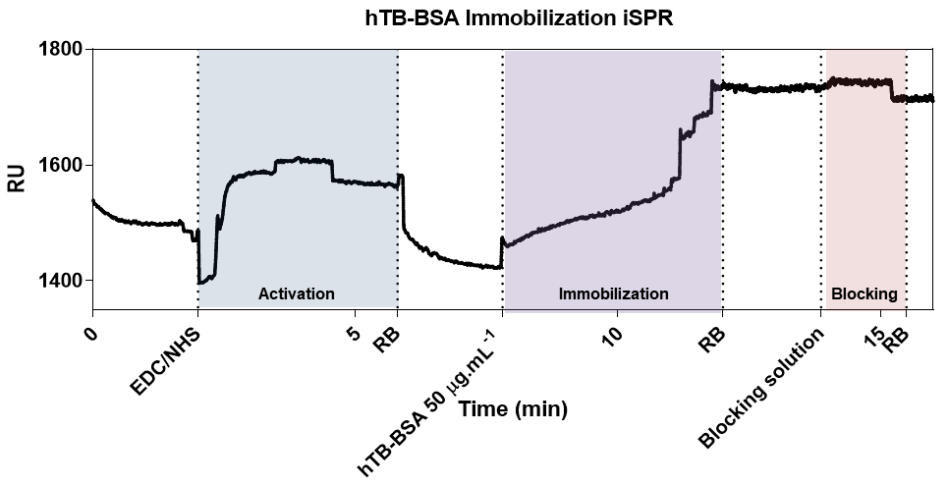

Figure 5.16 Surface immobilization of hTB-BSA in the iSPR system. The raw sensogram showing the steps involved during the immobilization protocol are represented. First, EDC/NHS surface activation, followed by hTB-BSA addition for covalent immobilization and finally a blocking step with 1M ethanolamine. RB refers to running buffer that in this case was MiliQ H_2O.

In the previous graph, is possible to see that the first increase in 100 RU's was obtained after addition of EDC/NHS solution, then the baseline was recovered and a difference of 300 RU's became detectable as consequence of the BSA conjugate immobilization attributed to the covalent coupling of BSA to the activated dextran surface and finally the blocking step was monitored without relevant response. In an attempt to visualize the data of the plasmonic strategies utilized, although the signal was not strictly comparable, the response obtained during hTB-BSA immobilization utilizing benchmark devices like Biacore™ and OpenSPR™ was represented in the Figure 5.17.

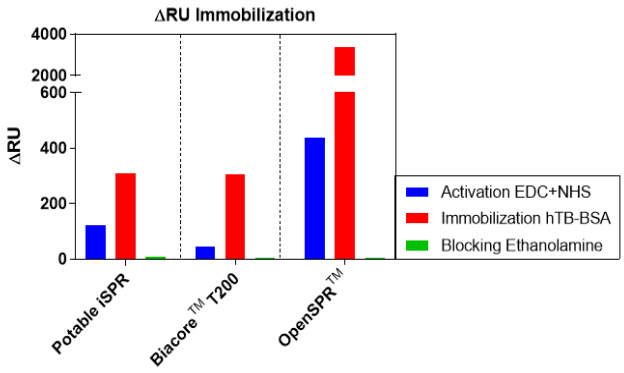

Figure 5.17 Sensor response detected during immobilization of hTB-BSA in different SPR devices. The comparison of the ΔRU (difference in response units) detected using the portable iSPR, Biacore T200 and OpenSPR instruments during immobilization is represented according to the main steps required during this period, activation with EDC/NHS, ligand immobilization and surface blocking.

Interestingly, a similar immobilization level was achieved with the portable and Biacore™ T200 detecting around 300 RU's, while the immobilization level for OpenSPR™ was 3300 RU's. In the first two approaches (portable and Biacore™) the same CM5 sensor chips were utilized while for the Nicoya system, a different sensor surface (nanogold coated) defined the LSPR phenomena, potentially explaining the 10-fold increase in the RU's detected. However, due to the successful monitorization of the immobilization procedure, the following step aimed to evaluate iSPR sensor response after the addition of the selective MAb interacting with the coating antigen following the typical single cycle kinetic scheme.

5.3.4.3. Proof of concept: Portable iSPR smartphone biosensor

For the purpose of demonstrating as a proof of concept, that the miniaturized device offered enough sensibility to monitor the binding event between our coating antigen (hTB-BSA, 68 KDa) and the MAb-Tyl (150 KDa). Increasing concentrations of MAb-Tyl solutions in 10 mM PBST were prepared and injected in the handheld device, followed by a regeneration step with 10 mM NaOH after each injection. The Figure 5.18 shows a representative sensogram of such kind of experiments.

One of the major limitations concerning the portable platform developed by the partners at LiU consisted on the lack of real time data visualization. Hence, the video had to be first recorded, including all the injections and then a computational post-processing step was required to extract the data and plot the sensogram using another data software (GraphPad Prism Software). Even though, our collaborators had envisaged that the final device would include the software integrating real time data visualization on the smartphone, the implementation of such utility, at that technological maturation level was still a challenge. Therefore, all the experiments required manual handling, not only of the video recording and analysis, but also the sample injections. This fact was a source of uncertainty across the different measurements. Furthermore, as it was observed in previous characterizations, the TYL reagents required particularly mild to aggressive regeneration conditions and this could not be monitored in real time which prevented from controlling this crucial step and the rest of the process.

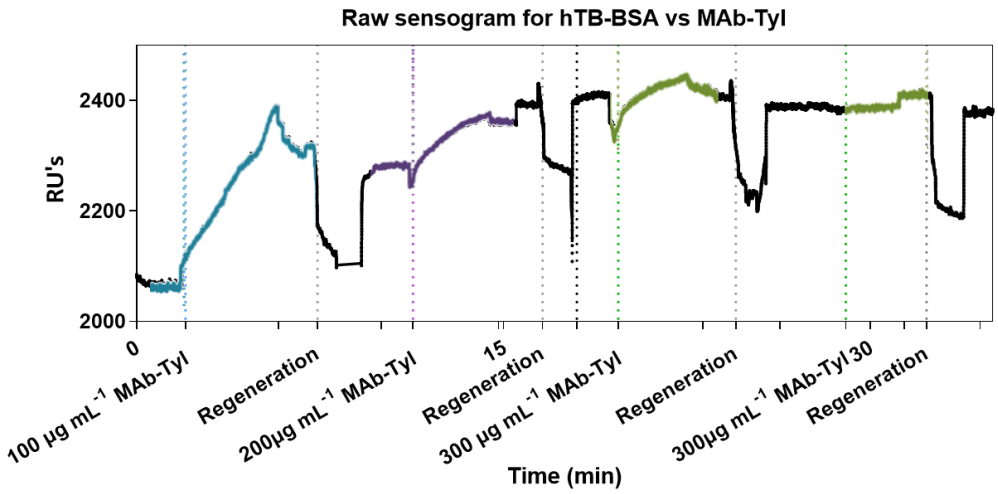

Figure 5.18 Raw sensogram recorded with the smartphone camera over the portable iSPR sensor. Single injections of MAb-Tyl solutions were performed with corresponding regenerations between each antibody addition.

After data processing, the sensogram was defined showing how the first injection of 100 µL of MAb-Tyl (100 µg mL^{-1}) produced an increase of almost 350 RU's as a consequence of antigen-antibody complex formation during association, and then the dissociation was recorded as a slight decay in the light blue response.

Afterwards, a regeneration step using 10 mM NaOH was observed as a drop in the signal detected. From this result is possible to estimate that the first regeneration was not satisfactory because the baseline was comparable as the one before the addition of NaOH at 2300 RU's, suggesting that a considerable amount of MAb-Tyl was still attached to the bioconjugate.

As this experiment was performed without visualizing in real time what was happening, after 12 minutes we proceed with the second injection of MAb-Tyl at 200 µg mL^{-1}. In this case, an increase of just approximately 70 RU's was registered indicating binding of just a small fraction of antibodies. A higher signal would have been expected considering that the first injection of less concentrated antibody (100 µg mL^{-1}) produced a shift of 350 RU's. We interpret this behaviour as a result of the unsuccessful regeneration in the previous step, leaving only few epitopes available for the interaction with the new antibody injection. The second regeneration was also evidenced as signal drop in the sensogram (minute 17), but again the original baseline was not recovered evidencing an inefficient regeneration. Therefore, the injection of the solution with higher concentration of antibody (300 µg mL^{-1}) did produce only a small response indicating saturation of the chip. The saturation condition was verified by injecting for the second time a solution of antibody at 300 µg mL^{-1} as replicate. In this case the signal remained stable suggesting that not only the regeneration was not occurring but also, that the chip was at the maximum binding capacity.

The portable iSPR platform has demonstrated to have enough sensitivity to detect BSA ligand immobilization, but consecutive additions of the antibody did not allow us recording reliable data due to the off-line smartphone readout system at this stage of development. These findings encourage the potential use of miniaturized portable optical sensing systems, but further efforts had to be made on the development and optimization of the platform to be implemented for bioanalytical purposes.

On the other hand, the reagents utilized in this proof of concept did not facilitated the regeneration step limiting accurate data adquisition. In this regard, it would be interesting to use a system (bioconjugate/antibody) with a weaker interaction to potentially improve each regeneration cycle and subsequently detect antibody injections with the corresponding dose dependent response expected. Probably the reagents for SA's would have been better

candidates for this characterization. However, with the actual prototype all these experiments had to be performed under blind conditions, which made each determination more complicated and time consuming.

At this point, it was decided to wait until a next and more advanced prototype available, however the dissolution of the research group at LiU because of the departure of the PI to another institution, followed by the finalization of the project prevented from continuing with the investigation of the performance of this portable smartphone based iSPR for onsite food reside analysis. Implementation of the DDI strategy could not be achieved, but according to the precedents in the literature combining DNA addressing with SPR [2, 22, 23] and our preliminary results, we are convinced that the development of a DDI-based smartphone portable iSPR device may be feasible.

In this section, appart from the MAb's characterization, it has been evidenced that monitoring biological interactions between antibodies and a hapten-BSA conjugates without labels is possible using a simple and inexpensive 3D printed optical SPR sensor although further improvements should be considered. Outstanding research has been recently reported in the context of SPR smartphone biosensing, as is the case of a 3D printed portable iSPR system coupled to a gold microarray chip for simultaneous detection of kidney injury biomarkers at ng mL^{-1} in urine samples [24]. The proposed inexpensive device works under Kretschmann configuration making use of the smartphone LED for plasmon excitation and the camera for the reflected light collection with a sensitivity of 1.78×10^{-5} RIU. Additionally, the updated version of the portable iSPR from LiU was employed for the detection of total hazelnut protein in plant-based milk, through the immobilization of selective antibodies. The experimental performance of the miniaturized system was contrasted with the reference Biacore 3000 device showing robust and comparable detectability, reaching limits of detection between 0.04 and 0.53 µg mL^{-1} in different plant derived milk samples [25]. According to the evidence discussed, this evolving field extends the possibility to work on the development of portable analytical devices with user friendly interfaces for the implementation in real life scenarios such as food safety, brining self-monitoring tools to the end consumers.

5.4. CHAPTER CONTRIBUTIONS

- Kinetic characterization of the immunoreagents through SPR highlighted that shorter incubation times could be explored in order to avoid partial dissociation of SA's reagents if longer periods are defined.
- The KD value of the MAb and hapten-BSA pair, was inversely correlated to the assay detectability over indirect competitive DDI microarray and ELISA formats. Suggesting that strong MAb-hapten interactions, may lead to worsen the affinity for the target analyte in solution.
- The establishment of a standardized protocol to assess kinetic interactions between MAb's and antibiotic hapten-BSA conjugates was successfully applied in a benchmark SPR system, a benchtop LSPR device and an experimental prototype.
- For the first time, the binding of a selective MAb with a hapten-protein conjugate (small molecule) was evidenced using a portable iSPR sensor integrating smartphone detection.
- The use of a reference MAb and bioconjugate pair with relatively weaker or average affinity would have been preferred in order to allow complete surface regeneration under single-cycle kinetic determinations. Alternatively, multicycle kinetic determinations could be considered.

5.5. MATERIALS AND METHODS

5.5.1. CHEMICALS, BUFFERS AND REAGENTS

The SPR experiments were carried out using carboxymethylated dextran sensor chips (CM5) from Cytiva (Marlborough, USA). For LSPR experiments, carboxyl sensors SEN-AU-100 were purchased from Nicoya (Waterloo, Canada).

All solutions were prepared using Ultrapure water (>18.2MΩ.cm^{-1}) from Barnstead™ Lab Water Purification Systems (ThermoFisher Scientific) and buffers were filtered and degassed prior implementation. Ethanol (EtOH >99%) was purchased at Sigma-Aldrich (Sweden). Immersion oil acquired from Cargille Laboratories (New Jersey, USA). The LED backlight module (model:1626) was purchased from Adafruit Industries (New York, USA).

PBS was 0.01 M phosphate buffer (1.48 mM KH_2PO_4 and 8.3 mM Na_2HPO_4) in a 0.8% saline solution (137 mmol L^{-1} NaCl, 2.7 mmol u^{-1} KCl), at pH 7.5. PBST is PBS previously described with 0.05% Tween 20. The solution of PBST Ca^{2+} corresponds to a PBST 10mM pH 7.5 solution that contains 1mM $CaCl_2$. As immobilization buffer 10mM sodium acetate pH 4.5 was used. Regeneration buffers were Glycine-HCl pH 2.2 containing 0.1 M Glycine and adjusting pH with HCl and 10mM NaOH. Blocking solution was 1 M ethanolamine hydrochloride (pH 8.4) all reagents purchased from Sigma-Aldrich. The pH and the conductivity of all buffers and solutions were measured with a pH-meter pH 540 GLP and a conductimeter LF 340, respectively (WTW, Weilheim, Germany).

5.5.2. EXPERIMENTAL PROCEDURES

5.5.2.1. Gold sensor chip preparation in Biacore™ T200

A standard amine coupling procedure was applied at 25 C to immobilize the BSA-hapten conjugates (PrEDA-BSA, SA2-BS-, hTB-BSA) over a sensor chip CM5. For an adequate immobilization, the BSA-hTB conjugate was diluted to 10 µg mL^{-1} in 10 mM sodium acetate at different pH's and tested using the pH scouting wizard

in the Biacore™ T200 control software (GE Healthcare). The most suitable immobilization level was archived using 10 Mm sodium acetate pH 4.5 as immobilization buffer following the next procedure with all the BSA bioconjugates.

The chip surface coated with carboxymethylated (CM) was divided in 4 microfluidic channels used for the immobilization of three conjugates in the same chip and the remaining channel used as reference for non-specific binding immobilizing only BSA. The surface activation took place after by injecting 150 µL of a mixture of EDC and NHS (1:1 *v*/*v*) at a flow rate of 15 µL min^{-1}. Then, BSA conjugates prepared at 25 µg mL^{-1} in the immobilization buffer (10 mM sodium acetate, pH 4.5) were injected in flow cells 2–4 respectively (2: PrEDA-BSA, 3: SA2-BSA, 4: hTB-BSA). Flow cell 1 was used as a reference channel for non-specific binding to BSA and therefore was activated by EDC/NHS and BSA (25 µg mL^{-1}) was injected. The immobilization protocol concluded with the addition of ethanolamine (1 M) to block remaining reactive groups over CM-dextran surface. The Response Units (RU) values for each after bioconjugates immobilization were automatically determined by Biacore™ T200 Software in BSA: 166 RU, PrEDA-BSA: 304 RU, SA2-BSA:71 RU, hTB-BSA: 236 RU. Low immobilization levels were preferred for kinetic determinations based on the mass of the ligands and the analyte in correlation with signal expected. The required target immobilization (RL) for each interaction was estimated through this calculation, $Rmax = RL \times MW_{analyte}/MW_{ligand} \times Sm$. (where Rmax = theoretical max response for analyte binding 100. Sm = stoichiometry of analyte/ligand. RL = RU of immobilized ligand.

5.5.2.2. Antibody binding experiments with Biacore™ T200

All the binding studies were performed in freshly prepared, filtered and degassed running buffer containing 10 mM PBST and 1mM $CaCl_2$ at 25 °C. The stock aliquots of respective antibodies (13.3 µM) were first diluted in 1/40 followed by serial dilutions 1/2 in the running buffer (with a final volume 400 µL). Single cycle kinetic experiments were performed, starting with three zero concentration injections (buffer only) to define the baseline. Then serial injections of 30 µL of antibody solution with 120 seconds for association and 300 seconds dissociation time at a flow rate 30 µL min^{-1} were performed. After each injection a surface

regeneration with 2 pulses of 5 µL of 0.1 M Gly-HCl, pH 2.2 was implemented for SA2-BSA and PrEDA-BSA, but the regeneration solution for hTB-BSA was 10 mM NaOH to return the biosensor signal to baseline.

Using the Biacore™ T200 Evaluation Software V 2.02, the estimation of the equilibrium dissociation constants, off-rates and on-rates were calculated from the sensograms obtained. By fitting a 1:1 Langmuir binding model while considering mass transfer (GE Healthcare).

5.5.2.3. hTB-BSA immobilization using Open SPR™

A similar experimental procedure to the one utilized with the Biacore™ system was utilized for hTB-BSA conjugates immobilization.

The OpenSPR™ platform requires carboxyl sensors for covalent coupling by conventional EDC/NHS chemistry to primary amine groups on the ligand. Once the chip was inserted and docked, the running buffer (PBS10mM) was flowed through the cell defining the baseline. The OpenSPR™ software offers a step by step immobilization protocol with pre-established flow rate conditions, although injections are performed manually in comparison with the fully automated Biacore™ T200 system.

Initially an injection of Isopropanol at 80% v/v was required to remove bubbles form the microfluidic compartments. After that, the first injection consisted on the mixture of 200 µl of EDC (0.2 M in water) and NHS (0.05 M in water) solution for activation of the surface at a flow rate of 20µL min^{-1}. Next, the addition of 200 µl of the coating antigen (hTB-BSA) at 50 µg mL^{-1} in NaOAc pH 4.5 was performed keeping a flow rate stable over the channel 2, while the channel 1 was used to monitor non-specific adsorptions to the sensor chip. To conclude surface coating, the injection of 200 µl of ethanolamine was applied to block active groups.

5.5.2.4. Kinetic determination of hTB-BSA and MAb-Tyl with OpenSPR™

For kinetic evaluation with OpenSPR™ system, the running buffer selected was PBS 10 mM. Several antibody MAb-Tyl dilutions were prepared in PBST 10 mM to be injected over the sensor. For this purpose, the concentrations assessed were 1, 5, 10 ,25 and 50 µg mL^{-1} and the regeneration solution was 10 mM NaOH. Through this procedure, consecutive antibody injections of 200 µl at 25 µl min^{-1} and regeneration took place in single cycle kinetic format. The signal obtained was monitored in real time by the OpenSPR™ software allowing direct estimation over the sensor response. After the experimental procedure, the data was analysed utilizing Trace Drawer software, to fit the experimental binding curves to theoretical 1.1 binding model.

5.5.2.5. Internal setup of smartphone-iSPR device

The 3D-printed attachment was mounted to include different platform components holding the light source, prism optics and the 3D printed microfluidic cells, as well as a top cover for smartphone-based SPR. A commercial BK7 60 prism (Crystran Ltd, Dorset, United Kingdom) was installed, with the top surface aligned horizontally. As the plane-polarized light source for SPR, a white LED was mounted on one side of the prism and covered with a linear polarizing film. Additionally, a resistor was included as part of the electric circuit connecting the light source to an external GP Super Alkaline 9V battery. To route the output light signal to the smartphone camera, a polished mirror surface created from a physical vapor deposition (PVD) gold-coated plastic foil was attached on the prism's opposite side. A fixed angle input light is used to run the imaging SPR (iSPR) while the image of the sensor surface displaying a dip spectrum was taken while the angle of the smartphone's LED input light was manually adjusted.

5.5.2.6. PDMS microfluidic cells preparation

A Form 3 (Formlabs Inc, USA) 3D printer based on low force stereolithography (LFS) technique was used to fabricate the microfluidic chip. The printing process generally takes approximately 1 hour for 10-chip printing. The photopolymer resin Clear Resin Version 4 from Formlabs Inc was utilized due to its optical

transparency, biocompatibility, and suitability for fluidics fabrication. The printed microfluidics chips were collected and washed with ethanol under sonication for 5 min to remove the resin residues. Finally, the microfluidic chips cleaned again with ethanol and then dried by compressed air and stored in a sealed container at room temperature.

5.5.2.7. Sensor characterization to RI changes with EtOH/water mixtures

A total of nine mixtures of EtOH/water with increasing content of 10 % EtOH (v/v) starting from 10 to reach 90 % EtOH were prepared and degassed. Then the inlet tube was connected to the microfluidic cell and attached to a syringe containing 200 µl of respective EtOH/water mixture with a continuous flow rate of 50 µl min^{-1} for 3 minutes each injection. The running buffer was ultrapure water, to define the baseline and changes in the RI were recorded with the camera of the smartphone for subsequent analysis in the respective software. The video was processed with the in-house analysis software in the computer and the sensogram obtained. Afterwards, the response units' values were plotted using GraphPad Prism v 6.0.

5.5.2.8. Immobilization of hTB-BSA conjugates in the portable iSPR sensor

The microfluidic cell was connected to the inlet and outlet tubes, and the first one was linked the 1 channel-syringe pump (MRC instruments, UK) and consecutive injections were performed during the experiment. The immobilization protocol consisted on the initial injection of 10 mM PBS at 50 µl min^{-1} for 10 min to establish the baseline (total volume injected 500 µl). Then the pump was stopped to change the syringe avoiding bubble formation in the tubbing's and is considered during every syringe change. Also, the video is paused when syringes are changed to generate shorter documents to facilitate the analysis and data transfer to the computer, eliminating non-relevant analytical information.

Then, 100 µl of EDC solution (15,35 mg EDC in 200 µl water) and 100 µl of NHS solution (5.75 mg of NHS in 200 µl in water) were taken and mixed in an

Eppendorf tube just before the injection. The flow rate for the injection was 25 µl min^{-1} adding 200 µl for a period of 5 minutes. Once again, the system was filled with 10 mM PBS at 50 µl min^{-1} for additional 3 minutes to recover the baseline. For ligand immobilization 200 µl of hTB-BSA conjugate (50 µg mL^{-1} 10 mM NaOAc pH 4.5) were injected at a controlled flow of 25 µl min^{-1} for approximately 5 minutes. Following the same procedure than Biacore™ and OpenSPR™, afterwards the system was filled with running buffer (10 mM PBS) at 50 µl min^{-1} for 3 minutes. In an attempt to block remaining active dextran molecules, 200 µl of ethanolamine 1 M were flowed at 25 µl min^{-1} and restored to baseline with 10mM PBS.

5.5.2.9. Proof of concept MAb-Tyl titration of hTB-BSA conjugate with smart iSPR system

Once the chip was functionalized with the corresponding BSA conjugate and bearing in mind that this system, the addition of increasing concentrations of monoclonal antibody solutions was assessed. MAb-Tyl aliquots of 400 µl were prepared in independent Eppendorf tubes at 100, 200 and 300 µg mL^{-1}. The running buffer consisting on 10 mM PBS was defining the baseline, and 200 µl of the first antibody solution were added at 25 µl min^{-1} for 5 minutes, followed by a regeneration injection of 200 µl of NaOH 10mM at 100 µl min^{-1}. Then, the second antibody injection took place following the same conditions of the previous injection and a regeneration step. Working under continuous flow, the injection of the third antibody dilution (300 µg mL^{-1}) was performed with the corresponding regeneration, and a duplicate addition of the same antibody dilution (300 µg mL^{-1}) was injected and regenerated, to then be restored in 10 mM PBS.

Once all the injections were done, the video was stopped and transfer to the computer for software analysis and data extraction. Excel sheets were obtained plotting the shift of the signal over time and this was represented in a graph using GraphPad Prism V.6.0 version, each step during the experimental procedure was assigned in the final sensogram to evidence the RU variations attributed to each injection.

5.6. BIBLIOGRAPHY

1. Xiao, C., et al., *Print-and-stick unibody microfluidics coupled surface plasmon resonance (SPR) chip for smartphone imaging SPR (Smart-iSRP).* Analytica Chimica Acta, 2022. **1201**: p. 339606.
2. Tort, N., et al., *Synthesis of steroid–oligonucleotide conjugates for a DNA site-encoded SPR immunosensor.* Bioconjugate Chemistry, 2012. **23**(11): p. 2183-2191.
3. Kramer, K., et al., *Production of Antibodies for the Quantitative Detection of the Anabolically Active Androgens 17β-Boldenone and Methylboldenone.* Analytical letters, 2007. **40**(7): p. 1461-1472.
4. Sparks, R.P., J.L. Jenkins, and R. Fratti, *Use of surface plasmon resonance (SPR) to determine binding affinities and kinetic parameters between components important in fusion machinery.* SNAREs: Methods and Protocols, 2019: p. 199-210.
5. Dobrovodský, D. and C. Di Primo, *Do conformational changes contribute to the surface plasmon resonance signal?* Biosensors and Bioelectronics, 2023. **232**: p. 115296.
6. Abbas, A., M.J. Linman, and Q. Cheng, *Sensitivity comparison of surface plasmon resonance and plasmon-waveguide resonance biosensors.* Sensors and Actuators B: Chemical, 2011. **156**(1): p. 169-175.
7. Cai, H., S. Shan, and X. Wang, *High sensitivity surface plasmon resonance sensor based on periodic multilayer thin films.* Nanomaterials, 2021. **11**(12): p. 3399.
8. Shrivastav, A.M., et al., *Engineering the penetration depth of nearly guided wave surface plasmon resonance towards application in bacterial cells monitoring.* Sensors and Actuators B: Chemical, 2021. **345**: p. 130338.
9. Zhang, D. and Q. Liu, *Biosensors and bioelectronics on smartphone for portable biochemical detection.* Biosensors and Bioelectronics, 2016. **75**: p. 273-284.
10. Mahmoud, M., et al., *Combining aptamers and antibodies: Lateral flow quantification for thrombin and interleukin-6 with smartphone readout.* Sensors and Actuators B: Chemical, 2021. **333**: p. 129246.
11. Cheng, Y., et al., *Reusable smartphone-facilitated mobile fluorescence biosensor for rapid and sensitive on-site quantitative detection of trace pollutants.* Biosensors and Bioelectronics, 2022. **199**: p. 113863.
12. Fabiani, L., et al., *based immunoassay based on 96-well wax-printed paper plate combined with magnetic beads and colorimetric smartphone-assisted measure for reliable detection of SARS-CoV-2 in saliva.* Biosensors and Bioelectronics, 2022. **200**: p. 113909.
13. Liu, Y., et al., *Surface plasmon resonance biosensor based on smart phone platforms.* Scientific reports, 2015. **5**(1): p. 1-9.
14. Preechaburana, P., et al., *Surface plasmon resonance chemical sensing on cell phones.* Angewandte Chemie International Edition, 2012. **51**(46): p. 11585-11588.

15. Guner, H., et al., *A smartphone based surface plasmon resonance imaging (SPRi) platform for on-site biodetection.* Sensors and Actuators B: Chemical, 2017. **239**: p. 571-577.
16. Zhang, J., et al., *Lipopolysaccharides detection on a grating-coupled surface plasmon resonance smartphone biosensor.* Biosensors and Bioelectronics, 2018. **99**: p. 312-317.
17. Liu, Q., et al., *Real-time biodetection using a smartphone-based dual-color surface plasmon resonance sensor.* Journal of biomedical optics, 2018. **23**(4): p. 047003-047003.
18. Comina, G., A. Suska, and D. Filippini, *Autonomous chemical sensing interface for universal cell phone readout.* Angewandte Chemie, 2015. **127**(30): p. 8832-8836.
19. Comina, G., A. Suska, and D. Filippini, *A 3D printed device for quantitative enzymatic detection using cell phones.* Analytical Methods, 2016. **8**(32): p. 6135-6142.
20. Day, Y.S., et al., *Direct comparison of binding equilibrium, thermodynamic, and rate constants determined by surface-and solution-based biophysical methods.* Protein Science, 2002. **11**(5): p. 1017-1025.
21. Drake, A.W., D.G. Myszka, and S.L. Klakamp, *Characterizing high-affinity antigen/antibody complexes by kinetic-and equilibrium-based methods.* Analytical biochemistry, 2004. **328**(1): p. 35-43.
22. Placido, A., et al., *A convenient renewable surface plasmon resonance chip for relative quantification of genetically modified soybean in food and feed.* Plos one, 2020. **15**(2): p. e0229659.
23. Wang, S., Y. Dong, and X. Liang, *Development of a SPR aptasensor containing oriented aptamer for direct capture and detection of tetracycline in multiple honey samples.* Biosensors and Bioelectronics, 2018. **109**: p. 1-7.
24. Zhang, Q., et al., *Smartphone surface plasmon resonance imaging for the simultaneous and sensitive detection of acute kidney injury biomarkers with noninvasive urinalysis.* Lab on a Chip, 2022. **22**(24): p. 4941-4949.
25. Xiao, C., et al., *A portable smartphone-based imaging surface plasmon resonance biosensor for allergen detection in plant-based milks.* Talanta, 2023. **257**: p. 124366.

PART II: UNDERSTANDING IMMUNE IMPLICATIONS ASSOCIATED TO SARS-COV-2 INFECTION THROUGH SEROLOGICAL DETERMINATIONS

I. COVID-19 PANDEMIC: A GENERAL OVERVIEW

By late 2019 the city of Wuhan, China began to evidence an increasing number of reports with unusual pneumonia. Immediately after, the disease was identified as COVID-19 in accordance to the agent responsible of infection named Severe Acute Respiratory Syndrome Coronavirus 2 (SARS-CoV-2) [1]. The novel virus was classified as member of the *coronaviridae* family with previous examples like SARS-CoV and MERS-CoV (Middle East Respiratory Syndrome-Coronavirus). The main concern arouses as consequence of a higher transmissibility and wider clinical symptomatology in comparison with other related viruses. Afterwards, the WHO declared the COVID-19 pandemic due to a rapid and uncontrolled viral dissemination, lacking of efficient treatments and preventive vaccines, threatening health care systems, governments and general society [2].

The limited knowledge regarding the viral behavior, in addition to the conflicting evidence reported during the first stage of the pandemic were determinant factors leading to the collapse of healthcare institutions in an attempt to address the rising number of patients with severe symptomatology. Unprecedently, social distancing and face masks were adopted by many authorities to mitigate the viral propagation among citizens. Common efforts from healthcare professionals, researchers, public and private institutions and governments worldwide lead to massive investment towards the understanding of the viral nature, development of effective vaccines and rapid diagnostic methods as well as different treatment options [3].

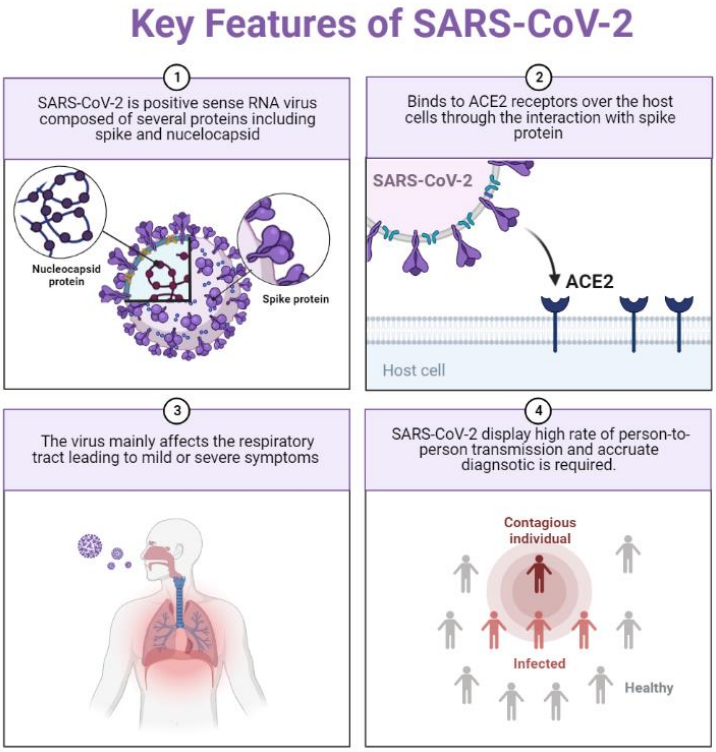

Figure II.I Schematic representation of some of the main features associated to SARS-CoV-2 infection like viral structure composition, cell entry mechanism and routes of transmissibility [4].

II. COVID-19 DISEASE AND MAIN CLINICAL FEATURES

Nowadays nobody doubts that aerosols and respiratory droplets are the main transmission routes for SARS-CoV-2 with a typical incubation period of 4-5 days before symptoms onset [5]. In this regard, most of the patients are exposed to mild or moderate disease including cough, fever, headache, myalgia and diarrhoea in addition to others that course with asymptomatic infection [6]. Generally, after one week of uninterrupted symptomatology severe disease is identified, experiencing dyspnoea (inability to breathe), increasing respiratory failure as well as hypoxaemia [7].

At this stage, most patients are diagnosed with acute respiratory distress symptom (ARDS) characterized by significant inflammation, pulmonary vascular leak and subsequent lung injury [8]. The excessive inflammation reported during

severe illness is mainly associated to pro-inflammatory cytokines release of interleukin-1 (IL-1), IL-6, IL-8, and Tumour Necrosis Factor (TNF) as well as higher levels of inflammatory markers like D-dimer, ferritin and C-reactive protein (CRP). The abundance of these proteins was evaluated through the course of the infection as potential biomarkers of disease progression [9].

According to the report "COVID-19 Clinical Management Living Guidance" published on January 25th, 2021, the WHO defines clinical severity as a measure of the extent of disease severity in COVID-19 patients based on their clinical manifestations. This document categorizes COVID-19 severity into three levels as: mild, moderate, and severe/critical. See Figure II.II.

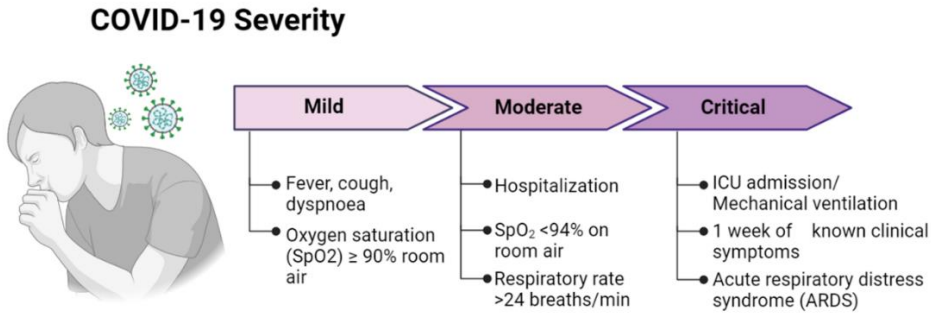

Figure II.II COVID-19 severity scale according to the WHO. Each category is based on the clinical manifestations reported after SARS-CoV-2 infection, ranging from mild disease, to moderate and finally critical or severe course. Adapted from [10].

In this sense, mild disease course was attributed to patients with upper respiratory tract complications including manifestation of symptoms such as fever, cough, sore throat and without evidence of pneumonia or hypoxia (low oxygen levels). Then, moderate cases evidencing lower respiratory tract disease such as pneumonia, but without signs of severe respiratory distress or hypoxia. Those patients may experience respiratory rate of >24 breaths per minute or higher with an oxygen saturation of 90 % or more on room air. Finally, severe and critical outcomes contemplate respiratory distress, hypoxia or multiorgan dysfunction. Characterized by respiratory rates around 30 breaths per minute or higher, oxygen saturation of less than 90 % and requirement of mechanical ventilation for respiratory support [10].

As a result of clinical data analysis, the main risk factors associated with severe COVID-19 identified include advanced age, obesity and male sex [11]. Diabetes, kidney failure, heart failure, cardiac arrhythmia, hypertension and chronic obstructive pulmonary disease have been found as prevalent co-morbidities too [12]. Moreover, extensive genetic comparisons elucidate some degree of predisposition to suffer severe outcomes mainly directed to genetical variants implicated in pulmonary fibrosis [13] and genes involved in Toll-Like Receptors 3 and 7 (TLR3 and TLR7) dependents form interferon (INF) pathway [14].

III. THE VIRUS AND ITS MAIN STRUCTURAL COMPONENTS

SARS-CoV-2 is an encapsulated virion (or viral particle) constituted by structural and non-structural proteins as well as a host-derived lipid bilayer that transports viral RNA into the infected cell. Although accessory proteins are not essential during replication, immunoreactive properties have been described amongst them [15]. This virus mainly infects the upper respiratory tract generating cold-like symptoms with relatively low mortality rates around 1 % for COVID-19 but according to the reports a 5-20 % requires hospitalization [16] and from this group up to almost 30 % is admitted to ICU [17; 12].

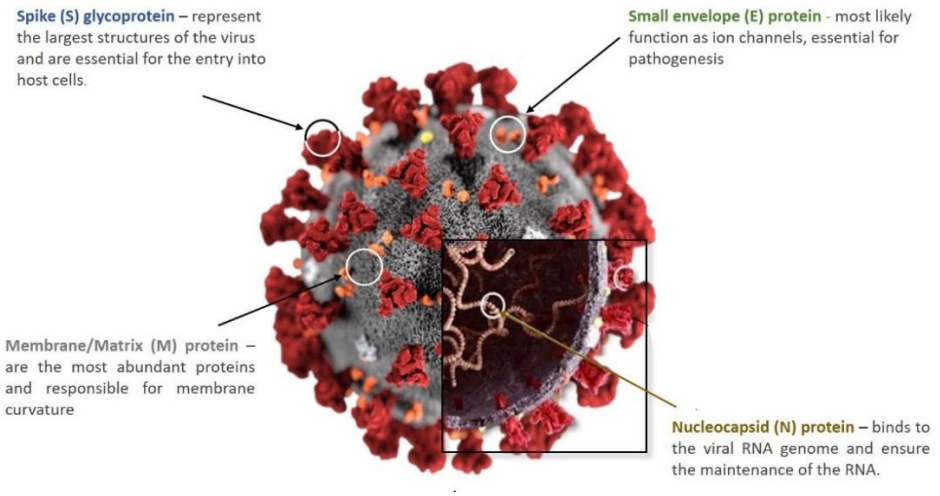

Figure II.III SARS-CoV-2 structural components. The image represents four of the main structural domains across the viral structure and the main functions associated. Adapted from [18].

Results interesting to emphasize that the first report describing Coronaviruses (CoV) dates from 1932 [19], followed by a relevant outbreak occurring in 2002 in

charge of SARS-CoV, evidencing the old and close relationship with humans. Coronaviruses are classified according to genetic differences in *alpha*-, *beta*-, *gamma*- and *delta*-CoV genera, belonging to the *Coronavirinae* subfamily. These viruses are typically described as enveloped, spherical or pleiomorphic structures comprising sizes between 80 to 120 nm. They possess the largest genome over all RNA viruses with a length between 26 and 32 Kb, carrying six or ten open reading frames (ORF's). More than half of their genome belongs to the first ORF that encodes for replicase proteins while the remaining fraction include genes from structural proteins [20]. Particularly, the emerging SARS-CoV-2 was described as a single stranded positive sense RNA virus carrying a genome of 29 Kb that encodes for a set of structural proteins (see Figure II.III) like the spike glycoprotein (S), the nucleocapsid (N), the envelope (E) and the membrane (M), non-structural proteins (in charge of viral replication and transcription) and accessory proteins [21].

a. Mediating viral-host interaction through S glycoprotein

From the structural basis, some essential proteins can be identified due to their relevance in the viral cycle. One of those is the S protein, naturally found as a homotrimer over the surface of the virus is responsible for the interaction with the angiotensin-converting enzyme 2 (ACE2) receptor in the host cell mediating its entry. The S protein size is 180 KDa with a length of 1273 amino acids (aa) and consists on a signal peptide (aa 1-13), the S1 subunit (aa 14-685) containing the receptor binding domain (RBD, aa 319-541) in charge of binding to ACE2, and S2 subunit (aa 686-1273) implicated in membrane fusion (see Figure II.IV). A natural advantage of the polysaccharide matrix covering the S protein was proposed favoring immune evasion during infection [22, 23]. Additionally, the trimeric S structure was reported in a dynamic state offering an open and close conformation of the RBD region conferring different functionalities [21].

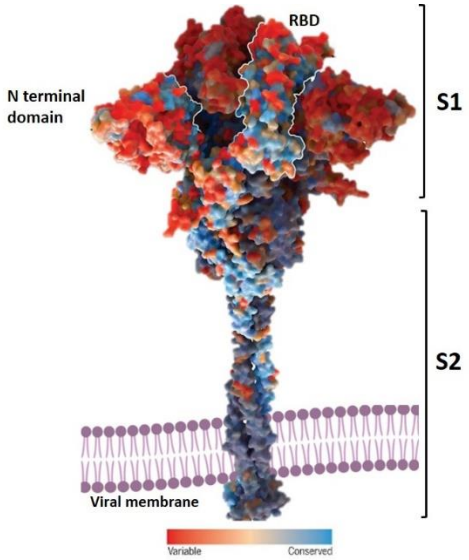

Figure II.IV Three-dimensional representation of S Trimeric Protein anchored to the viral membrane through S2 subunit, and exposing the S1 domain holding the RBD zone. Adapted from [24].

In the following table II.I, a detailed description at amino acid resolution of the principal domains described over the S glycoprotein are expressed.

Table II.I. Structural domains found on S at amino acid resolution

Regions of Spike Protein	Aa sequence
S1 Subunit	14-685
N Terminal Domain	14-305
Receptor Binding Motif	437-508
Receptor Binding Domain	319-541
S2 Subunit	686-1273
Fusion Peptide	788-806
Heptad Repeat 1	912-984
Heptad Repeat2	1163-1213
Transmembrane Domain	1214-1237
Cytoplasmic Domain	1238-1273

b. Relevance of receptor binding domain (RBD) in S protein

A crucial component of the S glycoprotein is the RBD region, with the ability to recognize and tightly bind to the ACE2 receptor to promote viral internalization

triggering the infective cycle. Structurally, this domain is composed of five antiparallel β sheets (β1, β2, β3, β4 and β7) with loops and helices interconnecting them. These structures are highly conserved amongst SARS-CoV and SARS-CoV-2 with almost 75 % of homology. Additionally, the expression of ACE2 as transmembrane receptor was reported in different tissues including lungs, heart, kidney and intestine making them susceptible to SARS-CoV-2 infection [25, 26]. Moreover, kinetic studies revealed that RBD was able to bind with 10-20 times more affinity to ACE2 receptor than the complete S protein [27], evidencing the importance of such region during viral-host interaction.

On the other hand, many therapeutic approaches have been proposed through the interference of this binding event, expecting to reduce the probabilities of viral infection based on a rapid immune clearance [28]. Experimental results indicated that the RBD region is the main responsible of neutralizing antibody (NAb's) production [29] and they can be quantified by plaque reduction neutralization tests (PRNTs), offering potential correlations with immune protection, but requiring live viral culture [30].

c. The nucleocapsid protein from a structural and biochemical perspective

Considering the inner side of the virus, the viral genome is packed into the helical N structural protein (Figure II.V), constituted by 5 different domains [20]. Characterized by a N-terminal tail ranging from aa 1 to 40, followed by the RNA binding region from aa 41 to 173 and the C-terminal dimerization domain between aa 250 and 364 [31] as the most relevant portions. The N protein is naturally expressed in high concentrations during initial stages of infection and the main functions described include packaging, replication and preservation of viral RNA. According to the evidence, the $arginine_{94}$ and $tyrosine_{122}$ residues are essential during RNA binding [32]. Additionally, N protein was identified as a highly conserved region sharing almost 90 % of homology with other N proteins from similar viruses like SARS-CoV [33].

Figure II.V Crystal structure of the C-terminal Dimerization Domain of N protein from SARS-CoV-2 (PDB ID: 6YUN).

Alternative biological implications were attributed to N protein, such as the inhibition of phosphorylation of the nuclear protein B23 in charge of cell cycle progression [34]. Also responsible of promoting inflammation through cyclooxygenase-2 pathway in the lungs [35] and activating NOD-, LRR- and pyrin domain-containing protein 3 (NLRP3) inflammasome, an essential protein complex mediating host immune response through interleukin-1β maturation and caspase activation [36]. Additional features suggest the suppression of type I interferon (IFN) response leading to abnormalities at innate immune levels [37]. In summary, N and S proteins can be considered fundamental viral components exhibiting a variety functions implicated in infective and spread related processes. The development of effective therapeutic approaches based on the interactions with these proteins could offer promising treatment alternatives. According to the next table II.II, main regions defined over N protein are represented indicating functional characteristics.

Table II.II. Principal domains of N protein sequence.

Functional N domains	**Aa sequence**
N terminal tail	1-40
N terminal RNA Binding Domain	41-17
Ser/Arg-rich linker region	174-249
C-terminal dimerization domain	250-364
C-terminal intrinsically disordered region	365-419

Adapted from [31]

IV. SARS-COV-2 EVOLUTION AND EMERGING VARIANTS OF CONCERN (VOC)

Over the course of the COVID-19 outbreak, viral replication and massive spread, led to the accumulation of changes in the genetic material of the original virus promoting the generation of new strains or variants of concern (VoC). These variants gained attention as a result of higher transmissibility rates, severe symptomatology or immune scape capacity from prior infection or vaccination. Sequencing techniques became essential tools for real time monitoring of viral prevalence and variants emergence worldwide. In this scenario, several actions took place in order to unify epidemiological criteria and accelerate reliable data generation. As an example, the advanced molecular detection (AMD) division of the center of diseases control and prevention (CDC) coordinates the SPHERES (SARS-CoV-2 Sequencing for Public Health Emergency Response, Epidemiology and Surveillance) consortium with the aim to harmonize and support health sequencing along the US collaborating with scientist, clinicians, public and private institutions [38]. The following Figure II.VI shows the number of analyzed sequences in the period between May 11th 2020 to Jan 31th 2022 across Spain illustrating the considerable abundance of the original strain (in red), followed by **Alpha**, **Delta** and lately **Omicron** spread across the country.

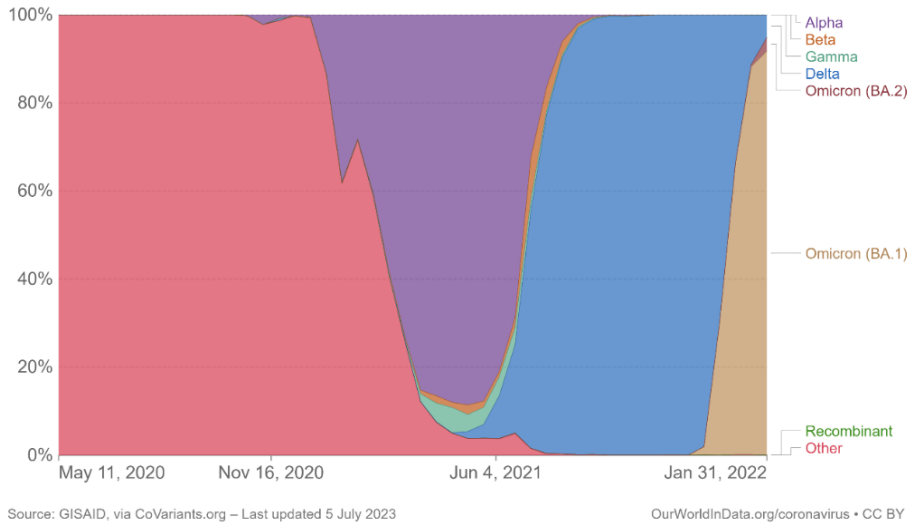

Figure II.VI Relative abundance of SARS-CoV-2 variants detected in sequences analyzed across Spain form the period between May 11,2020 to Jan, 31, 2022. The Wuhan variant is represented in red, while Alpha prevalence is in purple, followed by Delta in light blue and more recently Omicron in brown.

Looking back, the first SARS-CoV-2 VoC detected was the B.1.1.7 mutant (**Alpha**), popularly known as UK variant where was initially identified in December 2020. This subtype was characterized by several amino acid mutations, including N501Y which is thought to increase viral ability to bind to human ACE2 receptor form host cells. The B.1.1.7 variant displayed more transmissibility than the original strain and was associated with a higher risk of severe illness [39]. The following to appear was the B.1.351 variant (**Beta**), detected in South Africa and associated with an increased risk of severe illness and carrying several amino acid mutations, including E484K, linked to effective immune evasion [40]. Another relevant example was found over P.1 variant (**Gamma**) described as the Brazilian strain that included N501Y and E484K mutations also present in the B.1.1.7 and B.1.351 variants [41]. The P.1 variant was related with increased transmissibility and reported in reinfection cases.

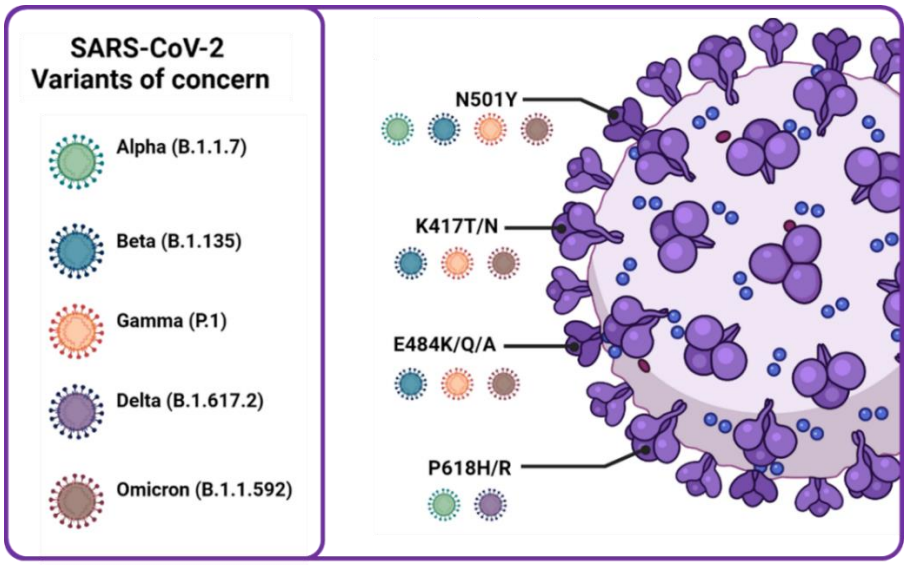

Figure II.VII Schematic representation of the most predominant mutations on S protein reported across different SARS-CoV-2 VoC's. Adapted from [42].

Continuing the viral evolution, the B.1.617.2 or **Delta** variant was originally detected in India and rapidly assigned as VoC owing to more transmissible phenotypes including multiple mutations in the spike protein like L452R and E484Q enhancing immune evasion [43]. Afterwards, other relevant variants were studied, leading to more contemporary ones like **Omicron** (B.1.1.529) variant, observed in South Africa by November 2021, and the sub-linages B.1.1.529.1 detected in Botswana [44], summarized in Figure II.VII. One of the key features

of this concerning mutant is its ability to rapidly spread in addition to the potential immune escape from vaccines or previous infections. These variants are characterized by accumulation of mutations in the spike protein and were under investigation to determine their potential impact on vaccine effectiveness and disease severity [45]. According to the previous description, it may seem that the mutation rate over N protein is lower or not comparable to S protein and this can lead to misinterpretations. Although a deeper analysis would be required in this sense, is clear that the pressure of selection over S protein is considerably higher than over N protein, due to the natural role and distribution of S protein mediating viral entry to the host cell. However, any viral protein including the N protein, can still undergo mutations but the frequency and impact on the viral behaviour may differ [46].

In this regard, an ambitious study aimed to correlate clinical severity with the variant causing the infection over more than 2700 patients but no significant differences regarding hospitalization, ICU admission or death were established within **Alpha**, **Gamma** and **Delta** variants. Interestingly, **Omicron** infected patients showed lower rate of hospitalization, oxygen requirement and ICU admission with no differences between sub variants BA.1 and BA.2 [47] probably due to pre-existent naturally or induced immunity. The characterization of emerging VoC's was essential assuming the increasing prevalence of specific sub-linages in different regions worldwide. As consequence, sequencing techniques became the reference methods to identify new mutations and track their global distribution. Nevertheless, sophisticated equipment and trained laboratory personnel are required, limiting their mass scale implementation. The potential application of high-throughput and affordable screening tools capable to discriminate VoC generating the infection would considerably help to understand the selective viral evolution opening the door to solutions for future outbreaks.

V. DETECTING THE NOVEL CORONAVIRUS: TRENDING METHODS AND REFERENCE TECHNIQUES

Diagnostic tests are a fundamental component of a successful outbreak containment strategy, being involved at every stage of an outbreak, from initial detection to eventual resolution. The COVID-19 pandemic has been the proof of

that. At the start of the COVID-19 pandemic, Tedros Adhanom Ghebreyesus, Director-General of WHO, urged countries to “test, test, test”. Proposing the **test-trace-isolate-quarantine (TTIQ)** strategy, where confirmed-positive carriers are isolated from the community and their recent close contacts to be preventively quarantined, expecting to break chains of transmission during the COVID-19 outbreak.

For a successful TTIQ strategy intensive testing is required. In the absence of specific treatments or vaccines the only alternative to control the COVID-19 pandemic was to reduce transmission by isolating symptomatic and asymptomatic individuals and, to achieve that goal the availability of diagnostic tools was required in a short period of time. The response from the diagnostic industry was overwhelming despite the scientific and technological complex challenges involved in the development, validation and implementation of the tests. Currently, more than 1000 brands of diagnostic test for COVID-19 are commercially available and more have remained in the pipeline. Following there is a short description of some of the main diagnostic strategies for COVID-19.

a. Platforms based on viral components

The rapid viral dissemination imposed an unprecedented challenge for diagnostic considering the lack of reliable detection tools during initial phases of the pandemic. Indeed, the absence of symptoms in mild or asymptomatic patients increased the chances of viral propagation [48, 49] requiring for faster, easier to use and cost-effective monitoring platforms to cover the massive testing needs and decentralize laboratory-based diagnostics [50, 51].

On this behalf, once the sequence of the virus was available, the first group of detection methods in appear were based on **polymerase chain reaction (PCR)** and were rapidly defined as gold standard. This technique relies on repeated amplification cycles of discrete viral sequences delimitated by a set of carefully designed primers until reach detectable number of copies monitored by fluorescence. In the case of SARS-CoV-2 detection, a reverse transcription step, to convert the starting RNA into cDNA was necessary before performing the PCR protocol. Most of commercially available PCR kits target ORF1ab region, N and E proteins genes [52, 53]. The main limitations were found on the need of trained

personnel and limited sample processing capacity, requiring a minimum of 2-3 hours to obtain results [54].

The second group of methods in charge of detecting viral proteins were **antigen tests**. They emerged as user-friendly alternatives allowing self-monitoring and mass screening capacity at affordable prices [50, 54]. The principle of detection consists on the use of selective antibodies for the recognition of structural components like N or in minor proportion S protein, both from nasopharyngeal swabs or saliva samples under lateral flow immunoassay formats offering results in 15-20 minutes [55, 56]. During the first stages of development, the antigen tests available lacked of enough sensitivity, increasing the risk of viral propagation and in some cases were useless against new emerging variants [57]. However, further on the antigen tests that appeared showed excellent features and played a crucial role in curbing COVID-19 infections, especially because their role to reduce transmission. Antigen detection provided a number of distinct advantages including; 1) high speed, low cost, and noninvasive small volumes of sampling; 2) equipment-free interpretation of qualitative results and mild equipment dependence to interpret semiquantitative results; 3) easy sampling and simple testing procedures; 4) long shelf-life and easily achievable storage conditions, and overall 5) the possibility to use them at home as point-of-care (PoC) testing devices. Antigen test provided an effective diagnostics alternative to monitor active infection at epidemiological scale, however, as with PCR, the sensitivity of these tests can be uncertain as the virus load gradually drops to a low concentration, which usually occurs in the first 5–7 days before symptom onset and the late post-symptom period. Nevertheless, their above-mentioned features allowed for daily screening and therefore improving test reliability Although the determination of viral components like genetic material (RNA) or proteins (S and N) is extremely necessary from the diagnostic perspective, their use is limited to the residence of the virus in the host during the period of incubation and up to now no solid evidence demonstrated a clear correlation with predictive clinical outcomes [58]. Therefore, the development of accurate diagnostic tools with the ability to correlate clinical severity with specific biomarkers of infection at host level is highly desirable (see Figure II.VIII)

b. Assessment of host immunological response

In order to evaluate host immune progression during and after SARS-CoV-2 infection, the third group of monitoring tools developed were **serological assays**. In this regard, immunity has been addressed as a principal component behind successful disease control and clinical progression [59]. Differences over innate immunity and adaptive response were associated to severe and mild outcomes [60].

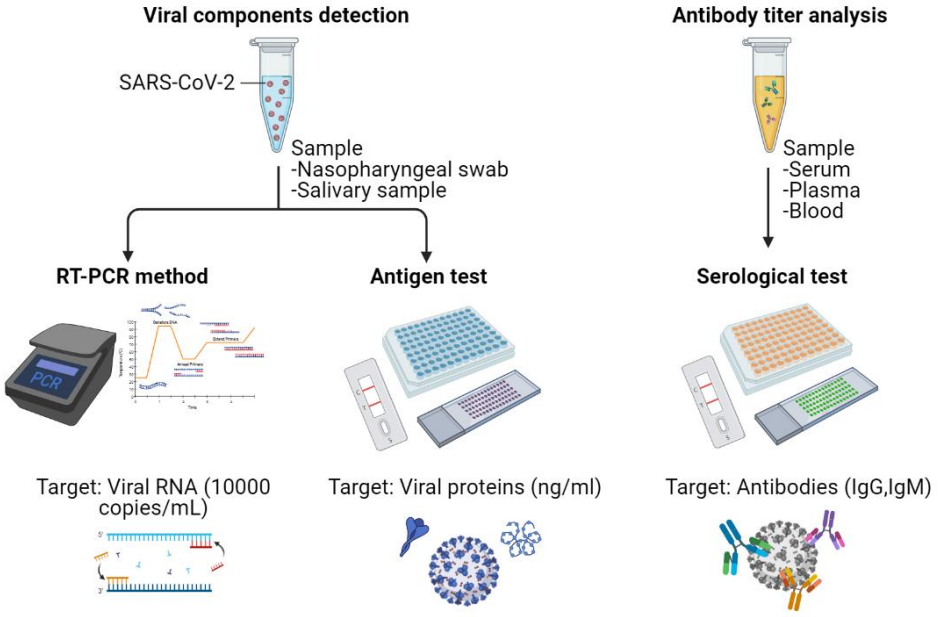

Figure II.VIII Graphical representation of three standard methods for SARS-CoV-2 diagnostic. Depending on the type of sample required, different detection strategies can be applied. For viral components determination, RT-PCR methods target viral RNA while antigen tests measure amount of viral proteins. On the other hand, anti-SARS-CoV-2 antibodies are determined through serological tests targeting mainly IgG's, IgM's and in some cases IgA's.

Serological assays are characterized by a relatively simple configuration that allows the determination of naturally generated antibodies (IgAs, IgGs or IgMs) from individuals exposed to a pathogenic component or vaccination, eliciting a measurable antibody mediated response. In the case of SARS-CoV-2, a wide variety of assays formats were explored but the use of nitrocellulose strips was broadly applied to immobilize structural proteins like S or N, promoting the interaction with specific antibodies in serum and plasma or even saliva samples

for IgA's detection [61, 62]. Despite the limited diagnostic performance, serological tests were rapidly produced and validated during the first pandemic period while antigen tests required more extensive optimizations as well as high-quality antibodies to commit the limits defined by the authorities.

c. General considerations towards more accurate serological diagnostics

As soon as the COVID-19 pandemic was announced, worldwide regulatory agencies like the FDA in North America and the EMA in Europe were committed to evaluate and authorize the use of several detection platforms, lacking of standardized reference materials and facing the urgent demand for reliable monitoring tools in a critical period. Leading to exceptions with approval for emergency use over devices without exhaustive validation in the case of FDA [63]. In this regard, by December 2020 the unit of reference materials from the European Commission launched a reference pool of serum samples obtained from different donors after SARS-CoV-2 infection that was extensively characterized, with the aim to implement it across the validation of new serological assays, neutralization studies and many other antibody related applications [64].

In an attempt to harmonize the data generated from the increasing number of serological platforms detecting SARS-CoV-2 response, the WHO also established different considerations to embrace validation and comparisons over these group of biochemical assays by defining tolerance limits for commercialization between 95-97 % sensitivity and 98-99 % specificity as acceptable criteria [65]. Furthermore, regulatory agencies recommended to express serological results in Binding Antibody Units (BAU) instead of antibody titers to standardize the values and limits of detection achieved by different devices. Particularly for the case of serology panels the results should be reported in International Units (BAU/mL) and the conversion factor for 1 arbitrary unit (AU/mL) corresponds to 4.33 BAU/mL [66]. According to these guidelines, future diagnostic developments should establish consistent validation protocols following a unified criterion, rather than exclusively innovative technological solutions [67].

Throughout the literature, a growing number of serological tools have been reported to estimate levels of Anti-SARS-CoV-2 IgG's and IgM's under lateral flow

formats (LFIA) [68, 69] or ELISA [70, 71]. Moreover, optical sensors based on surface plasmon resonance were proposed to define kinetic parameters over patient's IgG responses [72] as well as electrochemical platforms to be implemented as rapid immunity indicators [73, 74].

VI. DEFINING THE ROLE OF THE IMMUNE SYSTEM IN COVID-19

Over hundreds of additional relevant functions, the immune system is responsible of maintain homeostasis and mitigate potential threats from organisms undergoing through an infective process. Although the current understanding of the immune response has improved considerably over the past decades, the complexity of this system remains unclear over certain pathologies like autoimmune disorders and partially over SARS-CoV-2 infection. In a typical infectious process, the surveillance system will detect the presence of an abnormal agent raising the alarm to different subpopulations of immune cells with strictly defined functions to eliminate the threat in a coordinated manner [75].

Considering the cell types implicated and their functions, two types of immune responses can be broadly differentiated as innate immunity and adaptive immunity (See Figure II.IX). The first one is defined as a primary line of defense offering a generalized response against the agents causing the infection. This system is composed of anatomical barriers (like skin and mucosa) and white blood cells or leucocytes (as natural killer cells, mast cells, eosinophils, basophils and phagocytic cells that include macrophages, neutrophils and dendritic cells). This short-term response is mainly characterized by excessive inflammation mediated by cytokines and chemokines to induce the activation of specialized cells in charge of the elimination of the pathogen [76].

On the other hand, the adaptive immunity is a refined and long-term defense process that involves several steps and cell types with the ability to distinguish and eradicate the infective agent in a precise manner conferring memory against future re-infections. This type of immunity is divided into humoral and cellular responses, the first one mediated by B cells in charge of the production of antibodies and the second by T cells including CD4+ and CD8+ cells with different functions. A simplified representation considers T and B lymphocytes which are

responsible of external agents' recognition through an antigen presentation process, also to develop a tailored response distinguishing infected from non-infected cells and generate long term immunity across memory B cells producing antibodies and memory T cells [76].

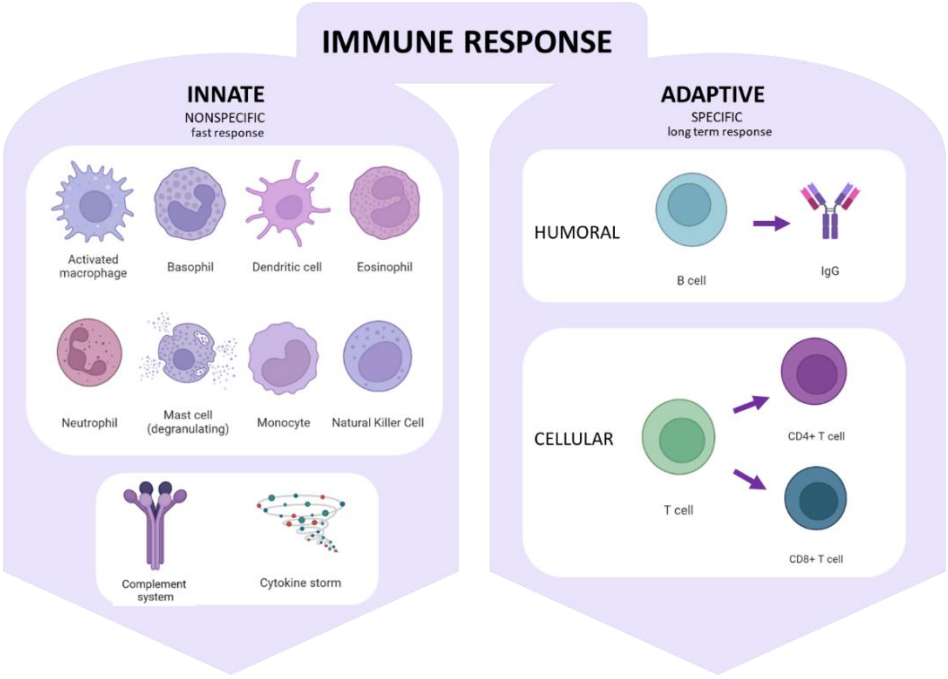

Figure II.IX Representation of the main cell types implicated in the immune response. Innate immunity is constituted by several immune cell populations and molecules acting as intermediate messenger. Adaptive response, defined as more specific can be distinguished in humoral response mediated by B cells and antibodies while cellular response is characterized by T cells (CD4+ and CD8+).

In the pandemic scenario, many efforts were dedicated to understand and explore the role of the immune system handling with SARS-CoV-2 infection. Special attention was pointed to establish the implications of innate response towards a rapid viral clearance associating a cytokine imbalance process also known as cytokine storm, to severe disease progression. Simultaneously, B cell mediated immunity through antibodies, was also addressed as a key element towards successful viral handling to generate alternative therapeutic solutions as well as effective vaccine candidates [77].

a. Innate immune dysregulations in SARS-CoV-2 infection

Viruses have evolved in many ways and with them immune evasion mechanisms. Particularly, SARS-CoV-2 immune evasion was described at innate immune level through the suppression via INF-I pathway. One of the earliest lines of host defense against viral infections is the innate interferon (IFN) response. Interestingly, the novel coronavirus is able to suppress anti-viral IFN-I response mediated by open reading frame 6 (ORF6) expression [78, 79]. Some authors proposed that children were better COVID-19 controllers based on the optimum performance of the innate immunity at initial stages of life directly attributed to elevated INF mediated response [80]. Additional evidence demonstrated that individuals with higher levels of autoantibodies against IFN I were more likely to undergo through severe clinical outcomes compared to those without detectable levels of this type of autoantibodies [81]. The capacity to develop effective antibody response against the virus was also attributed to the potential immune evasion strategies observed during INF I suppression mechanisms [82].

Furthermore, a critical step involving innate responses over life threatening patients was associated to the cytokine storm phenomena, described as an unregulated cytokine release triggering excessive inflammation. Similar biological processes have been reported in other pathologies caused by autoimmune disorders or sepsis mediated by cytokines like IL-1, IL-6, IL-8, IL-10, TNF-α and INF-γ showing despaired values [83]. The adequate control of such physiological conditions became promising as a therapeutic alternative towards COVID-19 handling in critical outcomes [84].

In summary, the dysregulation of IFN mediated immunity complemented with the increased level of cytokines like CXCL10, IL-6, and IL-8 has been related to inefficient control of SARS-CoV-2 infection linked to higher risk of severity according to different authors [85-87]. In this scenario, cytokines were evaluated as predictors of disease progression, demonstrating that high amounts of IL-6 in serum were correlated to lower survival expectancy [88]. While a higher probability of ICU admission was determined by increased levels of a group of cytokines like IL-2, IL7, IL-10, IP10, MCP1 and TNF-α [89]. The clinical relevance of innate immunity during the course of COVID-19 results evident. Nevertheless, the direct implications of the adaptive response should also be considered in

order to elucidate common pathways and provide a deeper understanding over the host-viral interaction.

b. Impact of SARS-CoV-2 exposure at adaptive immune level: The case of cellular response

Bearing in mind that the COVID-19 pandemic emerged from a novel virus, the lack of pre-existent immunity through natural or induced ways was a concerning element to face the increasing transmissibility rates and critical outcomes over the vulnerable population. Therefore, the assessment of humoral immunity was essential to underline potential mechanisms implicated in anti-viral protection.

As has been already described, the adaptive immunity is composed of three main cell groups with strictly defined protecting roles. On one hand, T cells are characterized by CD4+ T cells with helper and effector ability followed by CD8+ T cells in charge of eliminating infected cells. On the other hand, B cells are responsible of antibody production and long-term immune memory, expressed in Figure II.X.

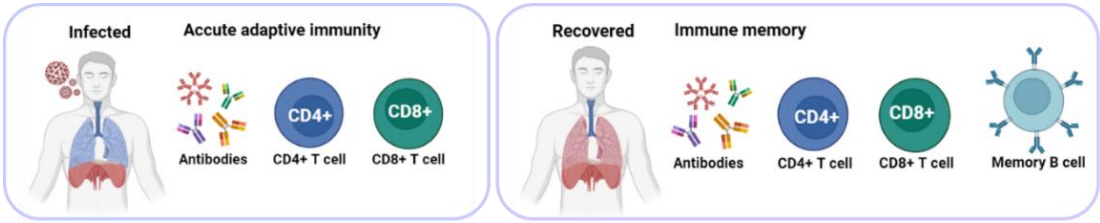

Figure II.X Schematic representation comparing adaptive immune response during and after infection. Mainly differentiated by the development of memory B cells post viral exposure.

During SARS-CoV-2 exposure, T cell mediated responses were detectable and particularly CD4+ T cell immunity showed more robust and effective prevalence during primary infection in comparison with CD8+ T cells [90]. Main interest was dedicated to comprehend T cell mediated response against S protein during infection and after vaccination [91] considering that CD4+ T cells could trigger the generation of anti-S antibodies [92]. In addition, the fast activation of CD4+ cells was linked to mild disease course and rapid viral elimination [93], while the low abundance of that subtype was mostly observed in fatal COVID-19 cases. Moreover, CD8+ T cell levels also showed to be determinant towards an effective

viral handling [92] indicating that both T cells subpopulations play a key role during SARS-CoV-2 infection.

c. Characterizing antibody mediated immunity

As already discussed in section 1.5.1, antibodies or immunoglobulins, are proteins secreted by humoral immune cells known as B lymphocytes in response to different pathogenic agents [94]. The natural function of these biomolecules consists on targeting a region of the pathogen (epitope) with the aim of neutralize it and elicit further elimination by other immune cells [76]. Antibodies can be found as transmembrane proteins acting as antigen-cell receptor or secreted proteins to neutralize components in the extracellular media [95]. As previously mentioned, B cells are responsible of antibody production after activation by CD4+ T cells, specifically Tfh type in SARS-CoV-2 infection.

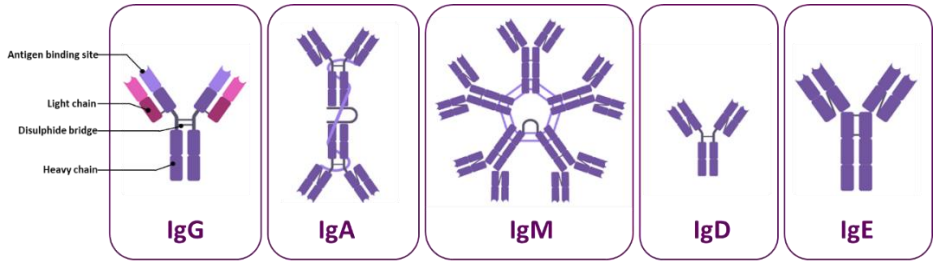

Figure II.XI Structure of different antibody classes. Description of the main components in IgG structure, followed by IgA, IgM, IgD and IgE from [96].

Different types of immunoglobulins are classified according to their function and structure represented in Figure II.XI [96]. The first to emerge are IgM's which are naturally found as pentamers secreted in early stages of immune response and constituting the 6 % of total Ab content in serum, followed by IgA's mainly secreted in mucus, saliva, tears and colostrum representing the 13 % of total antibody [97]. Complementary, other isotypes include IgD's associated with B cell activation and IgE's involved in allergic reactions. Finally, IgG's (gamma immunoglobulins) are the most abundant subtypes constituting the 80 % of total antibody content in serum. Structured in a conventional Y shape with modifications over the antigenic binding area, these glycoproteins are formed by two heavy chains (50 KDa) and two light chains (25 KDa) [98]. COVID-19 seroconversion occurs from day 5 to 14, first for IgM's and then for IgG's from the onset of symptoms, reaching a plateau by day 10-20 for the case of IgG's [99-

101]. A considerable part of the literature was focused on the utilization of antibodies as indicators of immunodominant regions derived from the complete viral proteome as well as assessing the immune protection provided by different vaccines with long term implications [102, 103].

VII. ANTIBODIES AS PROMISING COVID-19 BIOMARKERS IN DIFFERENT FIELDS

Particularly, the detection of IgM's was proposed as relevant early biomarker by many authors [104] but the clinical correlations are still not well defined yet, probably limited by a shorter sampling window (see Figure II.XII) [105]. Regrading IgA's, some articles state that higher levels of this isotypes are found over critically ill patients at early phases and may be used as good predictors but they clear much faster than IgG's limiting their implementation in prospective studies [106; 107]. Furthermore, based on their functions and properties, human IgG's can be classified in four different subtypes IgG1, IgG2, IgG3 and IgG4 and particularly during SARS-CoV-2 infection IgG1 and IgG3 were detected as the predominant classes over convalescent antisera [108]. Overall, IgG titers seems to offer the most robust and strong correlation with disease progression compared to other isotypes and due to this have been proposed as indicators of COVID-19 prognosis [109].

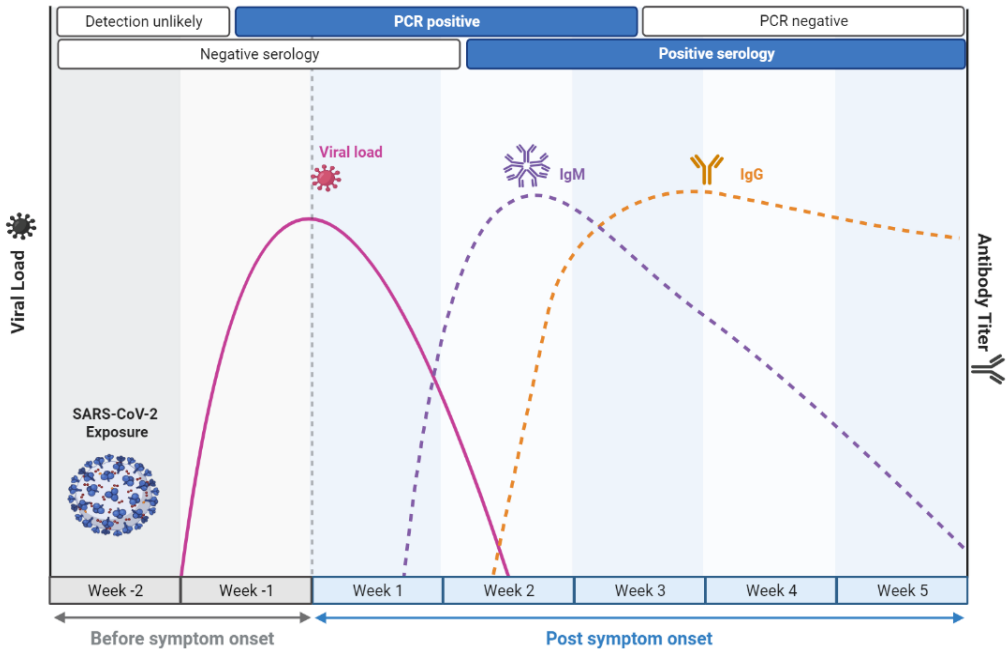

Figure II.XII Reported progression of the viral load and IgG/IgM mediated responses after SARS-CoV-2 exposure (expressed by weeks). The recommended method of detection considering the time point during infection is highlighted as well as the kinetic behavior of the components detected.

The long-term immunity as well as duration of IgG titters were questioned either after viral exposure or vaccination [110]. In this regard, immune protection was detectable after six months post symptom onset (PSO) and even during longer periods in severe cases [111]. In fact, convalescent serum samples were utilized to stratify seroconversion according to RT-PCR results based on IgG's and IgM's levels reaching high accuracy [112]. Additional studies emphasized on the importance of sample collection periods to correctly interpret serological results concluding that 20 days after the onset of symptom was sufficient to determine the immune state comparing commercial devices available in the market [113]

The difference in kinetics of antibody development were also approached stating that faster responses were associated with lower severity and on the contrary, delays in antibody response can lead to worst disease progression [110]. Additional evidence suggests that asymptomatic or mild COVID-19 patients went through the infection without developing a significative immune protection or extremely low in many cases and therefore are highly exposed to re-infection with different variants [99, 114].

A different area directly implicated with the role of antibodies during infection is described over vaccines development. Most of current vaccines available are directed towards the S glycoprotein with the aim to promote high neutralizing capacity and specificity. Nevertheless, N protein was proposed as ideal candidate because it triggers strong immunity, accumulate less mutations and is highly preserved among coronaviruses to develop broad spectrum alternatives [115].

Simultaneously, serological determinations at epidemiological level were used by public health authorities to get a better understanding of the true prevalence of SARS-CoV-2 infection over discreet populations and also to track the spread of the virus and identify areas where outbreaks were more likely to occur [116].

However, in this ever-evolving context, the emergence of novel detection tools to monitor antibody levels for diagnostic and prognostic purposes has been in continuous development and the main limitations arises as consequence of the significant amount of data that needs to be analyzed and interpreted. Due to this, artificial intelligence is playing a key role towards the understanding of the complex networks involved in personalized responses and thus facilitating upcoming developments of multiplexed and high-throughput platforms [117].

VIII. ARTIFICAL INTELLIGENCE ASSISTING FUTURE DIAGNOSTIC CHALLENGES

Artificial intelligence (AI) is a general definition that refers to the use of computers to simulate intelligent like behavior with minimum human influence [118]. This relatively new discipline is considered as an ever-evolving field of computer science with potential impact over distinct areas and in the context of this thesis, will be used to describe the implementation of mathematical models and algorithms to interpret complex data sets and establish correlations with clinical outcomes.

A relevant area where AI has proven direct and useful influence is over biostatistical analysis, consisting on the application of statistics to biological and medical data. The accelerated use and development of these techniques had led to automate processes and enhance the accuracy as well as processing capacity, to get results and provide new insights over complex biological systems [119].

a. Fundamentals on biostatistics

Nowadays, the most common techniques utilized in AI-based biostatistical analysis include machine learning and deep learning processing. These approaches involve the use of algorithms and statistical models to identify patterns and relationships across the data [120]. Some of the most relevant aspects to consider before embracing the implementation of biostatistical tools includes:

A) Appropriate design of data collection procedures following well-structured and homogenous conditions.

B) Consider a representative number of samples to evidence the phenomena under study.

C) Predefine the most suitable analysis strategy based on the variables assessed and the objectives of the study.

D) Report the level of uncertainty desired.

In biostatistics and medical prediction, receiver operating characteristic (ROC) curves (see Figure II.XIII) are graphical representations of a system performance towards binary classification. The ROC curve plots the true positive rate (sensitivity) against the false positive rate (1-specificity) of the classifier [121]. In the diagnostic field this type of analysis represents the platform capacity to assign a suspected sample between two categories, such as healthy or disease. Another parameter commonly assessed during biostatistical determinations is the area under the curve (AUC), considered as indicator of diagnostic accuracy. The AUC value ranges from 0.5 to 1 (perfect accuracy) and reflects the probability of the classifier to rank a randomly chosen “positive” sample with higher value than a randomly chosen “negative” sample. A higher AUC indicates a better diagnostic accuracy [122].

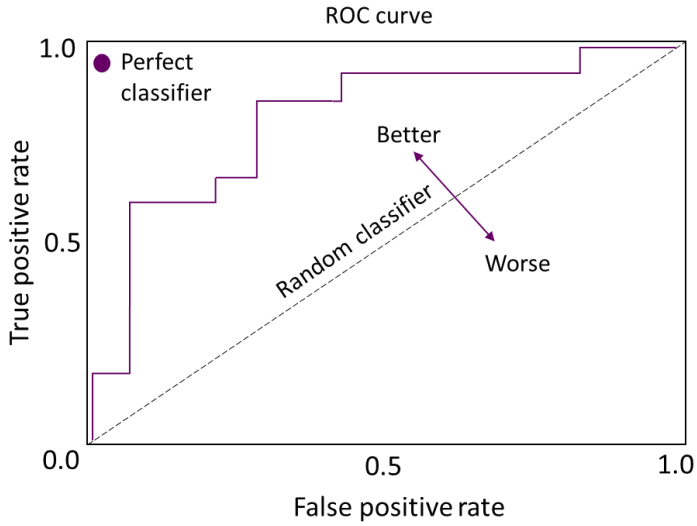

Figure II.XIII Standard ROC curve components. Interpretation of ROC curve characteristics plotting false positive rates (x-axis) and true positive rate (y-axis) to determine the accuracy of the method.

Deeper understanding over data implications can be extracted from Pearson's correlation coefficient determination. This is another statistical approach to measure the strength and tendency of the linear behavior between two variables to define positive or negative correlations [123]. It is important to highlight that correlation does not necessarily imply causation [124].

b. Classification and regression models integrated in the biomedical field

Classification and regression models are commonly used in bioinformatics to analyze and interpret large datasets. Classification models considers the characteristics of the variable to assign it into a class or category (see Figure II.XIV and Figure II.XV). For example, under protein expression analysis, classification models could predict the function or type of protein based on their intrinsic characteristics. Some of the most commonly used classification models in bioinformatics include decision trees, random forests and neural networks.

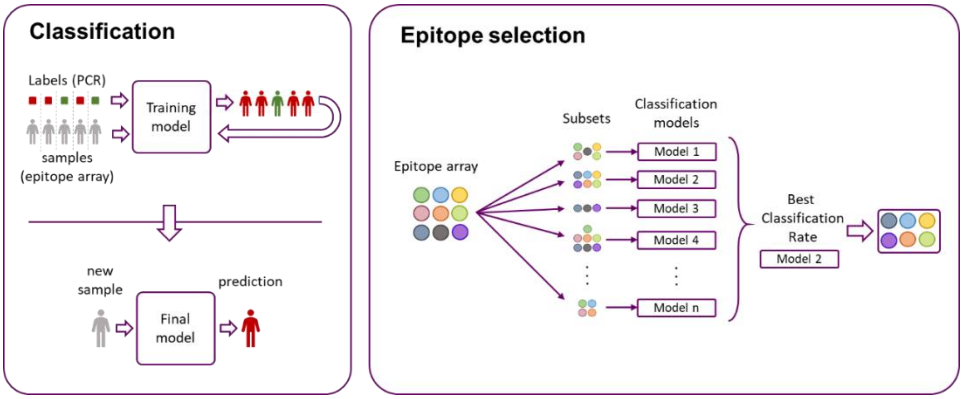

Figure II.XIV Classification models and epitopes selection. On the left side, labeled samples are utilized for training the algorithm until the definition of a final prediction model. At right, from the multiplexed matrix of epitopes evaluated different sub-sets are utilized to generate the model with the best classification rate.

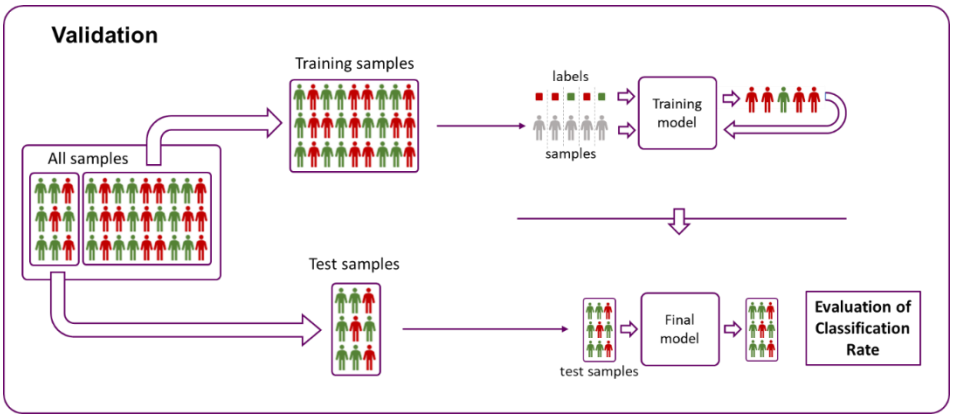

Figure II.XV Platfrom validation using clinical samples. The complete set of samples measured is divided in a training group (80 % of samples) to define the algorithm and the remaining 20 % of samples are used to evaluate the classification rate of the model generated in blind conditions [125].

Regression models, on the other hand, are used to predict a continuous outcome based on one or more variables. In the following example, regression models can be implemented to predict the expression level of a gene based on environmental factors. Commonly used regression models in bioinformatics include linear regression, logistic regression, and generalized linear models. Both classification and regression models can be trained using machine learning algorithms for the analysis of complex data in order to identify patterns and relationships between distinct clinical variables [126].

IX. NEXT GENERATION DIAGNOSTIC COMBINING MULTIPLEXED DETECTION FORMATS, LARGE DATA SETS AND ARTIFICIAL INTELLIGENCE FOR SARS-COV-2

Since the original definition, diagnostic was understood as the ability to discriminate between absence or presence of disease and infection making use of selective biomarkers. Nowadays, considering the progress in research and technological fields, the possibility to predict disease evolution was addressed as an additional motivation over traditional diagnostic platforms. On this behalf, during COVID 19 pandemic the lack of experience handling with this viral infection led to unpredictable clinical scenarios and diagnostic methods were proposed to anticipate patient's progression in many cases. Due to this, the integration of multiparametric determinations applied to large numbers of samples to generate results and extract conclusion using computational analysis are leading current developments. For instance, the susceptibility to suffer sequelae after COVID-19 infection was evaluated through a multi-omic and longitudinal approach over more than 300 patients and the main factors contributing to residual side effects were associated with type 2 diabetes, Epstein-Barr virus viremia, SARS-CoV-2 RNAemia and specific auto-antibodies [127].

A different multiplexed proposal, contemplated the analysis of chest computed tomography (CT) that was coupled to machine learning techniques to predict COVID-19 disease course. During the following investigation, patient's stratification based on image analysis was correlated with inflammatory levels, aging and higher neutrophil-to-lymphocyte ratio (NLR) to guide clinicians towards more accurate diagnostics [128]. Similar studies also declared successful discrimination of severe outcomes with deep learning models achieving 97.4 % of accuracy considering CT image analysis from 408 COVID-19 confirmed patients evidencing the potential over these hybrid diagnostic methodologies [129]. Nevertheless, data variability was pointed out as a major limitation over machine learning-based analysis leading to biased interpretations in some cases [130].

From the clinical evidence, the first biomarkers showing significant correlations with disease progression were associated to increased levels of IL6 and CRP as well as different cytokines in serum [131]. Moreover, innovative approaches like urinary peptidomic analysis were explored to predict disease severity utilizing

capillary electrophoresis coupled to mass spectrometry for the identification of peptide profiles in urine samples from COVID-19 patients [132]**.** Alternatively, the evaluation of amino acid metabolic signatures across hospitalized and recovered COVID-19 patients were also proposed linking tryptophan and arginine metabolism as key elements over antiviral immune performance promoting different treatment options [133].

In this context, recent strategies also contemplate the integration of well-defined serological panels with large sample-sets combining biostatistical analysis and machine learning tools to associate personalized antibody profiles with clinical outcomes [134]. Additionally, some authors state that monitorization of IgG response against different antigenic domains should be considered as a substantial factor to increase diagnostic sensitivity [135].

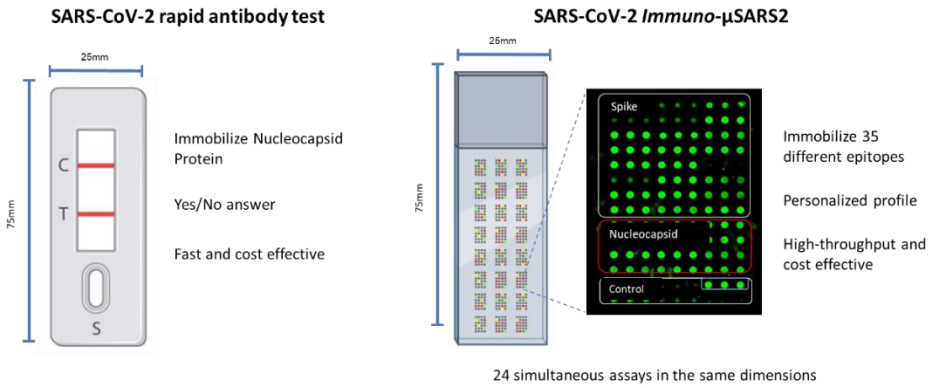

Figure II.XVI Comparison between conventional antibody tests under LFIA format(left) and the proposed platform under development through the following thesis discussed in chapter 6 and 7 (right).

Concerning this, some examples from literature explore serological determinations under microarray formats taking advantage of the extensive degree of multiplexation and high-throughput capacity in comparison with other sensing approaches as represented in Figure II.XVI [136-138]. For instance, *Whang et. al.* determined immunodominant regions with a peptide microarray containing the viral proteome with resolution of a single amino acid [139]. In addition, a similar proposal made by Jiang and collaborators studied the immunogenicity of 18 of the 26 viral proteins in microarray format, concluding that antibodies against N and S1 subunit were the most abundant sub-populations [140]. Furthermore, the analysis of the immune response against the

S protein and RBD zone over more than 2500 human serum samples revealed a group of peptides with high diagnostic capacity [141]. As can be seen, different serological studies and approaches based on microarray technologies are available, pointing to the possibility to use them for diagnostics and screening purposes [142]. However, most of serological arrays reported are focused on the analysis of the immunological response towards the complete proteome with a limited number of samples. This approach has a significant cost associated due to the high number of peptide sequences required in the microarray chip to accomplish that level of resolution. For instance, the chip from Wang *et al.* [139] contained 996 sequences, limiting the routine implementation of such platform for personalized diagnostic in clinical settings.

GENERAL AND SPECIFIC THESIS OBJECTIVES: POC4COV PROJECT

As already mentioned, the general objective of this thesis has been to investigate and extend the potential use of microarray technology to develop versatile bioanalytical solutions in different fields. In that respect, the research work performed in this second part of the PhD thesis is based on the hypothesis that profiling the antibody response against the main structural proteins of the SARS-CoV-2 virus could allow discriminating the different individual responses observed for COVID-19 while providing some clinical predictive value in respect to the prognostic of the disease.

The strategy proposed to achieve this goal consisted on developing a peptide epitope microarray, for which purpose the following working plan was proposed:

1. Rational selection of discreet panel of epitope peptide sequences of the Spike (S) and Nucleocapsid (N) proteins, based on the knowledge reported in the literature available during the first months of the pandemic and also using computational analysis.

2. Establishing a standardized methodology for the synthesis of the peptide epitopes selected, their bioconjugation to a protein and their characterization prior to their implementation in microarray format.

3. Developing a high-throughput and multiplexed peptide-protein microarray chip for profiling the human immunological response (IgG and IgM antibodies) towards a panel of selected epitopes after SARS-CoV-2 exposure.

4. Implementation of the microarray chip to the analysis of clinical samples.

5. Determining which immunoglobulin isotype provides the most accurate information about the patient's immunological status and identify the most immunodominant regions above the peptide sequences selected.

6. Investigating the potential correlation between the COVID-19 severity the characteristic serological signatures recorded using biostatistical analysis in populations lacking of vaccination schemes or pre-existing immunity.

7. Investigating the potential value of the microarray chip developed to identify the virus variants of concern (VoC) responsible of the infections by detecting a particular serological fingerprint.

8. To investigate the serological progression over time, after vaccination and reinfection

X. BIBLIOGRAPHY

1. Rothan, H.A. and S.N. Byrareddy, *The epidemiology and pathogenesis of coronavirus disease (COVID-19) outbreak.* Journal of autoimmunity, 2020. **109**: p. 102433.
2. Boni, M.F., et al., *Evolutionary origins of the SARS-CoV-2 sarbecovirus lineage responsible for the COVID-19 pandemic.* Nature microbiology, 2020. **5**(11): p. 1408-1417.
3. Hiscott, J., et al., *The global impact of the coronavirus pandemic.* Cytokine & growth factor reviews, 2020. **53**: p. 1-9.
4. Rasmussen, A., *Key Features of SARS-CoV-2*, in *Biorender*. 2021: https://app.biorender.com/biorender-templates/figures/5e99f5395fd61e0028682c01/t-609a986d2a2d6e00a4d3eaa8-key-features-of-sars-cov-2.
5. Guan, W.-j., et al., *Clinical characteristics of coronavirus disease 2019 in China.* New England journal of medicine, 2020. **382**(18): p. 1708-1720.
6. Chandra, A., et al., *Silent hypoxia: a frequently overlooked clinical entity in patients with COVID-19.* BMJ Case Reports CP, 2020. **13**(9): p. e237207.
7. Zhou, F., et al., *Clinical course and risk factors for mortality of adult inpatients with COVID-19 in Wuhan, China: a retrospective cohort study.* The lancet, 2020. **395**(10229): p. 1054-1062.
8. Force, A.D.T., et al., *Acute respiratory distress syndrome.* Jama, 2012. **307**(23): p. 2526-2533.
9. Del Valle, D.M., et al., *An inflammatory cytokine signature predicts COVID-19 severity and survival.* Nature medicine, 2020. **26**(10): p. 1636-1643.
10. Organization, W.H., *Living guidance for clinical management of COVID-19: living guidance, 23 November 2021*. 2021, World Health Organization.
11. O'Driscoll, M., et al., *Age-specific mortality and immunity patterns of SARS-CoV-2.* Nature, 2021. **590**(7844): p. 140-145.
12. Karagiannidis, C., et al., *Case characteristics, resource use, and outcomes of 10 021 patients with COVID-19 admitted to 920 German hospitals: an observational study.* The Lancet Respiratory Medicine, 2020. **8**(9): p. 853-862.
13. Fingerlin, T.E., et al., *Genome-wide association study identifies multiple susceptibility loci for pulmonary fibrosis.* Nature genetics, 2013.**45**(6):p.613-620.
14. Zhang, Q., et al., *Inborn errors of type I IFN immunity in patients with life-threatening COVID-19.* Science, 2020. **370**(6515): p. eabd4570.
15. Lamers, M.M. and B.L. Haagmans, *SARS-CoV-2 pathogenesis.* Nature reviews microbiology, 2022. **20**(5): p. 270-284.
16. Mahajan, S., et al., *SARS-CoV-2 infection hospitalization rate and infection fatality rate among the non-congregate population in Connecticut.* The American Journal of Medicine, 2021. **134**(6): p. 812-816. e2.
17. Wiersinga, W.J., et al., *Pathophysiology, transmission, diagnosis, and treatment of coronavirus disease 2019 (COVID-19): a review.* Jama, 2020.**324**(8):p.782-793.
18. Wang, M.-Y., et al., *SARS-CoV-2: structure, biology, and structure-based therapeutics development.* Frontiers in cellular and infection microbiology, 2020. **10**: p. 587269.

19. Hudson, C. and F. Beaudette, *Infection of the cloaca with the virus of infectious bronchitis.* Science, 1932. **76**(1958): p. 34-34.
20. Belouzard, S., et al., *Mechanisms of coronavirus cell entry mediated by the viral spike protein.* Viruses, 2012. **4**(6): p. 1011-1033.
21. Huang, Y., et al., *Structural and functional properties of SARS-CoV-2 spike protein: potential antivirus drug development for COVID-19.* Acta Pharmacologica Sinica, 2020. **41**(9): p. 1141-1149.
22. Watanabe, Y., et al., *Site-specific glycan analysis of the SARS-CoV-2 spike.* Science, 2020. **369**(6501): p. 330-333.
23. Bosch, B.J., et al., *The coronavirus spike protein is a class I virus fusion protein: structural and functional characterization of the fusion core complex.* Journal of virology, 2003. **77**(16): p. 8801-8811.
24. Cohen, J., *The dream vaccine*. 2021, American Association for the Advancement of Science.
25. Jia, H.P., et al., *ACE2 receptor expression and severe acute respiratory syndrome coronavirus infection depend on differentiation of human airway epithelia.* Journal of virology, 2005. **79**(23): p. 14614-14621.
26. Li, M.-Y., et al., *Expression of the SARS-CoV-2 cell receptor gene ACE2 in a wide variety of human tissues.* Infectious diseases of poverty, 2020. **9**(02): p. 23-29.
27. Tai, W., et al., *Characterization of the receptor-binding domain (RBD) of 2019 novel coronavirus: implication for development of RBD protein as a viral attachment inhibitor and vaccine.* Cellular & molecular immunology, 2020. **17**(6): p. 613-620.
28. Nayak, S.K., *Inhibition of S-protein RBD and hACE2 interaction for control of SARSCoV-2 infection (COVID-19).* Mini Reviews in Medicinal Chemistry, 2021. **21**(6): p. 689-703.
29. Yu, F., et al., *Receptor-binding domain-specific human neutralizing monoclonal antibodies against SARS-CoV and SARS-CoV-2.* Signal Transduction and Targeted Therapy, 2020. **5**(1): p. 212.
30. Theel, E.S., et al., *The role of antibody testing for SARS-CoV-2: is there one?* Journal of clinical microbiology, 2020. **58**(8): p. 10.1128/jcm. 00797-20.
31. Yang, M., et al., *Structural insight into the SARS-CoV-2 nucleocapsid protein C-terminal domain reveals a novel recognition mechanism for viral transcriptional regulatory sequences.* Frontiers in chemistry, 2021. **8**: p. 624765.
32. McBride, R., M. Van Zyl, and B.C. Fielding, *The coronavirus nucleocapsid is a multifunctional protein.* Viruses, 2014. **6**(8): p. 2991-3018.
33. Gralinski, L.E. and V.D. Menachery, *Return of the Coronavirus: 2019-nCoV.* Viruses, 2020. **12**(2): p. 135.
34. Zeng, Y., et al., *The nucleocapsid protein of SARS-associated coronavirus inhibits B23 phosphorylation.* Biochemical and biophysical research communications, 2008. **369**(2): p. 287-291.
35. Yan, X., et al., *Nucleocapsid protein of SARS-CoV activates the expression of cyclooxygenase-2 by binding directly to regulatory elements for nuclear factor-kappa B and CCAAT/enhancer binding protein.* The international journal of biochemistry & cell biology, 2006. **38**(8): p. 1417-1428.

36. Pan, P., et al., *SARS-CoV-2 N protein promotes NLRP3 inflammasome activation to induce hyperinflammation.* Nature communications, 2021. **12**(1): p. 4664.
37. Lu, X., et al., *SARS-CoV nucleocapsid protein antagonizes IFN-β response by targeting initial step of IFN-β induction pathway, and its C-terminal region is critical for the antagonism.* Virus genes, 2011. **42**: p. 37-45.
38. Control, C.f.D. and Prevention, *SARS-CoV-2 Sequencing for Public Health Emergency Response, Epidemiology, and Surveillance: SPHERES*. 2022.
39. Shen, X., et al., *SARS-CoV-2 variant B. 1.1. 7 is susceptible to neutralizing antibodies elicited by ancestral spike vaccines.* Cell host & microbe, 2021. **29**(4): p. 529-539. e3.
40. Zhou, D., et al., *Evidence of escape of SARS-CoV-2 variant B. 1.351 from natural and vaccine-induced sera.* Cell, 2021. **184**(9): p. 2348-2361. e6.
41. O'Toole, Á., et al., *Tracking the international spread of SARS-CoV-2 lineages B. 1.1. 7 and B. 1.351/501Y-V2 with grinch.* Wellcome Open Research, 2021. **6**.
42. Mistry, P., et al., *SARS-CoV-2 variants, vaccines, and host immunity.* Frontiers in immunology, 2022. **12**: p. 809244.
43. Mlcochova, P., et al., *SARS-CoV-2 B. 1.617. 2 Delta variant replication and immune evasion.* Nature, 2021. **599**(7883): p. 114-119.
44. Dhawan, M., et al., *Omicron variant (B. 1.1. 529) and its sublineages: What do we know so far amid the emergence of recombinant variants of SARS-CoV-2?* Biomedicine & Pharmacotherapy, 2022: p. 113522.
45. Ren, S.-Y., et al., *Omicron variant (B. 1.1. 529) of SARS-CoV-2: Mutation, infectivity, transmission, and vaccine resistance.* World journal of clinical cases, 2022. **10**(1): p. 1.
46. Rahman, M.S., et al., *Evolutionary dynamics of SARS-CoV-2 nucleocapsid protein and its consequences.* Journal of medical virology, 2021. **93**(4): p. 2177-2195.
47. Esper, F.P., et al., *Alpha to Omicron: disease severity and clinical outcomes of major SARS-CoV-2 variants.* The Journal of Infectious Diseases, 2023. **227**(3): p. 344-352.
48. García, L.F., *Immune response, inflammation, and the clinical spectrum of COVID-19.* Frontiers in immunology, 2020. **11**: p. 1441.
49. Chan, Y.H., et al., *Asymptomatic COVID-19: disease tolerance with efficient anti-viral immunity against SARS-CoV-2.* EMBO molecular medicine, 2021. **13**(6): p. e14045.
50. Mercer, T.R. and M. Salit, *Testing at scale during the COVID-19 pandemic.* Nature Reviews Genetics, 2021. **22**(7): p. 415-426.
51. Udugama, B., et al., *Diagnosing COVID-19: the disease and tools for detection.* ACS nano, 2020. **14**(4): p. 3822-3835.
52. Yu, F., et al., *Quantitative detection and viral load analysis of SARS-CoV-2 in infected patients.* Clinical Infectious Diseases, 2020. **71**(15): p. 793-798.
53. Russo, A., et al., *Current status of laboratory diagnosis for COVID-19: a narrative review.* Infection and Drug Resistance, 2020: p. 2657-2665.
54. Choi, J.R., *Development of point-of-care biosensors for COVID-19.* Frontiers in chemistry, 2020. **8**: p. 517.

55. Peto, T., et al., *COVID-19: Rapid antigen detection for SARS-CoV-2 by lateral flow assay: A national systematic evaluation of sensitivity and specificity for mass-testing.* EClinicalMedicine, 2021. **36**: p. 100924.
56. Peña-Rodríguez, M., et al., *Performance evaluation of a lateral flow assay for nasopharyngeal antigen detection for SARS-CoV-2 diagnosis.* Journal of Clinical Laboratory Analysis, 2021. **35**(5): p. e23745.
57. Giri, B., et al., *Review of analytical performance of COVID-19 detection methods.* Analytical and bioanalytical chemistry, 2021. **413**(1): p. 35-48.
58. Mattioli, I.A., et al., *On the challenges for the diagnosis of SARS-CoV-2 based on a review of current methodologies.* ACS sensors, 2020. **5**(12): p. 3655-3677.
59. Walter, L.O., et al., *The relationship between peripheral immune response and disease severity in SARS-CoV-2-infected subjects: A cross-sectional study.* Immunology, 2022. **165**(4): p. 481-496.
60. Mahmudpour, M., et al., *COVID-19 cytokine storm: The anger of inflammation.* Cytokine, 2020. **133**: p. 155151.
61. Ainsworth, M., et al., *Performance characteristics of five immunoassays for SARS-CoV-2: a head-to-head benchmark comparison.* The Lancet Infectious Diseases, 2020. **20**(12): p. 1390-1400.
62. Nicol, T., et al., *Assessment of SARS-CoV-2 serological tests for the diagnosis of COVID-19 through the evaluation of three immunoassays: Two automated immunoassays (Euroimmun and Abbott) and one rapid lateral flow immunoassay (NG Biotech).* Journal of Clinical Virology, 2020. **129**: p. 104511.
63. Zuckerman, D.M., *Emergency use authorizations (EUAs) versus FDA approval: implications for covid-19 and public health*. 2021, American Public Health Association. p. 1065-1069.
64. Freeman, J., et al., *Analytical characterization of the SARS-CoV-2 EURM-017 reference material.* Clinical Biochemistry, 2022. **101**: p. 19-25.
65. Organization., W.H., *Target product profiles for priority diagnostics to support response to the COVID-19 pandemic v.0.1; 2020*. 2020: https://www.who.int/publications/m/item/covid-19-target-product-profiles-for-priority-diagnostics-to-support-response-to-the-covid-19-pandemic-v.0.1.
66. Infantino, M., et al., *The WHO International Standard for COVID-19 serological tests: towards harmonization of anti-spike assays.* International immunopharmacology, 2021. **100**: p. 108095.
67. Gundlapalli, A.V., et al. *SARS-CoV-2 serologic assay needs for the next phase of the US COVID-19 pandemic response*. in *Open forum infectious diseases*. 2021. Oxford University Press US.
68. Weidner, L., et al., *Quantification of SARS-CoV-2 antibodies with eight commercially available immunoassays.* Journal of Clinical Virology, 2020. **129**: p. 104540.
69. Perez-Lopez, B. and M. Mir, *Commercialized diagnostic technologies to combat SARS-CoV2: advantages and disadvantages.* Talanta, 2021. **225**: p. 121898.
70. Krähling, V., et al., *Development and characterization of an indirect ELISA to detect SARS-CoV-2 spike protein-specific antibodies.* Journal of immunological methods, 2021. **490**: p. 112958.

71. Reiners, N., et al., *Performance of a SARS CoV-2 antibody ELISA based on simultaneous measurement of antibodies against the viral nucleoprotein and receptor-binding domain.* European Journal of Clinical Microbiology & Infectious Diseases, 2021. **40**(12): p. 2645-2649.
72. Calvo-Lozano, O., et al., *Label-free plasmonic biosensor for rapid, quantitative, and highly sensitive COVID-19 serology: implementation and clinical validation.* Analytical chemistry, 2021. **94**(2): p. 975-984.
73. Mojsoska, B., et al., *Rapid SARS-CoV-2 detection using electrochemical immunosensor.* Sensors, 2021. **21**(2): p. 390.
74. Yakoh, A., et al., *based electrochemical biosensor for diagnosing COVID-19: Detection of SARS-CoV-2 antibodies and antigen.* Biosensors and Bioelectronics, 2021. **176**: p. 112912.
75. Nicholson,L.B.,*The immune system.*Essays in biochemistry,2016.**60**(3)p.275-301
76. Chaplin, D.D., *Overview of the immune response.* Journal of allergy and clinical immunology, 2010. **125**(2): p. S3-S23.
77. Jordan, S., *Innate and adaptive immune responses to SARS-CoV-2 in humans: relevance to acquired immunity and vaccine responses.* Clinical & Experimental Immunology, 2021. **204**(3): p. 310-320.
78. Xia, H., et al., *Evasion of type I interferon by SARS-CoV-2.* Cell reports, 2020. **33**(1): p. 108234.
79. Lei, X., et al., *Activation and evasion of type I interferon responses by SARS-CoV-2.* Nature communications, 2020. **11**(1): p. 3810.
80. Pierce, C.A., et al., *Natural mucosal barriers and COVID-19 in children.* JCI insight, 2021. **6**(9).
81. Bastard, P., et al., *Autoantibodies against type I IFNs in patients with life-threatening COVID-19.* Science, 2020. **370**(6515): p. eabd4585.
82. Mohammed, R.N., et al., *A comprehensive review about immune responses and exhaustion during coronavirus disease (COVID-19).* Cell Communication and Signaling, 2022. **20**(1): p. 1-10.
83. Kim, J.S., et al., *Immunopathogenesis and treatment of cytokine storm in COVID-19.* Theranostics, 2021. **11**(1): p. 316.
84. Mehta, P., et al., *COVID-19: consider cytokine storm syndromes and immunosuppression.* The lancet, 2020. **395**(10229): p. 1033-1034.
85. Kuri-Cervantes, L., et al., *Comprehensive mapping of immune perturbations associated with severe COVID-19.* Science immunology, 2020. **5**(49): p. eabd7114.
86. Radermecker, C., et al., *Neutrophil extracellular traps infiltrate the lung airway, interstitial, and vascular compartments in severe COVID-19.* Journal of Experimental Medicine, 2020. **217**(12).
87. Schurink, B., et al., *Viral presence and immunopathology in patients with lethal COVID-19: a prospective autopsy cohort study.* The Lancet Microbe, 2020. **1**(7): p. e290-e299.
88. Ruan, Q., et al., *Clinical predictors of mortality due to COVID-19 based on an analysis of data of 150 patients from Wuhan, China.* Intensive care medicine, 2020. **46**(5): p. 846-848.

89. Huang, C., et al., *Clinical features of patients infected with 2019 novel coronavirus in Wuhan, China.* The lancet, 2020. **395**(10223): p. 497-506.
90. Grifoni, A., et al., *Targets of T cell responses to SARS-CoV-2 coronavirus in humans with COVID-19 disease and unexposed individuals.* Cell, 2020. **181**(7): p. 1489-1501. e15.
91. Krammer, F., *SARS-CoV-2 vaccines in development.* Nature, 2020. **586**(7830): p. 516-527.
92. Sette, A. and S. Crotty, *Adaptive immunity to SARS-CoV-2 and COVID-19.* Cell, 2021. **184**(4): p. 861-880.
93. Tan, A.T., et al., *Early induction of functional SARS-CoV-2-specific T cells associates with rapid viral clearance and mild disease in COVID-19 patients.* Cell reports, 2021. **34**(6): p. 108728.
94. Greenfield, E.A., *Antibodies.* A laboratory manual, second edition Cold Spring Harbor, NY: Cold Spring Harbor Laboratory.[Google Scholar], 2014.
95. Boyden, S.V., *Natural antibodies and the immune response*. Advances in immunology, 1966. **5**: p. 1-28.
96. Schroeder Jr, H.W. and L. Cavacini, *Structure and function of immunoglobulins.* Journal of allergy and clinical immunology, 2010. **125**(2): p. S41-S52.
97. Natvig, J. and H. Kunkel, *Human immunoglobulins: classes, subclasses, genetic variants, and idiotypes.* Advances in Immunology, 1973. **16**: p. 1-59.
98. Kandari, D. and R. Bhatnagar, *Antibody engineering and its therapeutic applications.* International Reviews of Immunology, 2023. **42**(2): p. 156-183.
99. Long, Q.-X., et al., *Clinical and immunological assessment of asymptomatic SARS-CoV-2 infections.* Nature medicine, 2020. **26**(8): p. 1200-1204.
100. Moderbacher, C.R., et al., *Antigen-specific adaptive immunity to SARS-CoV-2 in acute COVID-19 and associations with age and disease severity.* Cell, 2020. **183**(4): p. 996-1012. e19.
101. Premkumar, L., et al., *The receptor-binding domain of the viral spike protein is an immunodominant and highly specific target of antibodies in SARS-CoV-2 patients.* Science immunology, 2020. **5**(48): p. eabc8413.
102. Le Vu, S., et al., *Prevalence of SARS-CoV-2 antibodies in France: results from nationwide serological surveillance.* Nature communications,2021.**12**(1)p. 3025.
103. Brisotto, G., et al., *IgG antibodies against SARS-CoV-2 decay but persist 4 months after vaccination in a cohort of healthcare workers.* Clinica Chimica Acta, 2021. **523**: p. 476-482.
104. Shen, B., et al., *Clinical evaluation of a rapid colloidal gold immunochromatography assay for SARS-Cov-2 IgM/IgG.* American journal of translational research, 2020. **12**(4): p. 1348.
105. Jin, Y., et al., *Diagnostic value and dynamic variance of serum antibody in coronavirus disease 2019.* International Journal of Infectious Diseases, 2020. **94**: p. 49-52.
106. Zervou, F.N., et al., *SARS-CoV-2 antibodies: IgA correlates with severity of disease in early COVID-19 infection.* Journal of medical virology, 2021. **93**(9): p. 5409-5415.

107. Hennings, V., et al., *The presence of serum anti-SARS-CoV-2 IgA appears to protect primary health care workers from COVID-19.* European Journal of Immunology, 2022. **52**(5): p. 800-809.
108. Yates, J.L., et al., *Serological analysis reveals an imbalanced IgG subclass composition associated with COVID-19 disease severity.* Cell Reports Medicine, 2021. **2**(7): p. 100329.
109. Gaebler, C., et al., *Evolution of antibody immunity to SARS-CoV-2.* Nature, 2021. **591**(7851): p. 639-644.
110. Vanshylla, K., et al., *Kinetics and correlates of the neutralizing antibody response to SARS-CoV-2 infection in humans.* Cell host & microbe, 2021.**29**(6)917-929. e4.
111. Sherina, N., et al., *Persistence of SARS-CoV-2-specific B and T cell responses in convalescent COVID-19 patients 6–8 months after the infection.* Med, 2021. **2**(3): p. 281-295. e4.
112. Xie, J., et al., *Characteristics of patients with coronavirus disease (COVID-19) confirmed using an IgM-IgG antibody test.* Journal of medical virology, 2020. **92**(10): p. 2004-2010.
113. Whitman, J.D., et al., *Evaluation of SARS-CoV-2 serology assays reveals a range of test performance.* Nature biotechnology, 2020. **38**(10): p. 1174-1183.
114. Post, N., et al., *Antibody response to SARS-CoV-2 infection in humans: A systematic review.* PloS one, 2020. **15**(12): p. e0244126.
115. López-Muñoz, A.D., et al., *Cell surface SARS-CoV-2 nucleocapsid protein modulates innate and adaptive immunity.* Science Advances, 2022. **8**(31): p. eabp9770.
116. Radon, K., et al., *Protocol of a population-based prospective COVID-19 cohort study Munich, Germany (KoCo19).* BMC public health, 2020. **20**(1): p. 1-9.
117. Hotop, S.-K., et al., *Peptide microarrays coupled to machine learning reveal individual epitopes from human antibody responses with neutralizing capabilities against SARS-CoV-2.* Emerging microbes & infections, 2022. **11**(1): p. 1037-1048.
118. Hamet, P. and J. Tremblay, *Artificial intelligence in medicine.* Metabolism, 2017. **69**: p. S36-S40.
119. Gerstman, B.B., *Basic biostatistics*. 2014: Jones & Bartlett Learning, LLC.
120. Sullivan, L.M.,*Essentials of biostatistics for public health*. 2022:Jones & Bartlett.
121. Nahm, F.S., *Receiver operating characteristic curve: overview and practical use for clinicians.* Korean journal of anesthesiology, 2022. **75**(1): p. 25-36.
122. Cantor, S.B. and M.W. Kattan, *Determining the area under the ROC curve for a binary diagnostic test.* Medical Decision Making, 2000. **20**(4): p. 468-470.
123. Cohen, I., et al., *Pearson correlation coefficient.* Noise reduction in speech processing, 2009: p. 1-4.
124. Dua, S., et al., *Body mass index relates to blood pressure among adults.* North American journal of medical sciences, 2014. **6**(2): p. 89.
125. Vabalas, A., et al., *Machine learning algorithm validation with a limited sample size.* PloS one, 2019. **14**(11): p. e0224365.
126. Breiman, L., *Classification and regression trees*. 2017: Routledge.
127. Su, Y., et al., *Multiple early factors anticipate post-acute COVID-19 sequelae.* Cell, 2022. **185**(5): p. 881-895. e20.

128. Feng, Z., et al., *Early prediction of disease progression in COVID-19 pneumonia patients with chest CT and clinical characteristics.* Nature communications, 2020. **11**(1): p. 4968.
129. Xiao, L., et al., *Development and validation of a deep learning-based model using computed tomography imaging for predicting disease severity of coronavirus disease 2019.* Frontiers in bioengineering and biotechnology, 2020. **8**: p. 898.
130. Sáez, C., et al., *Potential limitations in COVID-19 machine learning due to data source variability: A case study in the nCov2019 dataset.* Journal of the American Medical Informatics Association, 2021. **28**(2): p. 360-364.
131. Herold, T., et al., *Elevated levels of IL-6 and CRP predict the need for mechanical ventilation in COVID-19.* Journal of Allergy and Clinical Immunology, 2020. **146**(1): p. 128-136. e4.
132. Wendt, R., et al., *A urinary peptidomic profile predicts outcome in SARS-CoV-2-infected patients.* EClinicalMedicine, 2021. **36**: p. 100883.
133. Ansone, L., et al., *Amino acid metabolism is significantly altered at the time of admission in hospital for severe COVID-19 patients: findings from longitudinal targeted metabolomics analysis.* Microbiology spectrum, 2021. **9**(3): p.0338-21.
134. Rosado, J., et al., *Multiplex assays for the identification of serological signatures of SARS-CoV-2 infection: an antibody-based diagnostic and machine learning study.* The Lancet Microbe, 2021. **2**(2): p. e60-e69.
135. Brochot, E., et al., *A multiplex serological assay for the characterization of IgG immune response to SARS-CoV-2.* Plos one, 2022. **17**(1): p. e0262311.
136. Klüpfel, J., et al., *Automated, flow-based chemiluminescence microarray immunoassay for the rapid multiplex detection of IgG antibodies to SARS-CoV-2 in human serum and plasma (CoVRapid CL-MIA).* Analytical and Bioanalytical Chemistry, 2021. **413**(22): p. 5619-5632.
137. De Assis, R.R., et al., *Analysis of SARS-CoV-2 antibodies in COVID-19 convalescent blood using a coronavirus antigen microarray.* Nature communications, 2021. **12**(1): p. 6.
138. Ruano-Gallego, D., et al., *A multiplex antigen microarray for simultaneous IgG and IgM detection against SARS-CoV-2 reveals higher seroprevalence than reported.* Microbial Biotechnology, 2021. **14**(3): p. 1228-1236.
139. Wang, H., et al., *SARS-CoV-2 proteome microarray for mapping COVID-19 antibody interactions at amino acid resolution.* ACS Central Science, 2020. **6**(12): p. 2238-2249.
140. Jiang, H.-w., et al., *SARS-CoV-2 proteome microarray for global profiling of COVID-19 specific IgG and IgM responses.* Nature communications, 2020. **11**(1): p. 3581.
141. Li, Y., et al., *Linear epitopes of SARS-CoV-2 spike protein elicit neutralizing antibodies in COVID-19 patients.* Cellular & molecular immunology, 2020. **17**(10): p. 1095-1097.
142. Alpdagtas, S., et al., *Evaluation of current diagnostic methods for COVID-19.* APL bioengineering, 2020. **4**(4): p. 041506.

6. IMMUNOLOGICAL MULTI-EPITOPE SARS-COV-2 MICROARRAY: DEVELOPMENT, CHARACTERIZATION AND CLINICAL ASSESSMENT

SUMMARY

Expecting to assess the immunological response mediated by IgG's and IgM's of COVID-19 patients with different symptomatology, throughout this chapter the development of a high-throughput serological microarray chip based on SARS-CoV-2 peptide epitopes and proteins (*Immuno*-µSARS-2 V1.0) is reported. Initially, a rational design and selection of a discreet set of immunogenic peptides followed by their synthesis and implementation in a multiplexed microarray platform is discussed. To then, introduce the methodological and experimental platform characterization, reaching to the final application in clinical samples. The work, carried out during the initial phases of the COVID-19 pandemic, was performed in collaboration with Luciano Sappia, PhD from the Nb4D group and the Multivalent Systems for Nanomedicine (MS4N) group leaded by Miriam Royo, PhD.

6.1. INTRODUCTION

6.1.1. PEPTIDES IN THE BIOMEDICAL FIELD

Peptides are defined as short chains of amino acids generally ranging between two to 50 units, linked by peptide bonds. In accordance to the IUPAC definition, a differentiation between oligopeptides constituted by 10-20 amino acids from polypeptides including more than 20 residues is established [1]. These biomolecules can be naturally produced by living organisms, playing a wide variety of important biological roles such as enzyme catalysis, hormone regulation and cell signaling. Peptides can also be artificially synthesized, either for research purposes or for use in medical applications. One of the main features of peptides is found on the ability to interact with other molecules in highly specific ways, making them valuable in a number of different fields including medicine, biotechnology and materials science. For example, peptides can be designed to target specific receptors on the surface of cells to then be applied in drug development [2]. Peptides can also be used as bioreceptors in

diagnostic, helping during the identification of specific biomarkers that are associated with certain diseases [2].

Based on the previous definition, SARS-CoV-2 peptides consists in artificially synthesized amino acid chains derived from the viral structure. Some of the most remarkable applications including SARS-CoV-2 peptides, are focused on the use of these biomolecules as therapeutic elements mimicking ACE-2 binding domains to interact with S protein and minimize the rate of infection [3]. On the other hand, viral derived peptides have been used as vaccine candidates based on immunogenic sequences capable to elicit comparable immune responses avoiding the need of complex protein synthesis and characterization procedures [4]. Moreover, different strategies have been developed to determine immunodominant peptide sequences based on IgG or IgM responses after infection as potential serological indicators [5].

6.1.1.1. Peptides as emerging serological indicators in COVID-19

By the time this work started, back on May 2020, the first serological tests started to appear in the market. No other technology aiming at getting additional insights on the role of the immunological system in the progress of the disease did exist. Since then, a great number of companies have placed lateral-flow immunoassay test into the market. Most of the serological platforms are targeting the detection of anti-SARS-CoV-2 antibodies by immobilizing structural proteins like S or N on particular supports, assuming certain limitations associated to the high costs of protein production and relative low stability. On the other hand, a reduced number of examples have been described that tackle development of multiplexed peptide-based assays or arrays to investigate immunological profiles as result of SARS-CoV-2 infection. However, the few reported are addressed to analyze the immunological response towards the wide proteome after printing viral peptide sequences on solid supports. Subsequently, incubation of such chips with patient's serum samples allow defining common immunodominant regions across 3.000 or even 15.000 spots depending on the amount of peptides and replicates evaluated [6]. The main challenges towards the clinical implementation of these systems are found on the manufacturing techniques available, also due to the significant costs and relatively low

processing capacity, in addition to the extensive amount of data generated that need to undergo through complex analysis procedures.

Conventional serological tools are primarily focused on the rapid determination of immunoglobulins against viral components without considering further evaluation of patients' immune state. In this regard, a clear gap between both methodologies was underlined contemplating the need of high-throughput, multiplexed and cost-effective serological platforms with predictive potential over clinical progression or immunological state to facilitate the decision-making process at healthcare level. In the following table 6.1, some of the most relevant serological peptide-based microarrays extracted from the literature are compared based on the type of immunoglobulin detected, number of samples used in the published study, number of peptides constituting the array as well as matrix of analysis.

Table 6.1 Multiplexed peptide-based arrays for serological determinations for SARS-CoV-2

N peptides	N samples	Target	Matrix	Assay time	Samples/run	Ref
2592	66	IgG, IgA, IgM	Serum	O.N inc.	2	[7]
996 (+7 proteins)	10	IgM, IgG	Serum	1.5 h	1	[8]
5513	36	IgG	Serum	5.5 h	1	[6]
15	2,434	IgG	Serum	5.5 h	14 or 7	[9]
981	132	IgG and IgM	Plasma	O.N. inc.	12	[10]

O.N. inc (Overnight Incubation)

Considering the wide range of applications deriving from the use of these platforms, some common features are that all of them target IgG's and only three include IgM's determination. Additionally, the number of samples analyzed is mostly found below 100 and this may be related to the number of peptides evaluated and the platform processing capacity considering complex signal interpretation as more epitopes are included. Only one example evidenced high-throughput performance after the analysis of more than 2400 samples but against of a reduced set of peptides (<15), offering alternative uses apart from proteomic interpretations. In this regard and according to the literature, a potential necessity of novel technological solutions including high-throughput techniques for serological determinations is identified.

6.1.1.2. Commercially available SARS-CoV-2 serological arrays

From an industrial perspective, several companies were dedicated to develop serological profiling arrays incorporating peptides mainly for research purposes like PEPperCHIP® SARS-CoV-2 Proteome Microarray [11] and Nimble Therapeutics Inc. (WI, USA). Moreover, the COVID-19 test directory of the accelerator platform FIND (https://www.finddx.org/) contains more than 400 serological tests commercially available worldwide in different configurations. However, if the search is restricted to microarray platforms for antibody determination, is interesting to see that only five devices are accessible, mainly using viral proteins as antigenic structures. In the following table, commercial serodiagnostic platforms exploiting microarray configurations are compared.

Table 6.*2* SARS-CoV-2 serological microarray platforms commercially available

Manufacturer	Device name	Epitopes	Target	Samples/run	Regulatory status	Matrix
Intavis Peptide Serv.	Covid19-hullB CelluSpot Array	384 S peptides	IgG	2	None	Serum; Plasma
Nirmidas Biotech, Inc.	pGOLD COVID-19	S1 and RBD proteins	IgA; IgG;IgM	16	None	Serum; Plasma
Quotient Suisse SA	MosaiQ COVID-19	132 S1 peptides	IgG; IgM	1 per chip	CE-IVD	Serum; Plasma
Sengenics Corporation	ImmuSAFE Resp. Virus Array	9 domains of N and S proteins	IgG, IgA,IgM	1	None	Serum; Plasma
Tetracore Inc.	FlexImmArray SARS-CoV-2 IgG	3 S and N proteins	IgG	96 well plate bead assay	None	Serum; Plasma

[a] Data collected in June, 2023

Surprisingly, only one device presents certification for *in vitro* diagnostic purposes while the regulatory status of the other platforms is not defined, which means that their use is restricted to research purposes. Moreover, in most of the cases the processing capacity of these systems is limited to 1 or 2 samples per run with the exception of pGOLD array that allows 16 samples in parallel. The main competitive features are found on the simultaneous determination of different isotypes like IgG, IgM or IgA's, reaching shorter incubation periods as well as higher sensibility or specificity and even the capacity to differentiate natural immunity from artificially induced response. Nevertheless, other innovative approaches following similar objectives as those of this PhD thesis,

aim to stratify patient's severity according to differences based on IgG levels mostly with research purposes. Nowadays, it is widely accepted that a faster and stronger immune response against viral proteins like S and N, is found in patients with severe COVID-19 symptomatology [12-15], however the use of peptides to predict such condition was not extensively explored yet [16].

6.2. RESULTS AND DISCUSSION

6.2.1. EXPERIMENTAL PROPOSAL

The proposed platform (*Immuno*-µSARS2 V1.0) started to be developed during the initial period of the pandemic (May, 2020) in an attempt to meet the demand of diagnostic tools, but also the possibility to understand better the disease considering the wide variety of symptomatology that the infection by SARS-CoV-2 was presenting. By that time, the viral structure was recently resolved lacking of consolidated reports or data assessing immunological response during COVID-19 disease. Therefore, the workflow behind the initial system characterization was directed to evaluate the following aspects that are going to be discussed in detail along the ongoing section:

1. **Rational peptide design:** the selection and synthesis of ten potentially immunogenic sequences from S and N proteins to be implemented in the epitope array using *in silico* and experimental results from the literature available.
2. **Biofunctionalization of the glass slides:** definition of the most suitable immobilization conditions for each component of the matrix, considering slide derivatization and bioconjugates preparation.
3. **Development and analytical characterization of the platform:** assessment of platform specificity and sensitivity as well as performance in serum samples, minimizing non-specific adsorptions and defining standard assay conditions.
4. **Measurement of clinical samples**: system evaluation in clinical human serum samples from convalescent patients. The simultaneous determination of specific IgG profiles against viral epitopes was determined.
5. **Biostatistical analysis**: implementation of univariate statistical approaches across the data set measured, to define the individual classification capacity of selected epitopes towards patient's distribution according to RT-PCR methods as reference.

6.2.2. RATIONAL DESIGN OF IMMUNOGENIC PEPTIDES

The rational selection of a discreet panel of immunogenic peptide sequences was decisive towards the successful determination of serological responses with clinical predictive value in the final platform. The possibility to incorporate peptides instead of full-length proteins in the microarray, could avoid potential cross-reactivity from patients previously exposed to coronavirus infection, assuming that peptides antigenicity can be modulated towards specific regions [17], in addition to the automated, faster and cheaper production in contrast with recombinant proteins. On the other side, the use of mathematical and predictive models to select potential antigenic regions in biological systems is sometimes limited by the level of reproducibility achieved on *in vitro* studies. Consequently, the rational design of peptides sequences aimed to overcome such limitation combining reports in the literature based on *in silico* and experimental applications integrating data analysis with computational tools.

For this purpose, an extensive literature review was conducted to identify potential antigenic sites, glycosylation patterns and immune accessible regions of the main SARS-CoV-2 structural proteins, S and N. Such work was done using various databases including PubMed, NCBI, and UniProt. The literature also served to determine the preferred length and characteristics of peptide sequences used for the serological microarray. The selected sequences were analyzed using BLAST software, to ensure SARS-CoV-2 specificity and assessing potential similarity to other proteins.

Based on the results obtained after bioinformatic analysis and comparisons from reports available a first set of 10 peptide sequences were selected using the following criteria that was also applied for the new peptide incorporation described in the following chapter (from peptide **P11** to **P22**):

a. Antigenic regions determination: peptide sequences were selected from predicted antigenic regions based on literature reports evidencing common immunodominant sections and also due to the analysis of the viral proteome indicating seroprevalence in clinical samples.

b. Accessibility evaluation: peptides located in regions of the proteins S and N accessible to the recognition by the immune system. In this regard, the protein structure and three-dimensional configuration were considered as decisive

factors towards antibody mediated recognition, favoring those regions predominantly exposed.

c. Glycosylation sites: peptide sequences were designed to avoid potential glycosylation sites, aiming to prevent interferences during the determinations. Contradictory statements have been reported mainly across S protein glycosylation, either playing a protective role or contributing to immune evasion [18], and by the time that this project started the pattern of glycosylation of the virus was not fully consolidated.

d. Length and chemical coupling: the peptide sequences were designed to be 12-15 mer and to have a balanced distribution of hydrophobic and hydrophilic residues. Furthermore, a cysteine (Cys) amino acid was included in the N-terminal or in some cases over the C-terminal domain to be used as a coupling moiety to the BSA.

e.The specificity criteria: aimed to define peptides that were selective for SARS-CoV-2 and not for SARS-CoV and MERS, and for this purpose, reports comparing sequence alignment were used as reference during the epitope selection process [19]. Furthermore, the microarray chip included N and S1 recombinant whole proteins from SARS-CoV and SARS-CoV-2 expecting to evidence distinct responses. However, the first limitation emerged from the high degree of sequence homology across S1 subunits from SARS and SARS-2 reporting around a 65 % [19] while for N protein the similarity reached up to 90.3 % [20]. Nevertheless, due to the high prevalence of infection caused by the novel coronavirus this differentiation was not assumed as a limiting factor.

Another relevant area to define potential antigenic epitopes was the RBD region responsible for the selective interaction between S and ACE2 receptor in the host cell. As a result, a recombinant RBD protein was included in the microarray as well as peptides belonging to this region with the idea to evidence the presence of antibodies with potential neutralizing activity [21].

For the initial peptide selection based on literature reports, a distinction between experimental and *in silico* studies was considered, assuming the advantages and limitations that each approach could provide.

From *in silico* analysis, the work of Zheng et al [22] compared the S protein sequence of SARS-CoV-2, SARS-CoV and MERS-CoV looking for conserved and non-conserved domains to establish an epitope score based on surface epitope antigenicity and accessibility. In a different work, bioinformatic tools were utilized to identify unique B-cell epitopes over NSP1, NSP3 or S glycoprotein and most of the target sequences were highly conserved between SARS-CoV-2 and SARS-CoV [23]. On a different approach, common immunogenic regions were predicted with two *in silico* strategies targeting B and T cell epitopes. Five sequences with high antigenic scores were selected (residues 274–306, 510–586, 587–628, 784–803, and 870–893) three of them derived from S1 sequence [24]. The emerging data reporting common immunogenic domains was taken into consideration by Kumar and colleagues [25] to estimate the sequence variation and antigenic divergence of S protein in SARS-CoV-2 and its predecessor, finding not significant differences.

From experimental reports, a peptide-based ELISA targeting S, N, M and E protein regions revealed four immunogenic sequences derived from S and N that were properly validated with 79 COVID-19 samples [16]. Three of these epitopes were strongly correlated with clinical severity evidencing strong prognostic value. Two high density microarrays, one directed to N protein sequence study [26] and the other assessing the viral proteome [6], suggested the epitope 155-171 located in N protein as promising candidate.

In the study by *Wang et al*. [8] already discussed, IgM and IgG binding against almost 1.000 peptides was tested in 10 COVID-19 patients and 10 control patients, although more samples would have preferred the number of peptides evaluated offers a wide overview of possible antigenic domains. The most significant sequences deriving from S protein were between residues 806–820 (LPDPSKPSKRSFIED) and 456–460 (FRKSN) and form N protein residues 166–170 (TLPKG) being the last ones also reported through *in silico* studies by Grifoni [24]. Nevertheless, these results should be treated with great care since they are based on a very small number of infected patients, and as already mentioned, the casuistry of this disease is very large.

Following with experimental data, Li and colleagues developed a microarray of 211 S peptides aimed at distinguishing neutralizing antibodies using sera from 55 convalescent COVID-19 patients and 18 healthy donors as control without

previous viral exposure [27]. In this work, the authors identify the so called “hot” epitope regions across S protein including the CTD domain (553-654 region), a portion of RBD between aa 487-488 and the immunodominant area of the S2 domain defined by the residues 764 to 829 and 1148 to 1159. They conclude that additional neutralizing activity can be found in antibodies that are not targeting the RBD zone, but could be involved in other mechanisms interfering with S and ACE2 receptor interaction. The final peptide selection is summarized in the next Table 6.3 including the references reporting each specific sequence with *in silico* and experimental approaches.

Spike

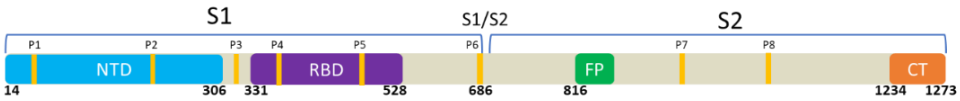

Nucleocapsid

Figure 6.1 Schematic representation of S and N sequences indicating the position of the rationally selected peptides from P1 to P8 in the case of S and peptides P9 and P10 deriving from the CTD over N protein. Adapted from [28 , 29].

As result of all these studies and taken into consideration the selection criteria mentioned above, eight peptide sequences were selected for the S structure (see Figure 6.1 top, fragments in yellow). and only two peptides for the N protein (see Figure 6.1, bottom, fragments in purple). On the selection of this initial panel, it was also expected that for S, there would be at least one peptide from each section of the protein. The table 6.3 shows the amino acid sequences of the peptide fragments selected, indicating the regions to which they belong and scientific evidence reporting those sequences.

Table 6.3 Final selection of 10 target peptide sequences rationally designed from S and N proteins.

ID	Target peptide sequence	SPIKE		Synthesized epitope	Ref
		Subunit	Region		
P1	L_{18}TTRTQLPPAYTNS	S1	NPD	C-LTTRTQLPPAYTNS	[8, 24]
P2	L_{110}DSKTQ	S1	NPD	C-TTLDSKTQSLL	[24]
P3	Q_{314}TSNFRVQPT	S1	NPD-RBD	C-QTSNFRVQPT	[24]
P4	A_{352}WNRKR	S1	RBD	C-ASVYAWNRKRISN	[22, 24]
P5	S_{469}TEIYQAGSTPC	S1	RBD	TEIYQAGSTP-C	[24, 25]
P6	Y_{674}QTQTNSPRRAR	S1	Furin site	C-YQTQTNSPRRAR	[22, 30]
P7	L_{806}PDPSKPSKRSFIED	S2	-	C-LPDPSKPSKRSFIED	[8, 23, 25, 30]
P8	A_{944}LGKLQDVVNQNAQALNTLV	S2	Porfirin site	C-LTTRTQLPPAYTNS	[23, 24]
NUCLEOCAPSID					
P9	K_{370}DKKKKADETQAL	NC	-	C- KDKKKKADETQAL	[8, 31]
P10	T_{393}LLPAADLDDFSK	NC	-	C- TLLPAADLDDFSK	[32]

According to this table, a differentiation between the target peptide sequence and the epitope synthesized is considered in separate columns. Referring as the target sequence to the original amino-acid chain from the virus, and the sequence finally synthesized that was truly used in this microarray, assuming experimental modifications as consequence of the peptide length required or even the cysteine (-Cys) residue incorporation.

6.2.3. SYNTHESIS OF THE PEPTIDES EPITOPES

The synthesis of the peptide epitopes was carried out by the Multivalent Systems for Nanomedicine (MS4N) group headed by Miriam Royo, PhD using a fluorenymethoxycarbonyl (Fmoc)/*tert*-butyl (*t*Bu) solid-phase peptide synthesis strategy on a Fmoc-Rink Amide CM (0.50 mmol/g) as polymeric support. All the peptides incorporated an additional Cys residue at the N- or C- terminal region (see Table 6.3) aimed to be used for coupling of the peptides to BSA (see below) using an orthogonal chemistry that do not interfere with the functional groups of other amino acid residues. The decision of whether the Cys residue had to be on one or another side of the peptide was taken based on the presence of this residue in the original sequence for some examples (like **P5**), but mostly attempting to favor the exposure of the peptide domain with higher antigenicity. Assuming that the amino acids closer to the Cys will not be as accessible as the ones in the other side of the peptide for antibody recognition.

All the synthesized peptides were acetylated at the N-terminal end of the peptide. Finally, the linear peptidyl resins were treated with a mixture of trifluoroacetic acid-triisopropylsilane-water (TFA:TIS:H_2O, 94:3:3, v/v/v) to cleave the peptide from the resin. Afterwards precipitation was achieved by adding TFA solution onto cold diethylether (Et_2O), discharging the supernatant and then lyophilizing the product. Peptides were purified by semi-preparative high-performance liquid chromatography (HPLC).

6.2.4. ESTABLISHMENT OF MULTI-EPITOPE MICROARRAY COMPONENTS

For the manufacturing of the peptide epitope microarray it was decided to use BSA bioconjugates instead of just the peptides. The reasons behind were that the BSA bioconjugates would allow exposing much better the peptides to the antibodies in the serum samples, with a more appropriate spacing between them which would reduce the chances of steric hindrance for the proximity of the antibodies to the peptides. Moreover, the BSA bioconjugates would provide a more biocompatible surface preventing at the same time potential non-specific interactions of the serum samples with the biofunctionalized surface. General microarray procedures involving peptide conjugation to BSA have been described in similar approaches [9, 27] and the key advantages include:

Increasing solubility: Considering that some peptides are hydrophobic and evidence difficulty to be dissolved in aqueous solutions. Their conjugation to carrier proteins like BSA can increase the solubility and stability in solution.

Improve specificity: Conjugate peptides to BSA can help to reduce non-specific binding and improve the specificity of the assay. This is because the carrier protein can block non-specific binding sites on the array surface, reducing background noise and enhancing specific response.

Facilitate immobilization: Peptides coupled to carrier proteins facilitate the immobilization process by providing a larger surface area for the attachment to the solid support and also defining homogenous surface chemistry conditions.

Higher accessibly: The 3D conformational distribution of peptides over BSA offers wider accessibility to the biomolecules interacting with the sequences favoring

the binding event, in contrast with conventional immobilization over planar and non-interspaced surfaces.

6.2.4.1. Peptide bioconjugation to BSA

The bioconjugation of the peptides (**P1** to **P10**), to BSA was performed making use of N-β-maleimidopropyl-oxysuccinimide ester (BMPS, see Figure 6.2) as heterobifunctional crosslinker interacting with the amino groups present in the BSA over the lysine residues available with the counterpart reacting with thiol groups (SH-) from Cys residues of the corresponding peptides. A simplified view of conjugation protocol is represented in the following scheme describing the order of reagents addition and optimized conditions utilized for the conjugation of all the peptides included in this work.

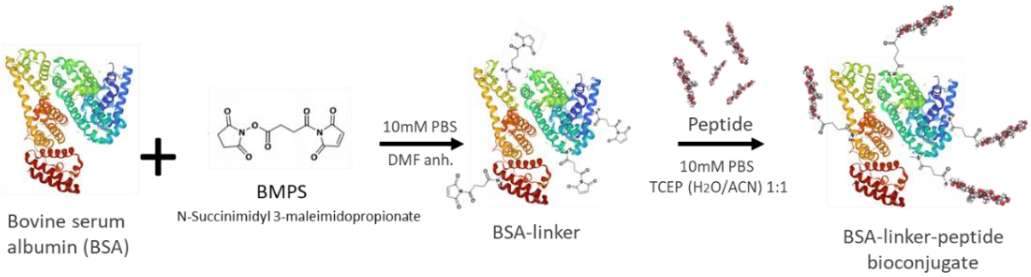

Figure 6.2 General scheme of the peptide bioconjugation reaction. On a first instance BSA reacts with BMPS crosslinker through the NHS (N-hydroxi succinimide) active ester to introduce maleimido groups into the BSA. After a purification step, the Cys-peptides react with the maleimido group on a specific manner without inteference from other chemical groups present on the aminoacid residues.

As described, the BSA molecule was resuspended in 10 mM PBS and incubated with the corresponding BMPS linker dissolved in anhydrous DMF. After reaction, chromatographic purification of the BSA-linker product was necessary to remove the excess of BMPS. The peptide solution was prepared in 10 mM PBS adding TCEP (tris(2-carboxyethyl) phosphine) as reducing agent to ensure absence of disulfide bonds resulting from the oxidation of the -SH groups of the Cys residues. After approximately 10 minutes, the peptide solution was added to the BSA-linker mixture for overnight incubation. The following day, purification by dialysis was carried out over each product and the subsequent characterization of the

bioconjugates was performed in MALDI-TOF-MS to estimate the average peptide density per BSA molecule obtained. Controlled bioconjugation conditions allowed the generation of peptide-BSA conjugates with an average density of 5 to 7 peptides per BSA molecule to perform adequate comparisons once implemented under the microarray configuration.

As an example, the Figure 6.3 shows a representation of a standard MALDI-TOF-MS spectrum, recording the molecular weight (MW) of the BSA through the different bioconjugation steps. In this regard, the initial BSA peak should be found at 66.5 KDa followed by the BMPS linker (MW: 266.21) addition, which loses the NHS moiety during coupling reaction with BSA (linker MW: 151.12). The amount of linker residues that have been introduced was estimated in 17 according to the displacement of the peak for BSA-BMPS conjugate. Finally, the covalent attachment to the peptide leads to a MW of 81.2 KDa, which corresponds to the incorporation of almost 7 peptides per BSA molecule. In the 6.4, the results from the characterization of the peptide-BSA bioconjugates using this approach is summarized.

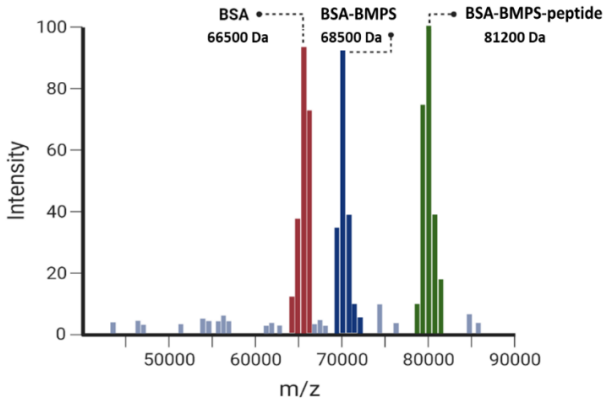

Figure 6.3 Schematic representation of a standard MALDI-TOF-MS spectra for peptide bioconjugates characterization. Commercial BSA (in red) was utilized as reference. Then, a purified aliquot of BSA-BMPS crosslinker in blue, used to define the number of binding sites available for peptides covalent attachment. Finally, the MW of the product of reaction, BSA-BMPS-Peptide in green was used to determine an average peptide density as part of the analytical characterization.

Table 6.4. Average peptide density of all the bioconjugates generated, determined by MALDI-TOF-MS

Peptide	Linker density (δ)	Peptide density (δ)
P1	14.8	5
P2	14.8	5
P3	14.8	5
P4	16.0	6
P5	16.0	6
P6	16.0	5
P7	17.7	5
P8	17.7	6
P9	17.7	4
P10	17.7	8

6.2.4.2. Establishment of experimental protocol

The same derivatization protocol applied in the section 3.5.6 was employed for this purpose. To covalently attach BSA-peptide conjugates to the glass slides. Probe immobilization consisted on protein and peptide-conjugates deposition utilizing a piezo-dispense arrayer, under standardized temperature and humidity conditions of 25°C and 65 %, respectively. The array design was adjusted to fit in the ArrayIt® slide gasket dimensions implemented for sample analysis (see Figure 6.4). As described previously (see Chapter 3), this holder allows the generation of 24 independent wells (3 columns and 8 rows) in a single glass slide. Respective sub arrays were spotted in each support with a variable number of spots based on the experiment propose

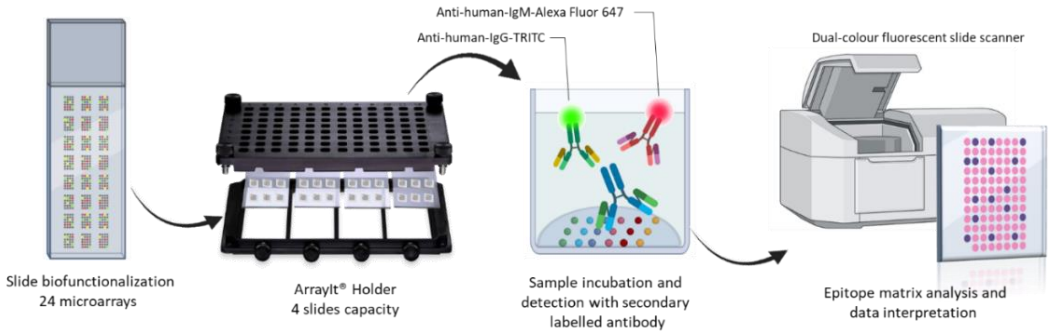

Figure 6.4 Immunoarray workflow: Slides were printed generating 24 independent microarrays of 6x9, then fitted in the 4-slide capacity slide holder. Sample incubation for 60 min followed by detection with two secondary labelled antibodies with distinct fluorophores to differentiate IgG's from IgM's took place. Afterwards, the signal was quantified in a dual colour fluorescent scanner and the data from each spot was processed for further analysis.

The principle of detection behind the proposed high-throughput multi-epitope microarray chip is represented in the previous scheme. Basically, consisting on the biofunctionalization of glass slides in 24 independent microarray chips. Then, the slides were placed in the holder, that is available in two formats, the first with 4-slide capacity generating a 96-well plate like configuration and the other for a single slide utilized to perform initial characterization experiments with 24 wells. In both cases, the serum samples were added to the wells defined by the gaskets. After an incubation period of 60 min in which the corresponding antibodies bind to the selected epitopes, a washing step was performed to allow the detection with a mixture of fluorescently labeled secondary antibodies (anti-human-IgG-TRITC and anti-human IgM-Alexa Fluor 647) for 30 min. The differentiation between IgG's and IgM's was possible through the use of distinct fluorophores in a dual laser microarray scanner. In this case, the emission wavelength of TRITC occurs at 572 nm while Alexa Fluor 647 at 668 nm allowing simultaneous signal acquisition. With a total assay time of almost 90 minutes and considering the high-throughput capacity of the system, rapid serological determinations are obtained compared to other microarrays exposed requiring overnight incubation [7, 10]. Although it was not experimentally corroborated in this work, the possibility to shorten incubation times is also contemplated depending on the application proposed and performing the corresponding characterizations studies.

6.2.4.3. In-house positive control serological samples

The lack of reference materials and the difficulties to get access to clinical samples during the initial pandemic stage prompted us to prepare in-house positive control ("CTR+As"). Availability of such positive samples was mandatory in order to develop and validate the diagnostic assay. Hence, positive antisera were produced in our facilities immunizing rabbits with S and N proteins (see Figure 6.5) respectively and monitoring the immunological progression of the antibody titers (IgG's/IgM's).

Three female New Zeeland rabbits identified as 409, 410, 411 were immunized with S glycoprotein and other three rabbits with N protein assigned 412, 413 and 414 respectively to obtain polyclonal antibodies against the corresponding proteins. The sera obtained during the immunization period were utilized as

CTR+As materials supposedly representative of the different stages of the evolution of the immune progression. The sera allowed us to evaluate the response of the peptide epitope microarray under development, which included also viral proteins like the S1 from SARS-CoV-2 and SARS-CoV, the RBD and N, last both from SARS-CoV-2, in addition to the first panel of peptides **P1** to **P10** (8 sequences from S and 2 from N). A considerable limitation of using rabbit antisera instead of human antisera for the microarray characterization is assumed, based on the presence of only one IgG isotype in rabbits, compared to the four typical IgG's isotypes (IgG1, IgG2, IgG3 and IgG4) present in humans. Additionally, rabbits present 10 functionally active IgA isotypes while only 2 are found in humans [33]. These differences may influence the response detected with the system once implemented in clinical samples, but due to the lack of human-derived reference materials this was the most adequate alternative to proceed.

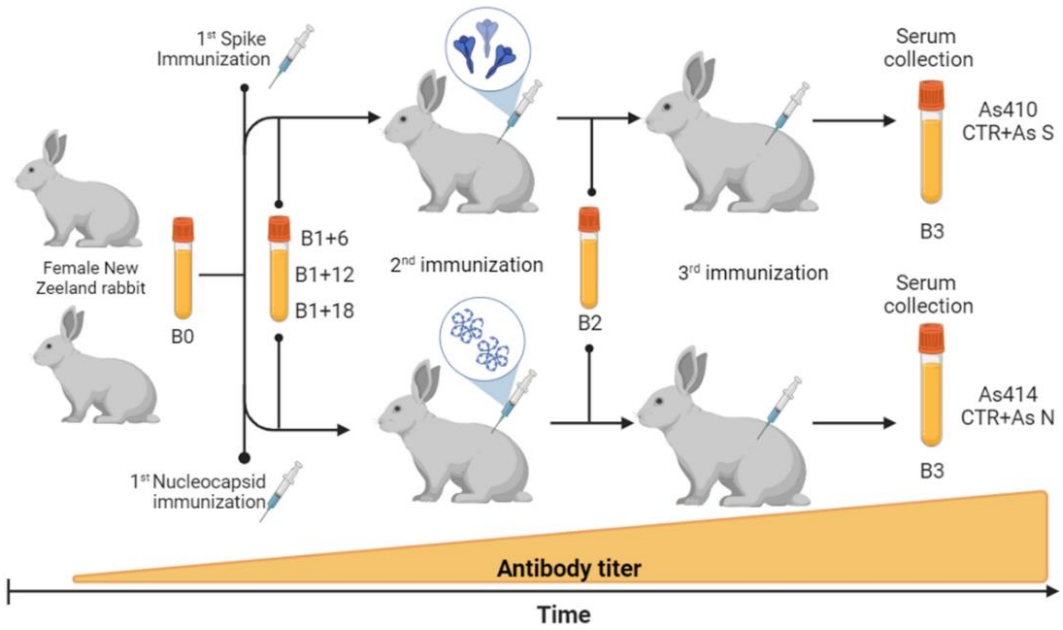

Figure 6.5 Scheme of rabbit antisera (As) production after several immunizations. Three female New Zeeland rabbits were immunized with recombinant S protein and other three with N protein. Pre-immune bloods were collected as negative control (B0) before the first immunization. After the first intradermal injections with the immunogen, 6, 12 and 18 days later B1+6, +12 and +18 were obtained. Two additional immunizations were carried out on each animal, one after thirty days and the other after sixty from the first challenge. In each case, ten days post immunization, B2 and B3 were obtained and the B3 As410 (S) with B3 As414 (N) were selected as positive control materials (CTR+As S and CTR+As N) for the microarray characterization.

Expecting to characterize the rabbit's immune response mediated by IgG's and IgM's after the first immunization, different partial blood samples were obtained from each of the six animals. A sampling interval window of 6 days was considered starting with B0 (pre-immune) as the negative control just before the first immunization, followed by B1+6, after 6 days post the first challenge, B1+12 and B1+18 as the following days. As an initial strategy for the evaluation of the antibody profile progression during this first stage, ELISA technique was utilized by coating the 96 well plates with S1-SARS2, RBD and NC-SARS2 proteins at 0.5 $\mu g\ mL^{-1}$. The antisera collected was diluted at 1/2000 in PBST and then incubated for one hour in triplicate wells. Partial blood from rabbits immunized with the S protein were assessed for the recognition of the S1 and RBD protein, while the other three against N protein. Figure 6.6 (Left) shows, a progressive evolution on the IgG response on each animal, apparently starting to reach a higher signal with the partial bloods collected after 18 days (B1+18), except for S1 protein which the plateau seems to be reached after 12 days for the three rabbits. Interestingly, anti RBD antibodies rise steeply from 12 to 18 days for two (409 and 411) of the three rabbits, pointing at the possibility that neutralizing antibodies recognizing this region need longer maturation of the T-cells to appear. The anti-N response reached strong intensity values on day 18 after the initial immunization for the three animals assessed suggesting that robust N immunity may be trigged after S1 response, at least in rabbits immunized with recombinant proteins. Nevertheless, this fact should be proven in patients infected by the virus in order to determine if such behavior was confirmed.

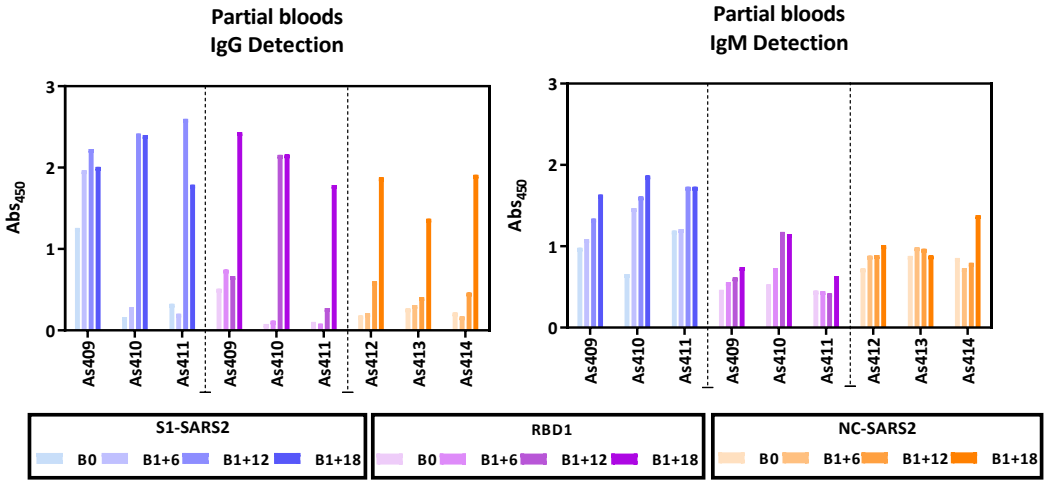

Figure 6.6. Partial blood immune profile progression estimation by ELISA. The three As from rabbits immunized with S (As409, As410; As411) and N (As412, As413, As414) proteins were evaluated through ELISA against S1-SARS2, RBD and NC-SARS2 recombinant proteins. IgG's and IgM's levels were determined for partial bloods consisting on pre-immune (B0) samples and different extractions after the first immunization, (B1+6, +12, +18, the numbers correspond to days post challenge).

As expected, and as it is shown in Figure 6.6 (right), IgM levels were quite high already after 6 days of immunization and it increased slowly on the sera from days 12 and 18. This behavior, which was consistent for the three proteins assessed, can be explained as a result of the natural development of IgM's which occurs earlier and faster compared to IgG isotypes on the initial phases of an immunization (or infection). Additionally, the maximum signal (Abs 450nm) reached for the IgG's was higher than for IgM's absorbance, which is in agreement with the relative abundance of each isotype in serum [34]. At this stage, the evaluation of the rabbit's serological profile against the three proteins through ELISA was done only using B0, B1+6, +12 and +18 while the immunization process was continuing, just as an initial approach to characterize each animal immune behavior due to the lack of B2 and B3 bloods.

Later on, the selection of the most adequate antisera to be used as reference was based on the results obtained once the epitopes were implemented in microarray (data not showed) indicating that maturation of IgG response was reached at B3. Therefore, the B3 antisera from rabbit 410 (referred as As410), was selected as CTR+As S (positive control) of "S" serological response while B3

antisera from rabbit 414 (As414) was selected as CTR+As "N" due to the highest IgG titers recorded. On the other hand, IgM's levels were more abundant at B1+18 samples, but due to practical reasons we decided to use only one control for S and another for N employing the B3, although the best approach would have been to have independent controls for each isotype. In this aspect, is worth mentioning that the same experiments were carried out also with the antisera from the other rabbits. Due to the extension required, these results are not displayed in the chapter but all of them showed similar immunological behavior, however, the candidates selected provided the most robust response with high level of antibodies against the epitopes selected.

6.2.5. DEVELOPMENT OF THE *IMMUNO*-µSARS2 V 1.0 MICROARRAY CHIP

6.2.5.1. Establishment of proteins and peptide-BSA conjugates concentration on the microarray

Aiming to define the optimum protein concentrations on the microarray chip, solutions of S1-SARS2, RBD_1, RBD_2 (two recombinant RBD's from different suppliers, see experimental section for details) and NC-SARS2 proteins at three different concentrations (100, 50 and 25 µg mL^{-1}) were printed in triplicate spots. Then B0 (pre-immune) diluted 1/6000 in PBST buffer and B3 samples from As410 (CTR+As S) at different increasing antisera dilutions (1/1600, 1/3200, 1/6400) were used to monitor the IgG responses in this case.

As the Figure 6.7 indicates, no signal was observed for the B0 diluted 1/1600 samples, due to the lack preexistent immunity used as negative control. From the three graphs is possible to evidence an increasing response when higher protein concentrations are immobilized that at the same time are correlated with the antisera dilution used. In the case of 100 µg mL^{-1} printed proteins, this effect is less evident using different dilutions of CTR+As S antisera, probably attributed to a saturation of the surface. Particularly, for the dilution 1/1600 at that protein concentration, the signal detected in RBD_1 and RBD_2 was comparable to the complete S1-SARS2 protein. As the RBD belongs to a discreet region of S1 protein, lower signal would be expected, thus validating saturating

conditions. Such effect was minimized working at higher dilutions like 1/6400 as can be seen and even more using lower concentration of proteins.

On the other hand, when 50 µg mL^{-1} of proteins were immobilized, high fluorescence signals were reached amongst the three dilutions evaluated. Finally, the deposition of proteins at 25 µg mL^{-1} allowed a clear differentiation of the signal from the spots for the three dilutions. Remarkably, the CTR+As S diluted at 1/6400 with the less concentrated protein spots, still showed enough fluorescent detectability. With the idea to reach comparable response to the peptide-BSA conjugates that theoretically could be less immunogenic (providing lower signal), fluorescence intensities around 10.000-20.000 RFU's were considered adequate for proteins. In this regard, even higher CTR+As S dilutions or less concentrated protein solutions could have been utilized.

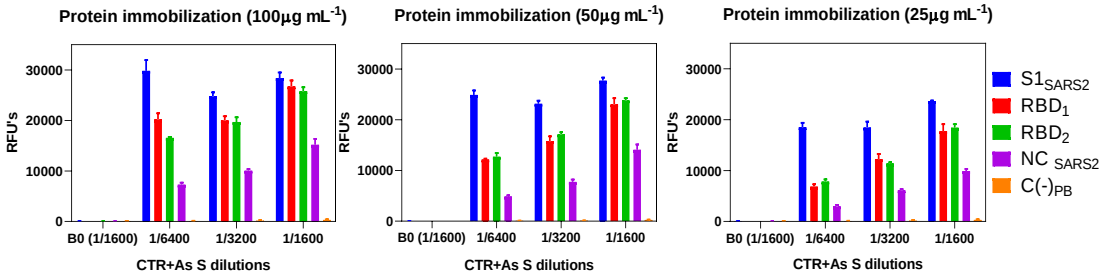

Figure 6.7 Results from the evaluation of the effect of protein concentration on the microarray chip after incubation with As410 (B0 at 1/1600 and CTR+As S at different dilutions). Three different concentrations of each protein were prepared and spotted using 5 drops/spot in the same matrix in triplicates. Then, different arrays were incubated with As410 B0 and CTR+As S (B3) at three dilutions to evidence the most suitable concentration of protein in and as dilution utilized. The SD corresponds to average signal from three independent wells.

It worth noticing the considerable signal recorded for the N protein, using CTR+As S", bearing in mind that the antiserum was raised against the S protein. According to these results, a spotted protein concentration of at least 25 µg mL^{-1} provides significant IgG response at 1/6400 dilution minimizing the recognition of the NC-SARS2 protein as can be seen in the next graph (Figure 6.8).

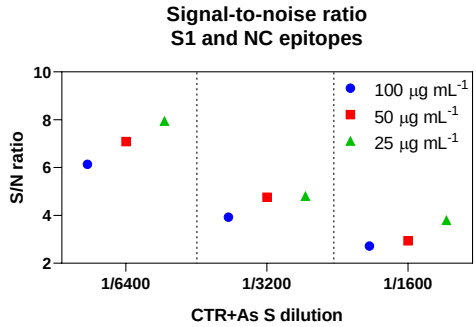

*Figure 6.8 Estimation of the signal to noise ratio for S1-SARS2 and NC-SARS2 proteins at different CTR+As S dilutions. The ratio was estimated considering the relation between the signal obtained from S1-SARS2 and NC-SARS2 after incubation with increasing concentrations of CTR+As S and protein immobilized. The higher the ratio, the more differentiated the response. The ratio was calculated from =10*Log(S1-SARS2/NC-SARS2) for each dilution and protein concentration.*

By estimating the signal-to-noise ratio between S1-SARS2 and NC-SARS2 responses considering the second as the interference, is possible to identify that higher ratios are achieved with the lowest dilution 1/6400 evaluated and the less concentrated protein solution. These means that the signal from S1-SARS protein is more differentiated from the signal detected in NC-SARS2 using such condition.

For the determination of the most suitable immobilization concentration for peptide-BSA bioconjugates in IgG and IgM detection, a series of experiments were performed aiming to achieve comparable fluorescent response to proteins already evaluated. In this case, it was preferred to immobilized the minimum concentration of bioconjugate, considering them as limiting reagents requiring a new synthesis and bioconjugation in case of running out of stock.

During this study, two different microarray chips were generated by immobilizing all the peptide-BSA conjugates at 1 and 0.5 mg mL^{-1}. To determine the effect on IgG's, the chips were incubated with CTR+As S and N solutions using a compromise dilution of 1/2000 to evidence if sufficient response was achieved, while for IgM's the B1+18 samples from As410 and As414 were employed at 1/100 dilution, considering the earlier expression of these isotypes. As both immunoglobulins are characterized by a different distribution and relative abundance over time, IgM's required a less diluted antiserum content (1/100) and were more abundant in samples collected earlier during immunization (B1+18).

After the analysis of IgG response, a considerably lower signal (1.000 RFU's) was observed using CTR+As S and N dilutions at 1/2000 above the peptides at both concentrations (Figure 6.9), in contrast with the protein already evaluated at 20.000 RFU's with a dilution of 1/1600 and 25 µg mL^{-1}. This observation limited the assessment of higher antisera (CTR+As) dilutions or even lower concentrations of peptide-BSA bioconjugates in view of a possible signal reduction.

However, during IgG and IgM assessment, no significant differences were observed in the maximum signal obtained if bioconjugates were immobilized at 1 or 0.5 mg mL^{-1}. On the contrary, when CTR+As S and CTR+As N were spotted in the microarray as internal controls (directly detected by the secondary antibodies) at both concentrations, a dose dependent effect was identified, as a result of the higher amount of antibody in the spots at 1 mg mL^{-1}. Thus, validating that the effect over peptides conjugated to BSA was specific and not influenced by the concentrations utilizied.

Interestingly, the response from **P4** and **P6** was detectable in the case of IgG with CTR+As S while **P10** was the only one showing response with CTR+As N, slightly higher with 0.5 mg mL^{-1}. In the case of IgM's, a relatively low response was observed with As410 (B1+18) and some unspecific adsorptions over **P9** at 0.5 mg mL^{-1}. While the response from As414 (B1+18) against **P10** was significantly different, reaching up to 10.000 RFU's at both concentrations of bioconjugate immobilized, suggesting high antibody titters against this linear epitope.

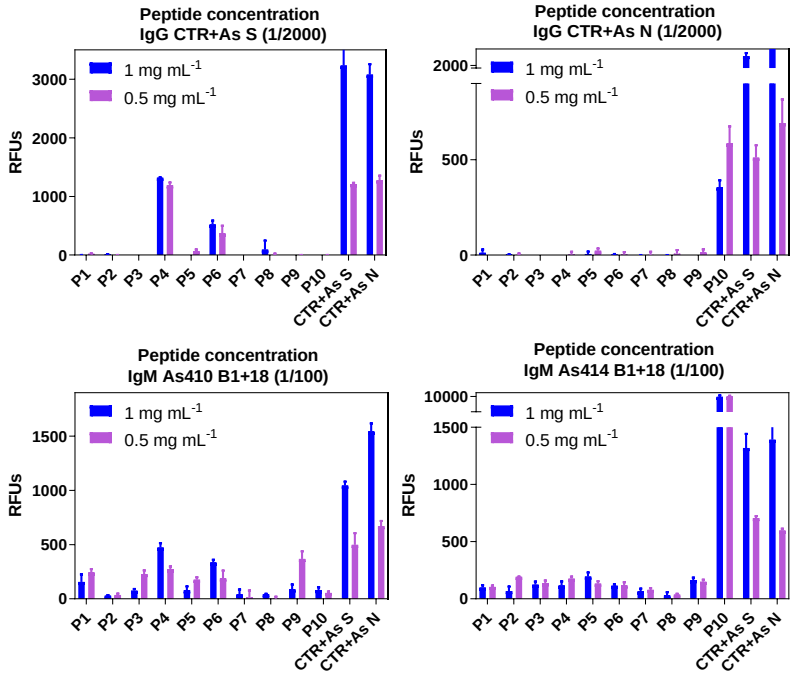

Figure 6.9 Effect of peptide BSA conjugates concentration during immobilization. All the peptide bioconjugates were spotted in triplicate spots, as well as CTR+As S and CTR+As N at 1 and 0.5 mg mL^{-1}. For the assessment of IgG's, different solutions of CTR+As S and CTR+As N at 1/2000 were incubated over separate peptide-BSA matrixes. For the determination of IgM's, distinct solutions of As410(S) and As414(N) from B1+18 at 1/100 dilution were required. The SD corresponds to the signal from three replicate spots.

Contemplating that no signal differences were attributed to the use of one or the other concentration and it was preferred to employ less amount of bioconjugates, the selection of 0.5 mg mL^{-1} as standard immobilization concentration for all the peptide-BSA conjugates was established. At the same time, at least a CTR+As dilution of 1/2000 for adequate IgG detection and a dilution 1/100 of B1+18 for IgM detection were proposed. On the other hand, protein immobilization was set at 25 µg mL^{-1} for comparable response evaluation, although the CTR+As dilution at 1/1600 showed higher fluorescence in contrast with peptide conjugates with 1/2000 dilution. Alternatively, a lower concentration of proteins for immobilization could have also been contemplated to allow comparable detectability with the peptide epitopes in the future.

Independently from the previous analysis, as a result of the simultaneous determination of IgG's and IgM's using different secondary labelled antibodies in

the same chip. During IgM's determination with the B1+18 from As410 at dilution 1/100, a strong fluorescent response was detected over IgG's at this dilution (data not showed). This was firstly assumed as a potential unspecific interaction with the peptide-conjugate matrix, as consequence of the high antisera concentration.

6.2.5.1.1. Influence of blocking agents in pre-immune signal detection

In an attempt to evaluate the origin of the effect observed after incubation of B1+18 from As410 at 1/100 in IgG's detection, B0 (pre-immune) samples from As410 were incubated at 1/100 dilution in the complete microarray combining peptide-BSA conjugates and proteins at the concentrations established. Surprisingly, positive signal was evidenced after analysis and this was attributed to unspecific adsorptions of the serum working at high concentrations. Bearing in mind that the platform was expected to be implemented in human serum and considering that non-specific interactions were detectable even in samples not exposed to the immunogen (B0), the incorporation of a blocking step to the general procedure was proposed. Due to this, the evaluation of different blocking agents was performed prior the incubation with the rabbit antisera, expecting to eliminate such interference to avoid similar effects when implemented in human samples.

The following day after slides biofunctionalization with peptide-BSA conjugates and proteins, an initial blocking step with different solutions was carried out for thirty minutes, followed by the addition of three As410 solutions (B0 and B1+18 at 1/100 dilution, and CTR+As S (B3) at dilution 1/2000 in PBST buffer) in different wells. Then, the slides were washed and incubated with the fluorescently labelled secondary antibody against IgG's for thirty minutes. As expressed in Figure 6.10, each column refers to a As410 solution and every row indicates the blocking step utilized in the three wells, such as 2% (w/v) BSA, 1% (w/v) gelatin, 2% (w/v) milk powder, 2% (w/v) polyethylene glycol 6000 (PEG6000), 2% (w/v) polyvinylpyrrolidone (PVP), 0.15% (w/v) casein and 2% (w/v) poly (vinyl alcohol) (PVA) all prepared in PBST.

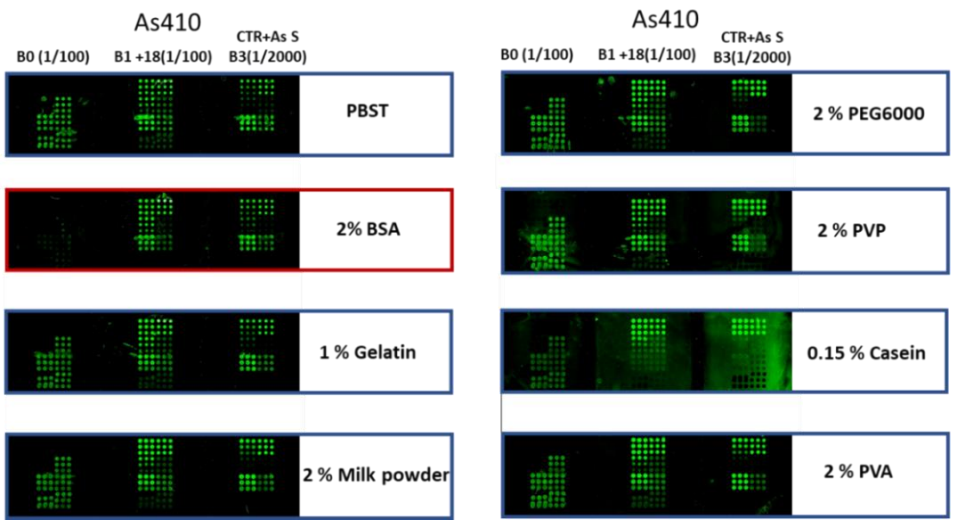

Figure 6.10 Effect of blocking agents. Seven blocking solutions and a control with PBST, were incubated for thirty minutes in the complete microarray. To then, determine the signal from As410 at different immunization points (B0 at 1/100 dil., B1+18 at 1/100 dil. and CTR+As S (B3)at 1/2000 dil.) The lack of fluorescent signal indicates no antibody binding to the epitopes in the surface.

From this analysis, is possible to highlight that only the blocking agent 2% (w/v) BSA in 10mM PBST, was able to completely eliminate non-specific adsorptions detected after incubation of pre-immune samples of As410 at 1/100 dilution. On the contrary, the rest of blocking agents assessed did not reduced effectively the unspecific signal and due to this the BSA was defined as the most adequate blocking agent to implement in the following assays. Moreover, the response form B1+18 at 1/100 was not reduced after the blocking with 2% (w/v) BSA or the rest of agents, evidencing that the signal was specific in this case.

Alternatively, the use of BSA as additive in the assay buffer was proposed to avoid the need of an additional blocking step (Figure 6.11). For this purpose, B0 or pre-immune samples from As410 and As414 at 1/100, B1+ 18 also at 1/100 and CTR+As S and N (B3) at 1/2000, were diluted in 10mM PBST as negative control and separately with 0.5 %, 1 % and 2 % (w/v) BSA in PBST respectively. As can be seen in the Figure 6.11, the effect over B0 from As414 at 1/100 in PBST was also detected, and for both antisera the unspecific adsorptions were successfully removed even with the lower BSA concentration of 0.5%. For the case of IgM's, a mild unspecific binding was removed in the case of B0 from As410 using BSA in the assay buffer.

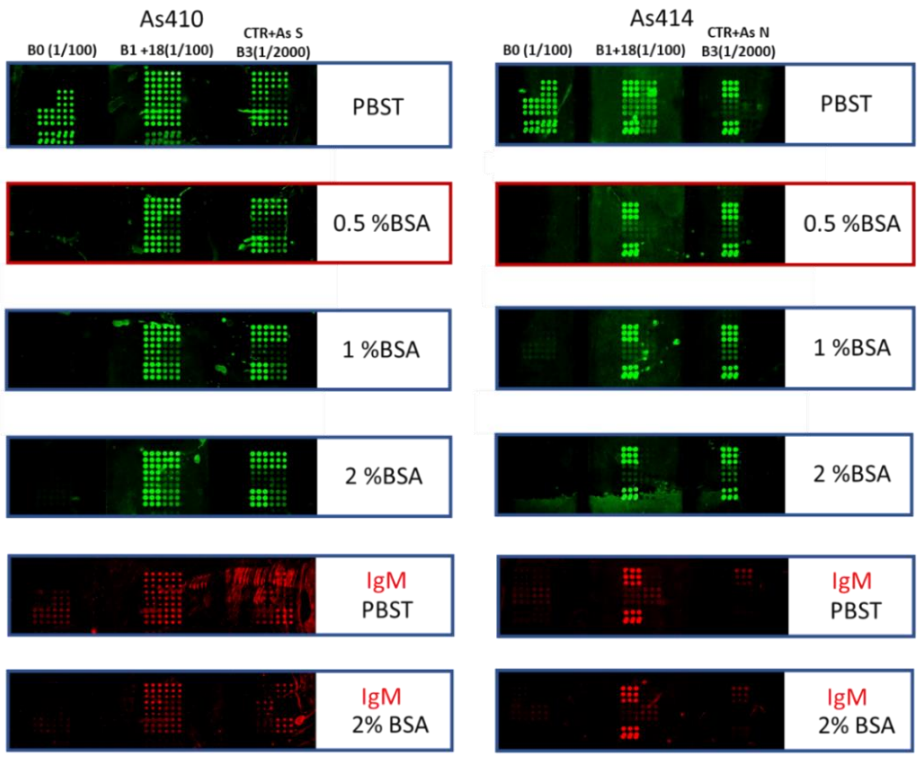

Figure 6.11 Effect of BSA as additive in assay buffer. For this, As410 and As414 from distinct immunization points (B0 at 1/100 dil., B1+18 at 1/100 dil. and CTR+As (B3) at 1/2000 dil.) were diluted in PBST buffer containing different concentrations of BSA (0.5, 1 and 2 % w/v) as additive and using PBST as control. IgM's and IgG's were determined using different fluorescently labelled secondary antibodies. The lack of fluorescent signal indicates no antibody binding to the epitopes in the surface.

As observed, the presence of BSA as additive in the dilution buffer helped to reduce nonspecific binding detected using B0 samples, working with high antisera dilutions (1/100). In accordance with these findings, the incorporation of 0.5% (w/v) BSA to the dilution buffer (PBST 10mM) was defined as part of the assay protocol to minimize potential contributions of the matrix, avoiding the need of blocking steps or laborious sample pretreatments once implemented in clinical samples.

6.2.5.2. Monitoring IgG and IgM response progression after consecutive immunizations with S and N proteins

Once all the epitopes were properly incorporated in the same microarray chip, the final hybrid matrix considering peptide-BSA bioconjugates and viral proteins was used to evaluate the IgG and IgM profile through the time and after each immunization step. In the graphs from Figure 6.12 the IgG's progression in B0, B1+18, B2 and B3 towards the epitopes of the S protein (As410) in and the N protein (As414) are shown. A single dilution of 1/2000 in 10mM PBST for IgG and 1/100 dilution for IgM detection was selected to favor the identification of peptide-BSA conjugates, as already explained. After incubation with both antisera for IgG detection, B0 samples represented in blue in the graph (see Figure 6.12), displayed non-detectable levels of immunoglobulins considering that were obtained before the first immunization lacking of specific immune response.

After 18 days (B1+18) post immunization, the samples showed only slight fluorescence over the structural protein S1-SARS2 in the case of As410, with no signal over the peptide epitopes while the incubation with the As414 rapidly showed detectable levels of **P10**, in addition to NC-SARS2 spots with the complete protein, indicating possible implications of such peptide epitopes during early immune response development. Following the second immunization (B2) serum samples from the As410 (S) started to evidence detectable response over the peptides **P4**, **P6** and stronger intensity over S1-SARS1, S1-SARS2 and RBD_2. Interestingly, during the analysis of B3 samples (CTR+As S), the fluorescence values were even higher reaching almost saturation values above 60.000 RFU's for the recombinant S1 portion of SARS-CoV-2 and a little bit less signal for S1 from SARS-CoV. On the other hand, a similar behavior was identified with As414 for the B2 samples were IgG's levels against **P10** and NC-SARS2 became considerably higher than the rest of epitopes. The fluorescent signal of **P10** in B2 samples was more intense than the one from B3 (CTR+As N) towards the same epitope. This is an anomalous result for which we have not found an explanation and should be repeated to corroborate reproducible behavior. The signal recorded for NC-SARS2 is in contrast comparable in both B2 and B3 samples.

Another remarkable aspect is that, cross reactivity was not evidenced between different selective antisera. Meaning that As410 specific for S epitopes, was diluted in 0.5 % BSA and then incubated with the complete microarray chip including epitopes from S and N protein, showing only specific response for S epitopes. The same can be said from the use of As414 that was specific for N protein and generated fluorescence response only against N epitopes (**P10** and NC-SARS2) demonstrating the specificity of the sequences included in the platform and that the positive control samples generated in rabbits performed correctly.

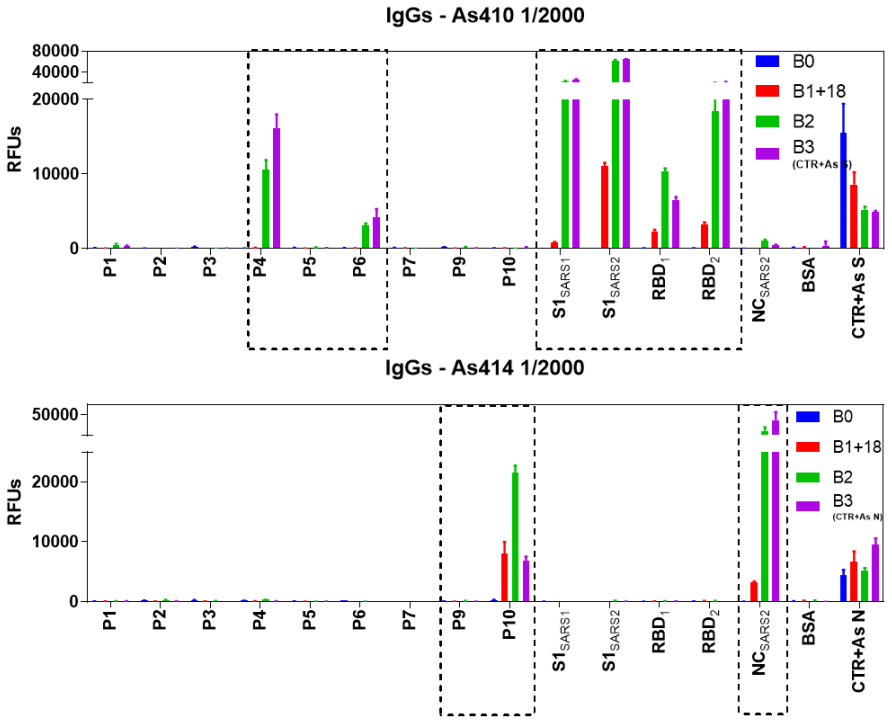

Figure 6.12 Progression of IgG titters along the immunization scheme. The IgG levels of As410 (above) and As414 (below) at 1/2000 dilution in PBST 0.5% BSA, comparing samples obtained along the period of immunization. For this, B0 samples were used as negative controls, then B1+18, B2 and B3 (CTR+As) were also determined making use of the complete matrix including peptides and proteins. The SD represented corresponds to the average of three replicate spots.

The same approach was followed to evaluate if the *Immuno*-µSARS2 v 1.0 chip could be useful to monitor IgM progression. For this purpose, a 1/100 dilution of As410 and As414 in PBST 0.5% BSA was required to evidence the presence of this isotype. The importance of IgM's determination relies on their intrinsic

expression during the early phase of infection providing faster response compared to IgG's. However, the detectability of IgM's in serum is limited to a rapid clearance and due to this the sampling window results critical to their accurate determination. Remarkably, a different behavior was evidenced during serological progression between IgG and IgM with our microarray. As it can be observed in Figure 6.13, the B1+18 and B2 As414 (N) samples showed the higher recognition also for the **P10** and the NC-SARS2 spots, as before, but the signal decreased for the B3 samples probably related to the rapid IgM clearance over time and even after several immunizations, in favor of the IgG's. It is worth noting the much higher response towards **P10** in respect to the spots containing NC-SARS2 with the structural protein, suggesting that this linear peptide is an important epitope, at least during the first stages of the infection (the IgG titers decreased in B3, se above). For the case of As410, the samples from B2 also displayed higher intensity values and decreased with B3 explaining the already discussed phenomena of early expression of IgM's. In addition, a high level of IgM's was recorded towards the RBD epitope, as also observed for IgG's suggesting that the immunization with the S protein triggered high neutralizing IgM's and IgG titers [35]. However, corroboration of this hypothesis would require performing *in vitro* neutralizing assays to quantify the real neutralization capacity of the antisera.

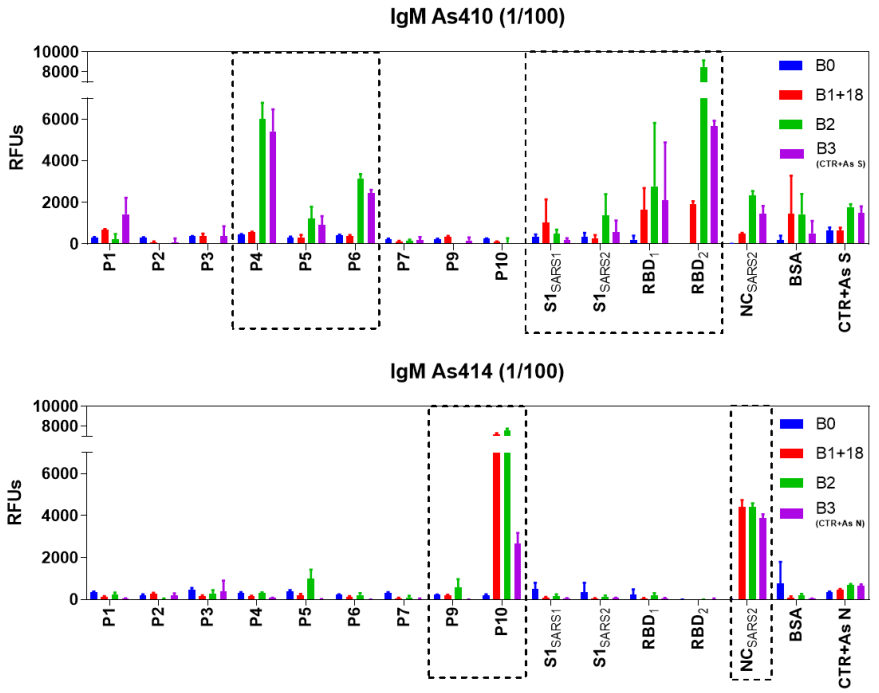

Figure 6.13 Progression of IgM titters along the immunization scheme. The levels IgM's for As410 (above) and As414 (below) at 1/100 dilution, after different days post immunization (B1+18, B2and B3 with B0 as negative control) with S and N proteins were determined making use of the complete matrix including peptides and proteins in triplicate spots. The SD represented corresponds to the average of two independent wells.

These preliminary findings pointed at the possibility to use the matrix selected to continue with our studies towards a potential implementation of the microarray platform to the analysis of the immunological progression of patients infected by SARS-CoV-2. On the other hand, there was a possibility for using just the peptide-BSA bioconjugates, instead of the more expensive recombinant proteins, to develop more affordable microarray chips. Overall these results were encouraging for the implementation of the multi-epitope microarray platform to the analysis of the profile of expression of IgG and IgM titters after viral infection or vaccination studies.

6.2.6. ANALYTICAL CHARACTERIZATION OF THE *IMMUNO*-µSARS2 V 1.0 CHIP

6.2.6.1. Matrix effect studies in commercial human serum

On a first instance the potential unspecific matrix effect of human serum samples was evaluated. For this purpose, solutions of PBST 0. 5% BSA (control), undiluted commercial human serum (HS) and diluted HS at 1/2 and 1/5 in PBST 0.5 % BSA were spiked with the CTR+As S and N at 1/2000 dilution for IgG detection and 1/100 for IgM. The samples were analyzed with the *Immuno*-µSARS2 v 1.0 chip following the same procedure as before (see Figure 6.4).

As it can be observed in Figure 6.14, the CTR+As S IgG's response in undiluted HS was comparable to that obtained in PBST, while the 1/2 and 1/5 diluted samples still showed a significant response. The only difference in respect of the buffer was certain small level of recognition with some other peptide epitopes. In contrast, for the case of IgM's, a notably reduction of the recognition of S1-SARS2 was observed for the undiluted HS, but the signal was recovered after a 1/2 dilution with buffer, which pointed to a matrix effect when analyzing undiluted HS. The abundant content of proteins presents in serum such as albumins could be acting as blocking agents interfering with the binding compared to control sample conditions. Although dilution of the matrix to 1/2 has proven to eliminate such effect, it may have also an impact on the detectability at certain points of the infection. From these results, is not recommendable to use undiluted HS for the detection of IgM's to avoid unspecific binding.

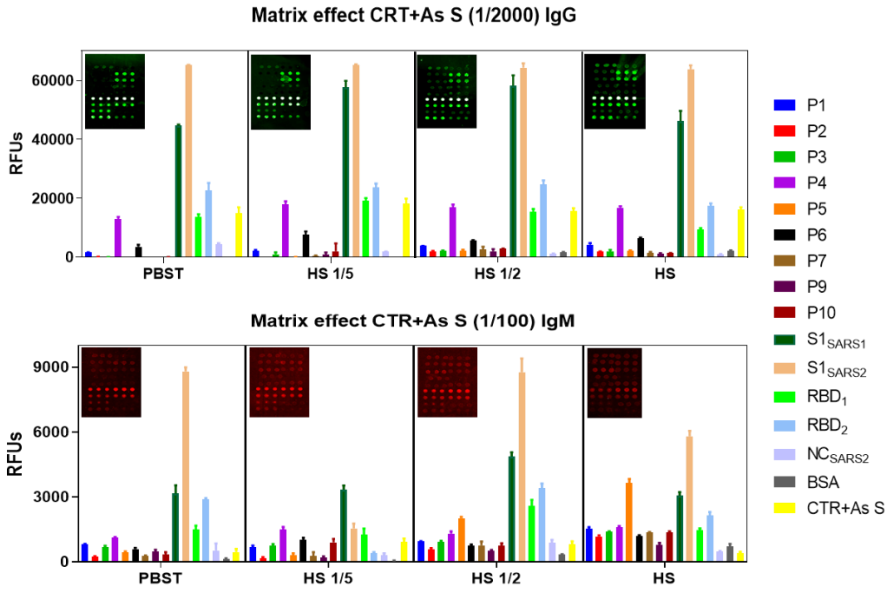

Figure 6.14 Matrix effect in commercial human serum (HS) with CTR+As S. The influence of increasing concentrations of commercial HS was evaluated after spiking the matrix with different dilutions of CTR+As S at 1/2000 for IgG's and 1/100 for IgM's determination using PBST as reference. The complete microarray was used in this experiment, the average epitope intensity was determined form three replicate spots and the SD corresponds to two independent wells.

When the same experiment was carried out using CTR+As N samples diluted 1/2000 for IgG, a higher fluorescence was recorded by diluting the serum whereas the undiluted antisera behave like the buffer (see Figure 6.15 above). At present we have not found an explanation for this behavior, since by diluting the matrix it would be expected that the IgG profile would be closer to the buffer, as it is observed for the IgM profile (see Figure 6.15, bottom). The undiluted HS apparently was blocking the interaction of the IgM's with the peptide's epitopes and proteins of the microarray and therefore for certain epitopes such as the **P10** or the NC-SARS2 protein the fluorescence was lower than for the spiked PBST samples. This matrix effect could be evaded by diluting the sample to the point that a comparable behavior was recorded at 1/5 dilution. The 1/2 diluted HS showed less matrix effect, but still was not identical to the buffer. However, the recognition of the rest of peptide epitopes and proteins of the microarray chip were not significantly affected by the HS matrix since, except for the P5 epitope, the profile of recognition appear to be independent from the dilution of the HS.

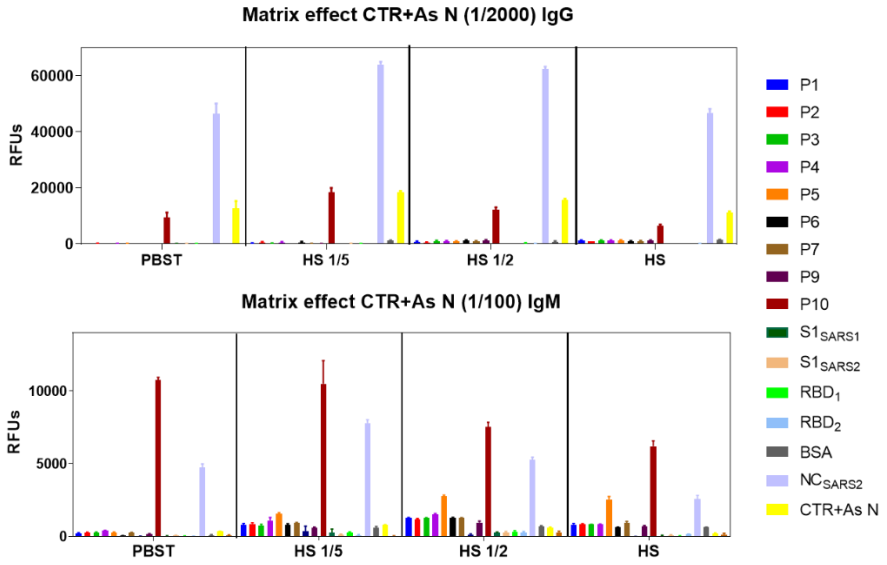

Figure 6.15 Matrix effect in commercial human serum (HS) with CTR+As N. The influence of increasing concentrations of commercial human serum was evaluated after spiking the commercial samples at different dilutions with CTR+As N (1/2000) for IgG's and CTR+As N (1/100) for IgM's determination using PBST as control. The complete microarray was used in this experiment, the average epitope intensity was determined form three replicate spots and the SD corresponds to two independent wells.

Summarizing both, CTR+As S and N, IgG's could be measured in undiluted or 1/2 diluted HS. In contrast detection of IgM's appears to be more affected by the HS, probably because of the complexity of the sample and the relative low abundance of this isotype. Potential alternatives such as those reported in section 6.3.5.1.1, could be used to minimize this effect analytical performance of the *Immuno*-µSARS2 V 1.0 microarray chip. Nevertheless, the use of BSA 0.5 % in the dilution buffer seems to contribute to the adequate detection of both isotypes at least at 1/5 HS dilutions and probably at higher dilutions.

6.2.6.2. Quality control assessment for the manufacturing of the *Immuno*-µSARS2 chip.

Considering the extensive production of biofunctionalized slides during this work, it was necessary to ensure manufacturing reproducibility due to batch to batch variations. Each printing session was limited to a maximum of 20 slides per run and due to this, an internal quality control procedure was implemented. For that purpose, B3 serum samples from As410 and As414 (CTR+As S and N) were

purified through affinity chromatography using protein A (see material and methods section 6.5.4.6). After the purification step the so-called antiserum (As) were technically converted into polyclonal antibodies (Ab) that will be identified as Ab410 and Ab414, but as they were used as positive controls through the following sections, will be named as CTR+Ab S and CTR+Ab N respectively, from now on. For this study, three concentrations (100, 20 and 5 µg mL^{-1}) of the CTR+Ab S (Ab410) and CTR+Ab N (Ab414), were prepared in PBST 0.5% BSA and used to assess microarray performance following the standard protocol described above (see Figure 6.4)

In this regard, Figure 6.16 shows the expected profile for each CTR+Ab S and N at 5 µg mL^{-1}. As it can be observed the signal intensity provided by CTR+Ab S is higher for the S1 proteins from SARS-CoV-2 and SARS-CoV, including RBD and **P4** as well as **P6,** demonstrating array specificity and the lack of cross-reactivity with other non-related epitopes. In respect to CTR+Ab N, the main signals recorded correspond to the NC protein from SARS-CoV-2 and SARS-CoV and also **P10**.

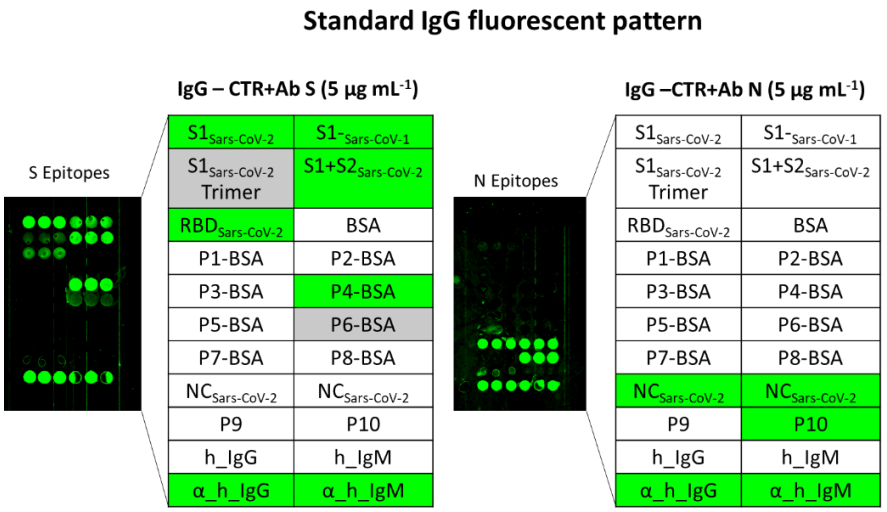

Figure 6.16 IgG's standard response profile. The fluorescent pattern of our immunoarray, after incubation of 5 µg mL^{-1} of purified CTR+Ab S and N are represented. The final matrix (6x11) was generated by printing triplicate spots of each epitope and incubated them with the respective CTR+Ab S and N, including internal controls. The pattern obtained after the analysis of the reference antisera is described in the picture in highlight selective epitopes in green.

As part of the biofunctionalization quality control procedure, the fluorescent response obtained from a new batch of slides printed was compared with the

pre-defined values determined for each epitope under standard conditions using CTR+Ab S and N. Moreover, the incorporation of this quality control has been crucial to stablish the maximum signal that could be achieved in each epitope and minimize variations attributed chip manufacturing conditions. Nevertheless, through the course of this research work no considerable differences were observed during the printing, indicating well standardized methodologies. As additional experimental considerations, different internal controls were included in the microarray to minimize variability in assay performance before reaching the use in human samples and are described as follows.

Internal control BSA: Three replicate spots containing BSA were used as negative control in the microarray, to evidence non-specific interactions with BSA considering that peptides were conjugated to BSA. A positive result for BSA may indicate presence of antibodies against albumin or non-specific adsorption of components in the sample.

Human IgG and Human IgM: identified as h-IgG and h-IgM in the Figure 6.16. These immunoglobulins were spotted in triplicates on the microarray with the idea to estimate the relative abundance of total IgG's and IgM's present in each sample to establish comparable determinations. The fluorescent intensity on these spots could be used to normalize the total amount of immunoglobulins at patient level, helping to identify negative samples from samples with low amount of antibodies for example.

Secondary labelled Anti-Human-IgG and Anti-Human-IgM: The solution utilized to generate these spots consisted on the aliquots of the secondary antibodies labelled for IgG and IgM detection, that were intended to be use during sample analysis in order to corroborate adequate fluorescence prior implementation. In the Figure 6.16 are named as α-h-IgG and α-h-IgM

Negative control solution (NEG-HS): Commercial human serum (HS) samples, already described for matrix effect studies, were measured in duplicate chips over each slide during the sample analysis, as negative control. The average fluorescent signal detected from both measurements was subtracted from the intensity detected over the rest of samples in the slide, to minimize background signal attributed to the serum sample.

6.2.6.2.1. Performance reproducibility of the chips

Inter-chip variability was studied by comparing the performance of four distinct chips printed on the same slide using the CTR+Ab S and CTR+Ab N samples at 100, 20 and 5 μg mL^{-1} in PBST-0.5% BSA. In these experiments each peptide-BSA bioconjugates and proteins were printed in triplicates. Some of the potential variables affecting array deposition include not homogenous surface immobilization, fluctuation in ambient conditions affecting spot shapes and evaporation rates, handling errors during the spotting solutions preparation and reagents stability.

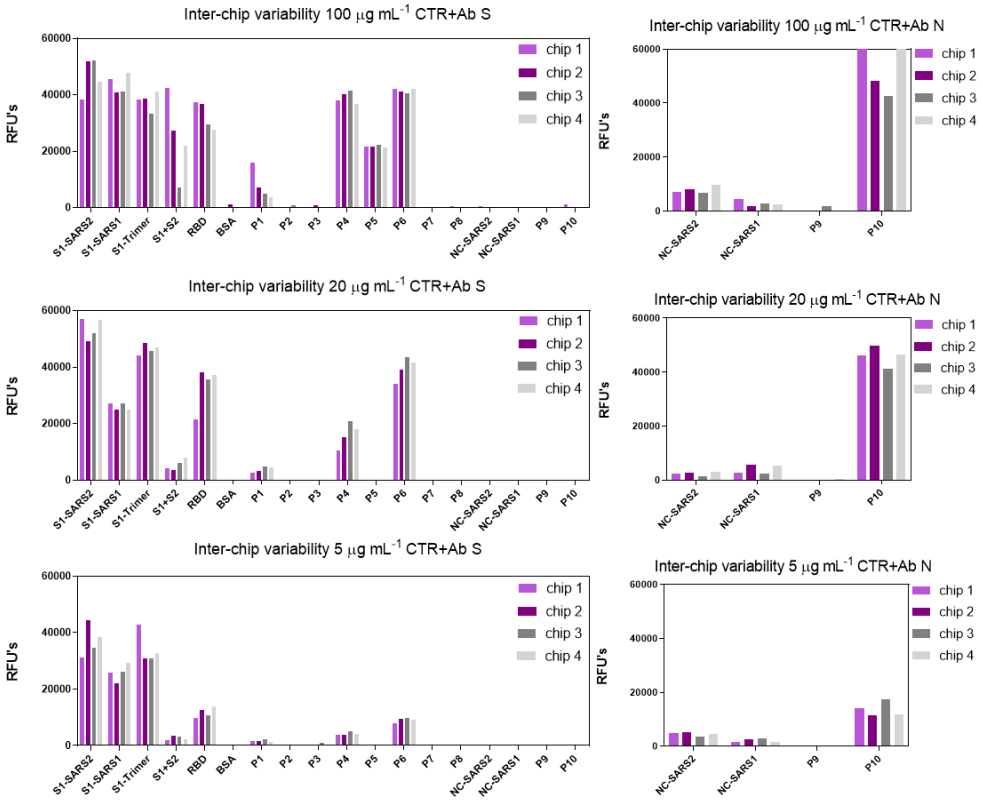

Figure 6.17 Results from the Inter-chip response reproducibility. On the same slide, four independent microarray chips were used to measure the profile of response of CTR+Ab S and CTR+Ab N at three concentrations (100, 20 and 5 μg mL^{-1}). Each bar corresponds to the average intensity of three replicate spots per epitope. The CV was lower than 15 %.

As can be observed in Figure 6.17, the distinct microarray chips provided comparable responses amongst the three CTR+Ab S and CTR+Ab N concentrations evaluated as evidenced by the profile of the S and N epitopes, respectively. In all cases, and as expected, a dose dependent response was observed in respect to the antibody concentration used for both, the S and N epitopes. According to these results adequate inter chip reproducibility is achieved working under high, medium and low concentrations of purified CTR+Ab S and CTR+Ab N. It must be considered, that experimental intensity values around 10.000 and 20.000 RFU's are sufficient to discriminate a positive response, depending on the background noise, that in this case is relatively low.

6.2.6.2.2. Inter-day and batch-to-batch variability of the assay

On another set of experiments the inter-day and batch to batch variability of the assay was evaluated by using the CTR+Ab S and CTR+Ab N at the three concentrations, but only showing 100 µg mL^{-1} as representative example in Figure 6.18 .For this, the fluorescence response from single chips printed in four slides generated in separate batches and measured in different days was compared. Each microarray chip contained three replicate spots of each peptide-BSA and protein, showing their corresponding SD in each column.

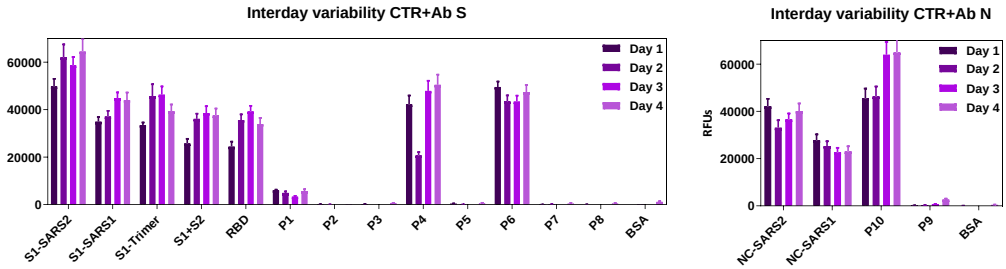

Figure 6.18 Inter-day variability using CTR+Ab S and CTR+Ab N. Each bar shows the average and standard deviation of the fluorescence intensity recorded for each epitope printed in three replicate spots on each microarray chip (SD) and processed in a single day using the CTR-POS antibodies S and N at 100 µg mL^{-1}. Experiments were carried out in four different days. Each day an independent slide produced in different batches was used. The CV was below 20 %.

As can be observed, a comparable signal was recorded on different days with the two CTR+Abs for each of the peptide epitopes and proteins of the different microarray chips manufactured on different batches. As no remarkable

fluorescence variability was observed after simultaneously assessing inter-day and batch to batch reproducibility, the platform robustness was corroborated, encouraging further experimental procedures. It is worth noticing that an independent quality control procedure has been performed for each group of slides manufactured and, because of this, an individual normalization is considered to minimize batch to batch variations.

6.2.7. IMPLEMENTATION OF THE *IMMUNO*-µSARS2 V 1.0 CHIP IN CLINICAL SAMPLES.

Once the first version of the *Immuno*SARS-2 chip v1.0 was analytically characterized, the implementation to the analysis of clinical serum samples was carried out in collaboration with partner healthcare institutions of Spain. Independent cohorts of human serum samples were provided by Hospital del Mar (HdMar), Biobanco de Zaragoza (BioZgZ) and Hospital Universitario Germans Trias i Pujol (HUGTIP) together with relevant clinical data associated to them to be evaluated with the microarray platform. A total of 755 human serum samples were collected and distributed according to the RT-PCR result associated, with the exception of a group of pre-pandemic clinical samples provided by HdMar to be used as negative reference samples. For the following studies a total of 572 samples were evaluated due to the lack of clinical information form the rest of them, but will be analyzed in the following chapter.

For the initial validation 298 human serum samples (143 from BioZgz, 61 from HUGTIP and 94 from HdMar) classified as RT-PCR+ were measured to elucidate the clinical performance of the microarray towards IgG mediated response of convalescent serum from infected patients. The experiments were performed with the aid of the Array It® holder with capacity of four slides. The microarrays used for these studies included three replicate spots of each epitope or protein, and the corresponding internal controls spots already described in section 6.3.6.2. Although they are not represented in the following Figure 6.19, performed adequately in each case. Additionally, from the 24 microarrays available in every slide two chips were designated to measure commercial HS samples at 1/5 dilution as negative control (NEG-HS) and the average intensity form these determinations for each epitope or protein was subtracted from the

signal detected in the clinical samples to eliminate the fraction of the signal resulting from unspecific adsorptions at slide level.

The analyses were carried out using 10 µl of human serum diluted with 40 µl of 10 mM PBST 0.5% BSA and processed as described before (see section 6.4.3.2). Then, raw signal expressed in relative fluorescent units (RFU's) was obtained from the scanner and normalized or referenced to 0 for the lower value detected and 100 % over the maximum fluorescence monitored considering each cohort independently to reduce batch effects.

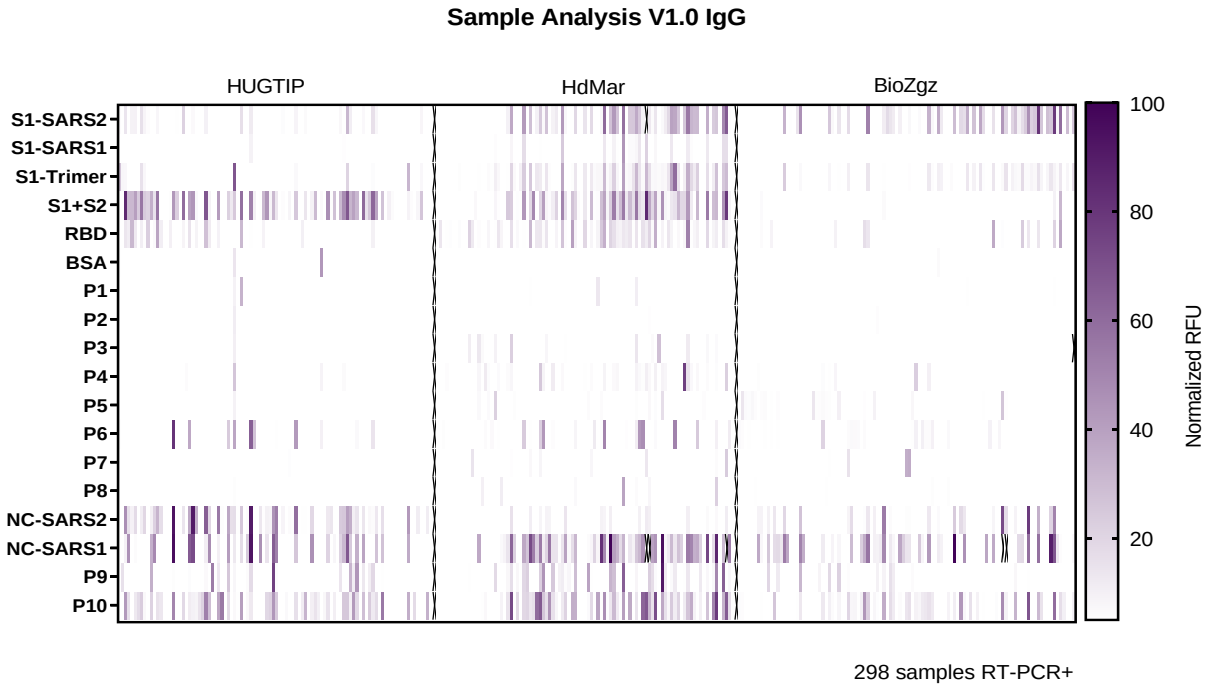

Figure 6.19 Landscape of IgG mediated response obtained from the analysis of 298 RT-PCR+ human serum samples from three different cohorts of patients with the immunoarray. The y-axis represents the individual epitopes constituting the microarray (viral peptides and proteins) while, the x-axis corresponds to the serum samples from patients with RT-PCR+ results. The intensity scale indicates the relative signal of antibody binding from 0 (white) to 100 (purple) in normalized RFU's. Normalization was defined by assigning 0% signal to the lowest value detected in each cohort and 100% to the maximum RFU's measured.

The main limitation behind the interpretation of these results was found on the lack of data homogeneity associated to each cohort during sample collection. The previous heatmap showed the relative IgG profile of the RT-PCR + samples from different cohorts. Over the three sample groups is possible to differentiate

common immunodominant epitopes that provide a characteristic serological response. Higher IgG levels were obtained against the structural proteins on the spots with NC-SARS2, NC-SARS1 assuming the intrinsic immunogenicity of these proteins. Interestingly, the linear peptide **P10** provided comparable response amongst different patients corroborating its excellent serological performance and potential relevance for further developments. Regarding epitopes related to S protein, the most prevalently found were also the structural proteins like S1-SARS2 together with S1-Trimer, S1+S2 and RBD while from the set of peptide epitopes only **P6** showed the most relevant contribution but not comparable to the proteins. Results interesting to highlight, that antibodies against **P6** were highly detected also from the rabbit CTR+As S (As410). On the other hand, using CTR+As N (As414) the **P10** peptide epitope showed increased response either in rabbits immunized with N protein and covalescent patients suggesting that the sequence can be considered as a promising seroprevalence indicator in both species reaching reproducible detectability.

Continuing with sample analysis, a set of 178 RT-PCR - samples was evaluated During the determination of IgG profiles of RT-PCR - serum samples it was important to consider that although the PCR was established as a sample classification method, the serological response does not have to be necessarily correlated with the PCR result. Hence, the immunological profile is mainly affected by the sampling period and the biomolecule detected, but RT-PCR - result could suggest; i) lack of infection with negative serology; ii) initial phase of an infection with undetectable levels or viral RNA (and negative serology), as well as iii) much more previous viral exposure with non-detectable RNA levels at the time of the analysis (positive serology). In agreement the literature, the most appropriate diagnostic strategy to discriminate between COVID-19 infected and non-infected patients with negative PCR should consider simultaneous determination through PCR and serology [36].

As the Figure 6.20 shows, the IgG profile of samples negatively classified through RT-PCR, evidenced relatively low abundance of anti-SARS-CoV-2 specific antibodies, probably attributed to the lack of pre-existent viral exposure. However, a moderate but sustained signal was observed in the first half of samples for the protein S1+S2. We hypothesized that potential protein denaturation could favor the unspecific interaction with negative samples explaining that effect, although it was not corroborated. Some patients displayed

signal against randomly distributed epitopes, probably as a result of a sort of immunity against other coronaviruses for which cross-reactivity was not evaluated. At the light of these results and the above-mentioned reasons, samples from the RT-PCR- groups were discharged from the subsequent analysis.

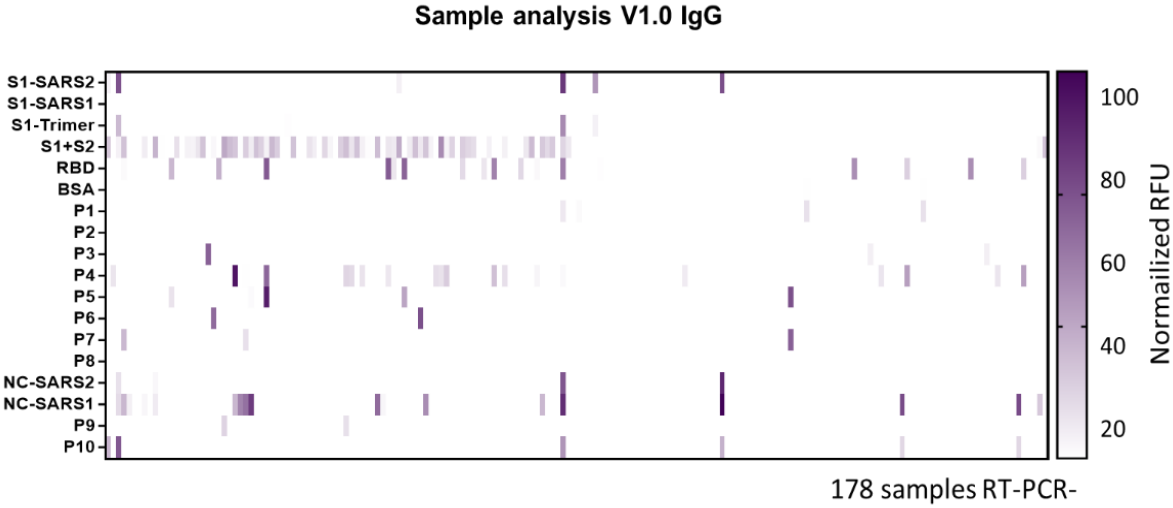

Figure 6.20 Landscape of IgG mediated response obtained from the analysis of 178 RT-PCR- human serum samples. The y-axis represents the individual epitopes forming the microarray constituted by viral peptides and proteins while, the x-axis corresponds to the serum samples from patients with RT-PCR- results. The intensity scale indicates the relative signal of antibody binding from 0 (white) to 100 (purple) normalized RFU's. Assigning 0 to the lowest signal detected and 100 to the highest fluorescence obtained.

In order to validate platform specificity, the evaluation of pre-pandemic samples was determinant, considering that these serum samples were obtained from patients who had not been exposed to viral infection. Hence, they were collected during early 2019. As can be seen in the Figure 6.21, the immune response profile detected in these samples was negligible using the *Immuno*-µSARS v1.0 chip. These results corroborate the specific response of the chip towards SARS-CoV-2 infection since only the serum from patients previously exposed to virus provided a profile of response to the epitopes on the chip. These findings were encouraging to continue studying the diagnostic and prognostic value of the platform developed for profiling the immunological response of SARS-CoV-2 infected patients.

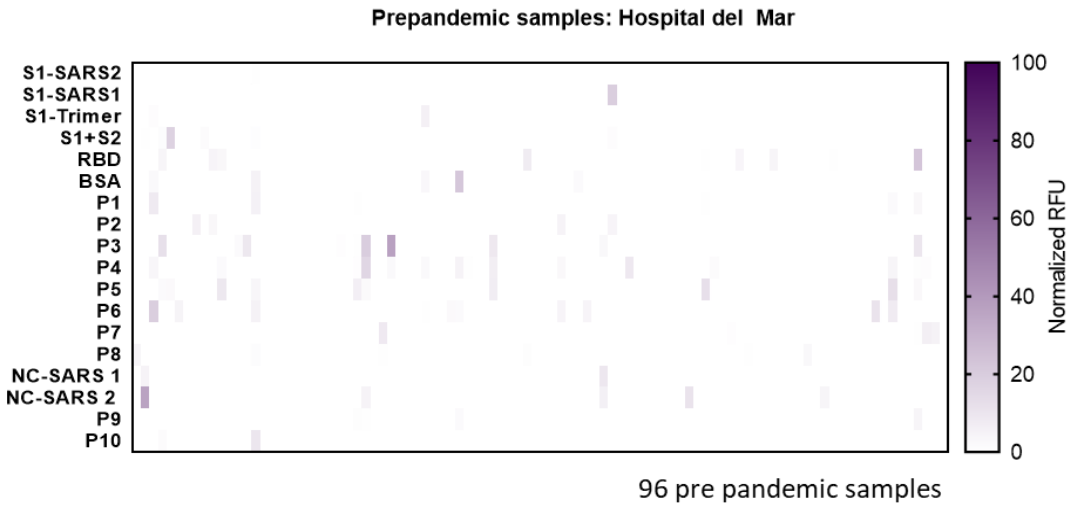

Figure 6.21 Landscape of IgG mediated response obtained from the analysis of 96 pre-pandemic human serum samples from HdMar. The y-axis represents the individual epitopes printed in the microarray (viral peptides and proteins) while, the x-axis corresponds to the serum samples from patients with RT-PCR+ results. The intensity scale indicates the relative signal of antibody binding from 0 (white) to 100 (purple) normalized RFU's.

Is necessary to mention that together with IgG's monitorization, IgM's were also detected using the cocktail of secondary labelled antibodies with different fluorophores over all the samples previously described. However, due to the lack of robust and consolidated response (data not showed), these results will be discussed in the following chapter, including an extended version of the epitope matrix using the second version of the immunoarray *Immuno*-µSARS2 chip 2.0.

6.2.7.1. Evaluation of IgG response progression in samples grouped according to days post symptoms onset (PSO)

Next step of the implementation, consisted on evaluating the profile of immunological response provided by the chip for serum samples collected at different time (days) after symptoms appear (PSO, post symptoms onset). The samples under study were collected in the period between 05/2020 and 07/2020, therefore those patients had been exposed to the virus for the first time, in the absence of vaccines or prior acquired immunity.

Early studies conducted by *Long et al*. [37] showed that the median days after symptoms to complete IgG's seroconversion was 13 days. In another study published by *Ma et al*. [38], different immunoglobulins were tested against SARS-CoV-2 proteins and it was found that IgG's reached the plateau after 20 days from symptoms. In this scenario detectable IgG levels were expected mostly after 8 to 10 days PSO.

Samples from the BioZgZ and HdMar cohorts were used for this study since had associated the information in respect the day of collection PSO. The serological results for these samples were already displayed in the heatmap from Figure 6.19, and in the next Figure 6.22 only the samples from HdMar are shown organized according to the days PSO reported in clusters of 5 days. As it can be observed, higher fluorescence intensity is recorded after 10 -15 days. It could be, that the intensity of the response could be detected earlier if contemporary samples are utilized, as a result of memory B cells generated from preexistent exposure to the virus or vaccination. From this analysis, is possible to infer that IgG levels against N epitopes are detectable much earlier than antibodies against S epitopes pointing to the possibility of using IgG's against N regions as earlier indicators. Hence, surprisingly the intensity of the response against NC from SARS-CoV-2 and P10 was already quite high in a representative amount of the samples from the 0-5 window, while the response towards the NC from SARS-CoV was not detected.

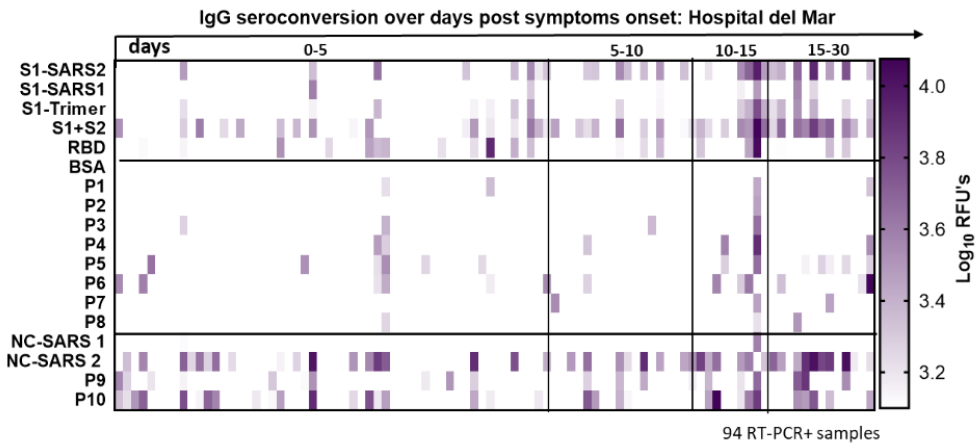

Figure 6.22 Landscape of IgG mediated response obtained from the analysis of 94 RT-PCR+ serum samples from HdMar distributed according to days PSO form serum collection date. The y-axis represents the individual epitopes printed in the microarray (viral peptides and proteins) while, the x-axis corresponds to the serum samples from patients with in clusters of days PSO. The intensity scale indicates the relative signal of antibody binding from 3 (white) to 4.6(purple) in Log_{10} RFU's.

In order to explore the predictive epitope capacity according to the onset of symptoms, the individual clinical sensitivity was determined for some of the most relevant components of the microarray in this set of samples (Figure 6.23). Comparing NC-SARS2 and **P10**, an increasing sensitivity of the protein is detected towards longer periods, reaching more than 75 % after 15 PSO.

On the other hand, the % of positive samples for S1 of SARS-CoV2 was only around 11% on the first-time frame (0-5 days), and the clinical sensitivity increased significantly on the following time frames reaching values of 42 % (5-10), 58 % (10-15) and 5 5% (15-30). These results are supported by previous reports suggesting that antibodies against N protein showed increased sensitivity compared to anti S antibodies [39].

Higher clinical sensitivity was provided by the S1+S2 protein with already a value of 25 % on the 0-5 days window, which also increased to 42 % (5-10), 75 % (10-15) and 80 % (15-30). In respect to the peptide epitopes from S, the **P6** appear to be one of the more sensitives although is no comparable to proteins with a clinical sensitivity of 9 % on the first-time frames which shifted to 11 % (5-10), 25 % (10-15) and 28 % (15-30). Next analysis has to move towards demonstrating whether if there exists a combination of peptide epitopes and proteins that allow increasing the clinical sensitivity in all time frames in a multivariate approach.

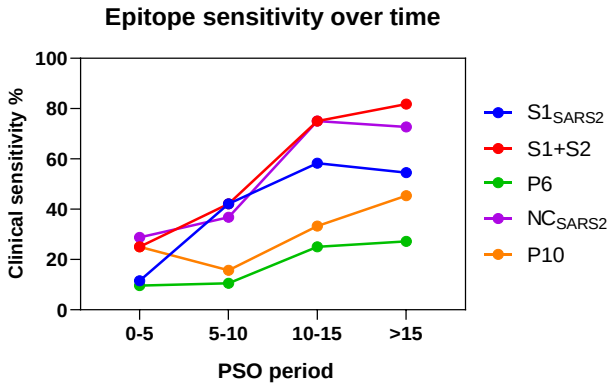

Figure 6.23 Clinical sensitivity of representative epitopes from HdMar cohort according to the time PSO. The clinical sensitivity was estimated for S1-SARS2, S1+S2 and P6 as relevant epitopes from S protein and NC-SARS2, and P10 from N protein. Each % was determined for the different time frames of days PSO, considering positive signals detected over the total of samples in each group.

At this point, and according to the data respecting to the rationally designed peptides, only **P10** showed comparable sensitivity to proteins during the first

period with 25 %, reaching up to 45 % after 15 days PSO. No data can be extracted at the moment of the clinical specificity of these epitopes since this would require testing serum samples from patients suffering other respiratory infections.

A similar analysis was made with the samples from the cohort of the BioZgz. Comparable behavior with the previous group from HdMar was identified, attributing a stronger fluorescence intensity after a minimum of 10 or more days from the onset of symptoms. However, unlike the HdMar, in this cohort the samples taken between day 0 to 5 did not showed significant IgG response (see Figure 6.24). With the time, the intensity increased for all epitopes, being the S1 from SARS-CoV-2, the S1 Trimer, the NC-SARS2 and NC-SARS1 the proteins that showed the strongest signal, however the samples from HdMar did not react with the N from SARS-CoV. Also, the trimer did not play a role in that cohort. These data point at intrinsic cohort differences to be taken into account when interpreting the data.

From the Figure 6.24, a difference in response is detected between the epitopes S1-SARS2 giving high positive signal and S1-SARS1 that is almost undetectable. This last epitope corresponds to the S1 subunit from the SARS emerged in 2002 indicating that IgG response seems to be specific for the novel SARS-CoV-2 considering structural differences over S protein at least along this cohort.

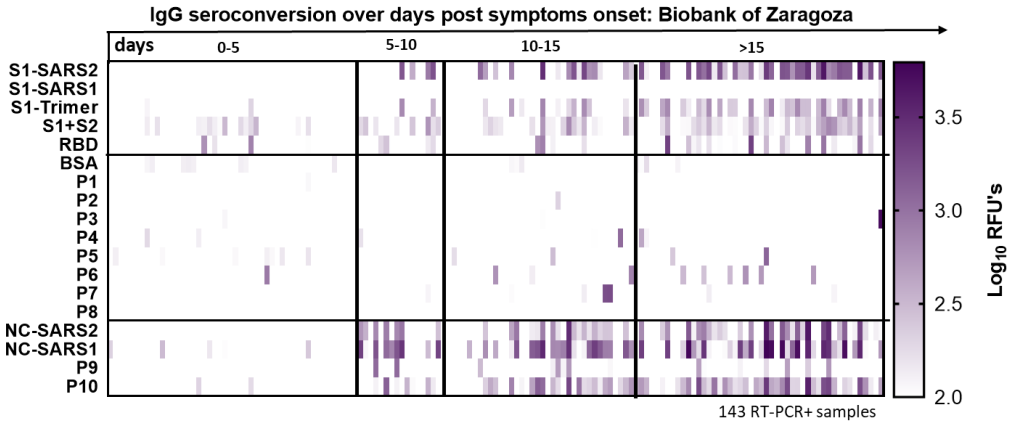

Figure 6.24 Landscape of IgG mediated response obtained from the analysis of 147 RT-PCR+ serum samples from BioZgZ distributed according to days PSO form serum collection date. The y-axis represents the individual epitopes printed in the microarray (viral peptides and proteins) while, the x-axis corresponds to the serum samples from patients with in clusters of days PSO. The intensity scale indicates the relative signal of antibody binding from 2 (white) to 3.8 (purple) in Log_{10} RFU's.

In line with this study, is possible to evidence the increasing trend of positive IgG response against S and N over time, reaching maximum sensitivity after 15 days PSO. These observations are in accordance with the normal distribution of IgG's reaching a plateau generally after day 20 [40]. In this cohort, a great clinical sensitivity was achieved by NC-SARS2 with 41 % in the frame of 5-10 days. After more than 15 days the S1-SARS2 reached almost 70 % sensitivity, being the most significant epitope from this group as evidenced in the next Figure 6.25.

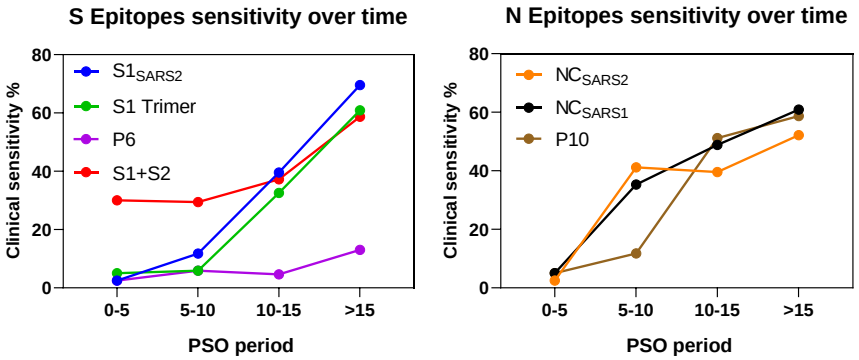

Figure 6.25 Clinical sensitivity of representative epitopes from BioZgz cohort according to the time PSO. The clinical sensitivity was estimated for S1-SARS2, S1-Trimer, P6 and S1+S2 as relevant epitopes from S protein and NC-SARS2, NC-SARS1 and P10 deriving from N protein. Each % was determined for the different time frames of days PSO, considering positive signals detected over the total of samples in each group.

Remarkably also in this cohort, **P10** is the only peptide sequence evidencing considerable sensitivity. Commencing with 5 % from day 0-5, but increasing over time to 11 % (5-10), 51 % (10-15) and 59 % (15-30). In respect to **P6**, the clinical sensitivity was also much lower with this set of patients, starting with 2.5 % on the first-time frame and then 6 % (5-10), 5 % (10-15) and 13 % (15-30).

During the evaluation of S proteins sensitivity, S1-SARS2 (69 %), S1+S2 (58 %) and S1-Trimer (60 %) showed the most remarkable values after 15 days PSO. On the other hand, the same analysis was carried out towards N epitopes. Both recombinant proteins NC-SARS2 and NC-SARS1 evidenced a similar sensitivity progression in the last time frame achieving 52 % and 60 % respectively. After comparing sensitivities against S and N epitopes over time with the cohort of BioZgz, is possible to infer that N proteins provide higher clinical sensitivity in early stages and S proteins with longer periods after the onset of symptoms.

In agreement with these results, **P10** showed consistent response and comparable with the recombinant proteins with less variability between patients. These findings suggest that **P10** is an excellent serological indicator to monitor IgG progression after viral infection over time comparable to S1-SARS2, S1+S2 and NC-SARS2. Additionally, a predominant immune behavior has been detected against epitopes like S1 Trimer or NC-SARS1 in the second cohort studied explaining potential differences between patient groups.

In summary, the correct determination of the sampling window results critical over antibody monitorization techniques and should be considered as a relevant factor in order to achieve precise and accurate detectability. According to *Whitman et al*., an ideal period of 18 to 20 days PSO provides accurate and robust IgG levels to perform serological studies minimizing unspecific responses or even lack of signal [41]. On the other hand, the global contribution of the epitopes under study could significantly increase the sensitivity obtained given the differences in response observed across the two cohorts. Due to this, integrated data analysis should be considered for future developments using samples after at least 10 days PSO.

6.2.7.2. Establishment of epitope classification rate with univariate analysis

Based on the signal obtained with the *Immuno*-µSARS2 chip, the individual epitope classification performance towards the differentiation between all the RT-PCR+ and prepandemic samples measured (see Figure 6.19 and Figure 6.21) was carried out using a univariate ranking analysis. For this analysis a training group of RT-PCR+ positive samples (80 % of the total) were measured together defining a positive threshold for each epitope, while a training group of prepandemic samples were used to establish the threshold for negative samples. After that, the rest of samples (test samples) were classified according to the pattern detected in blind conditions and the classification rate was plotted in the following Figure 6.26.

The potential utilization of a single epitope to classify a random sample as positive or negative (in respect to an ongoing or previous exposure to the virus) based on the fluorescent intensity detected was explored. In the next graph, from the 18 different epitopes and proteins studied only 6 displayed significant

individual classification rates and interestingly the best classifier was **P10** sequence leading over all the structural proteins such as S1-SARS2 and NC-SARS2 followed by S1-Trimer and NC-SARS1 with **P9** in the sixth place from all the samples. Is also remarkable that the only two peptides designed against N protein were good correlators while those sequences derived from S protein did not showed accurate performance suggesting higher immunogenicity over N epitopes rather than S epitopes. Nevertheless, the response detected over BSA epitopes was classified as non-significant with this model validating the platform specificity. This is also important because the peptide sequences were conjugated to BSA as carrier protein, therefore the signal detected over them is mostly attributed to the sequence rather than the albumin.

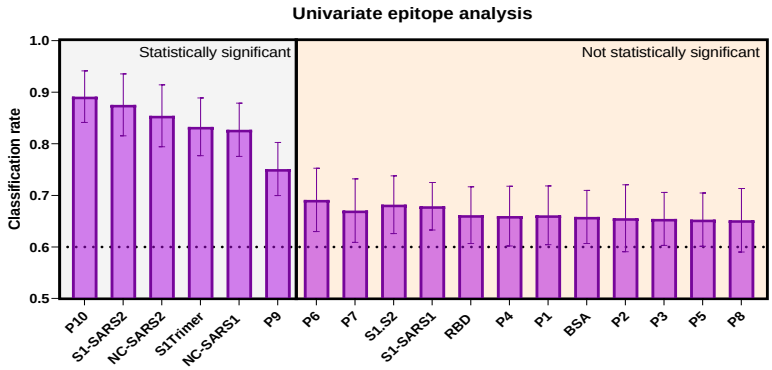

Figure 6.26 Epitope individual classification rate. From the samples measured, a univariate analysis was carried out to estimate the classification rate at individual epitope level to distinguish RT-PCR+ samples from pre-pandemic samples. Epitopes with more than 0.7 classification rate value were considered statistically significant predictors, while epitopes below this threshold were not assumed as statistically significant for this classification. The SD at epitopes classification rates were obtained from the values estimated from 394 human serum samples (298 RT-PCR+ and 96 pre-pandemic).

To summarize, the extensive work carried out to rationally define potential immunogenic sequences was crucial to end up with a first set of viral peptides that were further implemented in real samples. This approach demonstrates the relevance behind the combination of *in silico* studies and experimental data. The same principle can be applied to different pathogens in order to facilitate the selection of immunogenic candidate sequences based on aspects like antigenicity, accessibility, glycosylation pattern and chemical nature.

On the other hand, the analytical characterization of the platform was essential during the development of the proposed serodiagnostic tool. Allowing to

differentiate several immunization stages at IgM and IgG levels in rabbits, to translate that knowledge into human clinical samples. The high-throughput capacity of this system and relatively short time to answer facilitated the determination of the serologic profiles in more than 570 samples to define immunodominant regions amongst them. Aditionally, it was possible to monitor IgG progression over time from the onset of symptoms in separate cohorts and establish a clinical sensitivity value for some of the most relevant components of the microarray. From this study, seroprevalence discrimination could be considered using **P10** as ideal indicator of IgG response after SARS-CoV-2 exposure. However, viral proteins also demonstrated excellent performance, generally superior to the peptides selected, thus the idea to define highly immunogenic sequences should be further studied.

The next challenge would contemplate a new rational design based on consolidated evidence introducing bioinformatic tools to do so. In addition, another limitation was found on the individual evaluation of the epitopes conforming the chip and the intrinsic variability present in the samples under analysis suggesting that signal interpretation in multivariate approaches could offer a wider understanding of the complex interactions playing a role a patient level to discriminate profiles of IgG response instead of single epitope interactions.

6.3. CHAPTER CONTRIBUTIONS

Along this chapter the development of a multiplexed and high-throughput serologic microarray was defined contemplating several aspects like:

- The use of information gathered from *in silico* and experimental data, allowed the rational design of ten viral peptide sequences with potential immunogenic features during the beginning of the COVID-19 pandemic, circumventing the need of complex proteomic approaches.
- In rabbits, an increasing IgG response was induced after several immunizations with S and N proteins, reaching the higher titer with the third challenge, while significant IgM levels were detectable 18 days after the first immunization.

- Well-characterized rabbit antisera proved to be adequate positive control material during the development of the proposed platform, permitting a comparable transition to clinical samples.
- Although different antibody tests emerged during the pandemic, the establishment of a high-throughput serological microarray for IgG and IgM detection, combining 10 linear peptide sequences and 8 recombinant proteins form SARS-CoV-2 S and N regions was not widely explored. Also displaying adequate inter-well and inter-day reproducibility, lacking of sample pre-treatment and with a total assay time of 90 minutes.
- A clear differentiation based on the immunological response profile was observed in patients categorized as positives or negatives by RT-PCR, as well as prepandemic samples, in a total of 572 human serum samples.
- From three independent cohorts evaluated, a predominant IgG response towards N related epitopes was evidenced rather than S protein. Particularly **P10** and N recombinant proteins showed considerable immunogenicity.
- Progressive increase in IgG response was monitored from the onset of symptoms in clinical samples using the first version of the immunoarray. Antibodies against the N protein were identified earlier than anti-S antibodies.
- Proteins reached higher clinical sensitivity than the peptides tested individually over different time intervals PSO, with S1-subunit and N being the most significant. Specific IgG response was detectable after 10 days from the onset of symptoms.
- General differences in IgG profiles were observed amongst two independent cohorts (HdMar and BioZgz) attributing intrinsic variability to the healthcare provider institution.
- From 10 linear peptides evaluated, only **P10** showed comparable clinical sensitivity to proteins while performed as the most relevant epitope in rabbits. Additionally, **P10** was found to have the best classification rate with 89 % of accuracy differentiating PCR+ from prepandemic samples. Due to this, **P10** sequence is suggested as promising biomarker of seropositive conversion

6.4. MATERIALS AND METHODS

6.4.1. EQUIPMENT AND BUFFERS

The equipment utilized during this experimental work, was the same described in the previous chapters at material and methods section. MALDI-TOF-MS was used for bioconjugates characterization, pH-meter, conductimeter for buffer preparation. Spectrophotometer and plate washers for ELISA. The rest of equipment will be described if necessary.

Unless otherwise indicated, phosphate buffer saline (PBS) was 0.01 M phosphate buffer (1.48 mM KH_2PO_4 and 8.3 mM Na_2HPO_4) in a 0.8% saline solution (137 mmol/L NaCl, 2.7 mmol/L KCl), at pH 7.5. PBST is PBS previously described with 0.05% Tween 20. Dilution buffer is PBST with 0.5 w/v BSA at pH 7.5. Printing buffer is 10 mM PBS 10 (filtered 0.2um). Coating buffer is a 0.05 M carbonate-bicarbonate buffer pH 9.6. Citrate buffer is 0.04 M sodium citrate, pH 5.5.

6.4.2. PEPTIDES PREPARATION

6.4.2.1. Synthesis of peptide epitopes 1-10

The first generation of peptide epitopes (peptides **1-10**) were synthesized manually following the standard Fmoc/*t*Bu solid-phase strategy and using Fmoc-Rink Amide CM (0.50 mmol/g) as polymeric support. The resin was first conditioned using dimethylformamide (DMF, 3 x 1 min), dichloromethane (DCM, 3 x 1 min) and DMF (3 x 1 min). The Fmoc group was then removed by treating the resin with a solution of 20% piperidine in DMF (2 x 5 min) and the resin was washed with DMF and DCM. The C-terminal residue was incorporated by adding the Fmoc protected amino acid (3 equiv) together with N,N'-diisopropylcarbodiimide (DIC, 3 equiv) and ethyl cyanohydroxyiminoacetate (Oxyma, 3 equiv) in DMF for 1 h at rt. The peptide sequence was elongated performing cycles of Fmoc removal and coupling of the following amino acid. All the synthesized peptides were acetylated at the N-terminal end of the peptide. Acetylation was achieved by treating the peptidyl-resin with acetic anhydride

(Ac_2O, 10 equiv) and N,N-diisopropylethylamine (DIEA, 20 equiv) in DCM for 30 min at rt and followed by washing the peptidyl-resin with DCM (3 x 1 min), DMF (3 x 1 min) and DCM (3 x 1 min).

Cleavage of the peptide from the resin was achieved by treating the peptidyl-resin with a mixture of trifluoroacetic acid-triisopropylsilane-water (TFA:TIS:H_2O, 94:3:3, v/v/v) for 2.5 h. The solution was filtered and the peptide was precipitated by the addition of the TFA solution onto cold diethylether (Et_2O). The precipitate was centrifuged, and the supernatant was discarded. The peptide was washed twice with Et_2O, dissolved with water-acetonitrile and lyophilized.

All the peptides were purified using a semi-preparative high-performance liquid chromatography (HPLC). Crudes and purified peptides were analyzed by HPLC using a XBridge BEH130 column (4.6 x 100 mm, 5 µm) and a linear gradient of acetonitrile (0.036% TFA) in water (0.045% TFA) in 8 min and a flow rate of 1.0 ml min^{-1} and HPLC-MS using a XSelect C18 column (4.6 x 50 mm, 3.5 µm) and a linear gradient of 5-100% of acetonitrile (0.07% HCOOH) in water (0.1% HCOOH) in 3.5 min and a flow rate of 1.0 ml min^{-1}. Purity was determined by HPLC (UV).

6.4.2.2. Peptide BSA conjugates protocol

A BSA dilution was prepared at 10 mg mL^{-1} in 10 mM PBS buffer (30 mg in 3 mL^{-1} 10 mM PBS). Then, 2.08mg of BMPS (N-β-maleimidopropyl-oxysuccinimide ester) were diluted in 100 µL DMF (dimethylformamide). The BMPS solution was added dropwise over the BSA solution and left for 1 hour at room temp and overnight at 4°C under stirring. The following day, BMPS conjugated BSA was purified in ÄKTA Prime Plus using 2 HiTrap desalting columns both from GE Healthcare (Chicago, IL, USA) at a 1mL/min in 10 mM PBS buffer

The molar ratio of BSA-linker and peptides was established at 1:15. Then, peptides were reconstituted in ultrapure water (MiliQ H_2O) and hydrophobic peptides were resuspended in a mixture of ACN:H_2O. Simultaneously, 100 µl of tris(2-carboxyethyl) phosphine (TCEP) solution at 1,3mg/ml were added over resuspended peptides for 10 min at 37°C. Then, peptide and TCEP solution was added dropwise over BSA-linker solution and left 1-hour under stirring at R.T and O.N. at 4°C.

Finally, peptide conjugates were purified by dialysis against 0.5 mM PBS (4 × 5 L) and MiliQ water (1 × 5 L) and then freeze dried. Afterwards, each peptide was resuspended to a 1 mg mL^{-1} stock in 10 mM PBS and then separated in aliquots of 100 µl stored at -20°C until use. The table 6.4 summarize the peptide densities obtained per molecule of BSA determined by MALDI-TOF-MS following the same protocol already used for BSA conjugates characterization in chapter 3.

6.4.2.3. Final protein and peptide-BSA conjugates concentrations

Epitopes concentrations were optimized with a standard serum to minimize background noise and non-specific adsorptions. All dilutions were prepared in printing buffer and then subsequently dispensed over derivatized glass slides. The epitope RBD_1 was provided by collaborators from the National Center of Biotechnology in Madrid and due to the less selective detection in comparison with the RBD_2 acquired from RayBiotech, was removed from the final matrix. The following Table 6.5 expresses the final concentrations employed for the deposition of the corresponding reagents in the microarray chip considering slight modifications according to individual performance of the proteins once implemented in the matrix.

Table 6.5 Protein immobilization conditions over microarray chip and commercial source or reagents

Protein epitope	Concentration (μg mL^{-1})	Commercial source	Protein epitope	Concentration (μg mL^{-1})	Commercial source
S1-SARS2	12.5	Acro Biosystems (S1NC52H3)	NC-SARS1	6.25	Native Antigen
S1-SARS1	12.5	Native Antigen	Peptide-BSA	500	In-house
S1-Trimer-SARS2	64	Protein Production Platform, UAB	IgG from Human serum	50	Sigma-Aldrich (I4506)
RBD_2	20	RayBiotech (HEK)	IgM from Human serum	5	Sigma-Aldrich (I8260)
BSA	500	Sigma-Aldrich	Rabbit PAb to Human IgG (TRITC)	5	ABCAM (ab6756)
NC-SARS2	6.25	Acro Biosystems	Rabbit PAb to Human IgM (Alexa fluor 647)	5	ABCAM (ab150191)

6.4.3. FLUORESCENT SEROLOGICAL ARRAY PRODUCTION

6.4.3.1. Microarray printing

The same derivatization protocol utilized in the Chapter 3 and 4 was utilized in this experimental work. The optimized concentration of recombinant proteins utilized in the multiplexed matrix are expressed in Table 6.5. Peptide conjugates dilutions were prepared at 500 μg mL^{-1} (final volume of 100 μl) in printing buffer**.** The deposition was performed using an automated piezo-driven SciflexArrayer S3-Scienion AG spotter (Scienion AG, Berlin, Germany). For this approach a piezo dispense capillary (PDC) 70 type 4 (voltage 86 V and pulse width 49 μs) was employed. After optimization studies (data not showed), 5 drops of 350pL were deposited per spot at 25^{o}C and 60 % humidity, drying for 1 hour at R.T and then kept at 4^{o}C until use for a maximum of five days.

Over each glass slide, 24 independent arrays (matrix 6x11) including 22 epitopes in three replicate spots were printed. The matrix size was adjusted to fit with the dimensions of the ArrayIt® holder (Arrayit Corp, Sunnyvale, CA, USA) utilized for simultaneous samples analysis.

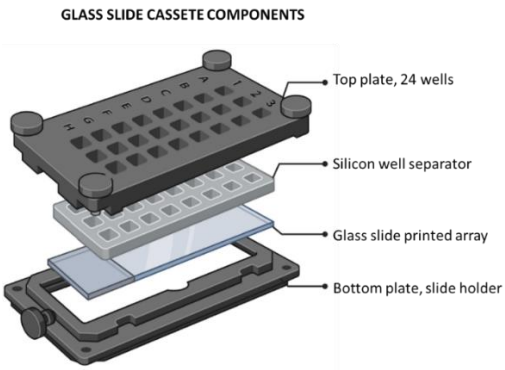

Figure 6.27 Scheme of the single glass slides holder components. The ArrayIt® gasket was utilized to generate 24 independent sub-microarrays allowing simultaneous determinations.

6.4.3.2. Immunoarray standard assay protocol

The standard microarray protocol applied for all the determinations performed across the work presented with this approach consisted in the following procedure:

The assay protocol includes an initial wash with 200 µl/well of 10 mM PBST to then perform the incubation of 10 µl of human serum sample or rabbit antisera, with 40 µl of dilution buffer consisting on 10 mM PBST containing 0.5% BSA per well for 60 minutes. After that, three washes with 200 µl/well of 10 mM PBST were carried out followed by the addition of 100µl of the fluorescently labelled secondary antibodies.

A distinction regarding the use of different secondary antibodies is considered in the case of serum samples from rabbits like As410 or As414, Goat PAb anti-rabbit-IgG-(Alexa fluor 555) from Abcam was used in 1/250 dilution in 10 mM PBST buffer and Goat PAb anti-rabbit-IgM - (Alexa fluor 647) at 1/500 dilution were employed. When the immunoarray was assessed over human serum samples anti-human IgG and IgM (Rabbit PAb to Human IgG (TRITC) at 1/500 and Rabbit PAb to Human IgM (Alexa fluor 647) at 1/250 both purchased from ABCAM, were incubated for additional thirty minutes. After a final washing step with 3 x 200 µl/well of 10 mM PBST and one wash with MiliQ H_2O, slides were dried under N_2 stream.

Internal Quality controls were performed in each slide, by designating two wells (from the 24 available) to incubate the matrix with 10 µl of blank human serum samples (Sigma, H4522) and calculate average fluorescence for each epitope in blank serum.

6.4.3.3. Signal acquisition

For signal acquisition, the spots were measured by deducting the mean fluorescent background intensity to the mean of fluorescent foreground intensity using a two-colour microarray scanner InnoScan 710, (Innopsys, Carbonne, France) at different wavelengths simultaneously (555 nm for IgG determination and 647 nm for IgM detection). Mapix analysis software *V 7.4.0* (Innopsys Inc., Carbonne, France) was employed for slide signal acquisition under following conditions: 555 nm channel (green, IgG) Gain=3, Power Low 5mW and 647 nm channel (red, IgM) Gain=10, Power Low 5mW. Excel tables were generated and predesigned templates utilized to assign intensity values to the respective epitopes calculating the mean fluorescence of 3 replicate spots + 2SD.

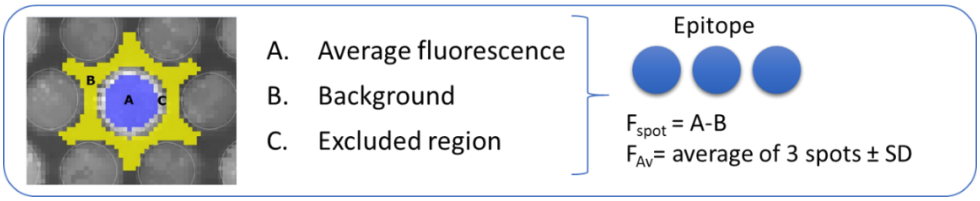

Figure 6.28 Representation of spot signal acquisition using Mapix Software by deducing background signal (B) from the average spot intensity (A) excluding edging fluorescence (C).

Then GraphPad Prism V 8.5.0 (GraphPad Software Inc., San Diego, CA, USA) was used to generate heatmaps showing the intensity of the group of slides per analysis in every sample and for every epitope.

6.4.4. EXPERIMENTAL DESCRIPTION

6.4.4.1. ELISA assays for the different rabbit's antisera

The microtiter well plates from Nunc (Maxisorp, Roskilde, Denmark) were coated with S1-SARS2, RBD and NC-SARS2 proteins at 0.5 µg mL^{-1} in triplicate wells using

coating buffer (100µl/well), incubated overnight 4°C. The following day, the microplates were washed four times with 300 µL/well of PBST. Then, different antisera collected during the first immunization (B0, B16, B1+12 and B1+18) of the three rabbits for S (409,410 and 411) and the three rabbits for N (412, 413, 414), were diluted 1/2000 in PBST and incubated for 60 minutes. After a washing step, 100 µl of a solution of anti-mouse IgG HRP (1/6000) in PBST was added and left for 30 min. Afterwards 100 µl of the substrate solution (citrate solution, 0.0004% H_2O_2 and 0. 375 µg mL^{-1}TMB) were added for 30 min, covered from light. The colorimetric reaction was stopped with 50µl/well of 4 M H_2SO_4 and absorbance was measured at 450 nm.

6.4.4.2. Optimization of protein and peptide-BSA conjugates concentration

The determination of the most suitable protein concentration was carried out printing a matrix of 6 columns per 7 rows, including 5 drops per spot. The protein solutions were prepared at three different concentrations 100, 50, 25 µg mL^{-1} and spotted in triplicate with the exception of the positive control row including 6 drops of CTR+As S at 10 µg mL^{-1}. Then standard microarray procedure was applied with the corresponding CTR+As S to assess the optimum protein concentration response with secondary labelled anti rabbit IgG antibodies.

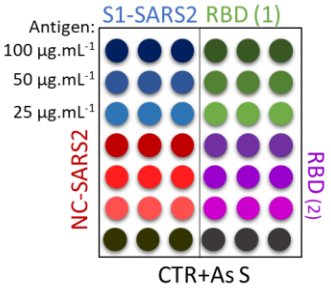

Figure 6.29 Microarray matrix utilized to select the optimum protein concentration.

For the peptide concentration determination, two different arrays were generated using 1 and 0.5 mg mL^{-1} of peptide-BSA conjugates solutions, dispensing 5 drops per spot in triplicates. After that the slides were incubated with CTR+As S and N samples at 1/2000 dilution in 10mM PBST for IgG's and samples from B1+18 (As410 and As414) were prepared at 1/100 dilution in 10

mM PBST. Then, standard assay protocol was applied using secondary labelled anti-rabbit IgG antibodies. The microarray templates utilized for this purpose are represented in the following image.

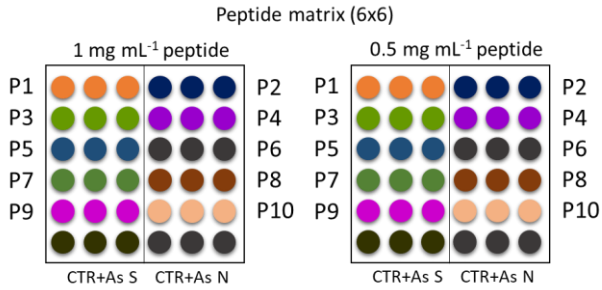

Figure 6.30 Microarray matrix utilized to select the optimum peptide concentrations.

6.4.4.3. Blocking agent's evaluation

Continuing with the already described chip, the incorporation of a blocking step to the assay protocol for thirty minutes prior the incubation with the sample was assessed. In this case 3 independent chips were incubated with 100 µl/well of the same blocking solution. After 30 minutes a washing procedure using 200 µl/well of 10 mM PBST for three times was performed to remove excess of blocking solution. After that, the chips were incubated with a different solution of As410 from B0 (1/100), B1+18(1/100) and B3 (1/2000) in 10mM PBST for one hour. Then the assay was carried out as described in the standard protocol procedure (section 6.5.3.2).

The blocking solutions were prepared under the following conditions. 1% (w/v) Gelatin in 10 mM PBS. using gelatin from cold water fish skin acquired from Sigma (St. Louis, USA). Then 2%(w/v) BSA in 10mM PBS solution making use of Bovine Serum Albumin Lyophilized Sigma (St. Louis, USA). Also 2% (w/v) of Skim Milk Powder from Milipore (Merck KGaA, Darmstadt, Germany) in 10mM PBST and polyethylene glycol 6.000 (PEG6000) at 2% w/v in 10mM PBST (Thermo Scientific, Massachusetts, USA). For, PVP (Polyvinylpyrrolidone) 2% (w/v) solution the use of PVP from Sigma (St. Louis, USA) was required. Casein 0.15% blocking solution was generated using Casein from Sigma (St. Louis, USA) for the stock 1% (w/v) in NaOH 1 N and then diluted to 0.15% (v/v) in 10 mM. PBS And finally, PVA 2% (w/v) in 10 mM PBS prepared using (Poly(vinyl alcohol) Mw

9,000–10,000, 80% hydrolyzed from Sigma-Aldrich, (cat. no. 360627-25G, St. Louis, USA)

For the study of BSA as additive in the assay buffer the predefined matrix configuration (6x9) was used in this case following the standard experimental procedure initially described without blocking step. For this study, different solutions of As410 and As414 were prepared changing the dilution buffer. For this B0 (1/100), B1+18 (1/100) and B3 (1/2000) were diluted in 0.5% (w/v), 1% (w/v), 2% (w/v) BSA in 10mM PBST and with PBST 10mM as control. Different arrays were utilized. Images were acquired in the fluorescent scanner and analyzed in mapix software.

6.4.4.4. Immune response progression after different immunizations

A matrix consisting on 6 columns and 9 rows was proposed for the final assignment of the epitope array including peptides and proteins under optimized conditions. Peptides solutions were prepared at 500 µg mL^{-1} in 10mM PBS and proteins concentration were expressed in the previously described table and were also diluted in 10 mM PBS for the immobilization. In the following scheme the distribution of the epitopes in the matrix is represented.

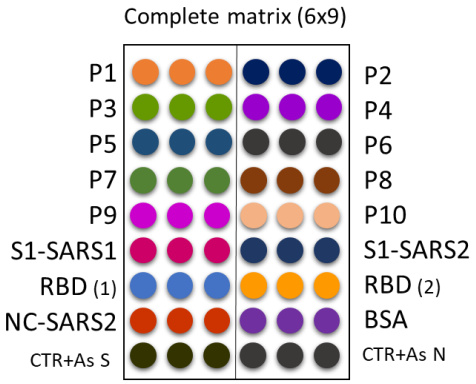

Figure 6.31 Schematic representation of the optimized matrix combining peptides and proteins with control solutions.

Then, four antisera (B0, B1+18, B2 and B3) collected during the immunization period of the animals with S protein As410 and N protein As414 were incubated with the hybrid protein peptide matrix. Respective antisera were diluted 1/2000

in 10 mM PBST for IgG determination and in a separate well IgM's were detected considering dilution of 1/100 after an incubation of one hour Afterwards, fluorescent detection was performed as described in the standard protocol.

6.4.4.5. Matrix effect in commercial human serum samples

The same matrix (6x9) including all the epitopes of the first array-generation was utilized to monitor human serum effect. In this regard, two dilutions of commercial Human Serum (HS) from Merck, were prepared at 1/2 and 1/5 in 10 mM PBST 0.5% BSA with additional solutions of undiluted HS and 10 mM PBST-BSA as control buffer. The corresponding solutions were spiked with CTR+As and N at 1/2000 for IgG's and 1/100 for IgM's estimation in a final volume of 100 µl/well and were incubated for a period of one hour, subsequently following the already described protocol.

6.4.4.6. Control of the surface biofunctionalization with purified polyclonal antibodies

The corresponding As410 and As414 from B3 were purified by affinity chromatography using a HiTrap Protein A HP column, eluted with 0.1 M Gly-HCl at pH 2.7 and stored in PBS adjusting the pH of the fractions collected to 7.4. Storage aliquots were prepared at 1 mg mL^{-1} stored at -20^{o}C until use.

One slide from the 20 prepared in the corresponding batch was incubated with the CTR+Ab S and CTR+Ab N at three different concentrations of 100, 25 and 5 µg mL^{-1} in PBST-BSA 0.5% (w/v) following the standard assay protocol already described and using anti rabbit IgG or IgM- labelled antibodies. Fluorescence detected in different wells was compared as inter chip variability. In the same line, inter day variability was assessed by comparing the signal obtained after different experiments following the already mentioned procedure performed in different days and over different slides from different batches considering the incubation of the microarray with 100 µg mL^{-1} of CTR+Ab S and CTR+Ab N.

6.4.4.7. Serum samples analysis

All human serum samples were obtained with the corresponding ethical committees' approval established in Spain (Law 14/2007, 3rd of July, of Biomedical Research) with the consent of enrolled patients for research purposes. As received, working aliquots were prepared to avoid defrizzing cycles and the samples were stored at -80°C.

All human serum samples were handled under P2 biosafety level laboratory. Three cohorts of samples were provided by different healthcare institutions of Spain with relevant clinical data regarding disease progression. The samples were collected during the period between 01/05/2020 to 01/08/2020 assuming the prevalence of Wuhan variant and first viral exposure in those individuals. Each group of samples was classified through quantitative RT-PCR in positive or negative groups with an additional prepandemic samples cohort obtained from healthy donors during the first months of 2019.

The following table 6.6, shows the final selection of samples analyzed and the distribution according to RT-PCR result and prepandemic condition, as well as clinical outcomes. Although a total of 755 samples were collected, for the initial determination only 572 were utilized.

Table 6.6 Distribution of clinical serum samples analyzed using RT-PCR method classification and separated according to the healthcare provider institution.

Cohort	**Sample group**		
	RT-PCR **+**	RT-PCR **-**	Prepandemic
BioZgz	143	-178	-
HUGTIP	81	-	-
HdMar	94	-	96

All samples analyzed were detected utilizing the standard assay protocol described and the subsequent analysis were performed using GraphPad Prism v 8.5.0.

6.5. BIBLIOGRAPHY

1. GDR, H.B., N. Sharon, and E.W. Australia, *Nomenclature and symbolism for amino acids and peptides.* Pure and Applied Chemistry, 1984. **56**: p. 595-624.
2. Wang, L., et al., *Therapeutic peptides: Current applications and future directions.* Signal Transduction and Targeted Therapy, 2022. **7**(1): p. 48.
3. Karoyan, P., et al., *Human ACE2 peptide-mimics block SARS-CoV-2 pulmonary cells infection.* Communications biology, 2021. **4**(1): p. 197.
4. Kalita, P., et al., *Design of a peptide-based subunit vaccine against novel coronavirus SARS-CoV-2.* Microbial Pathogenesis, 2020. **145**: p. 104236.
5. Xie, J., et al., *Characteristics of patients with coronavirus disease (COVID-19) confirmed using an IgM-IgG antibody test.* Journal of medical virology, 2020. **92**(10): p. 2004-2010.
6. Holenya, P., et al., *Peptide microarray-based analysis of antibody responses to SARS-CoV-2 identifies unique epitopes with potential for diagnostic test development.* European journal of immunology, 2021. **51**(7): p. 1839-1849.
7. Hotop, S.-K., et al., *Peptide microarrays coupled to machine learning reveal individual epitopes from human antibody responses with neutralizing capabilities against SARS-CoV-2.* Emerging microbes & infections, 2022. **11**(1): p. 1037-1048.
8. Wang, H., et al., *SARS-CoV-2 proteome microarray for mapping COVID-19 antibody interactions at amino acid resolution.* ACS Central Science, 2020. **6**(12): p. 2238-2249.
9. Li, Y., et al., *Systematic evaluation of IgG responses to SARS-CoV-2 spike protein-derived peptides for monitoring COVID-19 patients.* Cellular & Molecular Immunology, 2021. **18**(3): p. 621-631.
10. Mishra, N., et al., *Immunoreactive peptide maps of SARS-CoV-2.* Communications Biology, 2021. **4**(1): p. 225.
11. Schwarz, T., et al., *SARS-CoV-2 proteome-wide analysis revealed significant epitope signatures in COVID-19 patients.* Frontiers in Immunology, 2021. **12**: p. 629185.
12. Yan, X., et al., *Anti-SARS-CoV-2 IgG levels in relation to disease severity of COVID-19.* Journal of medical virology, 2022. **94**(1): p. 380-383.
13. Lynch, K.L., et al., *Magnitude and kinetics of anti–severe acute respiratory syndrome coronavirus 2 antibody responses and their relationship to disease severity.* Clinical Infectious Diseases, 2021. **72**(2): p. 301-308.
14. Ibarrondo, F.J., et al., *Rapid decay of anti–SARS-CoV-2 antibodies in persons with mild Covid-19.* New England Journal of Medicine, 2020. **383**(11): p. 1085-1087.
15. Plūme, J., et al., *Early and strong antibody responses to SARS-CoV-2 predict disease severity in COVID-19 patients.* Journal of Translational Medicine, 2022. **20**(1): p. 176.
16. Amrun, S.N., et al., *Linear B-cell epitopes in the spike and nucleocapsid proteins as markers of SARS-CoV-2 exposure and disease severity.* EBioMedicine, 2020. **58**: p. 102911.

17. Jiang, H.-W., Y. Li, and S.-C. Tao, *SARS-CoV-2 peptides/epitopes for specific and sensitive diagnosis.* Cellular & Molecular Immunology, 2023. **20**(5): p. 540-542.
18. Watanabe, Y., et al., *Site-specific glycan analysis of the SARS-CoV-2 spike.* Science, 2020. **369**(6501): p. 330-333.
19. Walls, A.C., et al., *Structure, function, and antigenicity of the SARS-CoV-2 spike glycoprotein.* Cell, 2020. **181**(2): p. 281-292. e6.
20. Tilocca, B., et al., *Comparative computational analysis of SARS-CoV-2 nucleocapsid protein epitopes in taxonomically related coronaviruses.* Microbes and infection, 2020. **22**(4-5): p. 188-194.
21. Wagner, A., et al., *Neutralising SARS-CoV-2 RBD-specific antibodies persist for at least six months independently of symptoms in adults.* Communications Medicine, 2021. **1**(1): p. 13.
22. Zheng, M. and L. Song, *Novel antibody epitopes dominate the antigenicity of spike glycoprotein in SARS-CoV-2 compared to SARS-CoV.* Cellular & molecular immunology, 2020. **17**(5): p. 536-538.
23. Guevarra Jr, L.A. and G.E.L. Ulanday, *Immune Epitope Map of the Reported Protein Sequences of Severe Acute Respiratory Syndrome Coronavirus 2 (SARS-CoV-2).* 2020.
24. Grifoni, A., et al., *A sequence homology and bioinformatic approach can predict candidate targets for immune responses to SARS-CoV-2.* Cell host & microbe, 2020. **27**(4): p. 671-680. e2.
25. Kumar, S., et al., *Structural, glycosylation and antigenic variation between 2019 novel coronavirus (2019-nCoV) and SARS coronavirus (SARS-CoV).* Virusdisease, 2020. **31**: p. 13-21.
26. Musicò, A., et al., *SARS-CoV-2 epitope mapping on microarrays highlights strong immune-response to N protein region.* Vaccines, 2021. **9**(1): p. 35.
27. Li, Y., et al., *Linear epitopes of SARS-CoV-2 spike protein elicit neutralizing antibodies in COVID-19 patients.* Cellular & molecular immunology, 2020. **17**(10): p. 1095-1097.
28. Wrapp, D., et al., *Cryo-EM structure of the 2019-nCoV spike in the prefusion conformation.* Science, 2020. **367**(6483): p. 1260-1263.
29. Bai, Z., et al., *The SARS-CoV-2 nucleocapsid protein and its role in viral structure, biological functions, and a potential target for drug or vaccine mitigation.* Viruses, 2021. **13**(6): p. 1115.
30. Li, Y., D.-y. Lai, and S.-c. Tao, *SARS-CoV-2 spike linear epitope scanning via a peptide microarray through sera profiling.* STAR protocols, 2021. **2**(3): p. 100707.
31. Li, S., et al., *The epitope study on the SARS-CoV nucleocapsid protein.* Genomics, proteomics & bioinformatics, 2003. **1**(3): p. 198-206.
32. He, Y., et al., *Mapping of antigenic sites on the nucleocapsid protein of the severe acute respiratory syndrome coronavirus.* Journal of clinical microbiology, 2004. **42**(11): p. 5309-5314.
33. Weber, J., H. Peng, and C. Rader, *From rabbit antibody repertoires to rabbit monoclonal antibodies.* Experimental & molecular medicine, 2017. **49**(3): p. e305-e305.

34. Khan, S.R., et al., *Determinants of serum immunoglobulin levels: a systematic review and meta-analysis.* Frontiers in immunology, 2021. **12**: p. 1103.
35. Gattinger, P., et al., *Neutralization of SARS-CoV-2 requires antibodies against conformational receptor-binding domain epitopes.* Allergy, 2022. **77**(1): p. 230-242.
36. Schneider, J., et al., *SARS-CoV-2 serology increases diagnostic accuracy in CT-suspected, PCR-negative COVID-19 patients during pandemic.* Respiratory Research, 2021. **22**: p. 1-10.
37. Long, Q.-X., et al., *Antibody responses to SARS-CoV-2 in patients with COVID-19.* Nature medicine, 2020. **26**(6): p. 845-848.
38. Ma, H., et al., *Serum iga, igm, and igg responses in covid-19.* Cellular & molecular immunology, 2020. **17**(7): p. 773-775.
39. Burbelo, P.D., et al., *Sensitivity in detection of antibodies to nucleocapsid and spike proteins of severe acute respiratory syndrome coronavirus 2 in patients with coronavirus disease 2019.* The Journal of infectious diseases, 2020. **222**(2): p. 206-213.
40. Isho, B., et al., *Persistence of serum and saliva antibody responses to SARS-CoV-2 spike antigens in COVID-19 patients.* Science immunology, 2020. **5**(52): p. eabe5511.
41. Whitman, J.D., et al., *Evaluation of SARS-CoV-2 serology assays reveals a range of test performance.* Nature biotechnology, 2020. **38**(10): p. 1174-1183.

7. *Immuno*-μSARS2 V2.0 CHIP COUPLED TO ARTIFICIAL INTELLIGENCE FOR PERSONALIZED ANTIBODY PROFILING AND DISEASE SEVERITY PREDICTION

7.1. SUMMARY

This chapter describes the updates and improvements performed with the microarray chip described on chapter 6 to achieve what we have called the *Immuno*-µSARS v2.0. The new platform includes additional peptide epitopes (total of 35 peptide epitopes and proteins) resulting also from a rational design aiming at increasing the power of the chip as a tool for better understanding of the implication of the adaptive immunity in the disease and convalescent patients. The complete collection of 755 human serum samples were analyzed with the updated version of the microarray chip for immunological profiling of IgG's and IgM's. The chapter reports the integration of the large data generated with biostatistical analysis to define diagnostic performance of the v 2.0 version and establishing correlations focusing on IgG mediated signatures recorded and disease severity.

For the biostatistical analysis and signal interpretation procedure, a collaboration with the group of Signal and Information Processing for Sensing Systems leaded by Prof. Santiago Marco Colás (Institute of Bioengineering of Catalonia) was established. The experimental analysis was carried out by Marc Alorda under supervision of Agustin Gutierrez, PhD. and Prof. Santiago Marco Cólas, respectively.

It should also be noticed that the research work reported in this chapter has been performed after the rushing period at the beginning of the pandemic during which a large part of the work of this part II of the thesis was carried out, seeking to be able to provide solutions to the global emergency that we were addressing. For this reason, some of the factors and parameters that affect chip development, and that should have been studied during the development of v1.0, were addressed during the development of this new version of the chip.

7.2. INTRODUCTION

7.2.1. APPROACHING SERODIAGNOSTIC WITH MUTIPLEXED PLATFORMS AND COMPUTATIONAL ANALYSIS

During COVID-19 pandemic, the critical need for accurate and reliable diagnostic tools to identify the virus and predict clinical progression was highlighted. From a medical perspective, the decision-making process behind patient's hospitalization or ICU admission requires consideration of several clinical manifestations that sometimes lead to irreversible conditions. Due to this, early and precise diagnostic is crucial to ensure better prognosis. Consequently, the development of effective detection platforms capable to anticipate and predict potential clinical outcomes have gained attention and is nowadays a major goal in diagnostic trends [1].

On the other hand, determination of the immunological signatures resulting from SARS-CoV-2 infection was contemplated as a promising an interesting strategy to understand disease severity and potentially predict clinical progression (see Figure 7.1). For instance, the use of Luminex technology to identify serologic fingerprints towards S and N proteins showed that convalescent individuals exhibited stronger immunity against the spike glycoprotein, while considerable nucleocapsid response was more prevalent among those with worst prognosis [2].

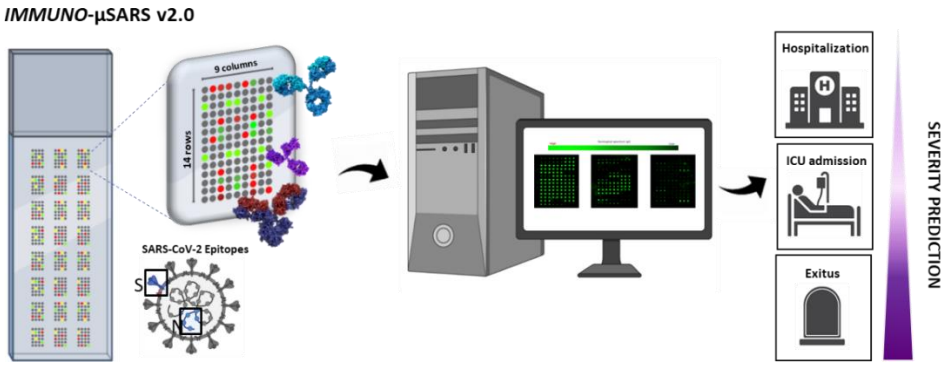

Figure 7.1 Schematic representation of the immunoarray determination integrated with bioinformatic analysis to predict disease severity based on IgG response.

Besides, phage display technology was implemented for epitope characterization studies generating viral peptide fragments (50-20 aa) to assess antibody mediated response against SARS-CoV-2 proteome. Interestingly, the authors state that higher prevalence of antibodies against the S2 subunit and N proteins are found over severe cases, while also associate stronger immune responses on men rather than women. In this work, the concept of "private" epitopes only recognized by limited patients and "public" epitopes detected in several clinical samples was proposed for further analysis [3].

Moreover, the interdependence of environmental and genetic factors along with life habits were pointed out as determinant features over the course of infection and the adequate immune response development [4]. Bearing in mind that the samples analyzed during the current experimental work were provided by healthcare institutions from Catalonia and Aragon, a seroprevalence study conducted in Catalonia revealed lower levels of total antibodies in asymptomatic patients compared to those requiring hospitalization or ICU admission [5]. Throughout this report an increased IgG response in severe outcomes was highlighted in contrast with IgA levels also monitored. Furthermore, the identification of a slight trend towards stronger anti-S responses in severe cases rather than N was elucidated.

Serological methods may provide accurate data at epidemiological scale and this was demonstrated in a study enrolling more than 60.000 Spanish individuals during the period between April 27th to May 11th, 2020. They were contacted and provided with PoC devices for self-determination of antibodies against SARS-CoV-2 and the results indicated that by that moment the seroprevalence estimated in Spain was around 5 % (95% CI 4·7–5·4) rising the alarm to the authorities and healthcare systems. During the following months, several outbreaks mainly caused by the emergence of new variants were reported and the correct implementation of immunological tools could have been useful to lay down political decisions [6].

Diagnostics is moving towards a new scenario in which molecular signatures will be used to interpret the disease, rather than single biomarkers. The research performed in this PhD thesis has been moving in that direction, in respect to the use of immunological data. The recent incorporation of bioinformatics tools over novel diagnostics strategies emerged to identify specific biomarkers in a faster

and accurate manner as well as define patterns based on clinical data to eventually anticipate disease progression. The outstanding potential behind the synergy of these approaches will be shaping forthcoming diagnostic developments.

7.3. RESULTS AND DISCUSSION

7.3.1. EXPERIMENTAL PROPOSAL

The same protocols already described in Chapter 6 were also used in the present chapter for peptide bioconjugation and glass slides functionalization. Remarkably, the incorporation of 18 new peptide sequences on the chip, followed by the evaluation and implementation to the analysis of clinical samples coupled to bioinformatic tools for extensive data interpretation is reported for the updated version 2.0 of the *Immuno*-µSARS2 chip.

The initial design and characterization of original 1.0 version was carried out during the first period of the pandemic to meet the need of detection tools with immediate application in the diagnostic field. At this point, limited knowledge regarding the structure and behavior of the virus was available. Then, lateral flow immunoassays (LFIAs) were rapidly proposed to develop antigen and antibody tests, so-called "Rapid Test", due to their inexpensive requirements, fast response (15-20 mins.) and user-friendly configurations. However, their implementation was restricted to qualitative interpretations. In contrast, our novel immunoarray chip was designed with the intention to provide a personalized immune profile data that could allow explaining the wide variety of individual responses to the virus and, if possible, assisting clinicians on predicting disease outcome. For this purpose, a technology endowed with high sample processing capacity, competence for delivering large amount of information and possibility for integrating suitable algorithms specifically developed for data interpretation was required (see Figure 7.2).

.

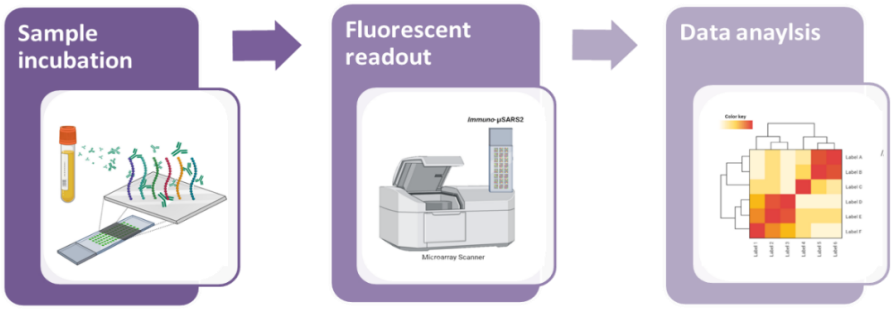

Figure 7.2 Experimental workflow to perform simultaneous analysis using the proposed immunoarray. Starting from serum sample incubation on the epitope matrix, to then quantify spots signals using a fluorescent readout system and finally establish potential correlations with bioinformatic tools.

In terms of months, an increasing amount of new evidence and information started to be reported and several diagnostic platforms became commercially available. The emergence of new variants of concern (VoC's) and the differences observed in clinical progression were highlighted as the next challenges to address with novel detection strategies. In this regard, the incorporation of additional peptide epitopes to identify the new VoC's to the array were proposed. Moreover, the necessity of implementing the chip with machine learning techniques became fundamental for our intention to define immunological signatures associated to different clinical outcomes with the idea to facilitate the decision-making process at clinical stages. Nowadays, relevant evidences suggest that the role of the immune system seems to be determinant to successfully course COVID-19 [7, 8].

7.3.2. EXPERIMENTAL UPDATES AND IMPROVEMENTS OF THE *IMMUNO*-µSARS2 CHIP V 2.0

7.3.2.1. Rational design of new immunogenic peptide epitopes

Considering performance of the *Immuno*-µSARS2 v 1.0 and the emergence of VoC's worldwide a set of additional 18 peptide epitopes were selected, synthesized and conjugated to BSA aiming to enhance the power of the chip. For

this purpose, extensive literature analysis of suggested immunodominant epitopes was conducted, bearing also in mind the low response recorded for the S derived peptides. In addition, the use of a B cell epitope predictor, BepiPred-2.0 software, was implemented to support our selection with the identification of other potential epitope candidates. The software uses information related to protein sequences and spatial arrangement, and the analysis was conducted increasing the epitope threshold (relation of the sensitivity/specificity of the prediction method) from 0.5 (default) to 0.6 favoring sequence specificity [9]. The on-line tool uses a random forest algorithm that has been trained on both, epitopes and non-epitope amino acids from crystal structures considering helix (H, pink), sheets (E, blue) and random coil (C, orange) configurations across the protein as well as accessible and non-accessible regions. Using this tool, the complete sequences of S (Uniprot, P0DTC2) and N (Uniprot, P0DTC9) proteins were analyzed. In Figure 7.3 the panel of peptides selected is represented over the sequence according to the target amino acid region.

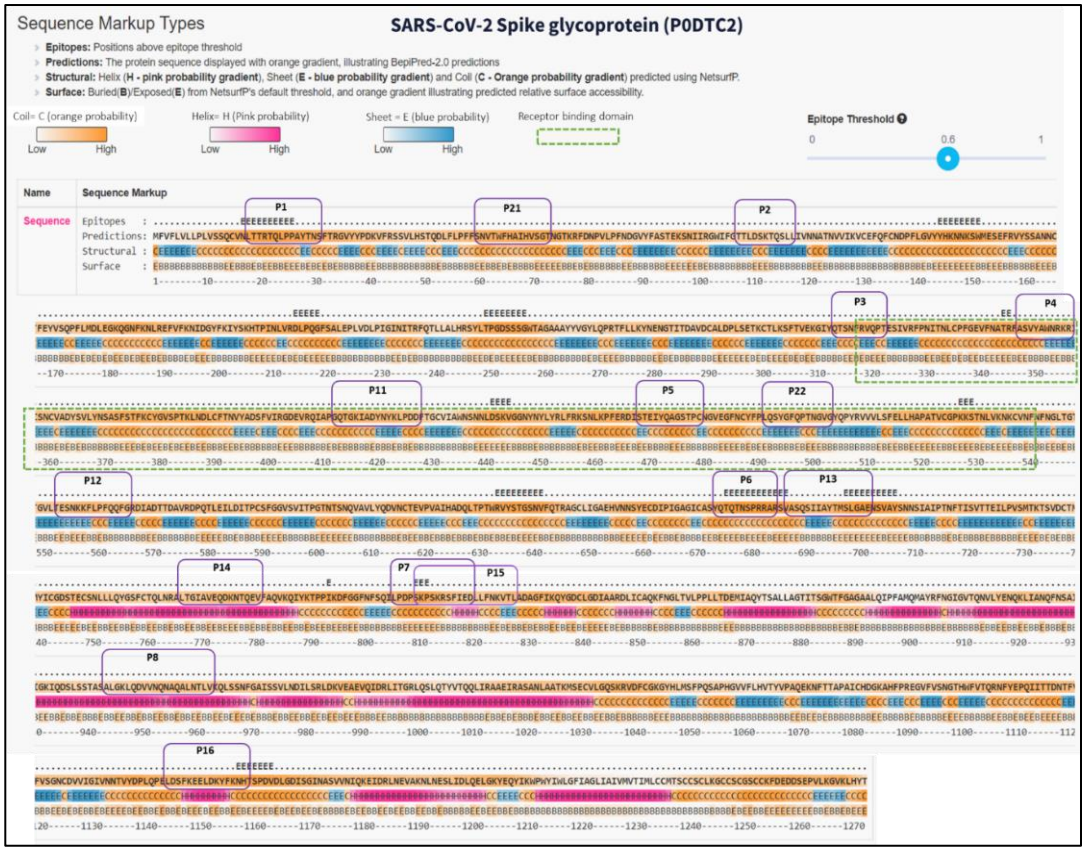

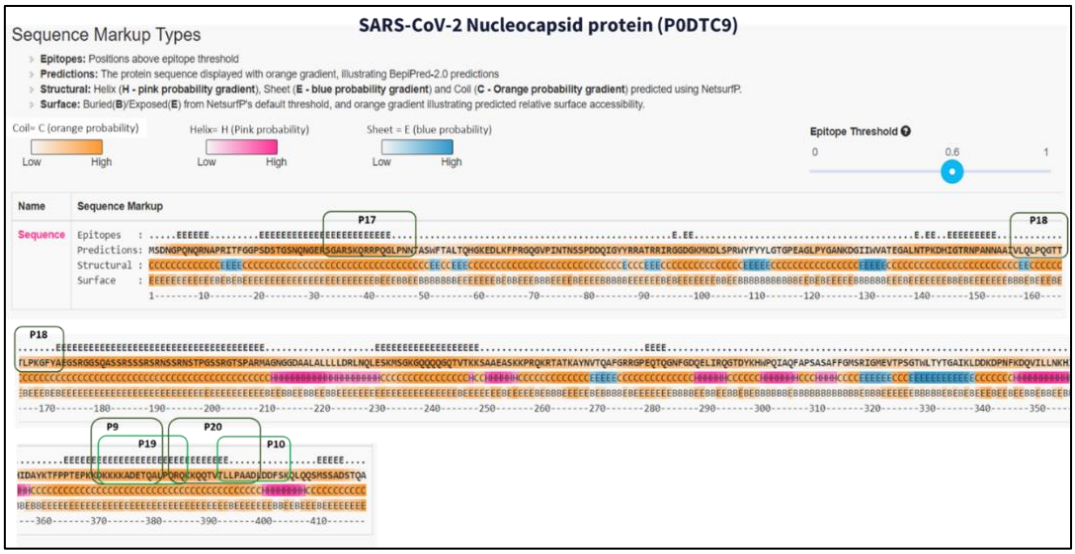

Figure 7.3 Results from B cell epitope prediction analysis. The open access software BepiPred 2.0 was utilized to predict potential B cell epitopes based on the structure of S (above) and N (below) protein sequences extracted from protein data bank (PDB). The software estimates probable epitopes position (with a threshold of 0.6) assigned with the letter E over the sequence. Also, in the structural row, highlight in orange the probability of random coil conformation, in pink the α-helix conformation and in blue the β-sheet structures considering the amino acids involved. Additionally, in the row indicated as surface, the letter E corresponds to exposed amino acids while the letter B refers to buried amino acids. Moreover, the final peptide sequence selected is indicated on the protein sequences with their corresponding numbers. A) S protein sequence is expressed at amino acid resolution indicating target regions for each peptide. B) N protein sequence was analyzed and the peptides selected are expressed [9].

Throughout this analysis, a structural correlation with antigenicity was defined for each peptide. An interesting feature observed while assessing the S protein was found on the relative abundance of β-Sheets (blue) and Random Coil (orange) conformations in the first portion of the protein mainly around S1 subunit, from aa 1 to 700. According to our prediction, a significant portion of immunogenic epitopes were identified across this section, probably because is the most exposed domain on the protein and also in charge of the interaction with the ACE2 receptor. On the other hand, the rest of the sequence (from aa 700 to 1270) evidenced more prevalence of α-helix (pink) structures along the S2 subunit, characterized by a transmembrane domain, where no relevant epitopes were predicted.

In the case of N protein, the peptides **P19**, **P20** and **P10** as well as **P17** are located in a hot epitope predicted region but no direct correlations with structural

characteristics were identified. Additionally, the software estimated surface accessibility, indicating buried and exposed amino acids with a B and E respectively. This information was analyzed by the time when the selection of additional peptide sequences was addressed and favoring the final choice of the most suitable epitopes ensuring accessibility to the antibodies.

Spike

Nucleocapsid

Figure 7.4 Schematic representation of the discreet peptides selected on the protein sequence. The original selection of 10 sequences already reported in the previous chapter is completed with the incorporation of 12 additional sequences rationally designed to enhance the immunoreactivity. Finally, a total of 16 peptides were selected from S sequences and the other 6 from N protein based on computational analysis and emerging literature.

The same considerations discussed in Chapter 6 were implemented in the scouting of the novel panel of peptide sequences (final selection in Figure 7.4). As part of the selection criteria, antigenicity was evaluated by addressing regions with high antigenic scores predicted with the already mentioned analysis software. Also, hydrophobic/hydrophilic balance was studied considering a standard peptide length of 12 to 15 amino acids, with a preference for non-conserved regions across the original sequence. By integrating all above mentioned parameters, the rational design was proposed as starting point to identify promising peptide candidates without the exclusive requirement of laborious, extensive and complex proteome characterization studies.

A deeper analysis of S protein sequence was conducted, expecting to increase the recognition of the peptides with greater immunogenicity and as a result, **P21** and **P12** were selected from S1 sub-unit. Moreover, in order to favor the potential determination of neutralized antibodies (NAb's) the **P11** and **P22** sequences and their mutated versions (**11b**, **11c** and **22b**) were defined on the RBD region according to several reports available in the literature. Furthermore, **P13**, **P14**, **P15** and **P16** were extracted from S2 subunit as highly immunogenic

peptide candidates, considered the behavior observed with S1+S2 in the previous v1.0 version.

For the case of N protein, **P17** and **P18** were incorporated to explore partially the N terminal domain, that in the first selection was not evaluated, in addition to **P19** and **P20**, located in the C terminal domain, expecting to enhance the performance observed around the closely related sequence of **P10** with previous encouraging results.

On the other hand, with the idea to potentially distinguish the VoC's causing the infection based on a characteristic serological profile, several peptide sequences carrying specific mutations form the original strain were included in the microarray. We referred to the CoV-Spectrum database [10] to identify the most prevalent variants across the Catalan region considering that the samples under analysis were restricted to that area, evidencing the presence of **Alpha** (B.1.1.7), **Delta** (B.1.617.2) [11], and **Omicron** (B.1.1.529) [12] and also **Beta** (B.1.351) and **Gamma** (P.1) variants with lower relative abundance. Is worth to mention that since the pandemic was announced until 2023, the VoC's were progressively de-escalated and re-assigned as variants of interests (VoI), variants under monitoring (VuM) or even considered not relevant. Nevertheless, based on the sequence of **P21** obtained from Wuhan strain, **P21b** was synthesized including deletions in ΔH69 and ΔH70 [13] present in the **Alpha** variant. Then for the case of peptide **P11**, the **P11b** (K417N) was designed for profiling the **Beta** and **P11c** (K417T) for the **Gamma** identification. In addition, a common mutation (N501Y) found in **Alpha**, **Beta**, **Gamma**, and **Omicron** (**P22b**) was contemplated and for the case of **P6** close to S1/S2 cleavage site **P6b** (P681H) was produced against **Alpha** and **P6c** (P681R) for **Delta** discrimination. A similar analysis was conducted over N protein, but due to the lower impact of representative and well characterized mutations over this sequence, no additional peptides were selected.

The following Table 7.1 represents each peptide sequence incorporated to in the array, identifying the location in the protein as well as peptide density obtained after bioconjugation to BSA.

Table 7.12 Selection of peptide epitopes rationally designed and characterized in this study

Peptide ID	Target Viral sequence	Protein region	Variant of Concern	BSA-peptide (δ) density
P1	L_{18}TTRTQLPPAYTNS	S1-Spike		5
P21	S_{60}NVTWFHAIHVSGT	S1-Spike		7
P21b[a]	S_{60}NVTWFHAISGT	S1-Spike	Alpha (ΔH69, ΔH70)	10
P2	L_{110}DSKTQ	S1-Spike		5
P3	Q_{314}TSNFRVQPT	S1-Spike (RBD)		5
P4	A_{352}WNRKR	S1-Spike (RBD)		6
P11	G_{413}QTGKIADYNYKLPDD	S1-Spike (RBD)		6
P11b[a]	G_{413}QTGNIADYNYKLPDD	S1-Spike (RBD)	Beta (K417N)	7
P11c[a]	G_{413}QTGTIADYNYKLPDD	S1-Spike (RBD)	Gamma (K417T)	7
P5	S_{469}TEIYQAGSTPC	S1-Spike (RBD)		6
P22	LQSYGFQPTN$_{501}$GVG	S1-Spike (RBD)		8
P22b[a]	LQSYGFQPTY$_{501}$GVG	S1-Spike (RBD)	Alpha/Beta/Gamma (N501Y)	10
P12	T_{553}ESNKKFLPFQQFGR	S1-Spike		7
P6	$_{674}$QTQTNSPRRAR	S1-Spike		5
P6b[a]	C_{671}ASYQTQTKSHRRAR	S1-Spike	Alpha(P681H)	6
P6c[a]	C_{671}ASYQTQTNSRRRAR	S1-Spike	Delta (P681R)	4
P13	V_{687}ASQSIIAYTMSLGAE	S2-Spike		7
P14	L_{767}TGIAVEQDKNTQEV	S2-Spike		5
P7	L_{806}PDPSKPSKRSFIED	S2-Spike		5
P15	S_{813}KRSFIEDLLFNKVTL	S2-Spike		6
P8	A_{944}LGKLQDVVNQNAQALNTLV	S2-Spike		5
P16	L_{1145}DSFKEELDKYFKNH	S2-Spike		6
P17	S_{33}GARSKQRRPQGLPNN	Nucleocapsid		5
P18	V_{158}LQLPQGTTLPKGFYA	Nucleocapsid		6
P9	K_{370}DKKKKADETQAL	Nucleocapsid		4
P19	D_{371}KKKKADETQALPQRQ	Nucleocapsid		5
P20	Q_{384}RQKKQQTVTLLPAAD	Nucleocapsid		4
P10	T_{393}LLPAADLDDFSK	Nucleocapsid		8

[a] *Peptide from a variant of concern, carrying a specific mutation considering the original sequence with the same number and no letters in the ID name. The ID numbers were assigned as peptides were selected, however in the table the order of peptides is related to the position in the sequence of each protein.*

Classification of peptides derived from VoC's regarding the original sequence selected for the rational design of peptides were synthesized.

7.3.2.2. Influence of the number of drops on the spot size and fluorescent intensity

With the aim to improve matrix array dimensions considering the introduction of 18 new epitopes with respective replicates, the influence of the number of drops over the spot diameter and intensity were evaluated. Figure 7.5 shows the spot diameter after deposition of decreasing number of drops (from 11 to 1 per spot) for each epitope at the pre-established concentrations. In this case, a matrix of 6 columns per 11 rows was printed and tested against the in house developed CTR+Ab S and CTR+Ab N samples. As can be seen, the number of drops directly influences the spot size, increasing the average diameter from 150 ±17 µm with one drop to almost 300 ±30 µm for eleven drops. Furthermore, for all the epitopes included the CV was below 14 % demonstrating the robust performance of the microarray spotter (SciflexArrayer S3). Mapix software was employed to analyze spots intensity and measure the corresponding diameter as the average of at least three replicates.

As result of these experiments, we concluded that a lower number of drops generating smaller spots was more suitable since increased the available surface over the slide for the incorporation of additional epitopes. A compromise between adequate fluorescence intensity and minimum spot size was considered.

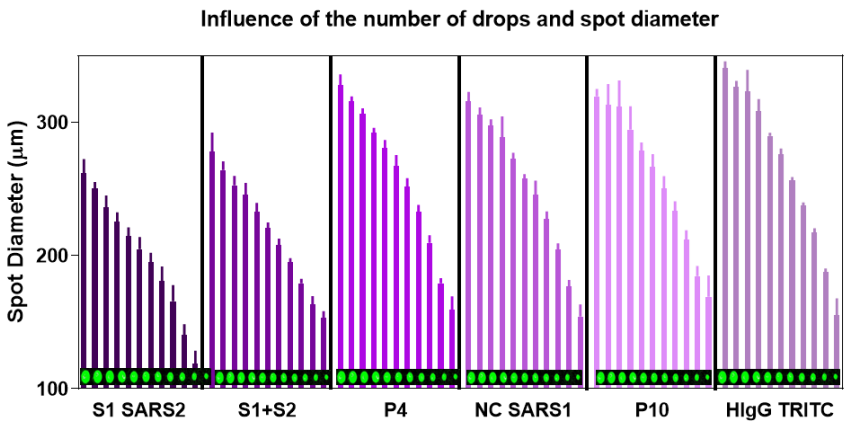

Figure 7.5 Influence of the number of drops in the spot size. The diameter of 3 replicate spots with a discreet number of drops ranging from 1 to 11, was measured after incubation with CTR+Ab S (S1-SARS2, S1+S2, P4) and CTR+Ab N (NC-SARS1, P10) and Human Anti-IgG TRITC as printing control. Spot diameters are expressed in µm. The average of CV was below 5 %.

On another set of experiments, we assessed the correlation between the fluorescence intensity and the number of drops per spot. The results from the Figure 7.6, demonstrated that higher amounts of drops in epitopes like S1-SARS2, S1+S2 and HIgG-TRITC (Human Anti-IgG TRITC) displayed increased fluorescence, reaching saturation after 9 drops per spot. While on the contrary, the signal detected over epitopes like **P4**, **P10** and NC-SARS was higher in spots with lower number of drops. Results interesting to emphasize that both peptides assessed, evidenced similar behavior displaying increased fluorescence at lower number of drops. This behavior could be related to a decrease on the peptide epitope availability on the BSA bioconjugates when multiple layers are deposited on the same spot. This effect is probable not as much evident when complete proteins are used since all the structure shows different epitopes that can be detected with CTR+Ab S and S showing a polyclonal antibody nature.

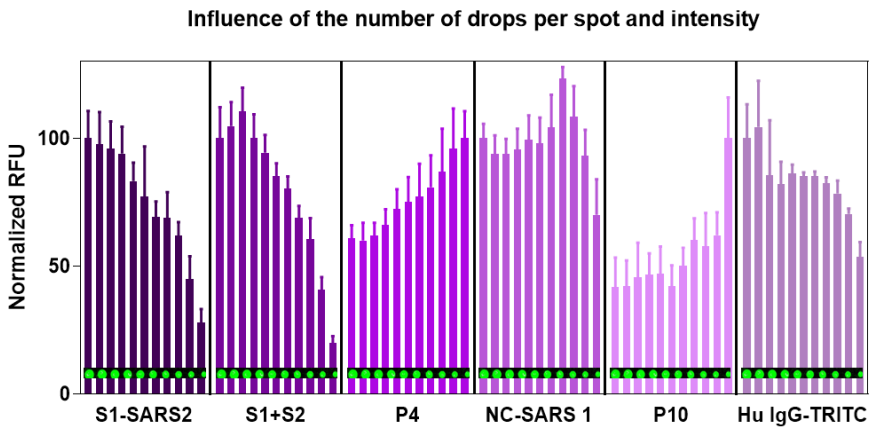

Figure 7.6 Influence of the number of drops per spot in the intensity detected. The average fluorescent signal from three replicate spots was measured and compared to spots with different number of drops ranging from 1 to 11, after incubation with CTR+Ab S (S1-SARS2, S1+S2, P4) and CTR+Ab N (NC-SARS1, P10) and Human Anti-IgG TRITC as printing control. Spot diameters are expressed in µm. The average of CV was below 15 %.

Finally, the spot quality was evaluated through image analysis of the microarray (see Figure 7.7) and it was possible to define that the use of lower number of drops also favored more homogenous fluorescence intensity. This can be attributed to the reduced surface area exposed to irregular evaporation effects in smaller spots [14] if environmental conditions are not strictly controlled. Several elements with the ability to interfere with spot shape and probe distribution have been described in the literature, for instance the "doughnut or coffee stain effect" characterized by high probe deposition at the edges of the spot [15, 16] due to diffusion limitations or geometrical constraint of the droplet surface. Or on the contrary, the so called "peak-shaped spots" showing higher densities in the center of the spot and diffusing at the edges as a result of a rapid evaporation during the printing process [17].

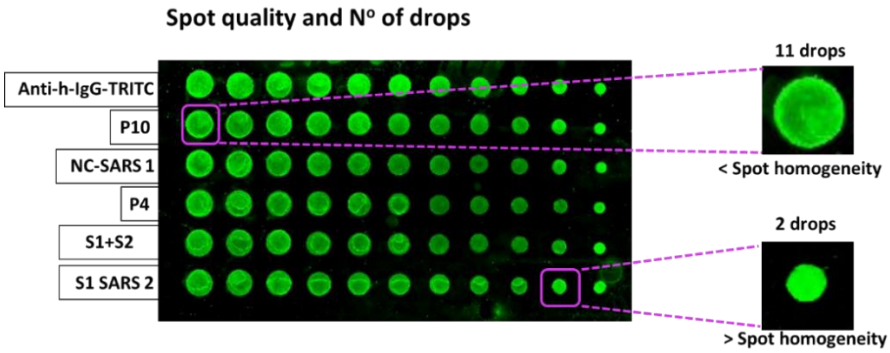

Figure 7.7 Micrography of a single sub-array containing the epitopes evaluated with different number of drops per spot. Each epitope solution was printed on the same row varying the number of drops to compare spot homogeneity after incubation with a mixture of CTR+Ab S and N. The images were acquired using a microarray scanner with a laser at excitation wavelength of 532 nm.

Based on the previous characterization, small numbers of drops evidenced comparable spot sizes with lower variability, independently from the type of epitope or protein, and better homogenous signal distribution. Moreover, higher fluorescence intensity was recorded for the case of peptide-BSA solutions. Taking into consideration all these data, printing the chips with just two drops per spot was defined as the most suitable conditions to eventually introduce additional epitopes to the chips without increasing considerably the spotting area, which for our purposes was limited by the ArrayIt® gasket.

7.3.2.3. Effect of peptide bioconjugation to BSA

During the first version of the immunoarray, the use of peptide-BSA conjugates was proposed to ensure homogenous immobilization conditions over the hybrid array combining viral peptides and proteins which also allowed using the same biofunctionalization protocol for each spot. However, on this version 2 of the microarray, we wanted to evaluate deeper the influence of BSA and assess if such approach was superior in terms of sensitivity. For this, microarrays were printed in which the peptides were immobilized directly on the surface of the chip and the signal compared to those in which the peptide-BSA bioconjugates were used.

In this case, APTMS (3-Aminopropyl) trimethoxysilane) derivatized glass slides were prepared and then treated with a Sulfo-SMCC (sulfosuccinimidyl 4-(N-maleimidomethyl) cyclohexane-1-carboxylate) solution to finally deposit five

different peptides (non-conjugated to BSA) at three concentrations of 50, 100 and 250 µg mL^{-1} in triplicate spots. As mentioned, a different functionalization protocol in two steps was required to covalently attach the single peptides through the thiol groups (-SH) from the terminal Cys residues to the glass surface as described by *Chen et al* [18]. Then, CTR+Ab S and CTR+Ab N purified antibodies at 20 µg mL^{-1} (in PBST 0.5% BSA) were used to assess the fluorescence intensity of those spots.

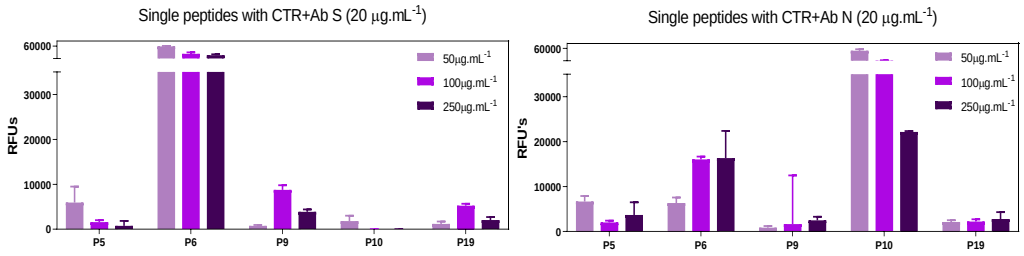

Figure 7.8 Evaluation of direct peptide immobilization response. Five selected peptides (P5, P6, P9, P10 and P19) non-conjugated to BSA were directly functionalized on the pretreated glass slide at three concentrations (50, 100 and 250 µg mL^{-1}. The fluorescent signal detected after incubation with CTR+Ab S and CTR+Ab N at 20 µg $mL^{-1}$was determined and plotted for each case. The SD was obtained from the average signal of five replicate spots.

As observed in Figure 7.8, single peptides immobilization was successful and displayed considerable fluorescence intensity after incubation with CTR+Ab S over **P5** and **P6** and with CTR+Ab N over **P9**, **P10** and **P19**. However, non-specific interactions were observed after incubation with the last one displaying dose dependent response with the **P6** epitope that was specific for S protein. This effect could be partially attributed to the high content of immunoglobulins in the sample. On the other hand, the use of BSA bioconjugates instead of the single peptides perhaps was also preventing the non-specific adsorption acting as a blocking agent already. To probe some of these possible explanations, lower CTR+Ab S and N concentrations (5 µg mL^{-1}, data not showed) were also assessed and such effect was minimized. Nevertheless, the absence of unspecific binding when peptide-BSA conjugates were used even at high antibody concentrations pointed to the blocking contribution of the carrier protein. Regarding the S epitopes, after incubating with 20 µg mL^{-1} of CTR+Ab S, high fluorescence was observed over **P6** with minimum contribution from the rest of peptides. According to these results direct peptide immobilization provides high signal

intensity, but also promotes nonspecific interaction at higher antibody concentrations as observed for CTR+Ab N.

Experiments performed by printing peptides at 100 µg mL^{-1} and peptide-BSA conjugates at 500 µg mL^{-1} in the same slide, were done utilizing the CTR+ Ab S and N at three dilutions (100, 20 and 5 µg mL^{-1} in PBST-BSA 0.5%) to additionally assess the convenience to pursuit or not with the idea of using the single peptides. As can be seen in Figure 7.9, the fluorescent signal using peptide-BSA conjugates is highly specific across the three CTR+Ab dilutions, while non-specific signals were recorded for the chips with only the single peptides. Unspecific adsorptions were evidenced against **P9** and **P10** using CTR+Ab S at 100 µg mL^{-1} on a concentration dependent manner and also with CTR+Ab N over peptides **P5** and **P6**.

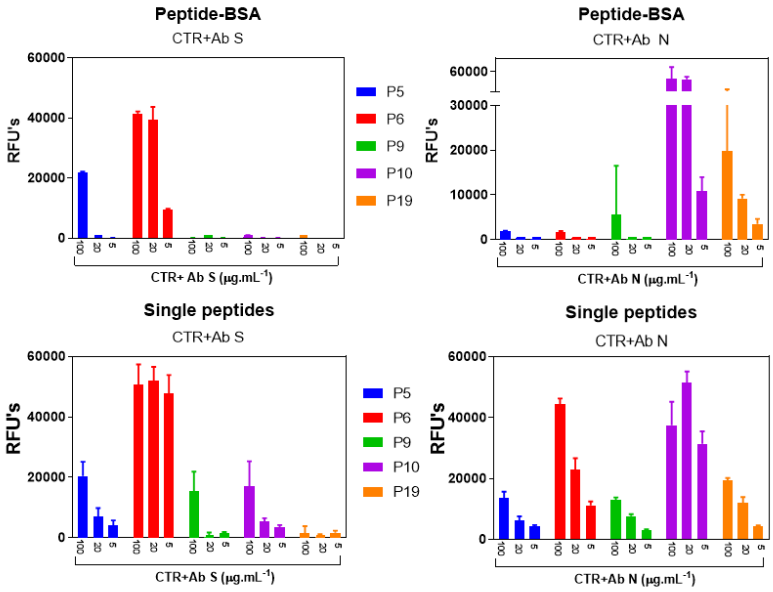

Figure 7.9 Influence of BSA conjugation in peptides immobilization. Comparison of single peptide and peptide-BSA conjugates immobilization in assay response was studied. In the upper section, the response of a matrix constituted by peptide-BSA bioconjugates (at 500 µg mL^{-1}) after the incubation with CTR+Ab S and CTR+Ab N at three different concentrations (100, 20 and 5 µg mL^{-1}) is represented. In the lower section, a different microarray composed by direct peptides immobilized at (100 µg mL^{-1}) after incubation CTR+Ab S and CTR+Ab N at three concentrations (100, 20 and 5 µg mL^{-1}) is evidenced. The SD is estimated from the average intensity of five replicate spots.

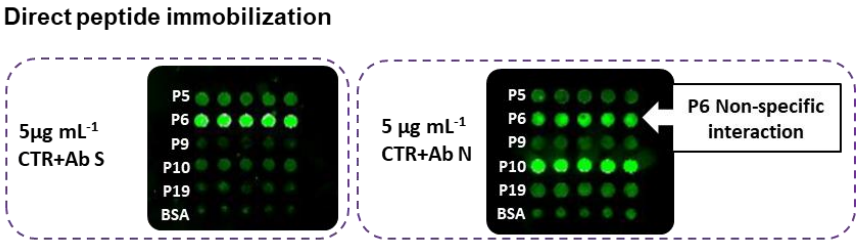

Figure 7.10 Scanned micrography of two microarray chips with peptides directly immobilized after incubation with 5 µg mL^{-1} CTR+Ab S (left) and CTR+Ab N (right), evidencing unspecific adsorption towards P6 in the last case.

Figure 7.10 shows the fluorescent image recorded for the microarrays where peptides were directly immobilized after incubation with the less concentrated CTR+Ab S and N solutions at 5µg mL^{-1}. Clear unspecific adsorption over the **P6** epitope of the S protein was observed when exposed to CTR+Ab N, that was specific for the N protein. Such effect was completely removed by using the corresponding peptide-BSA bioconjugates. According to these observations, it was concluded that using BSA bioconjugates is essential to prevent non-specific interactions, conferring appropriate peptide spatial distribution and enhancing specific peptide sequence recognition. From our concern, other authors in the literature also opted for using BSA bioconjugates [19, 20] assuming a blocking effect towards unspecific adsorptions promoted by sample components. On top of that, we consider that peptides conjugated to globular proteins may present a 3D like distribution that favors the interaction with the selective antibodies in serum, compared to linear peptides directly deposited over a glass surface that can be affected by steric hindrance effects limiting their recognition. On the other hand, the main limitation is found in the preparation of high-density peptide microarrays, requiring an additional synthetic step to bind the peptides to BSA. Thus, this application should be considered for a reduced sequence selection after proteomic studies.

7.3.2.4. Performance of the hybrid peptide-protein microarray chip

Previous experience with the *Immuno-µ*SARS2 v1.0 chip made us suspect of potential competitive phenomena due to the fact that epitope peptides of a protein, also present in the chip, could be affecting the signal of those spots.

Hence, the recognition of the native proteins could be favoured in respect to discrete linear peptide sequences. This was the reason because in the chip the selected concentration for the peptide-BSA bioconjugates was considerably higher than that proteins (500 µg mL^{-1} peptides and 5 to 15 µg mL^{-1} proteins).

With the aim to properly asses the influence behind the combination of peptides and proteins in the same chip, a group of clinical serum samples with increased response to our microarray chip were utilized to evaluate the assay perfromance under both conditions, mere peptide or protein microarrays or hybrid peptide-protein microarrays. The experiments were performed making use of the ArrayIt® gasket with a single glass slide for which 24 wells are defined (one for each microarray chip). As mentioned before, with this set-up, the chips are distributed in three columns and eight rows. Each column contained chips printed with a distinct matrix composition and each sample (PCR+: 19, 27 47 and 49; PCR-: 87, 113, 119) was analyzed on a different raw simultaneously over the three conditions. The first column was printed only with proteins (S1-SARS2, S1-SARS1, RBD, NC-SARS2 and NC-SARS1) at the already established concentrations. The second column contained chips in which only peptide-BSA bioconjugates (**P4**, **P6**, **P9**, **P10**, **P12**, **P13**, **P14**, **P15**, **P16**, **P17**, **P18** in that order) at 500 µg·mL^{-1} has been printed. Finally, the third matrix included microarray chips containing the combination of those peptides and the proteins at the same exact concentrations (see Figure 7.11).

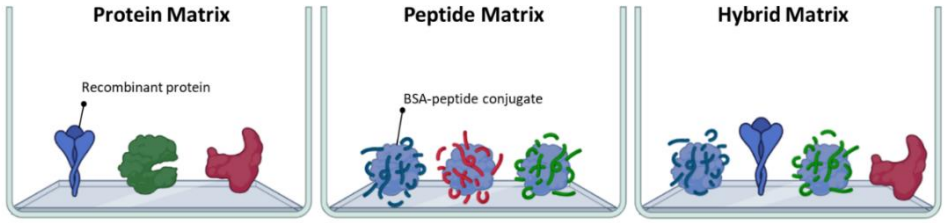

Figure 7.11 Schematic representation of the experiment comparing the influence of proteins and peptides combined in the same microarray. Three independent sub-arrays were generated by printing only proteins (left), in a separate well only peptide-conjugates (middle) and peptides and proteins combined (right) to explore potential competitive effects.

As displayed in Figure 7.12, the fluorescence intensity of the immunological profile of each sample was much higher on the mere chips containing only proteins or peptides (both upper heatmaps), than on the hybrid chips (lower heatmaps). The effect was more evident for certain patients on the signal

recorded for the proteins (Figure 7.12 left heatmap) while for others was more obvious than on the signal recorded for the peptides (right heatmap). Hence, the patient labelled as PCR+49 reach almost 8.000 RFU's over the epitopes of S1 SARS2 and RBD but when the same sample was measured in presence of the peptides, the signal decreases to almost 4.000 RFU's. On the other hand, for the sample PCR+19, a similar intensity of response was recorded for the different peptide-BSA bioconjugates on the mere peptide microarray, reaching fluorescence values around 5.000 RFU's, while the response of the same sample towards those epitopes in the hybrid microarray was very low, except for **P15** in this case. These results pointed to a sort of competitive effect between them. In this scenario, the proteins that evidenced the most significant signal reduction over the panel of samples evaluated were S1-SARS2 and RBD. Interestingly they are structurally related as RBD is part of the S1 portion, meaning that detection of neutralizing antibodies, which was one of our objectives, could be masked by the presence of peptides in the same microarray chip leading to signal reduction over these epitopes. On the other hand, after signal comparison between peptides, the epitopes mostly affected by the presence of proteins were **P12** and **P18** showing considerable signal fluctuations in presence and absence of proteins. **P12** belonged to S1-SARS2 region explaining potential response interactions with that epitope in the combined matrix that was also affected by the presence of peptides. While **P18** derived from N protein also showed differences in response with and without NC-SARS2 epitope, but in contrast the N recombinant protein printed in the chip was not affected. A potential explanation for this behavior could be attributed to the elevated immunogenicity of the N protein in comparison with the linear **P18** sequence.

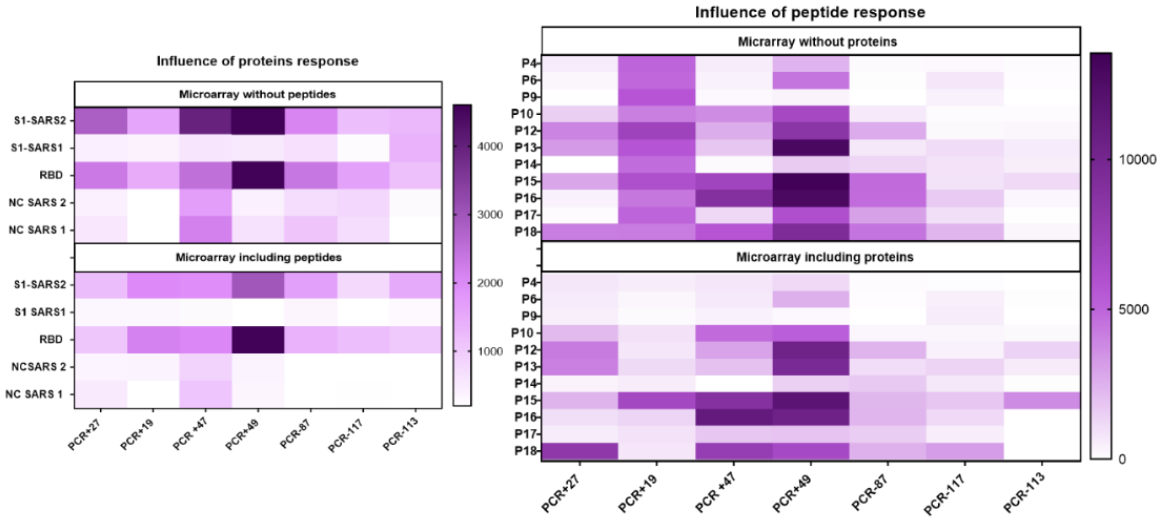

Figure 7.12 Competitive phenomena between peptides and proteins in the IgG's profile of human serum samples. The influence of the combination of peptides and proteins in the detectability of the corresponding epitopes (patient IgG response profile) was evaluated by comparing the signal obtained from a matrix constituted by proteins (up-left) and a different one combining proteins and peptides (low-left) after incubation with the same human serum samples. On the other side, IgG response against only peptides (up-right) was compared with the signal detected in the microarray combining peptides and proteins (low-right). Graphs on the left, represent the response of the proteins, while graphs on right represent the response of the peptide epitopes.

These results clearly point to the relative distribution of IgG's over the spots of the microarray that contain common epitopes, which on the hybrid chips are present in peptides and proteins. In contrast, when using the mere chips those immunoglobulins are only directed to one epitope increasing the fluorescence associated to those spots, as it has been experimentally observed due to the lack of competitive phenomena.

As a result of this observation, we have proposed that the further versions of the *Immuno*-µSARS2 chip should be divided in two sub-microarrays, one for proteins and other only for peptides. It is expected that such arrangement will promote comparable signal interpretations exclusively attributed to peptides and protein avoiding competitive effects. However, the main drawback associated to the selection of this configuration is that every sample will have be measured twice, doubling the number of slides required. However, probably a different response from the peptides will be promoted opening the door to additional immunological information that under this assay format was not detectable.

7.3.3. ESTABLISHMENT OF IMMUNOLOGICAL PROFILES IN CLINICAL SAMPLES WITH THE NEW VERISON OF THE MICROARRAY CHIP

7.3.3.1. IgM and IgG signal distribution and data analysis

After these experiments aimed at optimizing and better understanding the performance of the *Immuno*-µSARS v2.0 chip, we addressed the analysis of the same sample cohorts measured with the *Immuno*-µSARS2 v1.0. This time, the profile of IgG's and IgM's against the 35 different epitopes was explored by analyzing the total of 755 clinical samples (see Figure 7.13 and Figure 7.14). Another remarkable consideration was that during prepandemic sample analysis with the novel chip, we evidenced a significant fluorescent response in S1+S2 protein in most of the samples, which lead us to remove it from the study due to the lack of an adequate negative control. We assume that potential protein denaturation could have generated such unspecific effect in samples that were not exposed to viral infection, and we had already noticed a similar behavior in S1+S2 with the analysis of RT-PCR – samples in the previous chapter.

As described in chapter 6, the simultaneous determination of IgM and IgG levels in each sample was possible through the use of distinctly labeled secondary antibodies and the use of a dual color microarray scanner. The intensity values detected with the scanner are expressed in normalized RFU's. From the sample analysis using the complete array, the determination of the most immunogenic epitopes was based on raw signal interpretation, estimating that increased fluorescence was correlated with higher prevalence of immunoglobulins towards the respective epitopes.

As expressed over the heatmap in Figure 7.13, IgM mediated response was studied over two sample clusters classified as positive or negative by RT-PCR technique while prepandemic samples were utilized as negative control group. Across the heatmap, a stronger reddish intensity was observed in the RT-PCR+ clusters, in contrast with RT-PCR- and prepandemic groups in concordance with the fact the early development of IgM mediated response is detectable in samples from patients, most of them positive through PCR. Nevertheless, as already stated in chapter 6, the RT-PCR technique was used as reference to

classify the samples but in this case, it has not been strictly correlated with positive serology. Moreover, the PCR positive cohort from HUGTIP (cohort 3) is the only one displaying uniform response over peptides **P14 (S)**, **P15 (S)** and **P18 (N)** with an estimated clinical sensitivity of 21, 26 and 35 %, respectively. However, the signal of these epitopes was not comparable to the other RT-PCR+ groups suggesting intrinsic variability at cohort level. This could be attributed to a shorter sample collection gap between the onset of symptoms and serum extraction, particularly in the cohort 3 (HUGTIP) reaching higher levels of IgM's during initial stages of disease. Since these studies have all been done using retrospective samples, this important parameter has been out of our control. Another explanation could be due to a batch effect, possibly attributed to changes in personnel, reagent batches and extraction conditions affecting this group of samples [21]. With the evidence discussed, is possible to infer that single epitope analysis may limit results interpretation, leading to worst clinical predictive values. However, the integration of multiple epitopes defining immunological fingerprints could increase platform accuracy and sensitivity providing additional information regarding disease progression and prognosis.

Another relevant aspect is that according to these results, the full-length proteins incorporated in the microarray, could be possibly substituted by the peptide epitopes, that are easier to mass produce and more affordable, without missing information on IgM's interactions with the chip, although further bioinformatic analysis should be required to confirm that they behave comparably. Remarkably, the prepandemic cohort didn't showed significant response to the epitopes under evaluation suggesting good sequence specificity. Only in the case of **P5** a slight fluorescent signal was detected and no clear explanation can be attributed, considering that this peptide didn't showed response during IgG's determination using the same prepandemic samples.

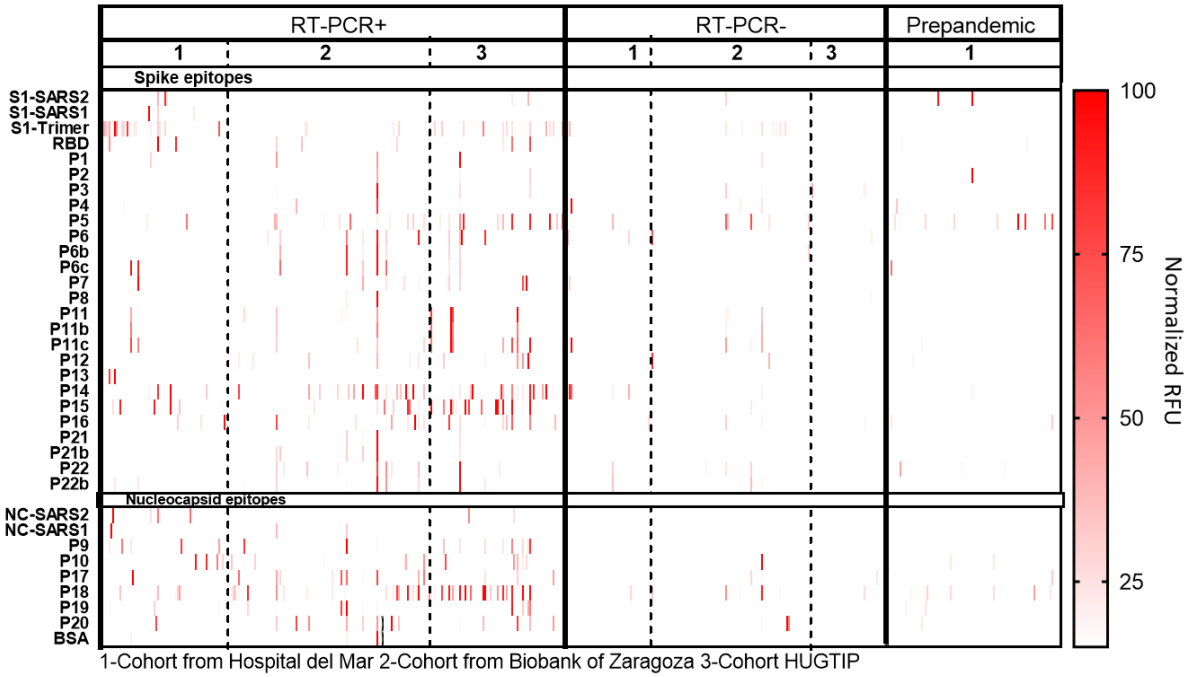

Figure 7.13 Landscape of IgM mediated response detected from the analysis of 755 human serum samples from three different cohorts of patients, classified according to RT-PCR groups and prepandemic samples as negative controls. The y-axis represents individual epitopes constituting the microarray (viral peptides and proteins) while, the x-axis corresponds to the serum samples from different patients. The intensity scale indicates the relative signal of IgM's antibodies binding from 0 (white) to 100 (Red) in normalized RFU's.

Throughout the literature, IgM's predictive capacity has been widely questioned due to the narrow sampling window required for accurate determinations in comparison with robust IgG responses obtained after ten to fifteen days post infection [22]. From our concern, IgM's are relevant early indicators of disease but further optimization should be required to adequately detect this isotype with enough specificity using the proposed microarray. Although a relatively low intensity was monitored during IgM determinations in these samples, our results suggest that good clinical correlations could be estimated probably under a multivariate analysis and in combination with IgG profiles.

In addition to IgM's, the profile of IgG's in clinical serum samples was also evaluated with the *Immuno*-µSARS2 v2.0 chip. The first remarkable expected aspect is the higher intensity detected for IgG's profile in contrast with IgM's (see Figure 7.14). Although the secondary labeled antibody against human IgG's was

at half the concentration of Anti-human IgM, this effect was anticipated due to the natural abundance of that Ig isotype.

Notably, from the complete matrix assessed a well-defined group of peptides showed increased response across the three cohorts of patients confirmed by RT-PCR demonstrating the specificity and robustness of the epitopes selected under different sample batches allowing comparable results. In this case, the sequence of **P12** from the S1 subunit and **P14**, **P15** and **P16** belonging to S2 subunit in addition to the peptides **P10** to **P18** from the N protein displayed the highest signals in respect to the rest of epitopes analyzed. These results may indicate that sequences extracted from S2 subunit and N protein could be immunodominant regions, in accordance with additional reports discussing seroprevalence determined by the same domains [23]. Another relevant aspect is that the S2 subunit, is characterized by a transmembrane domain that is not directly exposed to the viral surface interacting with antibodies, but according to proteomic studies, a fusion peptide (FP) region over S2 could be a hot antigenic area. The authors claim that antibodies against this region could interfere with the cleavage site of the FP affecting its natural function in detriment of the virus [24].

Surprisingly, during signal acquisition from the structural proteins with the *immuno*-µSARS v.2.0, a higher fluorescence would have been expected as they naturally carry multiple epitopes and present 3D structure compared to the linear peptides. A possible explanation behind this effect, could be that the new peptides incorporated represents highly immunogenic regions that as was already demonstrated, may promote competitive events in the hybrid matrix diminishing the signal from proteins. Is worth to mention, that in the *immuno*-µSARS v.1.0 (only with 10 peptides, see section 6.3.7) the signal contribution from the proteins was considerably higher than the linear sequences, thus the objective to select more immunodominant epitopes in this chapter could be partially corroborated.

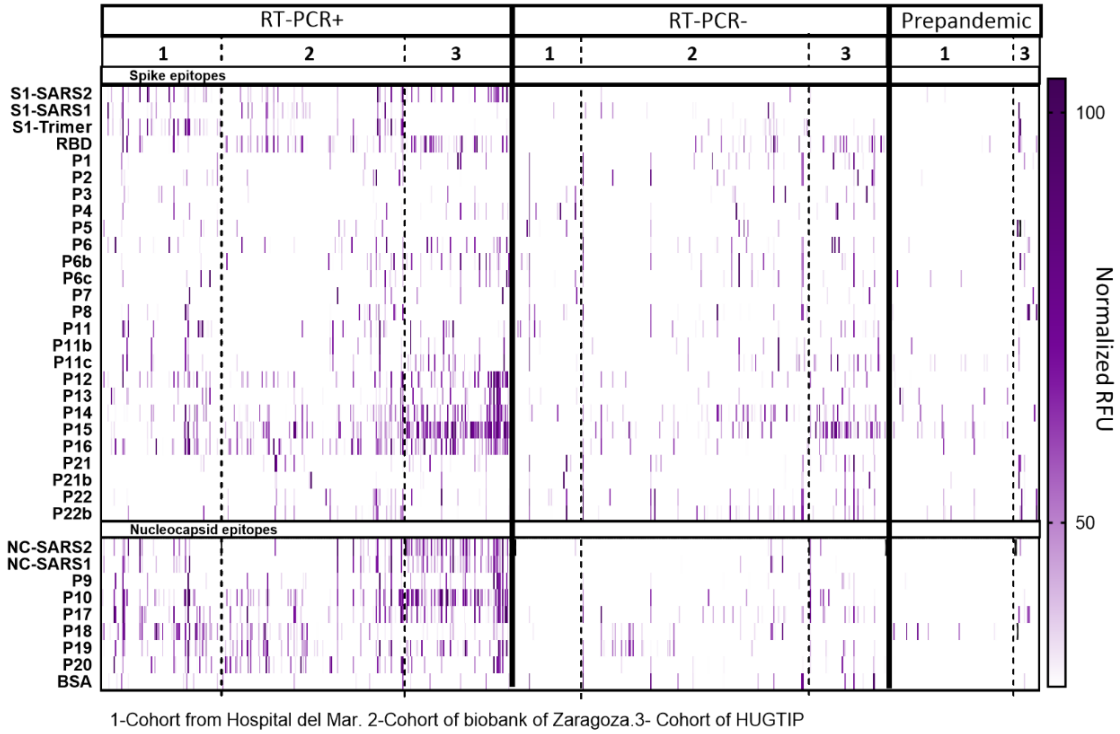

Figure 7.14 Landscape of IgG mediated response detected from the analysis of 755 human serum samples from three different cohorts of patients, classified according to RT-PCR groups and prepandemic samples as negative controls. The y-axis represents the individual epitopes constituting the microarray (viral peptides and proteins) while, the x-axis corresponds to the serum samples from different patients. The intensity scale indicates the relative signal of IgG's antibodies binding from 0 (white) to 100 (Purple) in normalized RFU's.

Interestingly, a distinctive serologic pattern was observed across the different groups of clinical samples (RT-PCR (+) or (-)), suggesting that IgG levels may serve as accurate predictors according to the RT-PCR used as reference method. Furthermore, the signal obtained from prepandemic group analysis was negligible using the v 2.0 chip, demonstrating the specificity behind the peptide sequences selected.

Another interesting observation was found over a small group of 5 samples that displayed significant fluorescent response amongst all the peptide epitopes in the matrix, also observed in the v1.0 of the microarray. This was initially attributed to a sort of unspecific binding but after some literature research, the presence of autoantibodies against albumin has been reported in patients with

systemic lupus [25]. Therefore, this could hypothetically explain such unexpected signal due a cross-reaction of antibodies against human serum albumin with bovine serum albumin. However, this potential explanation should be corroborated going deeper into the clinical histories of the patients, in general terms this is an eventuality that should be taken into consideration if this chip would finally be implemented in clinics.

Based on the results obtained after sample analysis and contemplating the signal achieved comparing both Ig subtypes, IgG levels demonstrated better correlation with specific viral epitopes. In this regard, our findings are in line with other reports suggesting more accurate serological predictions-based IgG response over time in respect to rest of isotypes [26]. On the contrary, IgM's displayed lower fluorescent response probably attributed to methodological aspects such as period of sample collection or amount of sample utilized. Nonetheless, the potential utility of this isotype as an early biomarker complementary to IgG's should be noted and further investigated. Given this, monitoring of both immunoglobulins (IgG/IgM) should be perused in order to further improve our understanding of individualized immune profiles. For the following studies, we decided to continue with the analysis of the response mediated by IgG's, delimiting the use of samples taken at least 10 days PSO, to minimize non-specific contributions.

7.3.3.2. Assessment of neutralizing antibodies identification with the *Immuno*-µSARS v 2.0 platform

Due to the important role of neutralizing antibodies in the protection against the viral infection, one of our objectives was to assess the value of the v2.0 chip to determine IgG's against the Receptor Binding Domain (RBD) and some associated peptides included in this new version of the chip. Hence, the version 1.0 did not show a robust and reliable response in that respect. Because of these disappointing results, and taking into consideration the effect observed with the hybrid chips (see section 7.3.2.4), we proposed a set of experiments in which a selected group of clinical samples would be measured in microarray chips manufactured with and without the recombinant RBD protein portion.

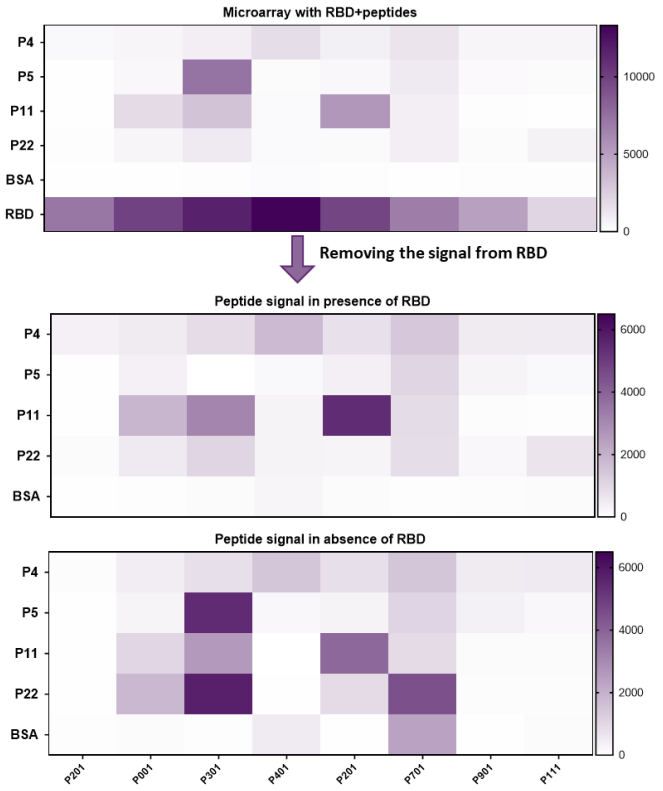

Figure 7.15 Influence of IgG response from RBD peptides in absence and presence of the recombinant RBD portion in the microarray using clinical serum samples. The y-axis represents the epitopes in the microarray and the x-axis shows the different clinical samples (from patients with robust RBD response). The upper heatmap corresponds to the signal detected after samples incubation in a microarray combining RBD peptides and recombinant RBD (firs graph) while the same heatmap eliminating the epitope from the recombinant RBD is expressed (second graph) changing the RFU's scales. In the lower section, a heatmap obtained after incubation of the same samples with a matrix only containing peptides from RBD without the recombinant proteins is observed.

In first place, is possible to highlight that our microarray was able to detect IgG's with potential neutralization capacity from patient's serum samples primarily binding to RBD protein, as expressed in the first heatmap of the Figure 7.15. In this case, the signal detected with the recombinant RBD portion (13.000 RFU's) was considerably higher than the one obtained with the peptide epitopes (6.000 RFU's), although some of them also showed response. From this result and in line with further evidence [24, 27], the RBD portion seems to lack of highly immunogenic linear peptides explaining the differences in the detectability observed. This may suggest that conformational epitopes seem to be essential

during the development of functional neutralizing antibodies. In fact, the gold standard technique to define the neutralizing activity of antibodies consists in plaque reduction neutralization tests (PRNT), preserving the native structure of the RBD but not widely implemented due to the requirement of living viral particles [28]. Therefore, a potential alternative contemplated for the third version of the *Immuno*-µSARS2 chip will include conformational peptides, considering the close proximity of two Cys residues located in the RBD sequence (-C_{480}NGVEGFNC_{488}-), that can be synthesized forming a loop-like structure mimicking a closer protein conformation. Through this approach we expect to obtain an increased response from the peptide in order to avoid exclusive need of the RBD portion.

On the contrary, as the Figure 7.15 shows, no significant differences were observed between the peptides analysed in one or another chip attributing that competitive effects are not prevalent with RBD portion in the chip. With the exception of **P22** (LQSYGFQPTN$_{501}$GVG), for which clear signal reduction was observed in some clinical samples when the recombinant RBD was present. The fact that only **P22** detectability was affected by the incorporation of RBD and not the rest of peptides needs to be further explored, however one possible explanation could be related to conformational preferences of the antibodies in the serum samples towards this particular sequence located in the protein rather than for the linear peptide. This conformations differences perhaps do not affect in the same extent to the other linear peptides and this is why the competence phenomena previously discussed is not manifested.

The signal differences detected over peptide **P22** in absence and presence of RBD protein in the chip among the different clinical samples assayed are represented in detail over Figure 7.16. The possibility of error during dilution preparation is discharged because the intensity detected over the rest of epitopes is comparable amongst both measurements and only interfere with **P22** sequence signal.

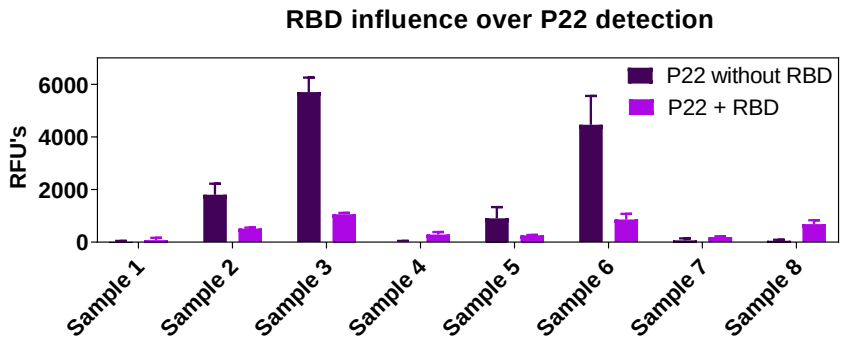

Figure 7.16 Influence of recombinant RBD in the determination of P22. The IgG levels from human serum samples against P22 were determined in absence (dark purple) and presence of the recombinant RBD protein (light purple) in the same microarray. The SD corresponds to the average of five replicate spots.

According to the literature, N501 residue present in **P22** and RBD forms a hydrogen bond with Tyr41 of ACE2 receptor, that may provide a distinctive conformational arrangement that is highly immunogenic and may increase the binding capacity [29]. Additionally, some variants of concern with increased transmissibility displayed mutations in the same amino acid and this modification could be promoting immune escape [30].

7.3.3.3. Identification of VoC-derived peptides in clinical samples exposed to the original SARS-CoV-2 strain

The continuous emergence of threatening VoC's displaying often higher infectivity prompted us to consider incorporating characteristic peptide sequences on the chip in such way that the immunological signature could also provide information of the causative variant of the infection. The hypothesis behind was that in addition to the presence of antibodies against such particular mutated sequence, the immunological profiles could also be altered. It should be noticed that version 1.0 of the chip contained peptides of the initial Wuhan strain. A major potential risk of this idea was that the polyclonal nature of the infected serum would not be able to differentiate a single amino acid mutation characteristic of a particular variant. On the other hand, an important limitation was that the three cohort patients that we had available were obtained during the prevalence of the original strain (Wuhan), making it difficult to validate the

chip for this purpose. However, within the context of the ongoing collaboration with HdMar, a prospective clinical studied has been approved to address such objective among other studies aiming at get deeper knowledge of the chip potential as prognostic tool for certain epidemiological studies, based on a more accurate and well-defined selection of the patients infected.

On the meanwhile, we assessed if the immunological profile of the samples already available would be affected by the introduction of VoC-derived peptides on the chip and if the specificity was high enough to distinguish these mutated sequences. To address such objective, for a set of serum samples, the signal recorded on the spot where the original peptide sequence was placed was compared to that of the spot of the mutated version.

The influence of single amino acid modifications (VoC's peptides) over fluorescent detection was initially assessed utilizing the CTR+Ab S on a chip that included the original peptides and the respective mutated sequences derived from S protein. As Figure 7.17 shows the CTR+Ab S immunological profile at 100 µg mL^{-1} differentiated between **P6** and **P6b** (**Alpha**, P681H), but the signal intensity of **P6c** (**Delta**, P681R) remains comparable to the original sequence. However, at 20 µg mL^{-1} of CTR+Ab S the signal from **P6** is significantly different from the other two peptides pointing to the possibility to discriminate between sequences and presumably identifying particular **Alpha** and **Delta** variants if appropriate optimized conditions are used. Contrarily, for **P11**, the highest concentration of CTR+Ab S (100µg mL^{-1}) revealed similar intensity with **P11c** (**Gamma**, K417T) but a considerable reduction of the recognition of **P11b** (**Beta**, K417N) while at lower antisera concentration (20 ug mL^{-1}), the signal of the three peptides was comparable. Finally, **P21** could be distinguished from **P21b**, although with a very low intensity for the last one, while **P22** did not provide any detectable fluorescence for either the original or the mutated sequences. From these findings, it could be assumed that immunological response towards the peptides evaluated and their corresponding variant-derived sequences, differing in a single amino acid could be discriminated by the chip using the rabbit CTR+Ab S sample, with the exception of **P22**. However, **P22** showed response in clinical samples as discussed in previous experiment assessing neturalizing antibody detection.

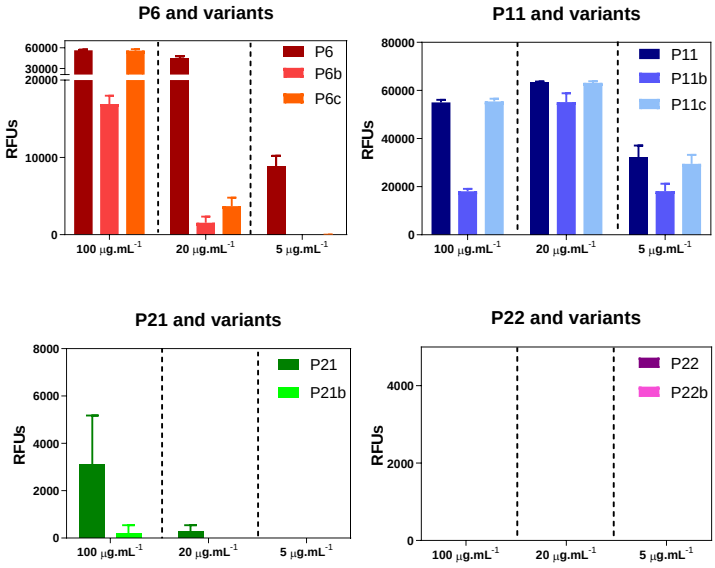

Figure 7.17 Determination of IgG response against peptides from Variants of Concern using CTR+Ab S. The fluorescent response from the original peptide sequences (P6, P11, P21 and P22) was compared with the peptides generated against the variants of concern in order to study if a single amino acid mutation was detectable after incubation with CTR+Ab S at three different concentrations (100, 20 and 5 µg mL^{-1}) evidencing signal differences. The SD corresponds to the average of three replicate spots.

To assess the performance with clinical samples, the profile of IgG response from the three clinical cohorts (RT-PCR+ samples: 94 HdMar,142 BioZgz, and 80 from HUGTIP) towards the original peptides and their respective variants was evaluated. Overall, the Figure 7.18 shows that structurally related peptides behave similarly in samples predominantly infected by the Wuhan strain. However, in some patients, both versions of the peptides are recognized in different proportions, suggesting that changes in the amino acid sequences can affect peptide recognition using the same sample, in this experiment competitive events should also be contemplated as they were printed in the same microarray chip. With this set of samples, it would be expected to obtain a higher response with the peptides generated from the original strain rather than the mutated epitopes.

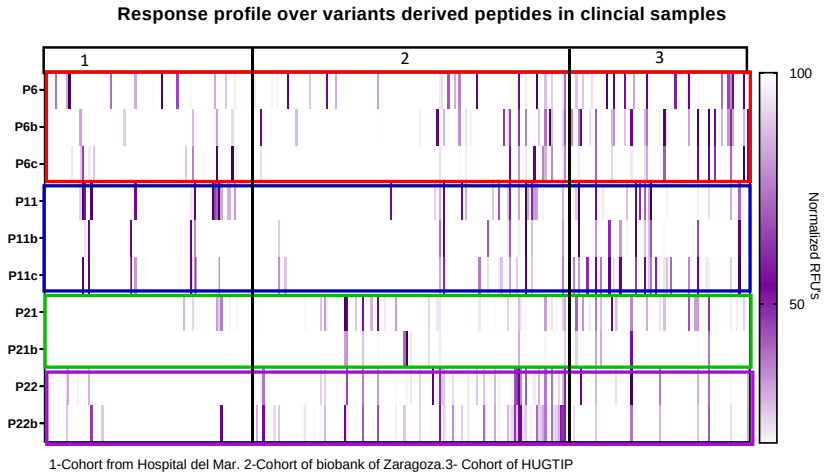

Figure 7.18 Recognition of IgG profiles in original peptides sequences and their corresponding derivates against specific variants of concern with clinical samples infected with Wuhan strain. The IgG levels detected over original peptide sequences were compared to the IgG levels of the same patients against the peptide's specifics for the VoC's in the same microarray. The y-axis represents the corresponding peptides grouped in clusters highlighted in different color. The x-axis contains the clinical samples analyzed from RT-PCR+ patients. The color scale represents the signal in normalized RFU's starting form 0 (white) to 100 (purple).

As observed in the previous heatmap, most of the peptides are still recognized in this group of samples, and some of them like **P6b**, **P11c** and **P22b** displayed considerable response in contrast with the original sequences. In an attempt to perform a comparative analysis, the percentage of samples providing at least 25 % or higher response to each peptide was estimated for every cohort. A threshold of 25 % was established in order to evidence differences in the detectability, considering the low signal obtained from these peptides in the previous microarray (Figure 7.18), however this value do not imply positive epitope response. It would be expected that the peptides from the original sequence could provide the higher response while the mutated peptides a comparable or even lower response. From this study (see Figure 7.19), the potential identification of mutated peptides with serum samples infected by the Wuhan strain was determined.

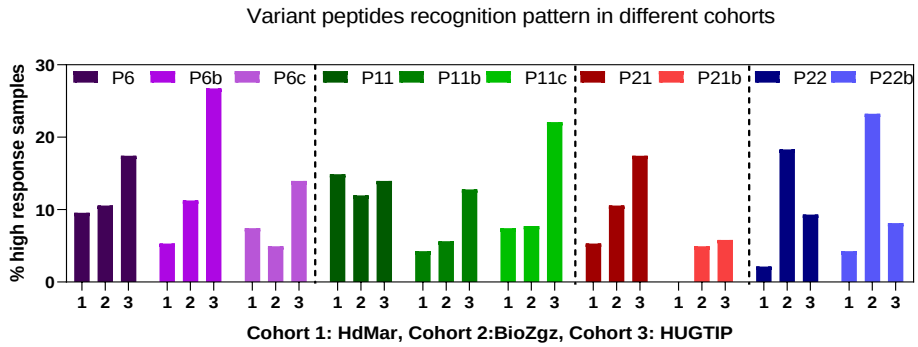

Figure 7.19 Comparative analysis of signal obtained from original peptides and variant peptides. The percentage of samples displaying at least a 25 % or more of response in the array was evaluated for each cohort independently. On the y-axis the % of samples showing more than 25 % of response is represented while in the x-axis the different peptides are represented in related colors according to the sequences compared and under the number assigned to each sample cohort being 1: HdMar, 2: BioZgz and 3; HUIGTP.

In the Figure 7.19, the **P6** showed relatively similar response (10-15 %) amongst the three patients' cohorts with a slight increase in the third one, while **P6b** was highly detected over cohort 3 (27 %) suggesting differential behavior in this group that can't be well understood. For the case of **P6c** a lower detectability was observed in contrast with the original peptide as expected, bearing in mind that the samples were exposed to the original strain. In the next example, the % of response from IgG's against **P11** was very similar in the three cohorts ranging from 11-14 %. Through the analysis of **P11b** (**Beta** variant, K417N) a considerable signal reduction was observed in respect to **P11** (except in cohort 3), while for **P11c** (**Gamma** variant, K417T) a lower response was evidence in the cohorts 1 and 2 but not in cohort 3 that reached even higher % values (22 %) than **P11**. This behavior was already described for **P6b** in the same cohort, indicating that this group of samples seems to react differently to the mutated versions of some peptides, which would require a deeper analysis to extract conclusions, ranging from a possible batch effect to a particular characteristic in the population at immunological level. Moreover, the signal from **P21** was different in the three cohorts indicating influence of the sample batch utilized, however **P21b** (**Alpha** variant, ΔH69, ΔH70) showed that the deletions included over the sequence considerably reduced the recognition of this peptide in contrast with **P21**. Finally, the signal towards **P22** was analyzed and displayed different behavior in each cohort being predominantly detected in cohort 2 (18 %, BioZgz) compared to cohort 1 (2 %, HdMar) or cohort 3 (9 %, HUGTIP). Which is even more surprising

is that P22b (Beta and Gamma variant, N501Y) response was found to be higher in cohort 1 and 2 than the original peptide. These means that both peptides are recognized, but is not possible to ensure that the IgG profile is affected because this would require to study the peptides in different matrixes independently. Consistently with the results using CTR+Ab S samples, the modified sequences and the original peptides can be recognized by serum samples from patients infected with the Wuhan strain. Thus, validating the idea of defining a particular serological pattern according to the variant causing the infection with the complement of artificial intelligence and multiparametric determinations.

7.3.4. DETERMINTATION OF THE PREDICTIVE CAPACITY OF THE *IMMUNO*-µSARS2 v 2.0 CHIP IN CLINCAL SAMPLES

Thie following section performed in this PhD thesis has been carried out in collaboration with Marc Alorda (Nb4D-CSIC) and the assistance of Dr. Agustin Gutierrez Galvez (IBEC) from the group of Signal and Information Processing for Sensing Systems leaded by Prof. Santiago Marco (IBEC). The elaboration of ROC curves was proposed to evaluate the diagnostic and prognostic value behind the updated version 2.0 of the chip. From the complete set of samples analyzed, only those classified as RT-PCR+ and prepandemic samples were utilized to generate the corresponding ROC curve in order to estimate the discrimination capacity of the chip-based on IgG responses. Although, as mentioned the RT-PCR and the immunological profile are not strictly comparable based on the target molecule analyzed, previous results (see section 6.3.7.2 in chapter 6) already showed that for this particular set of samples present high correlation. On the other hand, the aim here is just to probe if the chip is reliable in respect to providing positive result for those patients that have readily suffer the infection.

7.3.4.1. ROC curve establishment

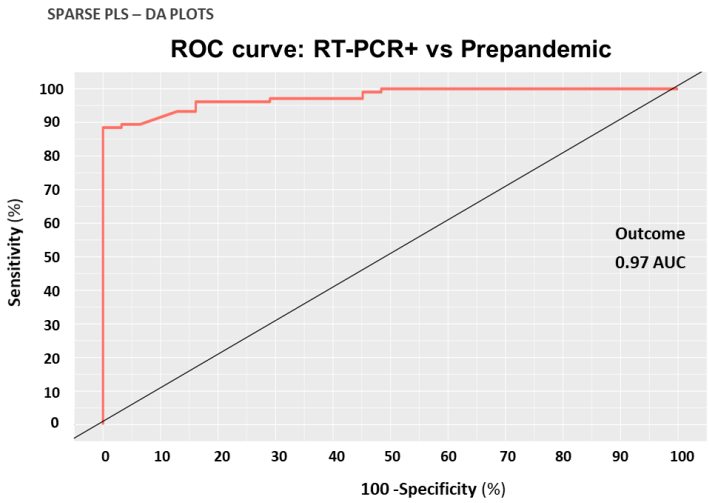

Figure 7.20 ROC curve of the Immuno-µSARS2 V 2.0 chip. The ROC curve obtained from a multivariate analysis of the hybrid peptide-protein matrix towards the discrimination of RT-PCR+ group (n =288) and control group (n = 96) IgG responses. The AUC value was calculated in 0.97 as a result of 98 % clinical specificity and 91 % clinical sensitivity.

Basically, the ROC curve (Figure 7.20) represents the sensitivity in Y axis (true positive rate) against 1-specifcifty (false positive rate) over X axis for each sample analyzed. It was build using the results from a total of 288 RT-PCR+ human serum samples and 96 prepandemic serum specimens. With this analysis, a 0.97 AUC value was obtained consisting in a 98 % of clinical specificity and 91 % of clinical sensitivity towards the capability of the chip of truly attribute the positive response to a person that has been exposed to the virus. From the diagnostic perspective, the interpretation of a 98 % of specificity is highly remarkable because it's indicating a low uncertainty towards false positives determinations. In other words, this represents the level of samples detected as negatives that are truly negative, feature extremely required over any diagnostic platforms. On the other hand, the 91 % sensitivity highlights that samples that are classified as positive are truly positive. According to our study, we encourage the transition from a laboratory-based platform to the potential clinical implementation, evidencing the accuracy of the chip to diagnose seropositivity towards COVID-19 on patients exposed to the virus.

7.3.4.2. Area under the curve (AUC) calculation with univariate analysis

In order to investigate the capacity of each epitope to individually discriminate between RT-PCR+ and prepandemic samples, the AUC and the classification rates were determined for each component of the matrix, using a *univariate* analysis as already performed with the first version of the array in the previous chapter 6.

The corresponding Figure 7.21, shows that over the 35 epitopes analyzed a total of 30 were consider significant classifiers of seroprevalence based on IgG response with an AUC value statistically relevant above 0.6. Notably, when the same analysis was conducted over the first version 1.0 of the array (see section 6.3.7.2), only peptides **P10** and **P9** were assigned as significant classifiers together with the recombinant proteins. Another remarkable aspect is that **P10** was again defined as the best epitope classifier, evidencing the potential behind this sequence to distinguish both groups of samples. Furthermore, the new sequences incorporated displayed higher AUC and classification rate values and were considered also significant markers indicating high specificity in respect to the determination of the IgG profile attributable to SARS-CoV2 infection. Results interesting to highlight that peptides that were not significant in the previous analysis, reached statistical relevant correlations in the new microarray, probably as a result of the already described optimizations and the cooperative effects after the incorporation of the new epitopes to the matrix including highly immunogenic sequences.

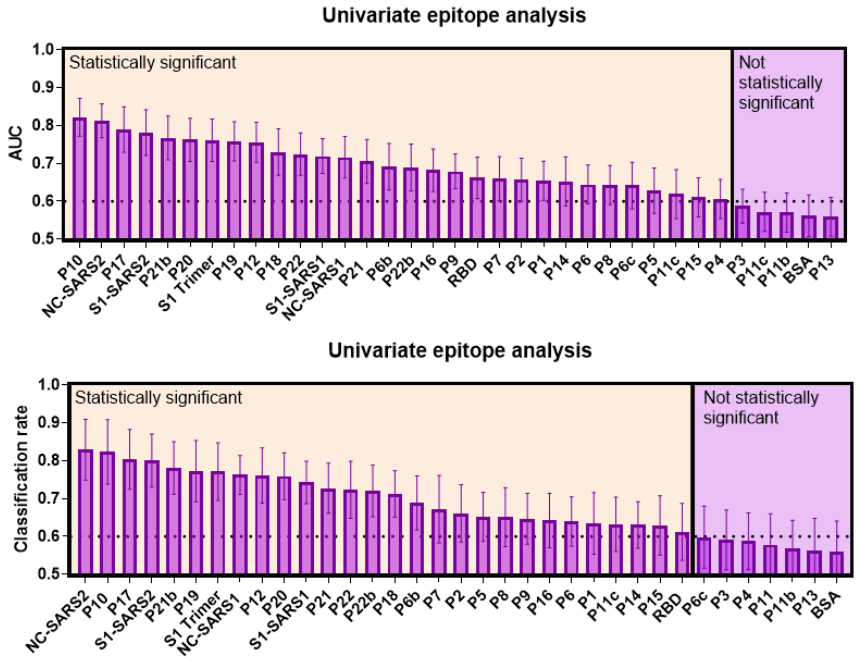

Figure 7.21 Individual epitope classification capacity. From the complete matrix utilized, a univariate analysis was conducted estimate the AUC value and the classification rate for each epitope to distinguish RT-PCR+ samples from pre-pandemic samples. In this case, epitopes with AUC and Classification rate above 0.6 were statistically significant predictors.

Across the following section is possible to identify that form the panel under analysis, **P10**, NC-SARS2, **P17** and S1-SARS2 present the highest classification rate over the rest of epitopes to distinguish between RT-PCR+ and prepandemic samples (see Figure 7.21). As already reported, structural proteins like NC-SARS2 and S1-SARS2 are widely employed for IgG determination [31], being implemented in most of the commercial serological devices [32]. On the contrary, the linear peptides **P10** and **P17** derived from the C- terminal and N-terminal domains of N protein respectively, were both grouped as equivalent classifiers to proteins. In agreement with these results, the implementation of **P10** and **P17** in detection platforms could be considered as substituent of the recombinant N protein due to the comparable serodiagnostic performance demonstrated. This would allow to reduce the analysis costs related to the protein production and probably increasing the shelf-life of the kits owing the greater stability of the peptides in comparison to that of the proteins.

Remarkably, the analysis of a BSA epitope included as internal control revealed non-significant correlation with positive serology, confirming that the signal obtained from each peptide was specific of the sequence conjugated and no due to interactions with BSA. In addition, **P3**, **P11**, **P11b** and **P13** were also included in the group showing non-specific response suggesting low individual predicative capacity.

Although slight variations in respect to the significance of the epitopes can be observed between AUC and classification rate estimations, both approaches consist on alternative techniques to evaluate the performance of a classification method and provided comparable results. Interestingly, after both types of analysis epitopes like **P3**, **P11b**, **P13** and BSA were always defined as non-significant classifiers evidencing lack of individual capacity to distinguish between the conditions evaluated. However, in a multiplexed analysis the incorporation of these epitopes becomes relevant because they may contribute to distinguish negative correlations adding different information to the profile measured rather than only a positive signal. Bearing in mind that the best classifier obtained with the *univariate* approach reached almost 0.80 AUC value and the multivariate prediction was estimated in 0.97 AUC towards patient's classification, results evident that multiparametric analysis is preferred over single epitope determinations due to the increase in the accuracy over the method classification.

7.3.4.3. Interpretation of the chip's predictive value in RT-PCR negative samples

Once the system was successfully validated in RT-PCR+ and negative control (prepandemic) samples, we addressed the study over RT-PCR- serum samples in order to interpret the information available from this group. Is important to notice that those samples were acquired together with the positive serum sets, obtained during initial pandemic stages when hospitals were at maximum capacity and every individual with suspected symptoms or possible contact with infected patients was tested through PCR method. There was a high risk of false negative results if the sampling window was not adequate. A limitation behind RT-PCR technique is found over the period of sample collection with higher uncertainty over initial phases or after the peak of infection [33, 34].

Therefore, the incorporation of RT-PCR negative samples was proposed considering three possible scenarios

1) Lack of infection: with a negative RT-PCR result and negative serology
2) Early infection phase: with non-detectable antibody titters or viral load, testing negative for RT-PCR and serology.
3) Late phase of infection, indicated by RT PCR negative result but positive IgG or IgM response.

Making use of the chip developed, the situation 2 would not be distinguished because infected patients start to display detectable IgG response after day 10 PSO. On the contrary, the situation 1 should be comparable to the results obtained with the prepandemic cohort due to the absence of infection and for the situation 3, a positive serology result will evidence pre-existent infection helping to estimate the true prevalence of SARS-CoV-2 at epidemiological level even though no RT-PCR was previously carried out. The simultaneous evaluation of immune response against S and N protein epitopes may also serve to distinguish immunity induced by vaccines, generally enhancing anti S response, as well as estimating long-term immune protection mediated by antibodies.

The signal analysis of RT-PCR negative samples through ROC curves estimation, identified approximately a 20-25% of false negatives showing detectable antibody response against the virus, although they tested negative for RT-PCR. The sensitivity of this technique was found considerably affected by the time of sample collection from the onset of symptoms, increasing the chances of false negative rates in early course of infection and after 10 days PSO [35-37]. Additional evidence also suggested that the sampling method could also contribute to increase false negative results, although is not assumed as the major cause [38]. The objective of antibody tests is not to intended to replace RT-PCR methods, but rather to complement them, helping to overcome the inherent limitation behind both approaches.

7.3.5. SEVERITY PREDICITONS CORRELATING IMMUNOLOGICAL PROFILES AND MACHINE LEARING TECHNIQUES

Taking advantage of the amount of data extracted form sample analysis against relevant viral epitopes, the next challenge aimed to explore the integration of machine learning techniques to predict disease progression based on IgG response. Due to this, severity correlations were established using well defined sample groups classified by clinicians during the period of collection to identify characteristic serological signatures in accordance with disease severity. The selected samples were stratified in asymptomatic, hospitalized, admitted to ICU and *exitus* and computational analysis was used to generate classification models towards the respective clinical manifestations based on the profile of antibodies detected in each group.

In the following table 7.2, the partial distribution of the 755 serum samples analyzed is represented according to the health provider institution classified in positive or negative RT-PCR and prepandemic groups. However, depending on the type of analysis performed a reduced number of samples from each group was implemented based on different selection criteria such as days post symptom onset or difference between PCR and serum extraction. The samples classified by clinical outcomes (asymptomatic, hospital, UCI admission and *exitus*) were extracted form patients testing positive for RT-PCR to corroborate that the symptomatology was consequence of SARS-CoV-2 infection.

Table 7.2 Clinical serum samples distribution according to the healthcare provider institution and grouped through RT-PCR results and clinical manifestations

Cohort	RT-PCR+	RT-PCR-	Prepandemic	Clinical outcomes		
				Hospitalized	ICU	*Exitus*
HdMar	96	51	97	47	28	2
HUGTIP	81	82	18	17	6	9
BioZgZ	143	187	-	55	24	37

In order to perform the comparative analysis, the 80 % of the samples over each category, were randomly selected and used as “training group” to provide the inputs needed to instruct the algorithm for adequate signal identification. Once the final classification model (algorithm) was established, the remaining 20 %

was used to validate the accuracy of the method included in the analysis as blind samples and classified according to the prediction model generated. The performance was estimated considering the results obtained over test samples by calculating the accuracy of the method and reporting true positive and true negative response as sensitivity and specificity respectively.

As expressed in thetable 7.3 a characteristic fluorescent pattern was determined to predict with 66 % accuracy (p value= 0.03*, 55 % specificity and 77 % sensitivity) the requirement of hospitalization over asymptomatic disease course. Followed by a distinct serological signature to distinguish ICU admission with 70 % of accuracy (p value= 0.01*, with 82 % specificity and 58 % sensitivity). Finally, *exitus* prediction was possible making use of a different IgG profile reaching the most significant predictive capacity over the three conditions evaluated against asymptomatic disease course with 81 % accuracy (p value= 0.0004*, 71 % specificity and 92 % sensitivity)

Table 7.3 Severity predictions calculated using the IgG response profile from patients with different clinical manifestations compared to asymptomatic individuals.

Clinical condition	Accuracy	P value (*<0.05)	Specificity	Sensitivity	SD
Hospitalization	66%	0.03*	55%	77%	6%
ICU admission	70%	0.01*	82%	58%	6%
Exitus	81%	0.0004*	71%	92%	6%

*statistically significant value. SD refers to standard deviation)

Results interesting to emphasize that the most accurate prediction was achieved over patients suffering from irreversible condition (or *exitus*) compared to “less” critical outcomes as ICU admission or hospitalization regarding asymptomatic infection. According to our results, lethal outcomes seems to be associated to a well-defined immunological imbalance reflected over the IgG pattern detected along the three cohorts under analysis. These findings may indicate that the differences observed in respect to the profiles recorded for patients with less survival expectancy could be implemented to anticipate clinical progression offering alternative treatments options.

In the same line, further evidence also supports the assessment of host immune dysregulation based on a gene expression assay (SeptyCite RAPID test) generally

applied for sepsis diagnosis as predictive tool of COVID-19 disease severity [39]. Interestingly, a higher accuracy between critical outcomes and mild disease differentiation was evidenced with this method showing correlation with our findings. A similar technological approach aiming to evaluate antibody levels to estimate disease severity was proposed, in this case determining IgG, IgA, IgE and IgM responses to multiple viral epitopes and proteins under microarray format [40]. The authors claim that stronger IgG and IgA levels towards full length S protein could serve as indicative of COVID-19 severity as we have observed, however they couldn't find specific epitopes or peptide with predictive capacity while our rational selection proposal demonstrated to be useful in this sense and also implementing multiparametric analysis to define signatures instead of single markers determinations. This suggests that COVID-19 severity could be estimated through the evaluation of the immunological performance using antibodies as promising clinical predictors. On the other hand, it is important to highlight that a positive *exitus* classification based on the prediction model generated is not strictly defining causative condition but may contribute to identify candidates with higher predisposition to develop severe symptomatology.

7.3.5.1. Severity estimation based on single epitope contribution

A detailed analysis of the relative intensity defined for each epitope to predict individually different clinical outcomes was performed and the results are presented in Figure 22. As can be seen, each chart represents the average intensity measured from clinical samples belonging to each severity scale (*Exitus*, ICU admission, Hospital and control or asymptomatic) on every epitope. The corresponding signal distribution was analyzed through regression models to define the most accurate approach associated to a particular clinical outcome.

Notably, is possible to differenciate positive and negative correlations towards COVID-19 severity based on the amount of antibodies detected against each component of the chip. For example, higher IgG responses against epitopes like S1-SARS2, S1-SARS1, S1 Trimer, RBD, **P10** and **P6** were positively correlated with increased severity indicating that antibodies targeting predominantly those regions may serve to anticipate worst prognosis. In agreement with this, some

reports state that higher neutralizing titers lead to severe disease course and in this case anti-RBD antibodies showed increased response according to severity [41]. Additionally, other authors state that higher antibody levels were associated with clinical severity and in this case the epitopes under study were displaying higher intensity values revealing serological predominance over the rest of epitopes [42].

On the contrary, antibodies against **P14**, **P5** or **P11** behave differently and were classified as negative correlators to severe progression meaning that prevalence of IgG's towards these sequences was generally found in patients with better prognosis. In particular, during sample analysis **P11** and **P5** did not showed considerable fluorescence response and that could explain the negative correlation. However, the epitope **P14** was detectable in clinical samples and higher titers against this sequence are observed in asymptomatic individuals suggesting possible protective implications that should be further evaluated.

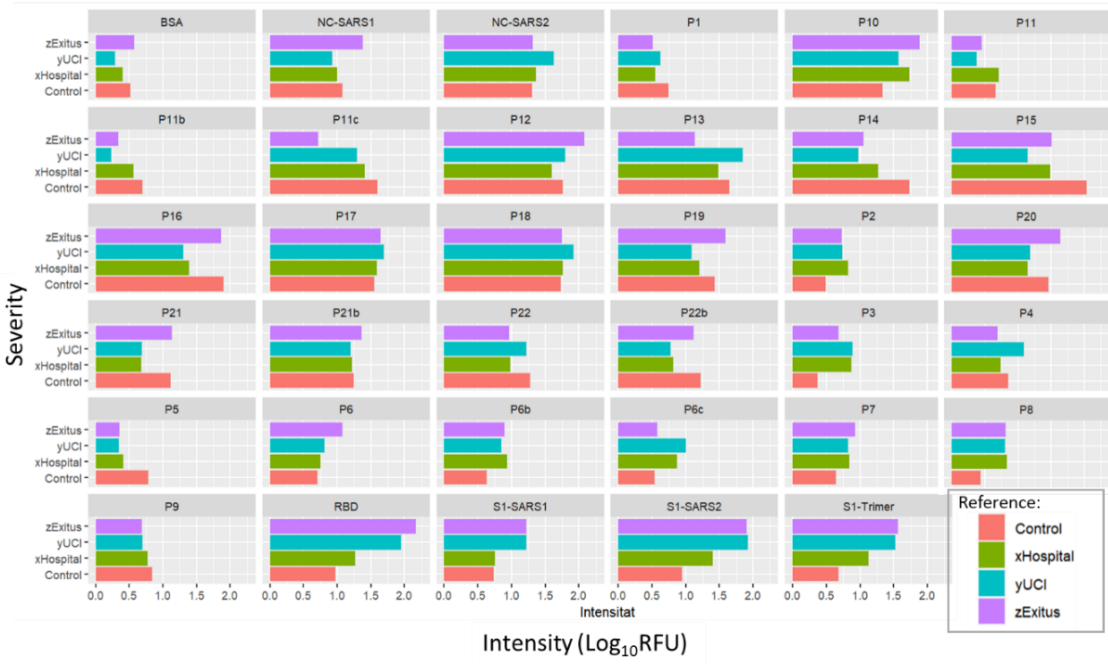

Figure 7.22 Single epitope correlation of IgG mediated response with clinical severity. The relative intensity detected in every epitope after measuring the different severity groups was represented in Log_{10} RFU and assigned to hospitalization, ICU admission, Exitus and asymptomatic (or control). The contribution of each epitope towards severity determination is represented and analyzed.

An interesting aspect to discuss arises from serological differences detected over peptides from Wuhan strain and the variants of concern after the modification in one amino acid. Surprisingly, **P11** shares a comparable signal pattern with **P11b** changing the lysine$_{417}$ for asparagine (K417N, South African Variant) but if the same lysine$_{417}$ is substituted for a threonine (K417T Brazilian variant) like the case of **P11c**, the intensity patter differs considerably allowing better *exitus* discrimination from the rest of outcomes. In the other peptides including variant mutations, the behavior seems to be comparable to the original sequence taking into account that the samples analyzed were prevalently infected by the Wuhan variant by the time of serum extraction. Furthermore, BSA epitope displayed low relative intensity and no clear correlation with any clinical progression validating specific response form the rest of epitopes analyzed. Across the already discussed study, the importance of the individual epitope contribution towards more specific multiplexed approaches is manifested, showing how different epitopes could provide complementary information that if is integrated with bioinformatic tools could increase the accuracy behind prediction models with imminent applications in forthcoming diagnostic platforms.

7.3.5.2. Pearson's correlation analysis of peptide epitopes and proteins

With the idea to further analyze the complex response detected from epitopes included in the multiplexed array, Pearson's correlation studies were conducted. This approach was proposed to establish associations between the signal detected across the chip, enabling the identification of correlated epitopes and determining whether they provided redundant information. As primary objective, the comparison of linear peptides response with the detectability achieved using recombinant proteins was addressed. Additionally, we explored the possibility of using smaller peptide clusters that could retain the diagnostic and prognostic value while reducing costs and simplifying signal interpretation. Through Pearson's correlation estimations, two epitopes can be positively or negatively associated, indicating that if a peptide X is positively correlated with a protein Y, the information provided by both components is comparable. Although this correlation is not defining causative effects, this may help to understand common pathways implicated during serological response development. For this purpose, the signals obtained from the analysis of RT-PCR+

samples were correlated amongst the different epitopes included in the array to identify clusters of associated viral components as serological indicators.

Throughout the following Figure 7.23 is possible to identify different clusters based on the signal obtained after clinical sample analysis. From the section A) the first group of correlated epitopes are **P15**, **P16** and **P14** belonging to the N terminal domain of S2 subunit in addition to three peptides related with N protein identified as **P9**, **P19** and **P20** also including the epitope NC-SARS1. A remarkable feature is found over the positive association between these epitopes deriving from different viral components such as S2 subunit and N protein linked to the structural NC-SARS1 that shares more than 90% of homology with NC-SARS2. In this regard, N protein and S2 subunit has been reported as highly immunogenic promoting similar serological behavior over both regions mediated by IgG [3].

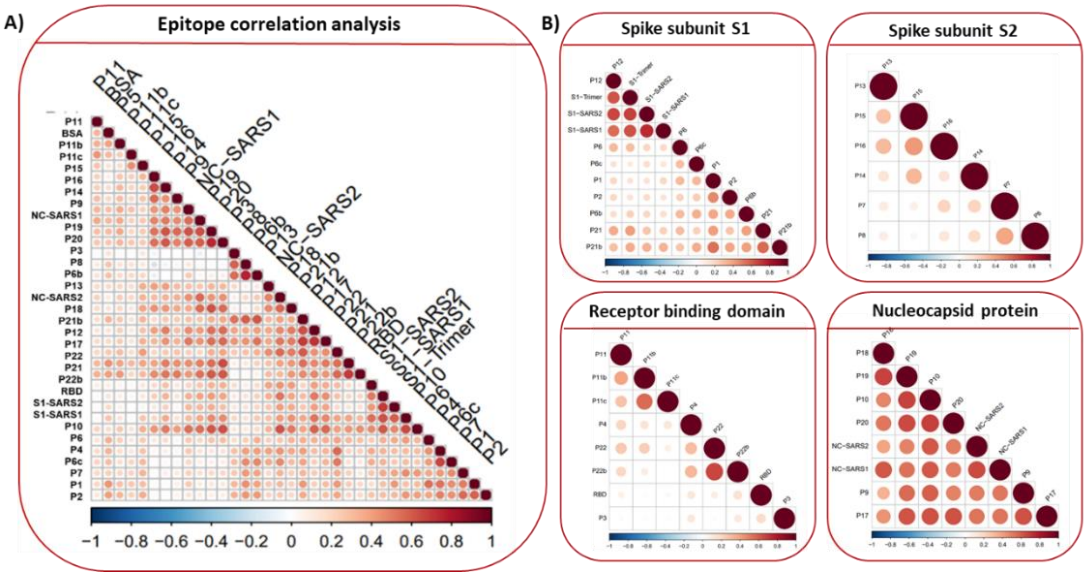

Figure 7.23 Pearson's correlation coefficients were estimated for a) complete matrix of epitopes analyzed, b) based on structurally and conformationally related peptides and proteins. Positive correlations are represented in color red and negative correlations in blue, while no correlation remains white.

Alternatively, other relevant cluster was defined by 13 epitopes including NC-SARS2 with **P18**, **P17** and **P10** deriving from N protein thus structurally correlated with this epitope. Then **P12**, **P22**, **P21**, **P6** from S protein with **P21b** and **P22b** that are peptides including one mutation derived from variants of concern.

Furthermore, the signal from these peptides was positively associated with S proteins such as S1-SARS2 and S1-SARS1 as well as the RBD epitope. These results support that the linear peptides selected provided specific response due to the close correlation to the proteins containing those sequences. Another remarkable finding emerged from the lack of correlation of these epitopes with the BSA included as negative control, contemplating that the linear peptides were conjugated to this protein and the signal obtained was not associated. Additionally, the strong correlation between N epitopes was also evidenced with high reddish intensity over NC-SARS1, NC-SARS2 with peptides **P19**, **P20**, **P18**, **P17** and **P10**.

Interestingly, the same type of analysis was carried out only considering structurally related epitopes including peptides and proteins from the matrix. As can be seen in section B) the N related epitopes are the most highly correlated in comparison with the other regions evaluated like S2 subunit, RBD or S1 subunit indicating similar serological performance in the samples. On the other hand, in the cluster of S1 subunit, the sequence of **P12** was highly correlated to the structural counterparts analyzed like S1-SARS2, S1-SARS1 and S1 Trimer showing positive IgG signal association. An interesting observation, is that immunoglobulins directed against peptide **P12** were previously reported as RBD independent neutralizing antibodies due to the close proximity of this sequence to RBD zone, interfering with ACE2 binding [19]. This could explain the high correlation detected across this sequence in regard with the structural S1 subunit, evidencing a relevant immunological role during IgG development in contrast with the rest of peptides. As the IgG mediated responses against linear N peptides (**P9**, **P10**, **P17**, **P18**, **P19** and **P20**) and **P12** from S1 subunit were positively correlated with the IgG levels detected in their protein counterparts, this may suggest that conformational arrangement is not determinant to promote immunogenicity across these regions. This feature can be mainly attributed to the N protein sequence, which results highly immunogenic even using N-derived linear peptides.

Regarding RBD zone evaluation, no positive correlations were established between the recombinant portion of RBD and the selected peptides (**P4**, **P11**, **P5** and **P22**). This could indicate low immunogenicity of the selected sequences, that may be overlapped by the signal from other immunogenic peptides (derived from S2 and N) considering that a single array was used to perform the

multiplexed determination. While another explanation started to be contemplated and points out that the 3D arrangement of the RBD portion is essential during NAb's development and for the biorecognition event. Therefore, the requirement of conformational peptides to map the RBD would be more accurate than the use linear sequences. This observation agrees with the work performed by Gattinger and collaborators [27] demonstrating that neutralizing antibodies are effective against the folded version of RBD region and not against the unfolded sequence. In this regard, a potential limitation of our platform could be evidenced due to the exclusive use of linear sequences without any conformational peptides. Although the use of recombinant proteins in the chip was proposed to overcome such limitation, for the future updates of the *immuo*-µSARS2, this should be considered.

7.3.5.3. Conclusions

In summary, the incorporation of new peptides to the matrix with the aim to extend the predictive capacity of the platform was successfully achieved. Initially considering the use of computational tools to establish potential antigenic sites from S and N proteins and emerging literature evidencing consolidated experimental results indicating immunodominant regions.

Although the use of serological platforms to predict disease progression has been extensively discussed contemplating certain limitations over assay performance which are influenced by adequate testing windows, response heterogeneity and cohort determination even due to the type of assay [43]. The updated version of the microarray showed more robust response compared to the first development, elucidating potential immune mechanisms involved during viral infections and defining correlations regarding disease progression. Additional limitations were found over the lack of standardized analytical procedures for the determination of antibody levels considering individual variance, method uncertainty or accuracy and positive predictive value making the implementation in the clinical fields even more challenging [44].

From the characterization experiments several concluding remarks were obtained such as the definition of lower number of drops per spot to increase the signal at a reduced surface area, to the preference of BSA bioconjugates rather than single peptides to avoid unspecific adsorption and the consideration

towards competitive effects detected after using a single matrix combining peptides and proteins for IgG determinations in clinal serum samples.

Moreover, the results obtained after sample analysis, showed that peptides derived from the C- terminal region of N protein as well as S2 subunit were highly immunoreactive. In this regard, additional evidence supports our findings indicating that the carboxyl terminal domain of N protein could be considered as a highly immunogenic region for IgG, IgA and IgM response in COVID-19 convalescent patients and epitopes belonging to S2 subunit were also detected as reactive towards IgG mediated immunity [45].

On the other hand, the integration of bioinformatic tools was essential during platform validation reaching considerable levels of sensitivity (91 %) and specificity (98 %) to further explore the predictive capacity of the system. In this line, almost a 20-25 % of the samples classified as RT-PCR- were identified as seropositive (potentially false negatives) through our immunodiagnostic method evidencing the potential implications at epidemiological level. Alternatively, the use of artificial intelligence to generate classification models for the accurate determination of clinical severity based on an IgG fingerprint was significant, mainly to define *exitus* condition which may indicate that early IgG development is closely related with the successful disease control and could be used as biomarker to prevent critical outcomes. After the extensive research conducted towards the development of the present high-throughput, cost effective and accurate *Immuno*-µSARS2 v.2.0 chip, we highly encourage the implementation of this system in the current post-pandemic scenario with the aim to explore epidemiological immune prevalence and evaluate protection induced by vaccines as well as introduce novel epitopes from different viruses.

7.4. CHAPTER CONTRIBUTIONS

- Peptide-BSA bioconjugates outperformed direct peptides immobilization in microarray format, exhibiting lower unspecific binding and better detectability. In addition, conjugated peptides present different spatial distribution, mimicking a 3D arrangement that

promotes the accessibility of bulky antibodies compared to direct peptide immobilization.

- Full length proteins and peptide-BSA conjugates showed competitive behavior when deposited in the same microarray chip. The IgG binding profile was different if peptides and proteins were printed separately. Different sub-microarrays would be necessary to avoid such effect.
- Antibodies with potential neutralizing capacity can be distinguished with the microarray developed, but a strong dependence on epitope conformation seems to be related to the RBD zone. The recombinant RBD portion showed higher IgG response compared to the linear peptides selected. Conformational peptides can also be explored as alternative approaches.
- From RBD peptides, only IgG's against **P22** exhibited a competitive effect when the recombinant RBD was in the same microarray. Suggesting that, the native conformation of the folded **P22** epitope in the protein seems to be more immunogenic than the linear sequence.
- Peptides derived from VoC's were recognized by serum samples form patients infected with the original strain, showing different IgG interaction in some cases. Cohort variability was evidenced in peptides like **P6b** and **P11c**.
- The updated version of the I*mmuno*-µSARS2 (2.0) increased the analytical performance compared to the original version (1.0), with a 98 % of clinical sensitivity and 91 % of clinical specificity in respect to RT-PCR. Seropositive patients were identified across RT-PCR – samples, suggesting a 20 % of false negatives results form the reference method.
- The detection of IgM's was also evaluated in the same chip, showing differences between PCR +, PCR - and prepandemic groups proposed as early indicator complementary to IgG's. However, due to a relatively low singnal further optimization would be required.
- The most relevant IgG responses were determined against linear peptides targeting the S2 subunit and the N protein, indicating that highly immunogenic linear epitopes are predominant over those regions.
- Once again, **P10** was selected as the best epitope for individual discrimination between RT-PCR + and prepandemic samples and thus is proposed as promising immunodiagnostic epitope showing comparable response in the version 1.0 of the microarray.

- The *multivariate* analysis increased the diagnostic capacity of the prediction model compared to *univariate* analysis. Scaling from a 0.89 AUC value with the *univariate* approach to a 0.98 AUC in the *multiplexed* format.
- Disease severity can be differenciated measuring IgG response profiles with the epitopes selected in the microarray. For the first time, an IgG fingerprint to predict *exitus* condition with 81 % accuracy was identified, evidencing that adaptive immunity performance could impact on patients' clinical outcomes.
- Peptides **P10**; **P17**; **P18**, **P19** and **P20**, derived from N protein and **P12** from S1 subunit, provided comparable IgG responses to the full-length proteins in clinical serum samples. The potential substitution of the recombinant protiens with those linear peptides could be considered to develop cost-effective serodiagnostic platforms.

7.5. MATERIALS AND METHODS

All common reagents and methods employed during this experimental section have been already described in the materials and methods section of the chapter 6. Additional procedures or modifications will be described in the ongoing section.

7.5.1. RATIONAL PEPTIDE DESIGN 2ND GENERATION

As already discussed, the rational selection of the new set of peptides was based on the utilization of a B-cell epitope predictor software BepiPred 2.0, to estimate potential antigenic sites across S and N protein sequences extracted from Uniprot database. The combination of computational protein characterization with experimental reports from the literature was crucial for the successful design of potential immunogenic candidates. The same criteria applied to the first selection was employed in this process, including studies of antigenicity, accessibility, length and chemical coupling conditions. Throughout this procedure some remarkable examples contemplated from the literature include the work published by *Amrun et al* [46], *Holenya* and collaborators [47] and *Wang et. al* [48], empirically demonstrating the robustness over specific viral peptide sequences as serological indicators.

7.5.1.1. Synthesis of peptide epitopes 11-20 and VoC-peptides.

The second generation of peptide epitopes assigned as **P11** to **P22** and the epitopes designed against SARS-CoV-2 VoC (**P6b**, **P6c**, **P11b**, **P11c**, **P21b** and **P22b**) were synthesized following the standard Fmoc/*t*Bu solid-phase strategy in an automated microwave-assisted peptide synthesizer (Liberty Blue, CEM). Fmoc-Rink Amide ProTide (0.56 mmol/g) was used as polymeric support for the syntheses. The Fmoc removal and coupling reactions were carried out using the standard protocols. The coupling reactions were performed using a solution 0.5 M of DIC in DMF as coupling reagent and 1.0 M of Oxyma in DMF as additive. All

the synthesized peptides were acetylated at the N-terminal end of the peptide as described above.

Cleavage of the peptide from the resin was achieved by treating the peptidyl-resin with a mixture of TFA-TIS-2,2'-(ethylenedioxy)diethanethiol (ODT) (95:2.5:2.5, v/v/v) for 2.5 h. The solution was filtered and the peptide was precipitated by the addition of the TFA solution onto cold Et_2O, centrifuged, and the supernatant was discarded. The peptide was washed twice with Et_2O, dissolved with water-acetonitrile and lyophilized. The corresponding peptides were purified using a semi-preparative HPLC and analyzed with the chromatographic conditions described above.

7.5.1.2. Peptide BSA conjugation protocol

Peptides were conjugated to BSA as carrier protein through N-[β-maleimidopropyloxy] succinimide ester (BMPS) linker, following the same protocol described in Chapter 6. The conjugates were purified and characterized by matrix-assisted laser desorption ionization time-of-flight mass spectrometer (MALDI-TOF/MS) defining an average density of 5 to 7 peptides per BSA molecule. Storage conditions were the same as for the first set of peptides developed.

7.5.2. FLUORESCENT MICROARRAY

7.5.2.1. Slides derivatization

Microscope slides (Micro slides, plain pre-cleaned 75x25mm) were acquired from Corning Inc (Corning, NY, USA) Following a derivatization protocol already described in previous chapter 6**.**

7.5.2.1.1. APTMS derivatization for direct peptide immobilization

In order to covalently attach peptides directly to the glass surface a different immobilization protocol was required in comparison with BSA bioconjugates. As mentioned above, the respective peptide sequences were synthesized containing a cysteine residue to use as coupling moiety to BSA, but in this case the thiol (-SH) group was employed for direct immobilization to the previously functionalized slides with maleimide groups instead of epoxy used for BSA conjugation.

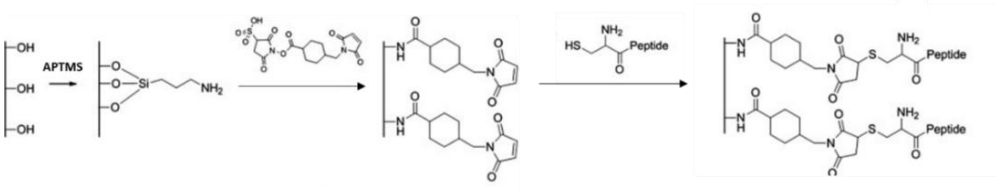

Figure 7.24 Derivatization scheme using APTMS to functionalize glass slides and then interact with Sulfo-SMCC crosslinker for the covalent attachment of (SH-) residues from cysteine modified peptides to the solid support.

Slides were initially washed in MiliQ H_2O and soap, placed in a glass holder and then immersed in Piranha solution (H_2SO_4conc:H_2O_2 7/3 (v/v)) for 30 minutes (50mL per slide support). After that, 6 washes with MiliQ H_2O took place followed by the incubation with 50 mL of 10 % NaOH solution for 1 hour for each slide container. Then 3 additional washes with MiliQ H_2O and other 3 with 60 % EtOH were required to proceed to the incubation with 2.5 % APTMS (Sigma-Aldrich, MO, USA) in Absolut EtOH with 10 mM Acetic Acid for three hours. Finally, 6 washes with 96 % EtOH (Merck KGaA, Germany) were performed followed by 20 min sonication in absolute ethanol (Merck KGaA, Germany), to dry them in N_2 flow. The next day prior direct peptide printing, a pre-incubation of the slides with a 2 mg ml^{-1} solution of the crosslinker Sulfo-SMCC (sulfosuccinimidyl 4-(N-maleimidomethyl) cyclohexane-1-carboxylate) (Thermo Fisher Scientific Inc., USA) was carried out in phosphate-buffered saline–ethylenediaminetetraacetic acid solution (PBS-EDTA, 50 mM phosphate, 0.15 M NaCl, 10 mM EDTA, pH 7.2) for 30 minutes.

7.5.2.2. Microarray printing conditions

The same concentrations of recombinant proteins and peptides were utilized in the multiplexed matrix already described in Chapter 6. The reagents deposition was performed using an automated piezo-driven SciFlexArrayer S3 (Scienion AG, *Berlin, Germany*). After optimization studies, 2 drops of 350pL each were deposited per spot at 25°C and 60% humidity, drying for at least 1 hour at R.T. and then kept at 4°C until use for a maximum of one week.

The distribution of the 24 array chips over a single slide are schematically represented in the following Figure 7.25, showing the distance between each printed array generating a 3 columns x 8 rows configuration. The assay protocol was the same as the one described in Chapter 6 see section 6.5.3.2.

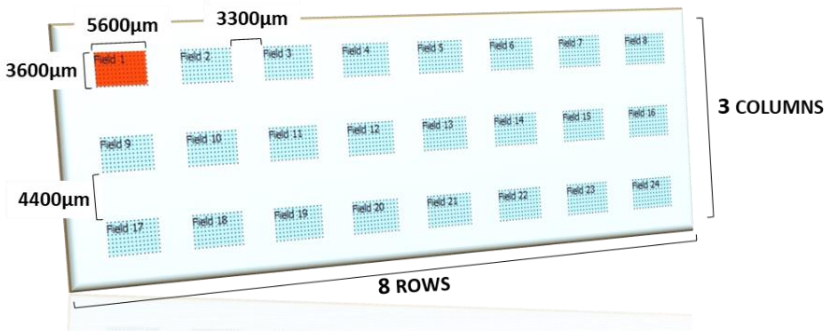

Figure 7.25 Rendered view of a single slide microarray. The spatial distribution of the general microarray in a single glass slide is represented, showing 24 independent sub-arrays by printing 35 epitopes in triplicate spots to simultaneously define a serologic profile from the samples under analysis.

7.5.2.3. Biostatistical analysis

The signal from each epitope was obtained as the average fluorescent intensity of three replicate spots from each sample subtracting the average fluorescence obtained with the control serum measured in each slide and then applying a logarithmic scale. Furthermore, from the total 755 human serum samples evaluated with the array only those with a lapse blood draw superior to 10 days from symptoms onset were considered for the biostatistical analysis.

Assay classification performance was estimated according to the gold standard RT-PCR technique through different data analysis models consisting on *univariate* and *multivariate* approaches. The first technique allows performance determination of each epitope individually, whereas the second evaluates the same performance considering more than one epitope at the same time. Across the *univariate* analysis, epitopes correlation was established and then the accuracy was estimated through ROC curves generation with their corresponding AUC values providing sensitivity and specificity for each component of the matrix classifying prepandemic vs RT-PCR+ patients. The correlation of the epitopes was calculated applying Pearson correlation coefficient with the Corrplot R package. The statistical significance and confidence interval of the ROC curves and AUC values was estimated using a binomial test. P-values for statistical analysis were adjusted using Benjamini – Hochberg correction. Analysis of significance and confidence interval for classification rate were obtained applying Wilcoxon test and bootstrap respectively.

For the *multivariate* analysis, classification and regression models were generated in order to predict RT-PCR+ results vs. pre-pandemic samples, and separately defining severity predictions. Additionally, feature selection techniques were applied to find a reduced number of epitopes with significant predictive performance. Principal components analysis was used throughout the data evaluation for visualization purposes. For classification and regression, partial least squares (PLS), random forest and K-nearest neighbors (KNN) were utilized. Random forests provided the best performance amongst all. Variance importance for decision trees in random forest was determined with VImp function. Double cross-validation with 10-fold cross-validation was implemented in this analysis. Epitope selection was performed using feed forward floating feature selection and genetic algorithms as search strategies following a wrapper approach based on KNN and random forests as criterium function.

7.5.3. EXPERIMENTAL DESIGN

7.5.3.1. Influence of number of drops per spot

The following matrix was created to monitor the influence of the number of drops over the spot size and intensity. For this purpose, peptide solutions for **P4** and **P10** were prepared at 500 µg mL^{-1} in 10mM PBS and protein solutions for S1-SARS2, S1+S2, NC-SARS1 and Hu-IgG TRITC were utilized at the already established concentrations on Table 6.5. Then, matrix incubation was carried out with CTR+Ab S and N at the three standard dilutions at 100, 25 and 5 µg mL^{-1} in 10 mM PBST 0.5 % BSA for sixty minutes continuing with the assay protocol as already defined. Spot diameter was determined using Mapix Software (Innopsys, Carbonne, France) also utilized for signal quantification.

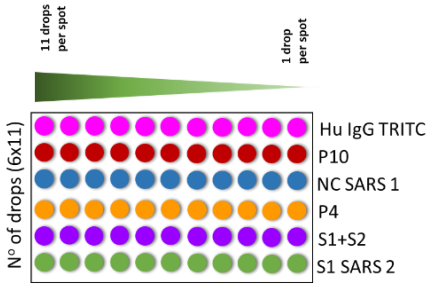

Figure 7.26 Matrix designed to evaluate the influence of the number of drops per spot in size, intensity and spot homogeneity.

7.5.3.2. Effect of BSA for peptide immobilization

For this experiment, three matrixes of 5x6 including peptides without prior BSA conjugation were developed using increasing immobilization concentrations adjusting the dimensions of the ArrayIt® holder creating 3x8 arrays over the slide. The order of the epitopes was the same as expressed in the Figure 7.27, but the first matrix was printed with 50 µg mL^{-1} peptide solution, the other 100 µg mL^{-1} and the third 250 µg mL^{-1} in 10mM PBS distributed in three columns across the single glass slides with eight replicate sub arrays each. Then, CTR+Ab S and N solutions were prepared at 100, 25 and 5 µg mL^{-1} in 10mM PBST 0.5% BSA and each solution was incubated over the three matrixes with increasing peptide

concentrations to assess the contribution of the peptides immobilized and the content of antibodies in the sample following standard array protocol.

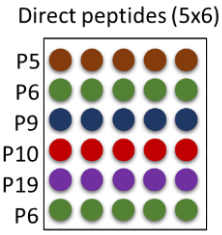

Figure 7.27 Microarray utilized for direct peptide immobilization with 5 replicate spots and a APTMS and Sulfo-SMCC derivatization protocol.

7.5.3.3. Competitive effect of hybrid-peptide protein microarray chip

Three different matrixes were prepared as described in the next Figure 7.28 using peptides solutions at 500 µg mL^{-1} in 10mM PBS and protein solutions at the corresponding concentrations. After that, 10 µl of seven selected clinal serum samples from BioZgZ were diluted in 40 µl of 10mM PBST 0.5% BSA and incubated over each array for one hour following standard assay protocol. The comparison of three matrixes with the same clinical samples was carried out making use of the ArrayIt® holder, in which each microarray chip was printed over a different column.

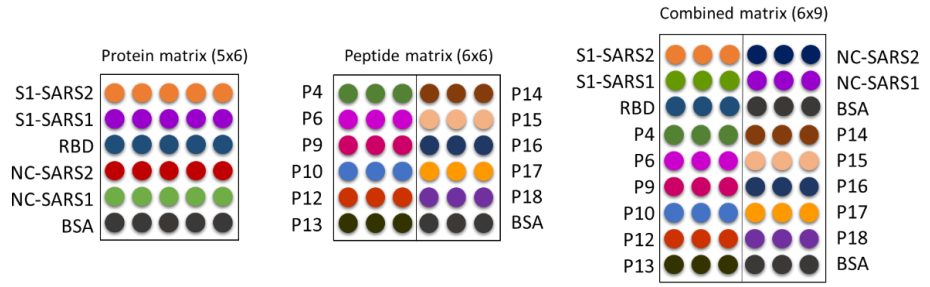

Figure 7.28 Evaluation of competitive phenomena. Three independent arrays were generated following the described distribution in a single glass slides dedicating one column to each matrix containing only the proteins, then peptide bioconjugates and the combination of peptides and proteins.

7.5.3.4. RBD influence in the matrix

For this study, two different arrays or 5x6 each, with 5 replicate spots were printed including only peptides without RBD (**P4**, **P5**, **P11**, **P11b**, **P22**) at 500 µg mL^{-1} and a different matrix containing RBD at 20 µg mL^{-1} in PBS with the same peptide solution used for the other array (removing **P11b**). Each matrix was incubated with the same samples to obtain comparable results attributed to the presence of RBD in the same array applying the standard assay procedure.

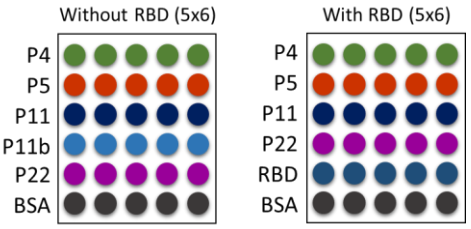

Figure 7.29 Influence of RBD presence towards the detection of RBD derived peptides. Two different matrixes were printed for this study, one of them containing only RBD peptides and BSA as control in five replicate spots while the other included the recombinant RBD at the concentrations established for the standard assay.

7.5.3.5. Effect of VoC-derived peptides detection in serum samples

In this case the matrix generated (6x6) included three replicate spots per epitope utilizing peptide solutions at 500 µg mL^{-1} in PBS. The following day, three CTR+Ab S solutions (100, 25 and 5 µg mL^{-1} in 10mM PBST 0.5% BSA) were used over the corresponding arrays. The exact experimental protocol was applied and epitope signal was analyzed.

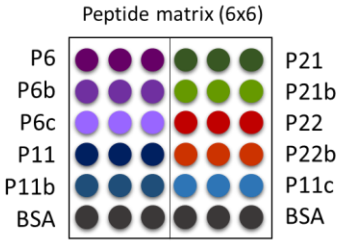

Figure 7.30 Effect of peptides derived from variants of concern. The following matrix was utilized to study the effect of peptides selected from VoC using triplicate spots of each bioconjugate at standard assay concentrations.

For the comparison of serological behavior on each peptide and the corresponding variant carried out over clinical samples. The final array matrix version 2.0 including 35 epitopes (9x12) was used. The signal from the epitopes of interest obtained after sample analysis with the complete array was extracted for each patient and plotted in the Figure 7.18 expressed. Qualitative interpretations were defined as a result of signal pattern monitored. For the Figure 7.19 the percentage of samples providing at least 25% of response for each epitope was calculated according to the total of samples belonging to every cohort and plotted in that graph.

7.5.3.6. Final matrix distribution of the *Immuno*-µSARS2 2.0 used in the analysis of clinical samples

Once the immobilization concentrations were defined for every immunoreagent, the decision to use two drops per spot and three replicate spots per epitope. The final array configuration was defined as a 9x14 matrix. As can be observed in the following Figure 7.31, the corresponding distribution in the printed array is expressed. The epitope concentrations solutions utilized were the same as implemented in the first version of the array, as only new peptides were included they were spotted at 500 µg mL^{-1}, to allow comparable determinations.

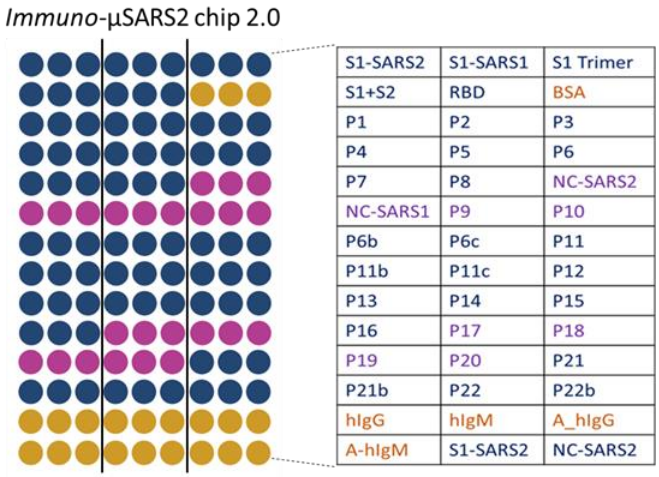

Figure 7.31 Immunoarray 2.0. Final epitope distribution of updated version of the microarray containing 35 different epitopes in triplicate spots to assess IgG/IgM mediated response after SARS-CoV-2 infection including internal controls.

7.6. BIBLIOGRAPHY

1. de Fátima Cobre, A., et al., *Diagnosis and prediction of COVID-19 severity: can biochemical tests and machine learning be used as prognostic indicators?* Computers in biology and medicine, 2021. **134**: p. 104531.
2. Atyeo, C., et al., *Distinct early serological signatures track with SARS-CoV-2 survival.* Immunity, 2020. **53**(3): p. 524-532. e4.
3. Shrock, E., et al., *Viral epitope profiling of COVID-19 patients reveals cross-reactivity and correlates of severity.* Science, 2020. **370**(6520): p. eabd4250.
4. Abdelzaher, H., et al., *COVID-19 genetic and environmental risk factors: a look at the evidence.* Frontiers in pharmacology, 2020. **11**: p. 579415.
5. Karachaliou, M., et al., *Infection induced SARS-CoV-2 seroprevalence and heterogeneity of antibody responses in a general population cohort study in Catalonia Spain.* Scientific Reports, 2021. **11**(1): p. 21571.
6. Pollán, M., et al., *Prevalence of SARS-CoV-2 in Spain (ENE-COVID): a nationwide, population-based seroepidemiological study.* The Lancet, 2020. **396**(10250): p. 535-544.
7. Moderbacher, C.R., et al., *Antigen-specific adaptive immunity to SARS-CoV-2 in acute COVID-19 and associations with age and disease severity.* Cell, 2020. **183**(4): p. 996-1012. e19.
8. Janssen, N.A., et al., *Dysregulated innate and adaptive immune responses discriminate disease severity in COVID-19.* The Journal of infectious diseases, 2021. **223**(8): p. 1322-1333.
9. Jespersen, M.C., et al., *BepiPred-2.0: improving sequence-based B-cell epitope prediction using conformational epitopes.* Nucleic acids research, 2017. **45**(W1): p. W24-W29.
10. Chen, C., et al., *CoV-Spectrum: analysis of globally shared SARS-CoV-2 data to identify and characterize new variants.* Bioinformatics, 2022. **38**(6): p. 1735-1737.
11. Mlcochova, P., et al., *SARS-CoV-2 B. 1.617. 2 Delta variant replication and immune evasion.* Nature, 2021. **599**(7883): p. 114-119.
12. Ren, S.-Y., et al., *Omicron variant (B. 1.1. 529) of SARS-CoV-2: Mutation, infectivity, transmission, and vaccine resistance.* World journal of clinical cases, 2022. **10**(1): p. 1.
13. Meng, B., et al., *Recurrent emergence of SARS-CoV-2 spike deletion H69/V70 and its role in the Alpha variant B. 1.1. 7.* Cell reports, 2021. **35**(13): p. 109292.
14. Dugas, V., J. Broutin, and E. Souteyrand, *Droplet evaporation study applied to DNA chip manufacturing.* Langmuir, 2005. **21**(20): p. 9130-9136.
15. Diehl, F., et al., *Manufacturing DNA microarrays of high spot homogeneity and reduced background signal.* Nucleic acids research, 2001. **29**(7): p. e38-e38.
16. Mujawar, L.H., et al., *Influence of the relative humidity on the morphology of inkjet printed spots of IgG on a non-porous substrate.* RSC advances, 2014. **4**(37): p. 19380-19388.
17. Kim, H.Y., et al., *Characterization and simulation of cDNA microarray spots using a novel mathematical model.* BMC bioinformatics, 2007. **8**(1): p. 1-11.

18. Chen, R., et al., *Characterization of chemoselective surface attachment of the cationic peptide melimine and its effects on antimicrobial activity.* Acta biomaterialia, 2012. **8**(12): p. 4371-4379.
19. Li, Y., et al., *Linear epitopes of SARS-CoV-2 spike protein elicit neutralizing antibodies in COVID-19 patients.* Cellular & molecular immunology, 2020. **17**(10): p. 1095-1097.
20. Lu, L., et al., *SARS-CoV-2-specific antibody response characteristics in COVID-19 patients of different ages: SARS-CoV-2 antibody response in different aged patients.* Acta Biochimica et Biophysica Sinica, 2022. **54**(4): p. 556.
21. Leek, J.T., et al., *Tackling the widespread and critical impact of batch effects in high-throughput data.* Nature Reviews Genetics, 2010. **11**(10): p. 733-739.
22. Sun, B., et al., *Kinetics of SARS-CoV-2 specific IgM and IgG responses in COVID-19 patients.* Emerging microbes & infections, 2020. **9**(1): p. 940-948.
23. Zamecnik, C.R., et al., *ReScan, a multiplex diagnostic pipeline, pans human sera for SARS-CoV-2 antigens.* Cell Reports Medicine, 2020. **1**(7): p. 100123.
24. Li, Y., et al., *Linear epitope landscape of the SARS-CoV-2 Spike protein constructed from 1,051 COVID-19 patients.* Cell reports, 2021. **34**(13): p. 108915.
25. Nehring, J., et al., *Autoantibodies against albumin in patients with systemic lupus erythematosus.* Frontiers in immunology, 2018. **9**: p. 2090.
26. Wu, L.x., et al., *Clinical significance of the serum IgM and IgG to SARS-CoV-2 in coronavirus disease-2019.* Journal of Clinical Laboratory Analysis, 2021. **35**(1): p. e23649.
27. Gattinger, P., et al., *Neutralization of SARS-CoV-2 requires antibodies against conformational receptor-binding domain epitopes.* Allergy, 2022. **77**(1): p. 230-242.
28. Liu, K.-T., et al., *Overview of neutralization assays and international standard for detecting SARS-CoV-2 neutralizing antibody.* Viruses, 2022. **14**(7): p. 1560.
29. Lan, J., et al., *Structure of the SARS-CoV-2 spike receptor-binding domain bound to the ACE2 receptor.* nature, 2020. **581**(7807): p. 215-220.
30. Leung, K., et al., *Early transmissibility assessment of the N501Y mutant strains of SARS-CoV-2 in the United Kingdom, October to November 2020.* Eurosurveillance, 2021. **26**(1): p. 2002106.
31. Rikhtegaran Tehrani, Z., et al., *Performance of nucleocapsid and spike-based SARS-CoV-2 serologic assays.* PloS one, 2020. **15**(11): p. e0237828.
32. Bryan, A., et al., *Performance characteristics of the Abbott Architect SARS-CoV-2 IgG assay and seroprevalence in Boise, Idaho.* Journal of clinical microbiology, 2020. **58**(8): p. e00941-20.
33. Kanji, J.N., et al., *False negative rate of COVID-19 PCR testing: a discordant testing analysis.* Virology journal, 2021. **18**(1): p. 1-6.
34. Takahashi, H., N. Ichinose, and Y. Okada, *False-negative rate of SARS-CoV-2 RT-PCR tests and its relationship to test timing and illness severity: A case series.* IDCases, 2022. **28**: p. e01496.
35. Mallett, S., et al., *At what times during infection is SARS-CoV-2 detectable and no longer detectable using RT-PCR-based tests? A systematic review of individual participant data.* BMC medicine, 2020. **18**(1): p. 1-17.

36. Wikramaratna, P.S., et al., *Estimating the false-negative test probability of SARS-CoV-2 by RT-PCR.* Eurosurveillance, 2020. **25**(50): p. 2000568.
37. Kucirka, L.M., et al., *Variation in false-negative rate of reverse transcriptase polymerase chain reaction–based SARS-CoV-2 tests by time since exposure.* Annals of internal medicine, 2020. **173**(4): p. 262-267.
38. Kinloch, N.N., et al., *Suboptimal biological sampling as a probable cause of false-negative COVID-19 diagnostic test results.* The Journal of infectious diseases, 2020. **222**(6): p. 899-902.
39. Montero, M.M., et al., *Evaluation of the host immune response assay SeptiCyte RAPID for potential triage of COVID-19 patients.* Scientific Reports, 2023. **13**(1): p. 944.
40. Plūme, J., et al., *Early and strong antibody responses to SARS-CoV-2 predict disease severity in COVID-19 patients.* Journal of Translational Medicine, 2022. **20**(1): p. 176.
41. Garcia-Beltran, W.F., et al., *COVID-19-neutralizing antibodies predict disease severity and survival.* Cell, 2021. **184**(2): p. 476-488. e11.
42. Li, K., et al., *Dynamic changes in anti-SARS-CoV-2 antibodies during SARS-CoV-2 infection and recovery from COVID-19.* Nature communications, 2020. **11**(1): p. 6044.
43. Peluso, M.J., et al., *SARS-CoV-2 antibody magnitude and detectability are driven by disease severity, timing, and assay.* Science advances, 2021. **7**(31): p. eabh3409.
44. West, R., et al., *COVID-19 antibody tests: a valuable public health tool with limited relevance to individuals.* Trends in microbiology, 2021. **29**(3): p. 214-223.
45. Camerini, D., et al., *Mapping SARS-CoV-2 antibody epitopes in COVID-19 patients with a multi-coronavirus protein microarray.* Microbiology Spectrum, 2021. **9**(2): p. e01416-21.
46. Amrun, S.N., et al., *Linear B-cell epitopes in the spike and nucleocapsid proteins as markers of SARS-CoV-2 exposure and disease severity.* EBioMedicine, 2020. **58**: p. 102911.
47. Holenya, P., et al., *Peptide microarray-based analysis of antibody responses to SARS-CoV-2 identifies unique epitopes with potential for diagnostic test development.* European journal of immunology, 2021. **51**(7): p. 1839-1849.
48. Wang, H., et al., *SARS-CoV-2 proteome microarray for mapping COVID-19 antibody interactions at amino acid resolution.* ACS Central Science, 2020. **6**(12): p. 2238-2249.

8. CONCLUSIONS

CONLCUSIONS PART I

- Under indirect competitive ELISA, the analytical performance of polyclonal and monoclonal antibodies targeting antibiotic residues was consistent. According to the experimental evidence, polyclonal antibodies achvied lower detection limits and robustness, as a result of the biophysical diversity favouring stability and the polyclonal nature, which allows the binding of different antigenic determinants of the target molecule.

-Highly selective immunoreagents have been effectively employed in single-analyte ELISA and multiplexed fluorescent microarrays exhibiting comparable bioanalytical characteristics in buffer and milk diluted. Moreover, a simple technological transition was demonstrated even under DNA-addressable microarray format.

-The conjugation of three haptenized antibiotic molecules with different oligonucleotides strands and their implementation in a DDI microarray assay was reported for the first time, although previous examples had proposed similar approaches using steroids-oligonucleotide conjugates.

-The use of class-selective antibodies allowed the detection of at least 18 different veterinary residues (FQ's, SA's, TYL) according EU regulatory levels with the same DDI chip after a single dilution of commercial milk samples. High-throughput performance was achieved with this microarray allowing the simultaneous analysis of 180 samples in 90 minutes.

-The kinetic characterization of the monoclonal antibodies and the hapten molecules through reference SPR techniques suggested that stronger interactions between antibody and hapten molecules could lead to lower analyte detectability in competitive assay formats, as was evidenced for the case of TYL reagents and showing the opposite behaviour with SA's reagents.

-For the first time reported, the binding between a monoclonal antibody (MAb-Tyl) and a small molecule (hapten) conjugated to a carrier protein was evidenced making use of a portable and inexpensive iSPR system coupled to smartphone detection as a proof of concept. These findings encourage the use of smartphones and plasmonic techniques as highly compatible tools in the development of label free and real time biosensing devices.

CONCLUSIONS PART II

-A rational design and selection of potentially immunogenic linear peptides derived from S and N proteins from SARS-CoV-2 demonstrated to be an effective strategy to define candidates with relevant immunodiagnostic performance. The extensive literature analysis based on *in silico* and experimental evidence showed to be useful but the most immunogenic epitopes were selected with consolidated experimental reports and utilizing a B cell epitope predictor software.

-The first version of the chip allowed simultaneous monitoring of IgG and IgM progression over time using antisera from rabbits immunized with S and N proteins. Defining a high and robust response for IgG's after three immunizations and the detecting considerable levels of IgM's eighteen days post first immunization. Additionally, the use of rabbit's antisera and the purified polyclonal fractions showed to be adequate positive controls for the chip characterization and transition to human samples.

-Competitive phenomena between linear peptides and proteins affecting IgG interactions from clinical samples were evidenced when they were printed in the same microarray. Future developments should consider the use of separate peptide-specific and protein-specific sub-microarrays to make comparable determinations.

- The clinical sensitivity of some peptide epitopes and mostly proteins, increased with longer time intervals between sample collection and onset of symptoms, demonstrating the chip's ability to track IgG progression in clinical samples. In addition, intrinsic cohort variability towards different epitopes was observed suggesting that multi-epitope immune profiling is more accurate that single epitope determinations.

-The profile of IgG's and IgM's in a total of 755 human serum samples was successfully analysed with the second version of the microarray. The chip was able to significantly discriminate seropositive samples according to RT-PCR technique using prepandemic serum as negative control for IgG's. A 98 % of clinical sensitivity and 91 % specificity were achieved with *multivariate* analysis.

-It has been demonstrated that *multivariate* analysis considerably improves the accuracy of the method (0.98 classification rate) increasing the diagnostic performance compared to *univariate* analysis (0.89 classification rate). Therefore, the establishment of immunological fingerprints against relevant peptide epitopes and viral proteins could serve as more efficient immunodiagnostic approach.

-Immunological signatures were significantly correlated with clinical outcomes using the panel of epitopes selected in the microarray chip 2.0 combining artificial intelligence. These results evidenced that clinical progression towards more severe outcomes can be better differentiated monitoring IgG response. Remarkably, *Exitus* condition was predicted with 81 % accuracy, followed by ICU admission (70% accuracy) and finally hospitalization requirement (66% accuracy) based on fingerprints established with clincal samples.

-The identification of immunodominant linear peptides was predominantly found over N protein sequence, and S2 sub unit region even in some cases with comparable IgG responses than the proteins. In addition, potential substitution of full-length proteins, for some correlated peptides was demonstrated mainly with N derived sequences (**P10**, **P17**; **P18**, **P19** and **P20)** and **P12** from S1 subunit to generate cost effective immunodiagnostic tests.

-The linear sequence of **P10** was identified as the most promising individual peptide epitope for discrimination of positive serological samples according to PCR, offering better performance than S1-SARS2 and NC-SARS2 proteins separately. Thus, we strongly suggest the potential use of this sequence as serodiagnostic element targeting SARS-CoV-2 IgG's.

-Antibodies with possible neutralizing capacity were detectable with the *immuno*-µSARS2 2.0 chip against the RBD protein and in a lower level to the linear epitopes selected from this region. In the case of **P22** sequence, a clear conformational preference of the antibodies was observed toward the sequence located in the folded RBD protein rather than the linear peptide.

-VoC-derived peptides including point mutations or deletions were detected and differentiated from the original peptides, utilizing clinical serum samples from patients exposed to the initial SARS-CoV-2 strain.

9. ACRONYMS AND ABBREVIATIONS

2D	Two Dimensional
3D	Three Dimensional
Ab	Antibody
aa	Amino Acids
Abs	Absorbance
ACE2	Angiotensin-converting enzyme 2
Ag	Antigen
AMR	Antimicrobial Resistance
Anh	Anhydrous
APTMS	(3-Aminopropyl) trimethoxysilane
aq	Aqueous
As	Antiserum
AUC	Area Under the Curve
AuNP	Gold nanoparticle
BAU	Binding Antibody Units
BioZgz	Biobanco de Zaragoza
BMPS	N-β-maleimidopropyl-oxysuccinimide ester
bp	Base Pair
BSA	Bovine Serum Albumin
°C	Degrees Celsius
CDC	Centers for Disease Control and Prevention
cDNA	Complementary DNA
CIBER-BBN	Centro de Investigación Biomédica en red – Bioingeniería, Biomateriales y Nanomedicina
CMOS	Complementary Metal Oxide Semiconductor
COVID-19	Coronavirus disease
CR%	Cross Reactivity
CRP	C-Reactive protein
CSIC	Spanish Council for Scientific Research
CTR+Ab	Positive control antibody
CTR+As	Positive control antisera
CV%	Coefficient of variation
Cys	Cystein
δ	density
Da	Dalton
DCC	N-dicyclohexylcarbodiimide
DDI	DNA directed immobilization
DMF	N-dimethylformamide

DMP	Dimethyl pimelimidate
DMSO	Dimethylsulfoxide
DNA	DeoxyriboNucleic Acid
EC	European Comission
EDC	1-Ethyl-3-(3-dimethylaminopropyl)carbodiimide
EFSA	European Food Safety Authority
ELISA	Enzyme-Linked ImmunoSorbent Assay
EMA	European Medicines Agency
EtOH	Ethanol
EU	European Union
FDA	Food and Drug Administration
FITC	Fluorescein isothiocyanate
Fmoc	9-fluorenylmethoxycarbonyl
FQ	fluoroquinolone
Fv	Fragment variable
g	Grams
GC-MS/MS	Gas chromatography coupled to mass spectrometry
GPTMS	3-(Glycidyloxypropyl)trimethoxysilane
h	hours(s)
HCH	Horseshoe Crab Hemocyanin
HdMar	Hospital del Mar
HPLC	High Performance Liquid Chromatography
HRP	HorseRadish Peroxidise
hTB	Tylosin hapten molecule
HUGTIP	Hospital Universitario Germans Trias i Pujol
IA	ImmunoAssay
IBEC	Instituto de Bioingeniería de Cataluña
IC_{50}	Concentration in which the signal is 50 % inhibited
IC_{90}	Concentration in which the signal is 10 % inhibited
ICU	Intensive Care Unit
IgG	Immunoglobulin G
IgM	Immunoglobulin M
IL	Interleukin
INF	Interferon
IQAC	Institute of Advanced Chemistry of Catalonia
iSPR	Imaging Surface Plasmon Resonance
ITN	Innovative Training Network
IVD	In Vitro Diagnostic

K_a	Association rate constant
K_d	Dissociation rate constant
KDa	KiloDalton
KD	Equilibrium Dissociation Constant
L	liter
LC-MS/MS	Liquid Chromatography coupled to Mass Spectrometry
LED	Light-emitting diode
LFIA	Lateral Flow immunoassay
LiU	Linköping University
LOD	Limit of Detection
LOQ	Limit of quantification
LSPR	Localized Surface Plasmon Resonance
µ	micro
MAb	Monoclonal Antibody
MALDI-TOF-MS	Matrix Assisted Laser Desorption Ionization - Time of Flight Mass Spectrometry
max	maximum
MERS-CoV	Middle East respiratory syndrome coronavirus
milliQ	milli-Q deionized and purified water
MIP	Moleclularly Imprinted Polymer
mL	milliliter
mm	millimeter
mM	millimolar (moles per liter)
mmol	millimole(s)
MRL	Maximum Residue Limit
mRNA	Messenger Ribonucleic Acid
MRPL	Minimum Required Performance Limit
MW	Molecular Weight
m/z	mass to charge ratio (in MS)
N	Nucleocapsid protein
$N4_{up}$	20-mer oligonucleotide, CTCTGTACACTAACGCTGGA
$N4_{down}$	20-mer oligonucleotide, TCCAGCGTTAGTGTACAGAG
$N5_{up}$	20-mer oligonucleotide, CCTGTTGAGCACAACCATTG
$N5_{down}$	20-mer oligonucleotide, CAATGGTTGTGCTCAACAGG
$N6_{up}$	20-mer oligonucleotide, TGAACTTCCACTTGCACAGG
$N6_{down}$	20-mer oligonucleotide, CCTGTGCAAGTGGAAGTTCA
NAb	Neutralizing antibody
Nb4D	Nanobiotechnology for Diagnostics Group

NHS	N-HydroxySuccinimide
nM	Nanomolar
O.N.	Overnight
ORF	Open Reading Frame
PAb	Polyclonal Antibody
PBS	Phosphate Buffered Saline solution
PBST	Phosphate Buffered Saline Tween-20 solution
PBT	Standard PBST with the absence of salts
PCR	Polymerase Chain Reaction
PDC	Piezo Dispense Capillary
PDMS	Polydimethylsiloxane
PEG	PolyEthylene Glycol
POC	Point-Of-Care
Ppb	Parts per billion
PrEDA	Hapten molecule derived from fluoroquinolones
PSO	Post Symptoms Onset
PVP	Polyvinylpyrrolidone
QDs	Quantum Dots
RBD	Receptor binding domain
RFU	Relative Fluorescence Units
RI	Refractive Index
RIU	Refractive Index Units
RNA	Ribonucleic Acid
ROC	Receiver operating characteristic curve
RPM	Revolutions per minute
RT	Room Temperature
RT-PCR	Reverse transcription polymerase chain reaction
RU	Resonance Units
S	Spike Glycoprotein
SA	Sulphonamide
SA2	Sulphonamide hapten molecule
SARS-CoV	Severe acute respiratory syndrome coronavirus
SARS-CoV-2	Severe acute respiratory syndrome coronavirus 2
SDS	Sodium Dodecyl Sulphate
SPE	Solid Phase Extraction
SPR	Surface Plasmon Resonance
SPY	Sulfapyridine
STC	Screening Target Concentration

Sulfo-SMCC	Sulfosuccinimidyl-4-(N-maleimidomethyl) cyclohexane-1-carboxylate
TAMRA	5-Carboxytetramethylrhodamine
TECP	Tris (2 carboxyethyl) phosphine
TMB	3,3',5,5'-TetraMethylBenzidine
TNFα	Tumor Necrosis Factor α
TRITC	Tetramethylrhodamine
TTIQ	Test-Trace-Isolate-Quarantine
Tyl	Tylosin
UV-Vis	Ultraviolet-visible absorption spectroscopy
VoC	Variant of Concern
WHO	World Health Organization